Kinesin Regulation:
Discovering the Mechanisms that Mediate Autoinhibition, Cargo Complex Formation, and Selective Microtubule Use in Neurons.

by

Jennetta Watson Hammond

A dissertation submitted in partial fulfillment
of the requirements for the degree of
Doctor of Philosophy
(Cellular and Developmental Biology)
in The University of Michigan
2008

Doctoral Committee:

Assistant Professor Kristen J. Verhey, Chair
Professor Lois S. Weismann
Associate Professor Catherine E. Krull
Assistant Professor Diane C. Fingar
Assistant Professor Jeffrey R. Martens

Acknowledgements

I would like to thank my Advisor and Committee Chair, Kristen Verhey for all of her invaluable teaching and mentoring over my time as a graduate student. I would also like to thank my thesis committee, as well as Professors: Billy Tsai, Edgar Meyhofer, and Gary Banker for their guidance and advice regarding my thesis work. I am indebted to the members of the Verhey, Tsai, Fingar, Meyhofer, Martens, and Banker labs for their contributions (whether direct or indirect) to my thesis work. I have learned a great deal from others about how to perform certain experiments as well as by following their advice about particular experiments I should try. Chapters 2-5, of this dissertation, includes some experiments contributed by others and I would like to acknowledge them as co-authors.

Chapter 2 Co-authors: Paul Jenkins, Jeffrey Martens, Kristen J. Verhey. Paul Jenkins, from Jeffrey Martens' lab, performed the KIF17 experiments in olfactory sensory neurons, Figure 2.7. In relation to this chapter, I would also like to acknowledge that Edgar Meyhofer generously permitted me to use his TIRF microscope. Dawen Cai, gave valuable advice on the single molecule experiments in Figure 2.1. He also developed an ImageJ plug-in to make data collection and analysis much easier and faster. Lynne Blasius performed crosslinking experiments on KIF17 that although the data was not included in Chapter 2 figures, did increase our understanding of KIF17 dimerization.

Chapter 3 Co-authors: Dawen Cai, T. Lynne Blasius, Gloria T. Jih, Edgar Meyhofer, and Kristen J. Verhey. Dawen Cai contributed the FRET data in Figure 3.1. Joel Swanson and Adam Hoppe, also deserve credit, as they generously provided the calibrated microscope and valuable experimental advice. I would additionally like to thank Dawen Cai for his recommendations and guidance with all the single molecule experiments. Lynne Blasius did all the crosslinking experiments on KIF1A constructs (Figures 3.1D, 3.4A, 3.5B). Gloria T. Jih, did some co-immunoprecipitation experiments that contributed to our overall understanding of the dimerization of KIF1A constructs,

although this data was not included in the figures shown. Edgar Meyhofer designed and built the microscope components required to perform the two-color single molecule motility assays (Figure 3.4 E-F). I would also like to thank Neha Kaul, Diane Wiener, and Dawen Cai as they helped with setup and alignment of the two-color TIRF system. Software to align the collected two-color images was developed by Dawen Cai.

Chapter 4 Co-authors: Kelly Griffin, Gloria T. Jih, Jeanne Stuckey, and Kristen J. Verhey. Kelly Griffin performed the yeast-two-hybrid experiment in Figure 4.4 D, and cloned the TPR mutants used throughout the paper. Gloria T. Jih contributed to the data collection in Figure 4.2. Jeanne Stuckey aligned the primary structure of KLC's TPR domains onto the crystal structures of other TPR containing proteins to make a structural model of KLC's TPR bundle (Figure 4.2 C and Supplemental 4).

Chapter 5 Co-authors: Chun-Fang Huang , Catherine Jacobson, Gary Banker, and Kristen J. Verhey. Catherine Jacobson, from Gary Banker's lab (Oregon Health and Science University), contributed the data showing that taxol treatment causes constitutively active Kinesin-1 to accumulate in dendrites over time (Figure 5.5 E and F). Although Chapter 5 does not contain any data contributed directly from Chung-Fang Huang (also from the Banker lab), she performed many of the same experiments I did, but in rat hippocampal neurons rather than neurons from mice. Publication of my work shown in Chapter 5, will eventually be a collaborative effort with Chung-Fang and the Banker lab.

Table of Contents

List of Figures

List of Abbreviations and Acronyms

aa	Amino acids
ACT	Activator of CREM in testis (CREM, cAMP-response element modulator)
AMPA	Alpha-amino-3-hydroxy-5-methylisoxazole-4-propionate (neurotransmitter)
AMPPNP	Adenylyl imidodiphosphate, a non-hydrolysable ATP analog
APC	Adenomatous polyposis coli
aPKC	Atypical protein kinase C
ApoER2	Apolipoprotein E receptor 2
APP	β-amyloid precursor protein
ARMS	Ankyrin-rich membrane spanning
AU	Arbitrary units
BSA	Bovine serum albumin
CA	Constitutively active
CAD	Mouse central nervous system catecholaminergic cell line
CaMKII	Calcium/calmodulin-dependent protein kinase II
CC	Coiled-coil
CFP	Cyan fluorescent protein
CNG	Cyclic nucleotide-gated
COS	African green monkey kidney cells
Co-IP	Co-immunoprecipitation
CRMP2	Collapsin Response Mediator Protein-2
CT	C-terminus, Carboxy-terminus
Dd	*Dictyostelium*
Dlg	Discs-large
DMP	Dimethylpimilimidate, a chemical crosslinker
E_{AVE}	Average FRET efficiency

EP-PCR	Error-prone PCR
EYFP	Enhanced yellow fluorescent protein
FEZ	Fasciculation and elongation protein zeta
FHA	Forkhead-associated
FL	Full-length
FP	Fluorescent protein
FRET	Fluorescence resonance energy transfer
GDI	Guanine dissociation inhibitor
GEFs	Guanine-nucleotide exchange factors
GFP	Green fluorescent protein
GRIP1	GluR2-interacting protein-1
GSK3β	Glycogen syntahase kinase-3β
HDAC	Histone deacetylase (HDAC6 is a tubulin deactylase)
Hs	Homo sapiens
IFT	Intraflagellar transport
IgG	Immunoglobulin G – control antibodies
IP	Immunoprecipitation
JB	JNK binding domain
JNK	c-Jun NH_2-terminal kinase
JIP	c-Jun NH_2-terminal kinase (JNK)-interacting protein
KAP	Kinesin associated protein
KHC	Kinesin heavey chain
KIF	Kinesin superfamily
KLC	Kinesin light chain
Kv4.2	Potassium channel subunit
LZ	Leucine zipper
MBS	Membrane associated guanylate kinases (MAGUKs) binding stalk
MAP	Microtubule associated protein
MCAK	Mitotic Centromere Associated Kinesin
mCFP	monomeric cyan fluorescent protein
mCit	monomeric citrine (variant of YFP)

min	minute
MKLP	Mitotic kinesin-like protein
MT	Microtubule
Mut	Mutant
NC	Neck coiled-coil or Neck coil
NMDA	N-methyl-D-aspartate (neurotransmitor)
NT	Non-transfected (Chapter 4)
NT	N-terminus, Amino-terminus (Chapter 2)
NXF2	Nuclear RNA export factor-2
Odora	Olfactory sensory neuron cell line
PAT1	Protein interacting with APP tail-1
PCR	Polymerase chain reaction
PDZ	Post-synaptic density (PSD)-95, Discs-Large, ZO-1.
PH	Pleckstrin homology
PI3K	Phosphotidylinositol-3-Kinase
PIP_3	Phosphotidylinositol(3,4,5) trisphosphate
PIP_3BP	Phosphotidylinositol(3,4,5)trisphosphate binding protein
PreImm	Pre-immune serum
PTB	phosphotyrosine binding domain
$PtdIns_{(4,5)}P_2$	Phosphotidylinositol(4,5)bisphosphate
PTMs	Post-translational modifications
RNAi	RNA interference
SAD	Synapses of amphids defective
SDS-PAGE	Sodium dodecyl sulfate polyacrylamide gel electrophoresis
sec	second
SEM	Standard error of the mean
SH3	Src homology 3
shRNA	short hairpin RNA
SLO	Streptolysin O, a bacterial toxin
TIRF	Total internal reflection fluorescence
TM	Transmembrane domains

TPR	Tetratricopeptide repeat
TSA	Trichostatin A
TTL	Tubulin tyrosine ligase
WT	Wildtype
YFP	Yellow fluorescent protein

Abstract

Kinesin motors play an indispensable role in intracellular trafficking by driving the long-distance transport of protein and vesicular cargoes along microtubules. My thesis work has focused on uncovering regulatory mechanisms that mediate 1) kinesin autoinhibition, 2) cargo complex formation, and 3) polarized transport due to preferential microtubule track selection. Kinesin motors generally are kept inactive in the absence of cargo. My work demonstrates that KIF17 (Kinesin-2) is self-inhibited by assuming a folded conformation that allows a weak coiled-coil region in its stalk to directly contact the motor domain. This interaction prevents KIF17 from moving on microtubules. The cargo binding tail does not play an inhibitory role, but is nevertheless important in regulation as it functions to load KIF17 into cilia. KIF1A (Kinesin-3) is also inactive in the absence of cargo due to inhibitory regions that include the FHA domain and two adjacent coiled-coils. My work further demonstrates that KIF1A motors undergo processive motility as dimeric rather than monomeric motors using their neck coil to dimerize. Kinesin motors are relieved of their autoinhibition by cargo binding. However, as there are many different cargoes that require transport by the same kinesin motor, I have investigated whether specific cargo proteins compete or cooperate with each other for transport. My work shows that while some cargos are transported independently, other cargos such as JIP1 and JIP3 do form cooperative complexes with a single motor that are essential for efficient transport. The JIP1/ JIP3/Kinesin-1 complex is formed due to an interaction between JIP1 and JIP3 and distinct binding sites on Kinesin-1 for each cargo. Once cargo is loaded, kinesin motors have to transport them to their correct subcellular destinations. I have investigated whether Kinesin-1's preference for certain types of modified microtubules can direct the polarized sorting of cargo into the axonal compartment of neuronal cells. My results indicate that several types of microtubule post-translational modifications additively or synergistically mediate Kinesin-1's preference for axonal microtubules and its sorting mechanism. Overall, my

work contributes to our understanding of how kinesin motors are activated and attached to their cargos in order to transport them to specific subcellular destinations.

Chapter 1:
Introduction

A cell relies on intracellular transport in order to maintain its proper morphology and functions. Molecular motors of the kinesin, dynein, and myosin superfamilies use the cell's microtubule or actin cytoskeletons as highways to transport cargoes to their appropriate cellular destinations. Typical cargos include large organelles, membrane bound vesicles of the secretory and endocytic pathways, cytoskeletal components, and protein or mRNA complexes [1, 2]. The mechanisms underlying individual motor regulation, cargo recognition and release, and sorting to appropriate cellular locales are only beginning to be discovered.

The kinesin superfamily is divided into 14 families that all contain a well-conserved motor domain [1, 3, 4]. This ~350 residue domain binds and hydrolyzes ATP. The motor domain couples this ATPase activity with its ability to attach to and generate movement along microtubules. Many kinesins contain the motor domain (or head) at one end, followed by a stalk region containing short or extensive alpha-helical coiled-coil regions which function to dimerize the motor. Cargo binding regions follow, or in some cases are intermixed within the stalk, and are quite divergent among the kinesin superfamily, and even within families, allowing for diversity in cargo binding and motor regulation [2]. The linker region between the motor and stalk is referred to as the neck, which in some cases has been shown to be important in motor regulation or determining direction of motility [5, 6].

In considering kinesin mediated vesicular transport, it is helpful to recognize the basic steps likely involved (Figure 1.1). First, kinesin motors must be activated by binding to cargo, possibly with the help of other regulatory complexes or post-translational modifications. Second, the activated motor/cargo complex binds to microtubules and begins processive movement, defined as taking multiple steps along microtubules without dissociating. Third, the motor reaches its destination where it

dissociates from the microtubule and its cargo. This step may occur spontaneously or may require the help of an "inactivating" complex or post-translational modifications. Finally the motor diffuses or is transported in an inactive state back to where it will be used again for cargo transport; although it is also possible that the motor is simply degraded at this point.

My research has focused on three specific questions relating to the first two steps of this kinesin transport cycle. 1) What are the molecular mechanisms keeping different kinesin family members inactive in the absence of cargo? 2) How do kinesins attach to and coordinate the transport of their various types of cargo? 3) Does kinesin's preference for certain types of modified microtubules direct polarized sorting of cargo to the axonal compartment of neuronal cells? To address these questions, I have focused on a small subgroup of the kinesin superfamily that are all well documented in their involvement in vesicular transport; specifically, Kinesin-1 (also known as conventional Kinesin or KIF5); KIF17, a Kinesin-2 family member; and KIF1A, a Kinesin-3 family member (Figure 1.2).

AUTOINHIBITION

Kinesin-1

Kinesin-1 was the first kinesin identified and is the most extensively studied of the kinesin family members. It is composed of two heavy chains (KHC), each containing an N-terminal motor domain, followed by an extensive coiled-coil stalk with multiple flexible hinge regions, and a globular, cargo binding tail. Two light chains (KLC) bind to the heavy chains using heptad repeats and are also composed of six tandom TPR protein-protein interaction domains that are responsible for binding cargo (Figure 1.2).

Kinesin-1 is a highly processive motor that coordinates its two motor heads to move in an alternating, hand-over-hand stepping manner over long distances. Each step is about 8-nanometers in size, corresponding to the length of a tubulin dimer, the building blocks of the microtubule lattice. Kinesin-1 moves toward the plus-end of microtubules or generally towards the cellular periphery [2, 6, 7].

Because Kinesin-1 uses a considerable amount of ATP to fuel its motility, it is essential that this activity be tightly coupled to cargo transport so energy is not

unnecessarily wasted. Consistent with the existence of an inactive state, soon after Kinesin-1 was identified, cellular fractionation studies revealed that a majority of Kinesin-1 resides in the cytoplasm as a soluble protein with inhibited microtubule-activated ATPase activity [8-10]. Electron microscopy, sedimentation assays, single molecule analysis, and FRET stoichiometry have since shown that without cargo bound, Kinesin-1 is inactive and folded head to tail [6, 11-19]. This autoinhibited state is maintained by the IAK region (consisting of the three amino acids: isoleucine, alanine, and lysine) of the KHC globular tail and by KLC, most likely through multiple weak electrostatic interactions with the neck and motor regions [6, 12, 14, 19]. These interactions in addition to folding the motor lengthwise, head-to-tail, separate the motor domains most likely through an unwinding of the neck coiled-coil [18]. Overall, this folded conformation prevents the motor from interacting with microtubules or exchanging ADP for ATP when not bound to cargo.

Autoinhibition of Kinesin-1 is relieved by cargo binding. As the two regions shown to mediate inhibition of motor activity, namely the IAK region of KHC's tail and KLC's TPR domains, are both regions known to mediate cargo binding, it is a compelling theory that cargo binding to either, or both, of these regions activates Kinesin-1. Indeed early studies showed that attaching beads to the KHC tail, as a cargo mimic, resulted in a motile Kinesin-1 [11, 12]. More recently, Blasius et al. showed that binding of a known cargo to either the KHC tail or KLC TPR domains is not sufficient for motor activation. Instead binding of two cargos, FEZ to KHC and JIP1 to KLC, is required in order to free the microtubule binding and processive motility activities of Kinesin-1 [20]. Cargo binding of Dlg to the motor-binding inhibitory domain of kinesin protein, Gakin/KIF13b [21], also relieves Gakin's autoinhibition, suggesting that the mechanism of cargo binding directly to regulatory regions is a general mechanism employed by kinesins for activation. Other mechanisms such as phosphorylation or dephosphorylation of kinesins have also been suggested to play a role in motor activation or regulation of cargo binding [22, 23].

As the motility/ATPase activities of other cargo-transporting kinesins must also be tightly coupled to cargo transport, the work on Kinesin-1 has led to the general hypothesis that kinesin motors are autoinhibited. Indeed full-length Kinesin-2 family

member Osm-3, homologue to mammalian KIF17 [24], and the Kinesin-3 family members, KIF1A/Unc104 and KIF13B/GAKIN [21, 25-27], have been shown to be autoinhibited. However regulatory domains and mechanisms for these kinesins are less clear than for Kinesin-1. Because kinesin superfamily members only share the motor domain in common [2], the evolution of diverse cargo binding domains and stalk structures must have co-evolved with motor regulatory regions and mechanisms. Consequently the detailed mechanisms of each kinesin protein are likely to be unique; although, the general principles learned from Kinesin-1 regulation may still be applicable.

KIF17

KIF17 is a homodimer that like Kinesin-1, moves processively towards the plus ends of microtubules. It has been implicated in the transport of NMDA and Kv4.2 vesicles in the dendrites of neuronal cells and CNG channels in olfactory cilia [28-31]. The C. *elegans* homologue Osm-3 is better characterized, playing an essential role in ciliary and flagellar transport [32]. Despite the handful of transmembrane proteins or protein complexes that are known to be transported by KIF17/Osm-3, only three direct binding proteins are known, Mint1, ACT, and NXF2 [29, 31, 33-37]. In the case of Mint1 (also known as mLin10 or X11) the extreme C-terminal residues of KIF17 bind one of two PDZ domains in Mint1 [31]. This interaction has been shown to be additionally regulated by phosphorylation of a nearby serine residue by CaMKII [23]. If KIF17 motor regulation is analogues to Kinesin-1, in that, cargo binding domains regulate motor function, it is possible these C-terminal residues, or the tail in general, are important in mediating autoinhibition (Figure 1.2). However other unidentified cargo binding regions may also exist.

Previous work on recombinant Osm-3 *in vitro* showed that motility is inhibited in the absence of cargo, and that the protein may shift from a folded, more compact form, to an extended conformation like Kinesin-1. A small hinge region between two coiled-coils in the stalk is essential for this folding and regulation [24]. Because inhibition was lost when the Osm-3 hinge was removed or mutated, it was hypothesized that a region C-terminal to the hinge likely interacts with residues in the motor/neck region; yet, the

specific domains and interaction mechanisms were not investigated [24]. Because of major structural differences between mammalian KIF17 and C. *elegan* Osm-3, specifically in the hinge and the following coiled-coil regions, it is difficult to conclude whether the same hinge mediated folding mechanism is likely to be conserved between the two homologues.

My work, detailed in Chapter 2, confirms that KIF17, like Kinesin-1 and Osm-3, is autoinhibited,in the absence of cargo. Processive motility is inhibited by direct contact of the motor domains with a region of the coiled-coil stalk that is only somewhat conserved with Osm-3. The cargo binding tail does not play a detectable role in motor regulation, but is essential for loading KIF17 into cilia.

KIF1A

KIF1A and the C. *elegans* homologue, Unc104, structurally look much different from Kinesin-1 and KIF17 because their stalk regions are not composed of large coiled-coiled regions. Rather the motor domain is followed by two very short and relatively weak coiled-coils, a forkhead-associated (FHA) domain, two more short coiled-coils, a large undefined region, and a C-terminal PH domain (Figure 1.2). Cargo protein Liprin-α's binding site includes a section of coiled-coil 2, as well as, a portion of the undefined region [38]. The PH domain has been shown to be important in connecting KIF1A/Unc104 motors to vesicular membranes via interactions with phosphotidylinositols (specifically $PtdIns_{(4,5)}P_2$; [39, 40]).

Full-length KIF1A/Unc104 is autoinhibited in the absence of cargo [25, 26, 41]. Inhibition of microtubule binding, and thus motility, is prevented by the FHA domain and adjacent c-terminal coiled-coil (CC2), although neither of these domains directly contact the motor nor neck domains, leaving the mechanism of regulation largely unknown [25]. The two coiled-coils adjacent to the motor also have suggested roles in regulating KIF1A activity in that they can pair with themselves on adjacent KIF1A molecules to form an intermolecular coil (dimer) or pair with each other in an intramolecular coil (monomer) (Figure 1.3)[27].

KIF1A has some of the highest velocities reported for kinesin molecules, running between 1-2 μm/second [26, 27, 42, 43]; yet, its mechanism of motility is controversial.

KIF1A/Unc104 has been postulated to function as a monomer. Recombinant and endogenous KIF1A proteins act like monomers in sedimentation and gel filtration assays [44-46] and truncated KIF1A proteins that are confirmed monomers, have motile properties *in vitro* [47-49]. A novel, biased-diffusion model of motility has been proposed to explain the motility of a single-motor driven KIF1A, used in place of the hand-over-hand model generally accepted for dimeric, or two-motor driven, kinesins [7, 47-49]. However, recent studies have brought into question the monomer-based movement hypothesis, and suggested instead that KIF1A and/or closely related family members do indeed dimerize, but may require high concentrations [26, 41, 45, 50-52]. Tomishege et al additionally showed this dimerization is likely required for processive motility [26]. Thus, a second model has been proposed where KIF1A binding to clustered cargos on a vesicle locally concentrates KIF1A and mediates a monomer to dimer switch, which has also been suggested, although not yet experimentally supported, to activate KIF1A's motile properties. In this model, KIF1A moves like Kineisn-1 in a coordinated hand-over hand fashion that allows the motors to take successive, unidirectional steps along a microtubule without dissociating [25, 26, 39, 40].

Because of unresolved questions about whether KIF1A moves as a monomer or dimer and whether a monomer to dimer transition relieves autoinhibition, I was interested in investigating KIF1A's regulation and motile properties in relation to dimerization state using some new and old experimental tools. My work, and that of my lab colleges, detailed in Chapter 3, shows that a significant population of endogenous and overexpressed KIF1A exists as a dimer, yet is still inactive for microtubule-based motility. Thus, dimerization is not sufficient to relieve the autoinhibition mediated by the FHA domain. KIF1A constructs without the FHA domain that dimerize via the short neck coiled-coil do move at a constant velocity of 1.3 μm/second over long distances. Although shorter, monomeric, constructs do display some motile properties, their motility is very short in duration and does not require ATP. Thus we support the conclusion that KIF1A moves as a dimer and that motility is regulated by both the FHA domain and the neck coiled-coil which functions to dimerize and coordinate the two motor heads in the full-length molecule.

MOTOR/CARGO COMPLEXES

As mentioned above, kinesin cargos take various forms ranging in size from large organelles to smaller protein complexes. Recent work has identified multiple binding partners for individual motor proteins and in many cases, these binding partners are soluble adaptor proteins that mediate the attachment of motor proteins to membrane-bound cargoes or other protein or mRNA complexes [2, 53]. KIF17 binds directly to the soluble adaptor protein Mint1, which mediates the transport of NMDA receptors through complexing first with at least two other adaptors, mLin-2 and mLin-7 [31]. Kinesin-1 transports the transmembrane proteins APP and ApoER2 via the JIP family of adaptor proteins [53-55]. Kinesin-1 also likely transports AMPA receptors via binding to GRIP1 [56].

The fact that it takes at least two proteins to activate Kinesin-1 and that it is easier to see motor binding to a particular cargo than to reconstitute active motility of kinesins with that particular cargo *in vitro*, suggests that cargo/motor complex formation and motor activation is often more complex than a single protein interaction or phosphorylation event [20, 57]. It is therefore critical to decipher not only the identity of cargo proteins and their direct or indirect binding mechanisms to kinesin motors, but also the combinations of cargo proteins (and/or other modifications) that are required for motor activation and thus truly define a kinesin cargo. Additionally, as more and more direct binding cargo proteins are identified for KLC or KHC, it begs the question of how one motor can coordinate and carry out the transport of its many different cargoes at specific times and to correct cellular locations.

In Chapter 4, I set out to investigate the transport of different Kinesin-1 cargoes that bind directly to the TPR domains of KLC, specifically JIP1, JIP3, Kidins220/ARMS, and PAT1 [54, 58-60] asking the specific question of whether these cargo proteins compete or cooperate for transport. For most cargo combinations, no competition or cooperative activity was found, suggesting independent transport by a non-limiting Kinesin-1 pool. Yet, in the case of JIP1 and JIP3, the two cargos cooperate for Kinesin-1 transport. JIP1 and JIP3 interact with each other and with independent sites on KLC forming a tri-molecular complex that is necessary for both proteins to be efficiently transported in neuronal cells. Thus, the complexities of the Kinesin-1 motor/cargo

complex grows as three binding partners, FEZ, JIP1, and JIP3, likely make up a functional motor activating and transportable unit. However, other essential, unidentified members of this particular cargo complex could still exist. JIP1 and JIP3 are scaffolding proteins known to bind and modulate the JNK signaling pathway [61], thus the JIP1/JIP3/Kinesin-1 transport complex likely contains many additional kinases as well as other transmembrane and soluble proteins.

MICROTUBULE PREFERENCE AND ITS ROLE IN POLARIZED TRANSPORT

Once a kinesin motor binds cargo and its autoinhibition is relieved, it is able to bind microtubules and begin processive transport. For Kinesin-1, KIF17, and KIF1A that involves moving towards the plus-end of microtubules or generally towards the cell periphery. However, like in a city where not all roads lead to one specific destination, in a cell, not all microtubule tracks lead to the cargos' targeted cellular endpoint. This is especially true in polarized cells were cellular compartments that require their own unique subset of proteins for proper function, like the axonal and dendritic processes of neuronal cells or the basolateral and apical membrane surfaces of epithelial cells, reside at rather opposite ends of the cell. Yet, it is also true in the case of non-polarized cells, where although most microtubules point towards the cell periphery, some microtubule tracks may still be under construction or are actively being removed and thus poor choices for transport. The necessity to transport cargo to its correct cellular destination through the use of complete microtubule roadways, suggest kinesins may have evolved intrinsic microtubule preference mechanisms or separate regulatory partners that direct them to preferred microtubule tracks and/or cellular destinations.

In neuronal cells, Kinesin-1 transports cargo primarily down microtubules of the axon [62, 63]. As truncated Kinesin-1 constructs show this same preference for axons over dendrites, the axonal sorting cue is thought to reside within the motor/microtubule binding interface [62]. However, a separate cargo directed sorting model has also been proposed [56]. The first model is especially intriguing when combined with multiple studies showing Kinesin-1, *in vitro*, has a binding preference for microtubules post-translationally modified by acetylation, detyrosination, and/or polyglutamylation [64-68]. These same post-translational modifications (PTMs) tend to accumulate on, or mark,

stable or long lasting microtubules and are enriched in axons over dendrites [69, 70]. Thus, this pool of microtubules marked with PTMs and preferred by Kinesin-1, could serve as an axonal signal. This seems to be the case in fibroblast cells, as Kinesin-1 preferentially uses the subset of microtubules that are acetylated and/or detyrosinated [64, 67] .

In chapter 5, I test the possibility that microtubule modifications direct Kinesin-1's axonal sorting in primary hippocampal neurons. My results indicate that there are probably several types of PTMs that together mediate Kinesin-1's preference for axonal transport. Drug treatments that increase multiple PTMs (i.e. taxol and GSK3β inhibitors), redirect Kinesin-1 to all neuronal processes; however, increasing microtubule acetylation alone is not sufficient to alter polarized transport.

DISSOCIATION FROM CARGO AND FATE OF KINESIN MOTORS AT THE TRANSPORT DESTINATION

Once kinesin/cargo complexes have transported along microtubules and reached their cellular destinations, kinesin motors must be inactivated and released from cargo and microtubules. The exact order of events, specific mechanisms, or accessory regulatory complexes mediating this step are still unclear. Phosphorylation of the motor or cargo is the most experimentally supported mechanism at this time mediating cargo release. Phosphorylation of Kinesin-1 by GSK3β or other unidentified kinases inhibits anterograde transport and has been shown to reduce the amount of kinesin bound to vesicles [71, 72]. Stagi et al recently showed that the JNK signaling pathway releases Kinesin-1 cargoes from microtubules [73]. Phosphorylation of KIF17 at Ser1029 by CaMKII, releases cargo protein Mint1 complexed to NMDA receptors likely in the vicinity of the synapse where it is needed [23].

The final step in the kinesin transport cycle requires that the motor return back to a place of cargo loading where it can be used again. Once more, details are very unclear; yet, multiple mechanisms have been proposed including diffusion of the motor, retrograde transport of the motor in an inactive state by dynein or other minus-end motors, or even the possibility that the motor is simply degraded at the transport end-point ([57, 74, 75]).

FIGURES

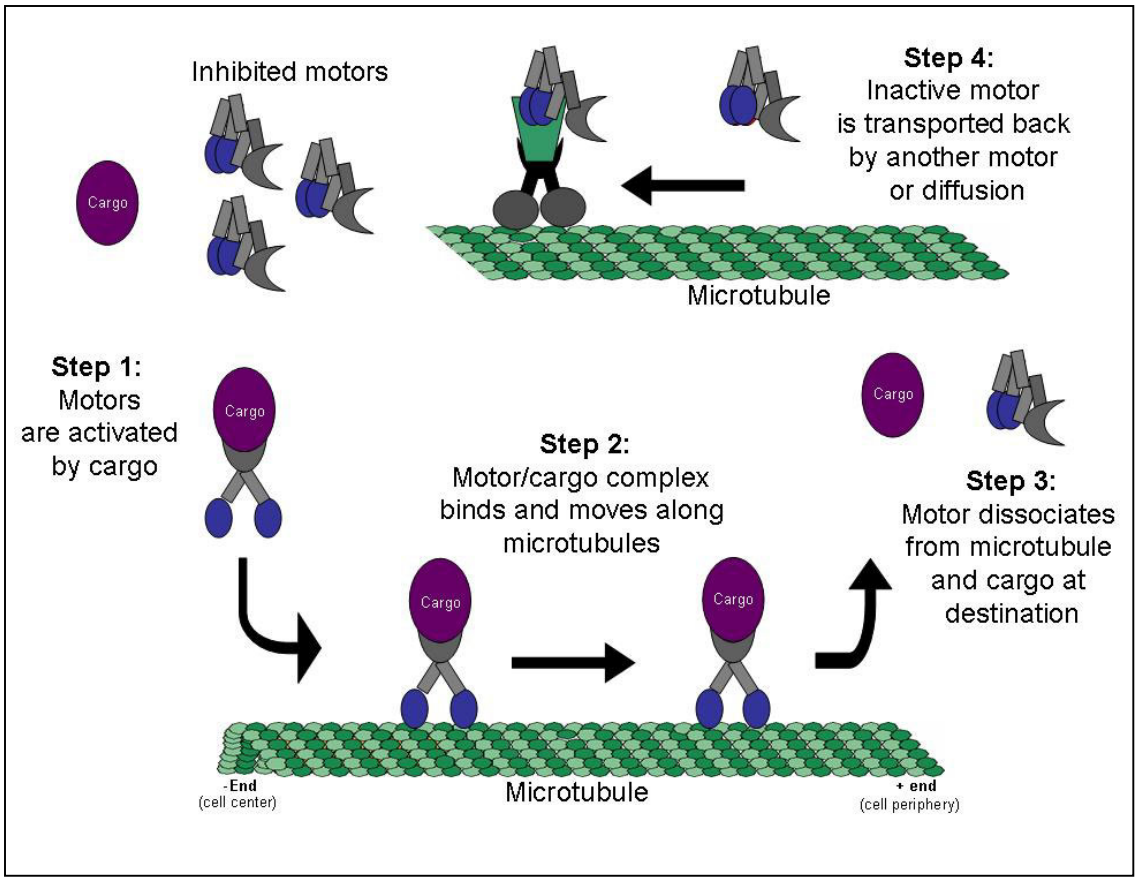

Figure 1.1: A simplified model of kinesin transport.

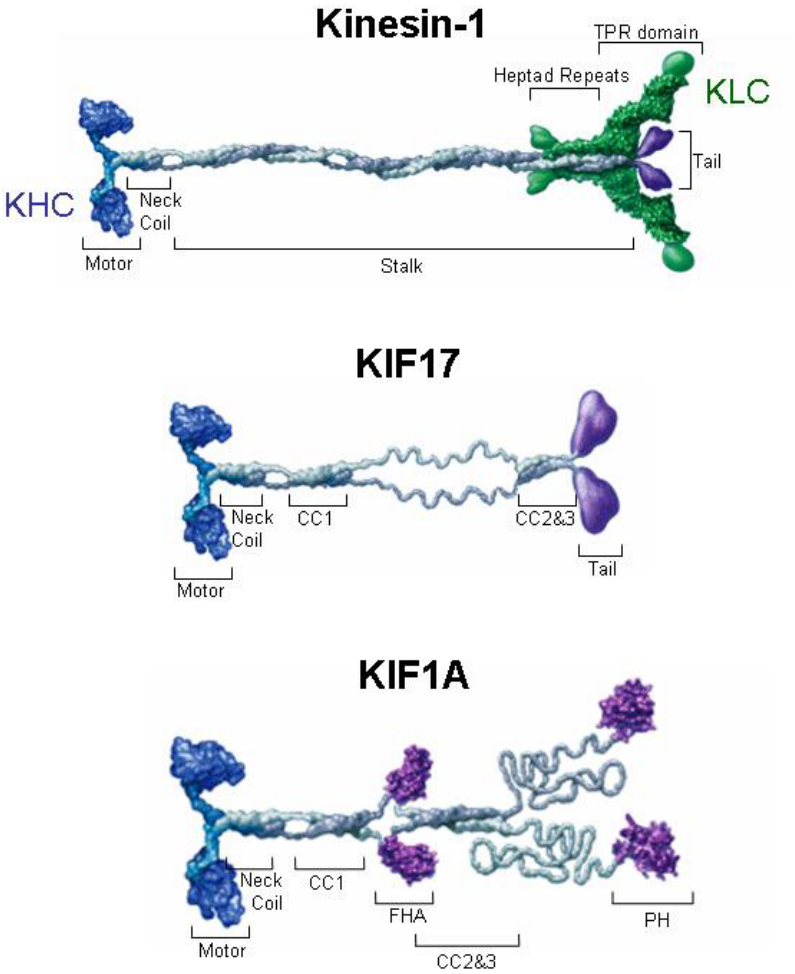

Figure 1.2: Schematic of Kinesin-1, KIF1A, and KIF17. The catalytic motor domains shown in blue are conserved among all kinesin motors while cargo binding and regulatory stalk/tail regions are unique. KHC, kinesin light chain; KLC, kinesin heavy chain; CC, coiled-coil; FHA, forkhead-associated domain. (Figure is modified from [2])

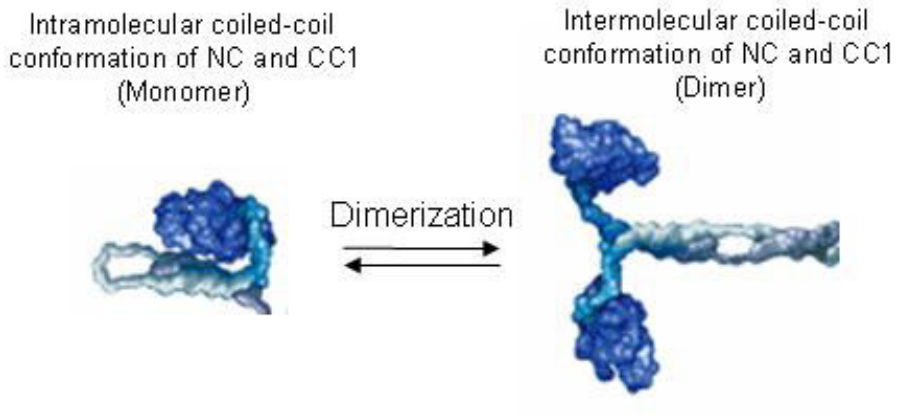

Figure 1.3: Two conformations of KIF1A's neck coil (NC) and coiled-coil 1 (CC1). Only the motor, NC, and CC1 regions of KIF1A are depicted. The NC and CC1 can from an intramolecular coiled-coil that may limit KIF1A to a monomeric state. Alternatively the NC and CC1 can form intermolecular coils with their counterparts on a separate KIF1A peptide consequently shifting KIF1A to a dimeric state with motor domains well coordinated for motility. (Figure is modified from [2])

REFERENCES

1. Hirokawa, N. and R. Takemura, *Kinesin superfamily proteins and their various functions and dynamics.* Exp Cell Res, 2004. **301**(1): p. 50-9.
2. Vale, R.D., *The molecular motor toolbox for intracellular transport.* Cell, 2003. **112**(4): p. 467-80.
3. Lawrence, C.J., et al., *A standardized kinesin nomenclature.* J Cell Biol, 2004. **167**(1): p. 19-22.
4. Miki, H., Y. Okada, and N. Hirokawa, *Analysis of the kinesin superfamily: insights into structure and function.* Trends Cell Biol, 2005. **15**(9): p. 467-76.
5. Endow, S.A., *Determinants of molecular motor directionality.* Nat Cell Biol, 1999. **1**(6): p. E163-7.
6. Adio, S., et al., *Review: regulation mechanisms of Kinesin-1.* J Muscle Res Cell Motil, 2006. **27**(2): p. 153-60.
7. Yildiz, A. and P.R. Selvin, *Kinesin: walking, crawling or sliding along?* Trends Cell Biol, 2005. **15**(2): p. 112-20.
8. Vale, R.D., T.S. Reese, and M.P. Sheetz, *Identification of a novel force-generating protein, kinesin, involved in microtubule-based motility.* Cell, 1985. **42**(1): p. 39-50.
9. Hollenbeck, P.J., *The distribution, abundance and subcellular localization of kinesin.* J Cell Biol, 1989. **108**(6): p. 2335-42.
10. Hackney, D.D., J.D. Levitt, and J. Suhan, *Kinesin undergoes a 9 S to 6 S conformational transition.* J Biol Chem, 1992. **267**(12): p. 8696-701.
11. Coy, D.L., et al., *Kinesin's tail domain is an inhibitory regulator of the motor domain.* Nat Cell Biol, 1999. **1**(5): p. 288-92.
12. Cross, R. and J. Scholey, *Kinesin: the tail unfolds.* Nat Cell Biol, 1999. **1**(5): p. E119-21.
13. Friedman, D.S. and R.D. Vale, *Single-molecule analysis of kinesin motility reveals regulation by the cargo-binding tail domain.* Nat Cell Biol, 1999. **1**(5): p. 293-7.
14. Hackney, D.D. and M.F. Stock, *Kinesin's IAK tail domain inhibits initial microtubule-stimulated ADP release.* Nat Cell Biol, 2000. **2**(5): p. 257-60.
15. Hackney, D.D. and M.F. Stock, *Kinesin Tail Domains and Mg(2+) Directly Inhibit Release of ADP from Head Domains in the Absence of Microtubules.* Biochemistry, 2008.
16. Stock, M.F., et al., *Formation of the compact confomer of kinesin requires a COOH-terminal heavy chain domain and inhibits microtubule-stimulated ATPase activity.* J Biol Chem, 1999. **274**(21): p. 14617-23.
17. Verhey, K.J., et al., *Light chain-dependent regulation of Kinesin's interaction with microtubules.* J Cell Biol, 1998. **143**(4): p. 1053-66.

18. Cai, D., et al., *Kinesin-1 structural organization and conformational changes revealed by FRET stoichiometry in live cells.* J Cell Biol, 2007. **176**(1): p. 51-63.

19. Dietrich, K.A., et al., *The kinesin-1 motor protein is regulated by a direct interaction of its head and tail.* Proc Natl Acad Sci U S A, 2008. **105**(26): p. 8938-43.

20. Blasius, T.L., et al., *Two binding partners cooperate to activate the molecular motor Kinesin-1.* J Cell Biol, 2007. **176**(1): p. 11-7.

21. Yamada, K.H., T. Hanada, and A.H. Chishti, *The effector domain of human Dlg tumor suppressor acts as a switch that relieves autoinhibition of kinesin-3 motor GAKIN/KIF13B.* Biochemistry, 2007. **46**(35): p. 10039-45.

22. Gunawardena, S. and L.S. Goldstein, *Cargo-carrying motor vehicles on the neuronal highway: transport pathways and neurodegenerative disease.* J Neurobiol, 2004. **58**(2): p. 258-71.

23. Guillaud, L., R. Wong, and N. Hirokawa, *Disruption of KIF17-Mint1 interaction by CaMKII-dependent phosphorylation: a molecular model of kinesin-cargo release.* Nat Cell Biol, 2008. **10**(1): p. 19-29.

24. Imanishi, M., et al., *Autoinhibition regulates the motility of the C. elegans intraflagellar transport motor OSM-3.* J Cell Biol, 2006. **174**(7): p. 931-7.

25. Lee, J.R., et al., *An intramolecular interaction between the FHA domain and a coiled coil negatively regulates the kinesin motor KIF1A.* EMBO J, 2004. **23**(7): p. 1506-15.

26. Tomishige, M., D.R. Klopfenstein, and R.D. Vale, *Conversion of Unc104/KIF1A kinesin into a processive motor after dimerization.* Science, 2002. **297**(5590): p. 2263-7.

27. Al-Bassam, J., et al., *Distinct conformations of the kinesin Unc104 neck regulate a monomer to dimer motor transition.* J Cell Biol, 2003. **163**(4): p. 743-53.

28. Chu, P.J., J.F. Rivera, and D.B. Arnold, *A role for Kif17 in transport of Kv4.2.* J Biol Chem, 2006. **281**(1): p. 365-73.

29. Guillaud, L., M. Setou, and N. Hirokawa, *KIF17 dynamics and regulation of NR2B trafficking in hippocampal neurons.* J Neurosci, 2003. **23**(1): p. 131-40.

30. Jenkins, P.M., et al., *Ciliary targeting of olfactory CNG channels requires the CNGB1b subunit and the kinesin-2 motor protein, KIF17.* Curr Biol, 2006. **16**(12): p. 1211-6.

31. Setou, M., et al., *Kinesin superfamily motor protein KIF17 and mLin-10 in NMDA receptor-containing vesicle transport.* Science, 2000. **288**(5472): p. 1796-802.

32. Scholey, J.M., *Intraflagellar transport motors in cilia: moving along the cell's antenna.* J Cell Biol, 2008. **180**(1): p. 23-9.

33. Chennathukuzhi, V., et al., *The kinesin KIF17b and RNA-binding protein TB-RBP transport specific cAMP-responsive element modulator-regulated mRNAs in male germ cells.* Proc Natl Acad Sci U S A, 2003. **100**(26): p. 15566-71.

34. Saade, M., et al., *Dynamic distribution of Spatial during mouse spermatogenesis and its interaction with the kinesin KIF17b.* Exp Cell Res, 2007. **313**(3): p. 614-26.

35. Burghoorn, J., et al., *Mutation of the MAP kinase DYF-5 affects docking and undocking of kinesin-2 motors and reduces their speed in the cilia of Caenorhabditis elegans.* Proc Natl Acad Sci U S A, 2007. **104**(17): p. 7157-62.

36. Takano, K., et al., *NXF2 is involved in cytoplasmic mRNA dynamics through interactions with motor proteins.* Nucleic Acids Res, 2007. **35**(8): p. 2513-21.

37. Kotaja, N., B. Macho, and P. Sassone-Corsi, *Microtubule-independent and protein kinase A-mediated function of kinesin KIF17b controls the intracellular transport of activator of CREM in testis (ACT).* J Biol Chem, 2005. **280**(36): p. 31739-45.

38. Shin, H., et al., *Association of the kinesin motor KIF1A with the multimodular protein liprin-alpha.* J Biol Chem, 2003. **278**(13): p. 11393-401.

39. Klopfenstein, D.R., et al., *Role of phosphatidylinositol(4,5)bisphosphate organization in membrane transport by the Unc104 kinesin motor.* Cell, 2002. **109**(3): p. 347-58.

40. Klopfenstein, D.R. and R.D. Vale, *The lipid binding pleckstrin homology domain in UNC-104 kinesin is necessary for synaptic vesicle transport in Caenorhabditis elegans.* Mol Biol Cell, 2004. **15**(8): p. 3729-39.

41. Rashid, D.J., et al., *Monomeric and dimeric states exhibited by the kinesin-related motor protein KIF1A.* J Pept Res, 2005. **65**(6): p. 538-49.

42. Lee, J.R., et al., *Characterization of the movement of the kinesin motor KIF1A in living cultured neurons.* J Biol Chem, 2003. **278**(4): p. 2624-9.

43. Zhou, H.M., I. Brust-Mascher, and J.M. Scholey, *Direct visualization of the movement of the monomeric axonal transport motor UNC-104 along neuronal processes in living Caenorhabditis elegans.* J Neurosci, 2001. **21**(11): p. 3749-55.

44. Okada, Y., et al., *The neuron-specific kinesin superfamily protein KIF1A is a unique monomeric motor for anterograde axonal transport of synaptic vesicle precursors.* Cell, 1995. **81**(5): p. 769-80.

45. Pierce, D.W., et al., *Single-molecule behavior of monomeric and heteromeric kinesins.* Biochemistry, 1999. **38**(17): p. 5412-21.

46. Nangaku, M., et al., *KIF1B, a novel microtubule plus end-directed monomeric motor protein for transport of mitochondria.* Cell, 1994. **79**(7): p. 1209-20.

47. Okada, Y., H. Higuchi, and N. Hirokawa, *Processivity of the single-headed kinesin KIF1A through biased binding to tubulin.* Nature, 2003. **424**(6948): p. 574-7.

48. Okada, Y. and N. Hirokawa, *A processive single-headed motor: kinesin superfamily protein KIF1A.* Science, 1999. **283**(5405): p. 1152-7.

49. Okada, Y. and N. Hirokawa, *Mechanism of the single-headed processivity: diffusional anchoring between the K-loop of kinesin and the C terminus of tubulin.* Proc Natl Acad Sci U S A, 2000. **97**(2): p. 640-5.

50. Dorner, C., et al., *Characterization of KIF1C, a new kinesin-like protein involved in vesicle transport from the Golgi apparatus to the endoplasmic reticulum.* J Biol Chem, 1998. **273**(32): p. 20267-75.

51. Dorner, C., et al., *The kinesin-like motor protein KIF1C occurs in intact cells as a dimer and associates with proteins of the 14-3-3 family.* J Biol Chem, 1999. **274**(47): p. 33654-60.

52. Pollock, N., et al., *Reconstitution of membrane transport powered by a novel dimeric kinesin motor of the Unc104/KIF1A family purified from Dictyostelium.* J Cell Biol, 1999. **147**(3): p. 493-506.

53. Schnapp, B.J., *Trafficking of signaling modules by kinesin motors.* J Cell Sci, 2003. **116**(Pt 11): p. 2125-35.

54. Verhey, K.J., et al., *Cargo of kinesin identified as JIP scaffolding proteins and associated signaling molecules.* J Cell Biol, 2001. **152**(5): p. 959-70.

55. Verhey, K.J. and T.A. Rapoport, *Kinesin carries the signal.* Trends Biochem Sci, 2001. **26**(9): p. 545-50.

56. Setou, M., et al., *Glutamate-receptor-interacting protein GRIP1 directly steers kinesin to dendrites.* Nature, 2002. **417**(6884): p. 83-7.

57. Sheetz, M.P., *Motor and cargo interactions.* Eur J Biochem, 1999. **262**(1): p. 19-25.

58. Bracale, A., et al., *Kidins220/ARMS is transported by a kinesin-1-based mechanism likely to be involved in neuronal differentiation.* Mol Biol Cell, 2007. **18**(1): p. 142-52.

59. Byrd, D.T., et al., *UNC-16, a JNK-signaling scaffold protein, regulates vesicle transport in C. elegans.* Neuron, 2001. **32**(5): p. 787-800.

60. Hammond, J.W., et al., *Co-operative versus independent transport of different cargoes by Kinesin-1.* Traffic, 2008. **9**(5): p. 725-41.

61. Whitmarsh, A.J., *The JIP family of MAPK scaffold proteins.* Biochem Soc Trans, 2006. **34**(Pt 5): p. 828-32.

62. Nakata, T. and N. Hirokawa, *Microtubules provide directional cues for polarized axonal transport through interaction with kinesin motor head.* J Cell Biol, 2003. **162**(6): p. 1045-55.

63. Jacobson, C., B. Schnapp, and G.A. Banker, *A change in the selective translocation of the Kinesin-1 motor domain marks the initial specification of the axon.* Neuron, 2006. **49**(6): p. 797-804.

64. Reed, N.A., et al., *Microtubule acetylation promotes kinesin-1 binding and transport.* Curr Biol, 2006. **16**(21): p. 2166-72.

65. Liao, G. and G.G. Gundersen, *Kinesin is a candidate for cross-bridging microtubules and intermediate filaments. Selective binding of kinesin to detyrosinated tubulin and vimentin.* J Biol Chem, 1998. **273**(16): p. 9797-803.

66. Ikegami, K., et al., *Loss of alpha-tubulin polyglutamylation in ROSA22 mice is associated with abnormal targeting of KIF1A and modulated synaptic function.* Proc Natl Acad Sci U S A, 2007. **104**(9): p. 3213-8.

67. Dunn, S., et al., *Differential trafficking of Kif5c on tyrosinated and detyrosinated microtubules in live cells.* J Cell Sci, 2008. **121**(Pt 7): p. 1085-95.

68. Larcher, J.C., et al., *Interaction of kinesin motor domains with alpha- and beta-tubulin subunits at a tau-independent binding site. Regulation by polyglutamylation.* J Biol Chem, 1996. **271**(36): p. 22117-24.

69. Witte, H., D. Neukirchen, and F. Bradke, *Microtubule stabilization specifies initial neuronal polarization.* J Cell Biol, 2008. **180**(3): p. 619-32.

70. Baas, P.W., et al., *Microtubule dynamics in axons and dendrites.* J Neurosci Res, 1991. **30**(1): p. 134-53.

71. Morfini, G., et al., *Glycogen synthase kinase 3 phosphorylates kinesin light chains and negatively regulates kinesin-based motility.* EMBO J, 2002. **21**(3): p. 281-93.

72. Sato-Yoshitake, R., et al., *The phosphorylation of kinesin regulates its binding to synaptic vesicles.* J Biol Chem, 1992. **267**(33): p. 23930-6.

73. Stagi, M., et al., *Unloading kinesin transported cargoes from the tubulin track via the inflammatory c-Jun N-terminal kinase pathway.* FASEB J, 2006. **20**(14): p. 2573-5.

74. Colin, E., et al., *Huntingtin phosphorylation acts as a molecular switch for anterograde/retrograde transport in neurons.* EMBO J, 2008.

75. Gross, S.P., *Dynactin: coordinating motors with opposite inclinations.* Curr Biol, 2003. **13**(8): p. R320-2.

Chapter 2:
KIF17's Coiled-Coil 2 Region Inhibits Processive Motility by Directly Interacting with the Motor Domain.

Kinesin motors use the energy of ATP to move membrane-bound organelles and protein or mRNA complexes along microtubules. The activity of kinesin motors in cells must be tightly coupled to cargo transport to ensure that energy is not wasted on futile movement. It is additionally important that motors transport the correct cargo, to the proper subcellular destination, at the relevant time.

A large body of work has shown that, in the absence of cargo, Kinesin-1 is inactive due to a folded conformation that allows the tail to directly interact with the motor domain and neck [1-6]. This interaction prevents Kinesin-1 from binding microtubules or exchanging ADP for ATP [5-7]. Additionally, in this autoinhibited state, Kinesin-1's motor domains are separated to ensure that the motor heads are unable to coordinate long-distance movement [6]. Studies on the Kinesin-3 family members, KIF1A and Gakin/KIF13B, show that these motors are also autoinhibited in the absence of cargo. For KIF1A, a coiled-coil and FHA domain region inhibit microtubule binding, while the neck coiled-coil folds with a second coiled-coil to inhibit motility [8, 9]. For Gakin, a MGB domain located in the stalk binds the motor domain and impairs motor function [10]. Thus, although the precise molecular details may be different between kinesins, autoinhibitory mechanisms are commonly used in motor regulation.

Whether the Kinesin-2 family member, KIF17 is likewise autoinhibited in the absence of cargo is currently unknown. Kif17 is specifically involved in transporting vesicles containing NMDA receptors and Kv4.2 channels in the dendrites of neuronal cells [11-13], as well as mRNA/protein complexes in multiple cell types [14, 15]. Work from C *elegans* has revealed an important role for the KIF17 homologue, Osm-3, in anterograde intraflagellar transport (IFT) which is essential for proper cilia formation, maintenance, and function [16-20]. Recently KIF17 has also been implicated in IFT, as it

carries CNG channels in olfactory cilia, and is crucial for the proper development of vertebrate photoreceptors, particularly the sensory outer segment [21, 22]. KIF17 and Osm-3 appear to have some unique IFT functions in certain types of cilia, but play a redundant role with the Kinesin-2 (KIF3A/B/KAP) in other cases [16, 19, 21, 23].

Previous work on recombinant Osm-3 *in vitro*, showed that Osm-3's motility is inhibited in the absence of cargo, and that the protein may shift from a folded, more compact form, to an extended conformation like Kinesin-1. A small hinge region (~15-20 residues in length) between two coiled-coils in the stalk is essential for this folding and regulation, suggesting an autoinhibition mechanism where stalk/tail domains are brought into proximity of the motor domain in order to inhibit motility [24]. As KIF17 and Osm-3 differ most in this hinge region, it is particularly unclear whether Kif17 is regulated in the same way. It is also unclear what regions of the stalk or tail may be responsible for negative regulation. Like Osm-3, KIF17, has an N-terminal motor domain, followed by a neck coiled-coil (NC) and coiled-coil 1 (CC1). In Osm-3 this CC1 is followed by the small hinge, but KIF17 has an approximate 300 residue insertion of undefined structure. This region is then followed by two more somewhat weak coiled-coils (CC2 and CC3) and a tail domain known to directly bind two, KIF17 cargo proteins Mint1 (also known as mLin10 or X11) and NXF-2 (Figure 1, [13, 15, 25]).

In this study, we confirm that Kif17, in the absence of cargo, is inhibited from binding microtubules and moving processively (that is taking many steps along the microtubule, without detaching). Removal of the CC2 region relieves the autoinhibition mechanism activating motor functions. As the CC2 region can inhibit constitutively active KIF17 motors *in trans*, the CC2 region is both necessary and sufficient for inhibition of processive motility. A direct interaction between CC2 and the motor was found to be responsible for this negative regulation. We additionally show that the cargo binding tail is required for loading KIF17 into cilia regardless of whether the motor is active or inhibited.

RESULTS

Molecular mechanism of KIF17 autoinhibition

To investigate the regulatory and motile properties of mammalian KIF17 we first tested whether full-length (FL) HsKIF17 is able to generate processive movement, or whether it is inhibited in the absence of cargo. Previous studies have shown that active kinesin motors often accumulate at the tips of cell processes [9, 26, 27]. Thus, we tagged KIF17 on its C-terminus with mCit (monomeric citrine—a yellow fluorescent protein variant) and analyzed its subcellular localization in the neuronal-like cell line, CAD. KIF17-mCit was localized diffusely throughout the cytoplasm and not concentrated in neurite growth cones (Figure 2.2 A, far left images). Thus we conclude KIF17 is inhibited for motility in mammalian cells.

For the autoinhibited motors, Kinesin-1, KIF1A, and GAKIN/KIF13B; truncation studies have been very helpful in identifying the structural domains that inhibit motor activity. Accordingly, we made mCit-tagged truncated versions of KIF17 that ended after each predicted coiled-coil region or the middle region of unknown structure (Figure 2.1 B and C). Deletion of the C-terminal cargo binding tail (1-846) or CC3 (1-795) had no affect on the processive motility of KIF17 (Figure 2.2 A). Like FL KIF17, these truncations when expressed in CAD cells showed a diffuse cytoplasmic localization. However, further truncation of CC2 resulted in a drastic change as the 1-738 construct accumulated at the ends of neurites. The ability to accumulate at neurite tips was maintained for truncation 1-488, but was lost upon further truncation where the CC1 (1-369) or the NC (1-347) was removed. Thus, the CC2 region (738-795) is critical to keeping KIF17 in an inactive state where it cannot move processively in mammalian cells. Additionally the NC is not sufficient to maintain KIF17's processive movement.

As a second method of testing whether or not FL or truncated KIF17 motors are active for processive movement, we tested the KIF17 constructs in an *in vitro* single molecule motility assay. We tagged the constructs on their C-terminus with three tandem copies of mCit and expressed them in COS cells. This 3xmCit tag results in a better signal-to-noise ratio, is less affected by photoblinking, and photobleaches much slower than a single mCit tag [28]. Lysates from COS cells expressing KIF17-3xmCit motors were added to a casein and BSA coated flow chamber containing polymerized

microtubules and assayed on a total internal reflection fluorescence (TIRF) microscope for motility. By timelapse imaging at 100ms intervals, individual motors could be seen moving along microtubules (representative tracks are shown in Figure 2.2 E). Only motility events that lasted at least 300ms were included in the analyzed data set to ensure that the same motor could be tracked through at least 3 timelapse images. In order to directly compare the number of motility events and the motile properties of velocity and track length for each KIF17 motor construct, the amount of expressed protein was normalized by western blot and each construct was analyzed for the same total amount of time.

Consistent with the *in vivo* processivity assay in CAD cells, KIF17(FL)-3xmCit and KIF17(1-369)-3xmCit were primarily inactive in the *in vitro* single molecule motility assay (Figure 2.2 B-F). These motors each showed very few motility events (n=21 and n=40 respectively) and when they did move along microtubules, they only moved for short distances (average track lengths: FL, 0.36 +/- 0.18 μm; 1-369, 0.45 +/- 0.39 μm) (Figure 2.2 C-F). KIF17(1-738)-3xmCit, on the other had, moved quite efficiently *in vitro,* as a large number of motility events were observed (n=112) (Figure 2.2 B-F). 1-738 moved with an average speed of 0.77 +/- 0.26 μm/second and for track lengths that were as long as 6-7 μm but averaged 1.13 +/- 1.06 μm/event. These motile properties are consistent with previous reports on KIF17 that showed *in vitro* microtubule gliding speeds of 0.8-1.2 μm/second [13] and *in vivo* KIF17 driven vesicle speeds of 0.76 μm/second [12]. Although data is not shown for the 1-846 and 1-795 truncations, they like full-length had limited single molecule motility. Thus, the dramatic activation of processivity in KIF17(1-738) again points to the critical role played by the CC2 region in repressing the processivity of KIF17.

FL and truncated versions of KIF17 dimerize

KIF17 has been shown to be a homodimer by gel filtration and sucrose gradient centrifugation experiments [13]. A large body of work on Kinesin-1, shows that it coordinates its two motor domains to step in an alternating hand-over-hand fashion from one tubulin dimer to the next tubulin dimer of the microtubule lattice. This hand-over-hand model of processive movement is generally thought to be conserved among cargo

transporting kinesins, including KIF17 [29]. As expected from this model, Kinesin-1 truncations that are monomeric are not processive [28]. Thus it was concerning that Imanishi et al reported truncation of Osm-3's tail domain resulted in unstable Osm-3 dimers [24]. In order to rule out the possibility that our KIF17 truncations also resulted in monomeric motors whose limited processivity would not be due to inhibitory regions, but the fact that they had only one motor domain, we analyzed their ability to dimerize using co-immunoprecipitation (Co-IP). As these Co-IP experiments were done with COS lysates basically identical to those added to single molecule motility assays, confirmation of dimerization by Co-IP is a good indication that our KIF17 motors were able to maintain dimerization in the *in vitro* motility assay.

We first confirmed that FL KIF17 is a dimer by co-expressing Flag- and mCit-tagged versions of FL KIF17 in COS cells. Cell lysates were then precipitated with antibodies to the Flag tag or with control antibodies (IgG). mCit-KIF17 was pulled down with Flag-KIF17 only in the presence of Flag antibodies confirming that FL KIF17 exists as a homodimer (Figure 2.3 A). Similar Co-IP experiments were done for the C-terminally tagged KIF17 truncations 1-846, 1-738, 1-490, and 1-369, except Myc tags and antibodies were used in place of Flag. In all cases, the mCit-tagged truncations co-precipitated with their Myc-tagged counterparts in the presence of Myc, but not control, antibodies (Figure 2.3 B). This confirms they maintain the dimeric state of FL KIF17. As KIF17(1-369) was able to dimerize efficiently, the NC is sufficient for KIF17 dimerization. However, dimerization by only the NC is not sufficient to maintain processive motility.

FL KIF17 is prevented from binding microtubules and truncation of KIF17 relieves this inhibition

The autoinhibition mechanism of Kinesin-1 restricts processive motility by first preventing the motor from binding microtubules [1, 6, 30]. Kinesin-1 is made up of two heavy chains (KHC) and two light chains (KLC); with the light chains being particularly important for preventing the motor from interacting with microtubules in the absence of cargo [6, 30]. The ability of kinesin motors to bind microtubules can be tested in live COS cells. Expression of Kinesin-1's KHC domain alone, at low levels, results in a

steady state cytoplasmic localization despite the fact that the motors are binding and falling off the microtubules (Figure 2.4 A). Treating the cells with the non-hydrolysable ATP analog, AMPPNP after permeabilizing the cells with sreptolysin O (SLO), causes active motors to be trapped on the microtubule because they cannot be released from their strong microtubule bound conformation by hydrolyzing ATP to ADP (Figure 2.4 A) [6, 31]. Co-expression of Kinesin-1's KHC and KLC domains, however, results in the motor being inhibited from binding microtubules, so AMPPNP treatment does not cause them to redistribute from a cytoplasmic to a microtubule-trapped localization (Figure 2.4 A and B) [6].

To determine whether inhibition of microtubule binding is also an important step used to prevent KIF17 from moving along microtubules in the absence of cargo, we tested the microtubule binding ability of KIF17 constructs tagged with mCit on their C-terminus in live COS cells. In the absence of AMPPNP, KIF17 constructs: FL, 1-846, 1-795, and 1-369 are diffusely localized in the cytoplasm similar to their localization in CAD cells (Figure 2.4 B). 1-738 and 1-490, are also largely cytoplasmic, but do show peripheral accumulation on microtubules, reflecting their ability to move processively. Surprisingly, after AMPPNP treatment, a significant portion of KIF17-mCit is present on microtubules showing it is active for microtubule binding. Indeed, all KIF17 truncations (1-846mCit, 1-795mCit, 1-738mCit, 1-490mCit, and 1-369mCit) are able to bind microtubules as they also accumulated on microtubules after AMPPNP treatment (Figure 2.4 B). The percentage of cells showing this microtubule accumulation was somewhat higher for the FL-mCit and 1-846-mCit motors than the other truncations (Figure 2.4 D). This suggests the possibility that residues 795-846 or CC3 may have some role in facilitating microtubule binding, either by interacting directly with the microtubule as has been reported in the case of Kinesin-1's KHC tail domain, or by promoting a conformation of the KIF17 motor that is more conducive to microtubule binding and/or keeping AMPPNP in the nucleotide pocket. It should also be noted, that while KIF17 motors do bind microtubules in the presence of AMPPPNP, all KIF17 constructs maintain a pool of motor in the cytoplasm (Figure 2.4B). This is in contrast to Kinesin-1 KHC, where AMPPNP treatment traps a vast majority of the expressed motors on microtubules, clearing the cytoplasm almost completely (Figure 3.4 B and C). Whether

this indicts that KIF17 does not bind to microtubules as strongly as KHC in the presence of AMPPNP, or whether KIF17 motors are partially inhibited for microtubule binding is unclear.

As the cargo protein Mint1 has been shown to bind KIF17's extreme C-terminal residues, we considered the possibility that the mCit tag on the tail of FL KIF17 may actually mimic cargo binding and thus lead to a partial activation of the motor. Although fluorescent protein tags do not interfere with the autoinhibitory mechanisms of Kinesin-1 or KIF1A, attaching beads to the tail of Kinesin-1 does mimic cargo binding resulting in an active, processive motor [2, 6, 24, 32]. Thus, we also generated FL KIF17 constructs that were tagged with mCit on the N-terminus (or motor) using both short and long flexible linkers (4 amino acids (4aa) and 18 amino acids (18aa) in length). We also used a smaller Flag tag in case the bulky mCit protein sterically hindered proper folding or regulation. COS cells expressing these N-terminally tagged FL KIF17 constructs, were permeabilized with SLO then treated with AMPPNP. Attachment of mCit to the motor domain with a 4aa linker gave similar results to KIF17-mCit; that is, it was active for microtubule binding (Figure 2.4 F). However, Flag-KIF17, mCit-18aa-KIF17, and mCit-Flag-KIF17 remained cytosolic after AMPPNP treatment, showing that they were inhibited for microtubule binding. As the smaller Flag tag, or a mCit that is attached with a longer linker, is less likely to interfere with motor regulation and/or folding conformations, we conclude that FL Kif17 is regulated by an autoinhibition mechanism that prevents microtubule binding in absence of cargo. But unlike other motors tested to date, presence of a fluorescent protein with short linkers on the N- or C- terminus of Kif17 interferes with autoinhibition, resulting in interaction with microtubules. As FL KIF17 tagged on the C-terminus with mCit or 3xmCit did not active KIF17 for processive movement (Figure 2.2), it appears that there two mechanisms to KIF17 autoinhibition. First, KIF17 is inhibited from binding microtubules. The exact region that mediates this inhibition is still unclear. Second, if KIF17 can bind microtubules, it is prevented from moving along them by the CC2 region.

Further analysis of CC2

As truncation results suggest CC2 is capable of negatively regulating KIF17's processive movement, we investigated whether CC2 is also required for negative regulation in the context of C-terminal regions using a KIF17 construct with an internal deletion of CC2 (Δ739-799) (Figure 2.5 A). In transfected CAD cells, Δ739-799 accumulated at neurite tips, in contrast to FL KIF17, which was diffusely localized primarily in the cell body (Figure 2.5 C). Thus the CC2 region is both necessary and sufficient for the autoinhibition of KIF17.

The CC2 region, is a rather weak predicted coiled-coil that contains a few helix breaking residues and many charged residues. To gain a better understanding of how CC2's coiled-coil structure and amino acid make-up contribute to regulation, we made two mutation constructs. First, we mutated the glycine residue at 754 to a glutamate (G754E). In Osm-3 a similar point mutation, G444E, activates the motor for processive motility. In Osm-3 this residue clearly lies in the small hinge between CC1 and CC2. KIF17, however, has a ~300 amino acid insertion into this same hinge. G444 and surrounding residues, although not well conserved, align with residues in the C-terminal portion of CC2 and in our estimation G444 corresponds best to G754 of KIF17. The G745E point mutant, results in a stronger coiled-coil prediction for the CC2 region (Figure 2.5 B). When expressed in CAD cells, the G754E point mutant accumulated strongly to neurite tips, showing this CC2 mutation was sufficient to relieve the autoinhibition of full-length KIF17.

A stretch of basic residues (KEKHKRRKR) in CC2 is also a rather conspicuous feature. We mutated these nine residues to alanine. Not surprisingly, this 764-772A mutation caused the coiled-coil prediction for CC2 to decrease in strength (Figure 2.5 B). When expressed in CAD cells, the 764-772A mutation also showed peripheral accumulation in neurites (Figure 2.5 C). As both increasing and decreasing the strength and rigidity of CC2 give the same effect—an active, processive motor—we propose that the predicted coiled-coil structure of CC2 is not necessarily a key feature to the mechanism by which it mediates KIF17's autoinhibition. Rather the charged and less-than-ideal coil forming residues in CC2 may have specific roles in mediating contact of CC2 with other motor regions.

CC2 directly interacts with the motor and can inhibit processive motility in trans

To test whether CC2 or any of the surrounding C-terminal regions interacted with the N-terminal domains of KIF17, we generated a series of constructs (Figure 2.6 A), co-expressed them in different combinations in COS cells, and then tested their interactions via co-immunoprecipitation. We first tested whether the Myc tagged constructs containing KIF17's undefined middle region and CC2 (466-846), the undefined middle region alone (466-738), CC2 and CC3 (735-846), CC2 alone (735-795), or CC3 and the tail (801-1028) could pull-down 1-738mCit (a motor construct truncated before CC2) in the presence of Myc-antibodies. We found that 1-738mCit was co-precipitated with all Myc-tagged CC2 containing constructs, including the Myc-735-795 construct which consisted of only CC2, but not constructs without CC2 (466-738 and 801-1028) (Figure 2.6 B). This suggested CC2 was both necessary and sufficient for the contact with 1-738mCit.

To further define what region of 1-738mCit CC2 interacted with, we tested whether the myc-466-846 construct could pull down constructs containing the motor and neck (1-369mCit), the motor domain only (1-347mCit) or CC1 (Flag-370-490) when precipitated with Myc antibodies. These experiments showed that CC2 interacts directly with the motor domain as both 1-347mCit and 1-369mCit co-precipitated with myc-466-846. The CC1, Flag-370-490 construct was not co-precipitated (Figure 2.6 C).

To confirm that this contact between the motor domain and CC2 mediates the autoinhibited state of KIF17, we investigated whether any of our Myc-tagged construct series could inhibit 1-738mCit's neurite tip accumulation *in trans*. CAD cells co-expressing 1-738mCit with Myc-tagged constructs containing CC2 (466-846, 735-846, or 735-795) showed no accumulation of 1-738mCit in neurite growth cones (Figure 3.6 D-E). However, 1-738mCit expressed alone, or with Myc-tagged constructs lacking CC2 (466-738 and 801-1028), showed efficient peripheral accumulation. Taken together these results show that the intramolecular interaction of CC2 with the motor domain inhibit motor function by preventing it from taking multiple steps along the microtubule.

Cargo-mediated activation of Kif17?

Evidence from Kinesin-1 suggests that cargo binding relieves its autoinhibition mechanism. Indeed, the regulatory regions that mediate autoinhibition are the same regions that bind cargo (KLC TPR domains and KHC tail) [1, 2, 4, 7, 33]. As of yet, no cargo has been shown to bind to KIF17's CC2 region. Cargo proteins, Mint1 and NXF-2, instead bind KIF17's tail domain (846-1028). We did explore whether or not binding of Mint1 could activate FL KIF17. Although we saw by co-immunoprecipitation that KIF17 and Mint1 did interact, this binding was not sufficient to activate the microtubule binding activity of FL KIF17 in our live-cell AMPPNP assay or its ability to move processively to neurite tips in CAD cells (data not shown). Why attachment of mCit to the C-terminus of KIF17 is sufficient to relieve the negative regulation on microtubule binding, but binding of Mint1 to the tail is not sufficient is unclear. As activation of Kinesin-1 requires the binding of two proteins, JIP1 and FEZ [33], activation of KIF17 may also require more cargo interactions, likely involving the CC2 region, or a specific phosphorylation state, to be relieved of its autoinhibition mechanism.

KIF17 tail domain is essential for sorting KIF17 to cilia

As Kif17 and Osm-3 have important roles in the intraflagellar transport (IFT) of cargo in cilia [19, 20, 22], we questioned whether a regulatory role for KIF17's cargo binding tail could be elucidated in a cilia context. We thus expressed mCit-tagged, KIF17 proteins in an olfactory sensory neuron cell line (Odora , [34]). Cells were fixed and stained with an antibody to acetylated tubulin to identify primary cilia. FL KIF17, regardless of whether the mCit tag was placed at the N- or C-terminus, did not accumulate at the cell periphery consistent with it being autoinhibited. However, FL KIF17 did accumulate at the tips of cilia (Figure 2.7). In contrast, the autoinhibited KIF17 constructs, 1-846 and 1-795, were unable to accumulate in cilia or the cell periphery. This suggests that the tail (846-1028) plays an essential role in sorting KIF17 into cilia. Indeed, constitutively active truncations that do not contain the inhibitory CC2 region or the tail (i.e. 1-738 and 1-488) are able to accumulate at the cell periphery in olfactory cells, but not in cilia. This confirms that the tail contains the cilia targeting signal. FL KIF17 with a G754E mutation accumulates both in cilia and at the cell

periphery. Together, these results confirm that in olfactory cells, like neuronal cells, the CC2 region is required to negatively regulate motor activity. However, activating the motor by removal or mutation of CC2 is not sufficient to direct the motor to where it is most needed in olfactory sensory cells that is to cilia. The C-terminal tail (846-1028), is required for loading KIF17 into cilia. As the tail is a known cargo binding region, this sorting into cilia is likely mediated through interactions with cargo or other IFT machinery.

DISCUSSION

Autoinhibition Mechanism of KIF17

We have shown that KIF17 is self-inhibited by assuming a folded conformation that allows the weak coiled-coil region of its stalk (CC2) to directly contact the motor domain. This interaction prevents KIF17 from moving on microtubules, but not necessarily from having interactions with the microtubule. The region that negatively regulates microtubule binding was not clear from our studies, but could reside in the cargo binding tail. Additionally, the cargo binding tail was shown to be essential for sorting KIF17 into cilia. These data support a model where KIF17 exists in the cytoplasm in an autoinhibited state. Binding of cargo targets the motor to specific cellular compartments, like cilia, and relieves the autoinhibitory mechanism allowing KIF17 to processively move along microtubules.

Autoinhibitory mechanisms appear to be a common feature of motor proteins. Kinesin-1, KIF1A, GAKIN/KIF13B, Osm-3, and KIF17 have now been shown to be autoinhibited in the absence of cargo [1, 8-10, 24, 33]. As only the motor domain is conserved among these and other kinesins [35], various divergent stalk/tail regulatory regions have been employed to inhibit motor activity. Despite the fact that these unconserved stalk regions may have developed their own methods to inhibit motor function, a few generalizations can be made about kinesin autoinhibition mechanisms. First autoinhibition often involves two different levels of regulation, prevention of microtubule binding and hindered processive motility. This two-level motor regulation has now been shown for Kinesin-1, KIF1A, and KIF17 [1, 4]. For these kinesins, sequences can be deleted or mutated that enable microtubule binding, yet the motors are

not capable of processive motility. Alteration of a second sequence activates motility. Second, motor activity is negatively regulated by direct interactions of the motor and/or neck with C-terminal stalk/tail regions.

More data is needed for KIF17 to pinpoint what residues of CC2 and the motor domain are responsible for this inhibitory intramolecular interaction. Additional structural data would be especially helpful to understand how this CC2/motor contact functions to inhibit the processive motility of KIF17. Recently, Dietrich et al showed that in Kinesin-1, tail residues QIAKPIRP directly interact with the switch 1 region of the motor [4]. As the Switch I region participates in nucleotide binding and release [36], this interaction likely prevents Kinesin-1's initial microtubule stimulated ADP release step, consequently, preventing Kinesin-1 from productively interacting with microtubules [1, 4, 5, 7]. As the tail can simultaneously interact with microtubules, it could also function to limit processive movement of Kinesin-1 when bound to microtubules [4]. This tail/switch I inhibitory interaction mechanism is strikingly similar to how GDI proteins function to inhibit small G proteins whose nucleotide binding pocket is similar in structure to that of kinesin motors [37, 38]. Thus, although the CC2 region of KIF17 is not conserved with the QIAKPIRP containing tail of Kinesin-1, the two kinesins could have co-evolved a similar inhibitory switch I-motor interactions.

Comparison of autoinhibition mechanisms of KIF17 and Osm-3

Osm-3, like KIF17, has been shown to be autoinhibited. For either motors, mutation or deletion of a central stalk region—CC2 for KIF17, or the hinge 2 region between CC1 and CC2 in Osm-3—results in an active, processive motor. For KIF17 we show that CC2 functions to inhibit motor activity by directly interacting with the motor domain. Imanishi et al showed that increased motor activity correlated with a less compact conformation of the protein. Thus, they proposed that Osm-3 folds at the hinge 2 region bringing more C-terminal regions in contact with the motor to mediate inhibition[24]. The stalk regions of Osm-3 and KIF17 are fairly well conserved, with the exception that KIF17 has a ~300 residue insertion of unknown domain structure, into the hinge 2 region. This insertion makes it difficult to conclude whether Osm-3 and KIF17 are likely regulated by the same mechanism, or whether they might have a slightly

different molecular basis for their autoinhibition. Both studies mutated a conserved glycine (G444, Osm-3; G754, KIF17) to glutamate. In Osm-3 this glycine and surrounding residues compose a region that has no predicted coiled-coil structure. As there are flexible residues, this region is defined as hinge 2. In contrast, KIF17 has a few alterations in the residues surrounding G754 which increase the coiled-coil probability for this same region causing it to be grouped with CC2 rather than the ~300 amino acid insertion that has no coiled-coil probability. Future studies will have to determine whether the hinge 2/CC2 regions should be considered together as the region that directly binds the motor domain, or whether there is a flexible part of KIF17's CC2 that serves as a hinge to facilitate binding of more C-terminal residues of CC2 to the motor domain.

Cargo-mediated activation and sorting of KIF17

The inhibitory mechanism of KIF17 is likely relieved by cargo. Attachment of beads as a cargo mimic to Kinesin-1 or Osm-3 activates their processive motility [1, 24, 32]. In our studies, we saw that attachment of a fluorescence protein to the C-terminus of KIF17 was enough of a cargo-mimic to activate the microtubule binding activity of KIF17, but not processive motility. This could indicate that the CC2-motor interaction requires additional cargo binding or post-translational modifications in order to be broken. As there are currently no know binding partners for the CC2 region, testing of this hypothesis will have to wait. KIF17's known direct binding cargo, Mint1 and NXF-2, interact with the tail region[13, 15, 25]. In the case of Mint1, phosphorylation of a serine residue in the tail, by CaMKII, regulates the ability of the cargo to bind KIF17 [25]. Whether this same phosphorylation event or others play a role in KIF17 motor regulation is unknown.

We show that the cargo binding tail is necessary for KIF17 to accumulate in the tips of cilia. This loading into cilia is likely dependent on interactions with IFT machinery, presumably cargo. As constitutively active motors without the tail were unable to accumulate in the distal cilia, loading into cilia is an additional level of regulation used by KIF17. KIF17 has also been shown to be important in vesicular trafficking in dendrites. Cargo binding to the tail of Kinesin-1 has been shown to be important for localizing the motor to dendrites as opposed to axons which the Kinesin-1

motor intrinsically prefers [27, 39]. It will be interesting to see if cargo binding to KIF17's tail could also be important in sorting KIF17 to dendrites.

MATERIALS AND METHODS

Plasmids and antibodies: Full-length or truncated KIF17 constructs tagged with mCit , Flag, or Myc were generated by PCR amplification from the Sport6-HsKIF17 cDNA vector. PCR products were cloned into the mCit-N1 or C1 vectors (modified from Clontech's EYFP-N1/C1 vectors by replacing EYFP with sequence for monomeric Citrine) the 3xmCit-N1 vector previously described [28], or the pcDNA3-Flag vector using convenient restriction sites. Additional KIF17 internal deletions and mutations were made by overlapping PCR. All plasmids were sequence verified. KHC-mCit and CFP-KLC have been described previously [6]. The following antibodies were used: Myc (Sigma and 9E10 hybridoma ascites), Flag (Sigma), GFP (used to recognize mCit; Invitrogen), and acetylated α-tubulin 6-11B-1 (Sigma).

Cell culture and immunofluorescence: COS and CAD cells were cultured, transfected, and processed for immunofluorescence as previously described (COS, Cai 2007; CAD, Verhey 2001 and Blasius 2007). Images were collected with a Nikon TE2000 microscope using a Plan-Fl 40X/NA 0.75 or a Plan-APO 60X/NA 1.4 objective and Photometrics CS ES2 camera. Odora cells were plated on uncoated glass coverslips in DMEM, 10% FBS, and PennStrep then maintained at 33 degrees C, in 5% CO2. Cells were transfected with Lipofectamine 2000. After 24 hour expression, cells were fixed and processed for immunofluorescence as described previously [22]. Images were taken on an Olympus Fluoview 500 confocal microscope with a 100x/NA 1.35 objective.

Co-immunoprecipitation: COS cells were first resuspended in lysis buffer 1 (LB1; 25 mM Hepes/KOH, 115mM potassium acetate, 5 mM sodium acetate, 5 mM $MgCl_2$, 0.5 mM, EGTA, 1% Triton X-100, and protease inhibitors; pH 7.4) or in Sabatini lysis buffer (SLB; 40mM Hepes pH 7.5, 120 mM NaCl, 1 mM EDTA, 10mM sodium pyrophosphate, 10mM ß-glycerophosphate, 50 mM NaF, 0.5% NP40, 0.1% Brij-35, and protease inhibitors). After removing insoluble material by centrifugation at 20,000xg at 4°C for 10mins, extracts were incubated with the specified antibodies for 2.5-18 hr at 4°C. Protein A agarose beads were then added and mixture was incubated for and

additional 20-40 mins at 4°C. Beads were pelleted and washed two times with lysis buffer, resuspended in Laemmli sample buffer, and analyzed by SDS-PAGE and Western blot.

In vivo microtubule binding assay: COS cells were plated onto glass-bottomed dishes (MatTek) and transfected with plasmids encoding the proteins of interest. Twenty-four hours later, cells were viewed on a Nikon TE2000 inverted microscope. Cells were treated with 0.1 μg/ml Streptolysin O in permeabilization buffer 1 (25 mM Hepes/KOH, 115mM potassium acetate, 5 mM sodium acetate, 5 mM $MgCl_2$, 0.5 mM, EGTA, and 10mg/ml BSA; pH 7.4) for 1 min. After washing 3 times with Buffer 1, cells were incubated with Buffer 1 containing 2mM AMPPNP. Cell were monitored every minute for an additional 15 minutes. Alternatively, cells were treated with SLO and AMPPNP in the presence of taxol for 10 minutes. Then, cells were fixed with 3.7 % formaldehyde and processed for immunofluorescence using Flag antibodies.

In vitro single molecule motility assays: Motility assays were performed in flow chambers as previously described [28] except P25 buffer (25 mM Pipes/KOH, 1 mM EGTA, and 2 mM $MgCl_2$, pH 6.8) was used in place of P12. Briefly, motor proteins were prepared by lysing transfected COS cells in SLB with 1mM ATP. 5-10μl cell lysate was added to flow-chambers containing taxol-stabilized microtubules and 40-45 μl of oxygen scavenger buffer (1 mM DTT, 1 mM $MgCl_2$, 2 mM ATP, 10 mM glucose, 0.1 mg/ml glucose oxidase, 0.08 mg/ml catalase, 10 mg/ml BSA, and 10 μM taxol in P25). An objective-type total internal reflection fluorescence microscope and a back-illuminated EMCCD camera (Cascade 512B; Roper Scientific) were used to image single molecule motility events at intervals of 100 ms. Single molecule tracking measurements for each construct come from at least two independent protein preparations and include motile events lasting at least 0.3 seconds. Velocity and track length measurements were obtained using home-made plug-ins written for ImageJ (NIH).

FIGURES

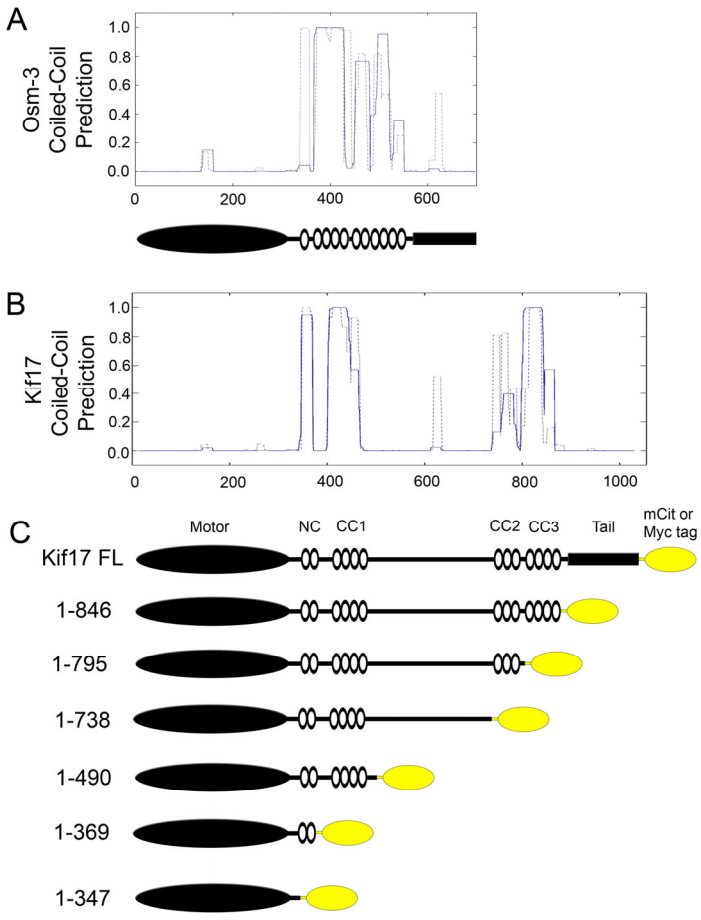

Figure 2.1: KIF17 and Osm-3 coiled-coil prediction and construct schematic. (A) Coiled-coil prediction for Osm-3 (C. *elegan* NP_001023308) and domain map. Gray dotted line, prediction using a window of 14 amino acids; Blue line, prediction using a window of 21 amino acids (based on COILS; Lupas method [40]). (B) Coiled-coil prediction for KIF17 (homo sapiens NP_ 001116291). (B) Map of KIF17 domains and construct schematics. NC, neck coiled-coil, CC, coiled-coil.

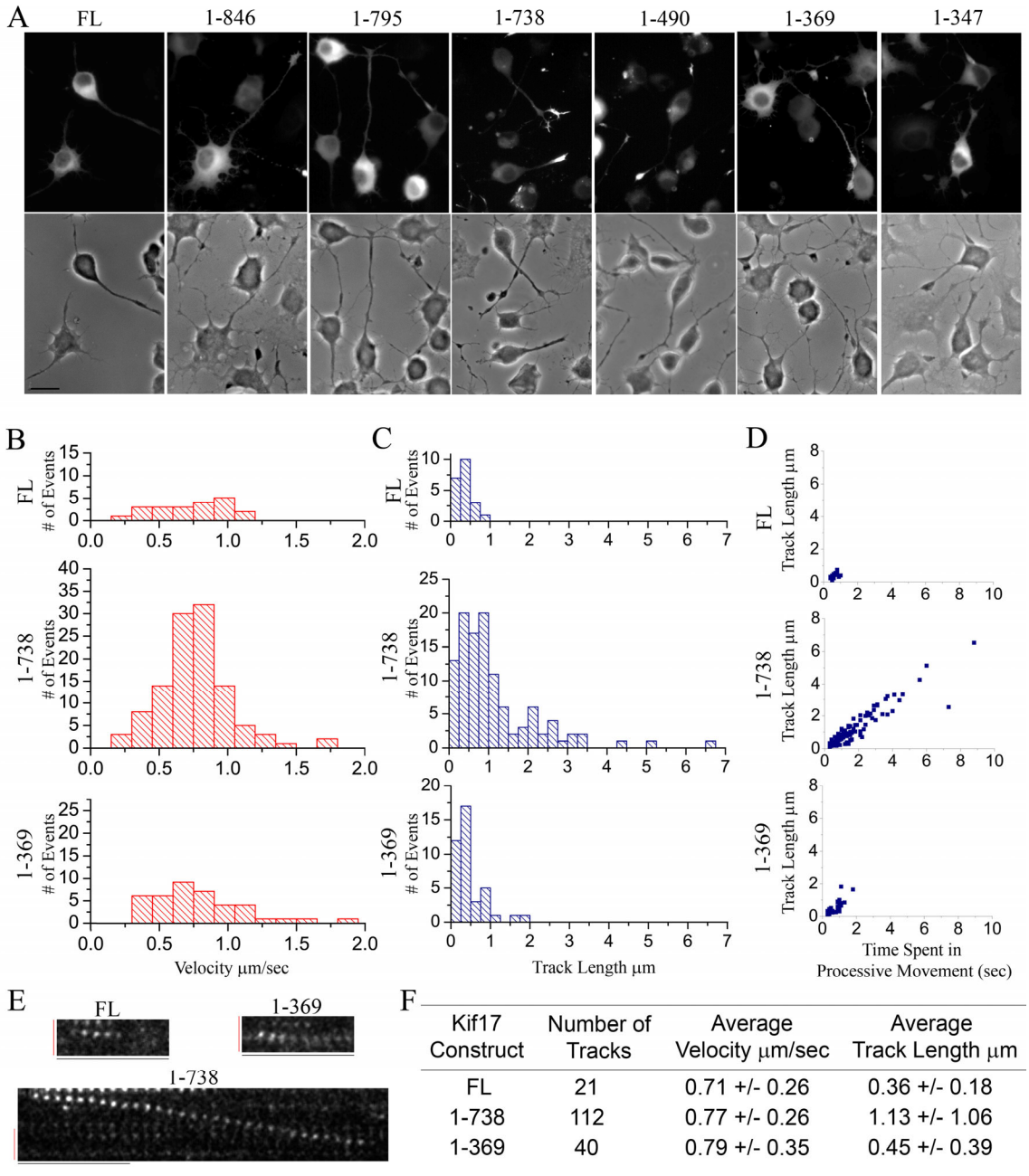

Kif17 Construct	Number of Tracks	Average Velocity µm/sec	Average Track Length µm
FL	21	0.71 +/- 0.26	0.36 +/- 0.18
1-738	112	0.77 +/- 0.26	1.13 +/- 1.06
1-369	40	0.79 +/- 0.35	0.45 +/- 0.39

Figure 2.2: KIF17 processivity is inhibited by coiled-coil 2. (A) Cell based-motility assay. CAD cells were transfected with full-length (FL) or truncated KIF17 constructs (C-terminally tagged with mCit) and differentiated for 40-48 hrs. Scale 20µm. (B-F) *In vitro* single molecule motility assay. COS cells were transfected with 3xmCit tagged FL or truncated KIF17 constructs. Motor proteins in cell lysates along with 1mM ATP were incubated with Taxol-stabilized microtubules and assayed with TIRF microscopy for motility. (B) Velocity histograms. (C) Track length histograms. (D) Distribution of track lengths as a function of time spent in 1-directional motility. (E) Representative kymographs for each motor construct. Scale bars: Red, 2 µm; Black 1 second. (F) Table of motile properties (mean+/-SEM).

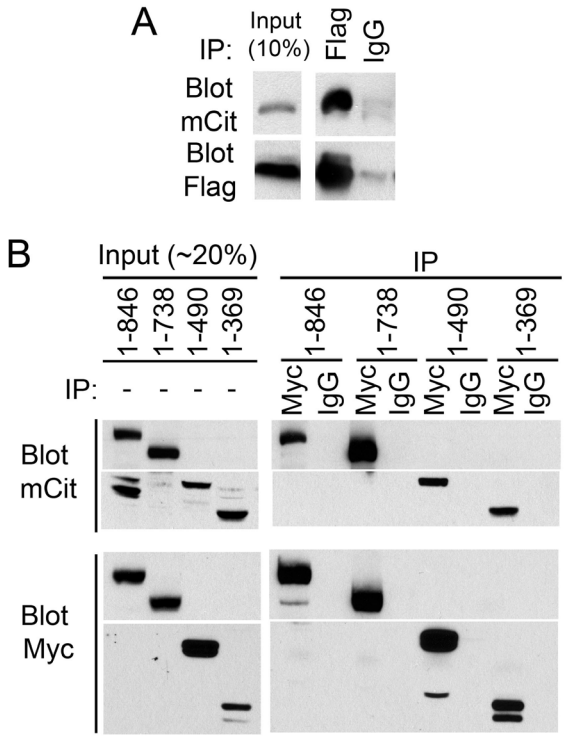

Figure 2.3: Full-length and truncated KIF17 proteins dimerize. (A-B) Co-immunoprecipitation. COS cells were co-transfected with plasmids encoding Flag and mCit tagged FL KIF17 constructs (A), or Myc and mCit tagged truncated KIF17 constructs (B). Lysates were analyzed by western blot either directly (input lysate) or after immunoprecipitation with anti-Flag and control IgG antibodies (A) or anti-Myc and control IgG antibodies (B).

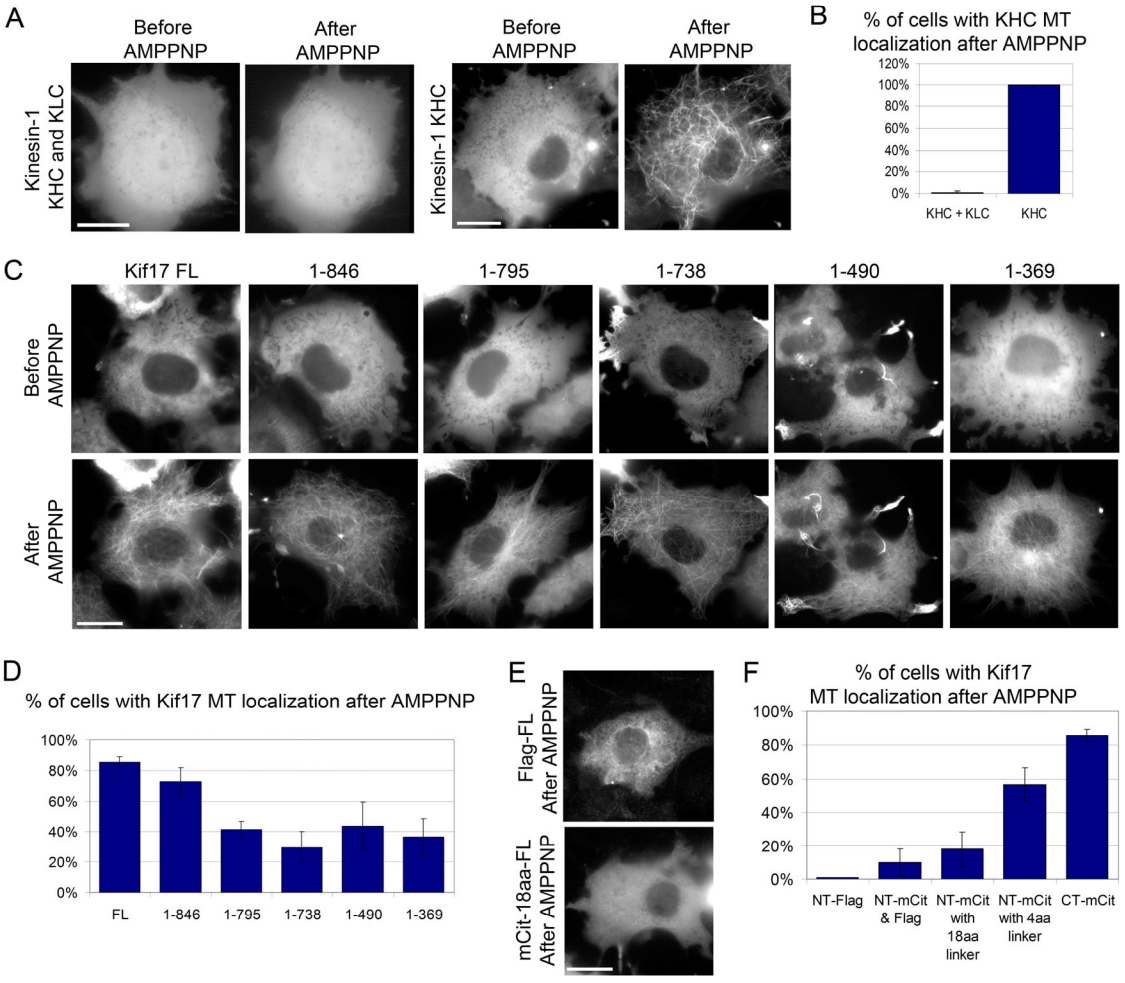

Figure 2.4: Full-length KIF17 is inhibited from binding microtubules. Truncation of KIF17 or using a fluorescent protein to mimic cargo relieves this inhibition. (A-F) Live cell microtubule binding assay. COS cell expressing the indicated Kinesin-1 or KIF17 proteins were permeabilized with SLO, washed, and treated 15 mins with AMPPNP. (A) Representative before and after AMPPNP treatment images shown for cells expressing Kinesin-1's KHC (mCit tagged) and KLC (CFP tagged, not shown) subunits (left); or the KHC subunit alone (right). Scale, 20µm. (B) Percent of cells where Kinesin-1 relocates from a cytoplasmic to microtubule (MT) bound localization after AMPPNP treatment. Averages from 3 experiments ~50 cells each. Error bars +/- SEM. (C) Representative before and after AMPPNP treatment images for FL or truncated KIF17 constructs C-terminally tagged with mCit. Scale, 20µm. (D) Percent of cells where KIF17 relocates from a cytoplasmic, to microtubule (MT) bound, localization after AMPPNP treatment. Averages from 3-5 experiments ~100 cells each. Error bars +/- SEM. (E-F) Tag type and location influences the microtubule binding ability of FL KIF17. (E) COS cells expressing FL KIF17 tagged on N-terminus with mCit or Flag after 15 mins AMPPNP treatment. For Flag-KIF17 cells were additionally fixed and immunostained with anti-Flag antibodies. Scale, 20µm. (F) Percent of cells with FL KIF17 localized to microtubules (MT) after AMPPNP treatment. Flag or mCit tags placed on N- or C- terminus (NT or CT respectively) as indicated. Error bars +/- SEM.

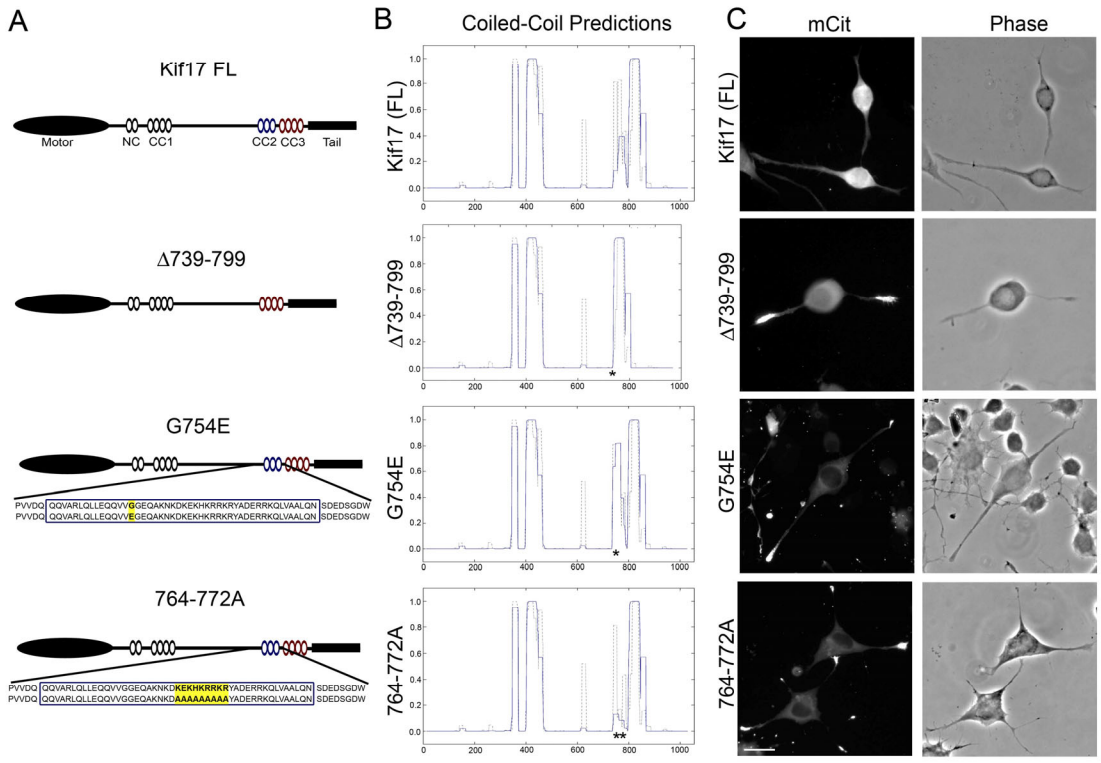

Figure 2.5: Removal or mutation of coiled-coil 2 results in an active, processive motor. (A) Construct schematic of FL KIF17 or constructs with internal deletions or mutations. Blue region, CC2; Red region, CC3. For G754E and 764-772A constructs, the mutated residue(s) are highlighted in yellow and the surrounding residues are shown. Amino acids within the predicted CC2 are boxed in blue. (B) Coiled-Coil predictions for constructs in A. Regions altered by deletions or mutations are marked *. Gray dotted line, prediction using a window of 14 amino acids; Blue line, prediction using a window of 21 amino acids (COILS, Lupas Method). (C) Cell based-motility assay. CAD cells were transfected with the indicated KIF17 constructs (tagged with mCit on C-terminus) and differentiated for 40-48 hrs. Scale 20μm.

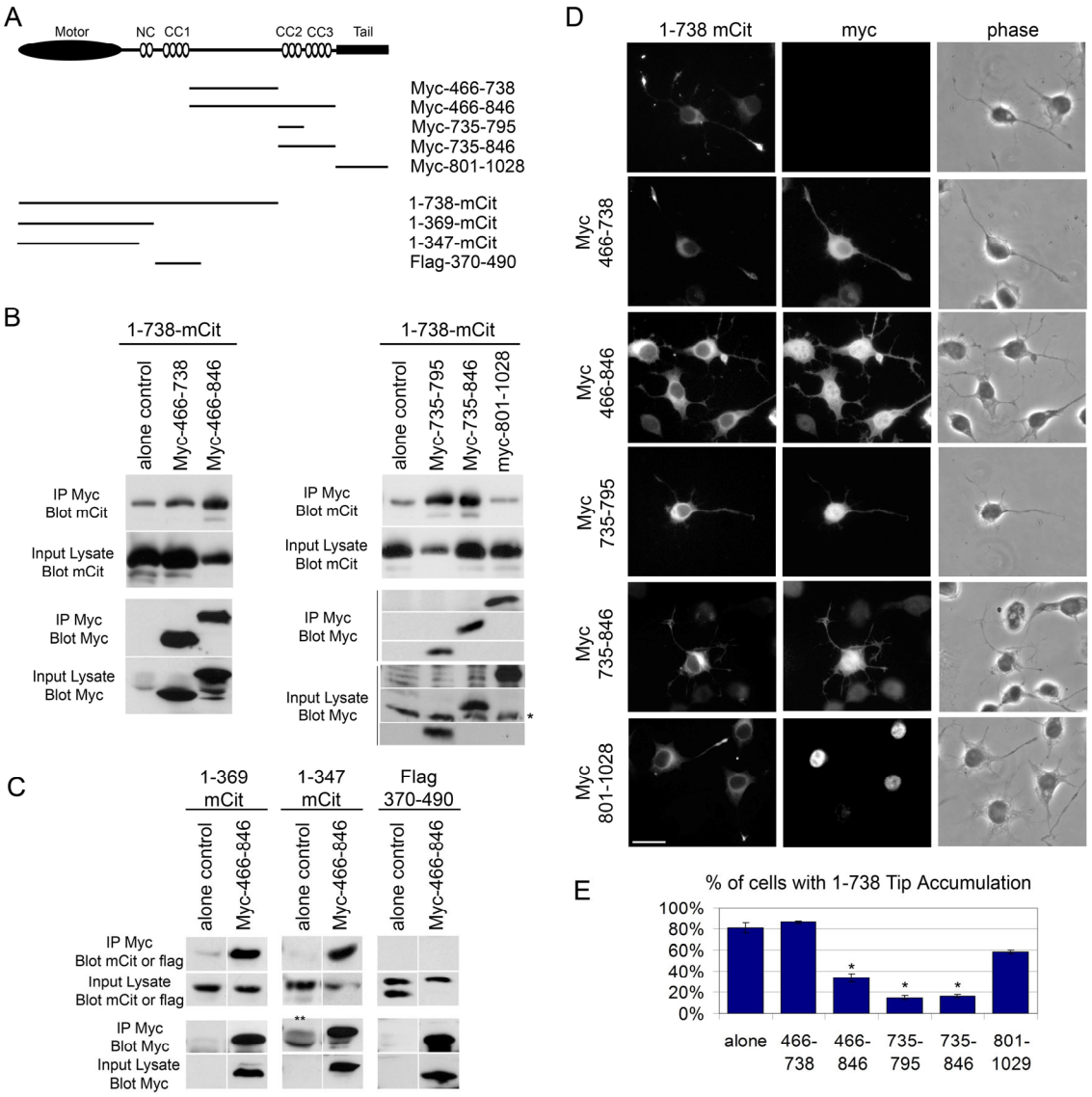

Figure 2.6: Coiled-coil 2 inhibits the motor by direct contact and can inhibit in *trans*. (A) Construct schematic. NC, neck coil, CC, coiled-coil. (B-C) Co-immunoprecipitation. COS cells expressing 1-738mCit, 1-369mCit, 1-347mCit, or Flag-370-490 and the indicated Myc C-terminal fragments were lysed and analyzed by western blot either directly (input lysate) or after immunoprecipitation with anti-Myc or control IgG antibodies. In C, the control and Myc-466-846 pairs for 1-369, 1-347, or 370-490 are from the same gel. ** indicates bands due to Myc antibody heavy chains. *background bands in total cell lysate. (D-E) Cell based-motility assay. Expression of Myc tagged constructs containing the minimal CC2 region, 735-795, can inhibit, in *trans,* the processivity or tip accumulation of KIF17 1-738. (D) CAD cells were transfected with 1-738 mCit alone or with the indicated Myc constructs and differentiated for 40-48 hrs. Scale 20µm. (E) Percentage of cells with 1-738 accumulated at neurite tips in the presence of the indicated Myc tagged construct. Averages from 2-3 experiments, 50-100 cells each. Students T-test (with comparison to 1-738mCit expressed alone control) * $p<0.1$. Error bars +/- SEM.

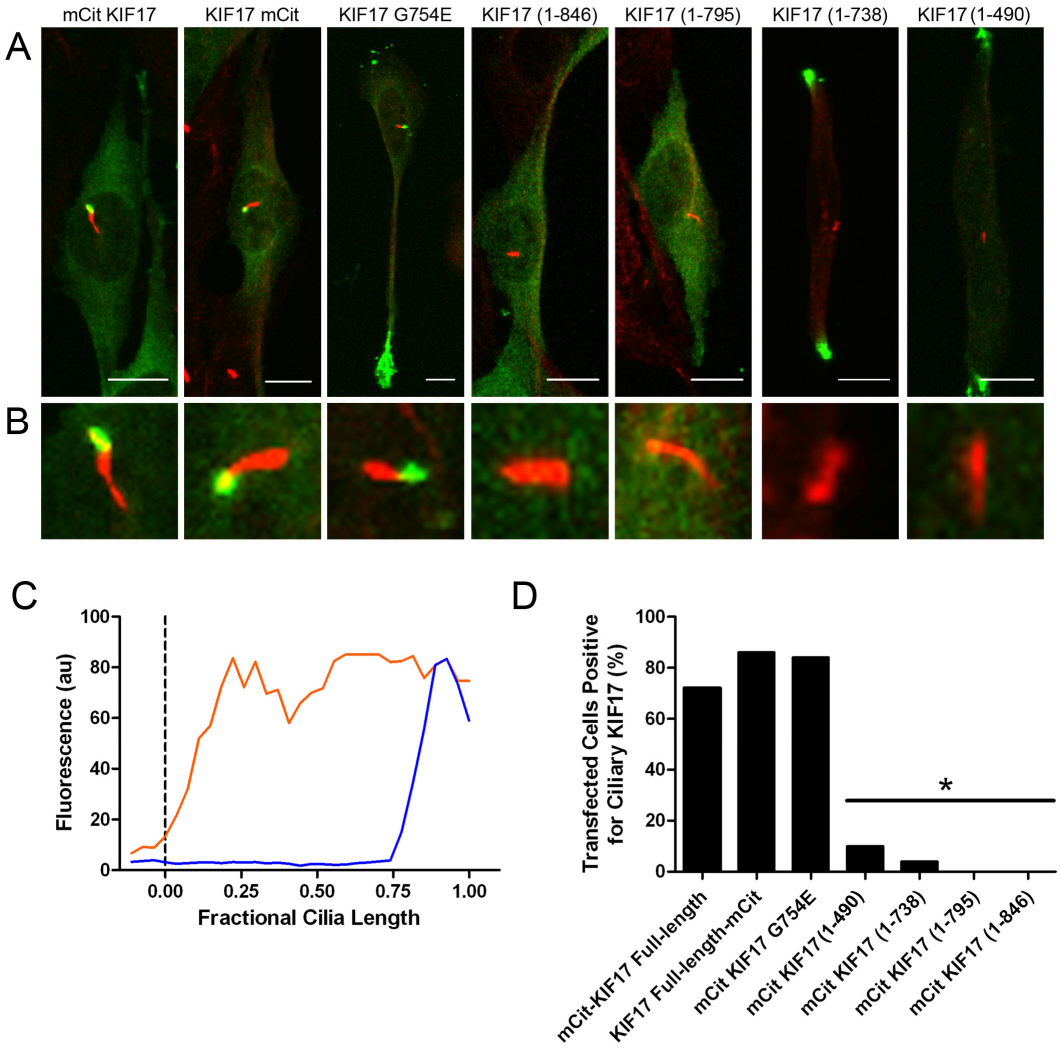

Figure 2.7: The KIF17 tail is required for peripheral accumulation in cilia. (A-D) Olfactory cells were transfected with the indicated mCit tagged KIF17 plasmids and allowed to differentiate for 48hrs. Cells were then fixed and immunostained with anti-acetylated tubulin antibodies to reveal cilia location (shown in red). Full cell images shown in (A), with cilia regions enlarged in (B). (C) KIF17 accumulates at the distal tip of cilia. A line was drawn down the proximal-to-distal length of the cilia shown in B, for mCit-KIF17. Fluorescence intensity (AU, arbitrary units) of mCit-KIF17 was measured and graphed as a function of cilia length. (D) Quantification of the percent of transfected cells that had KIF17 accumulated in cilia. *Chi-squared test, $p < 0.002$. Acknowledgements: This figure was generously contributed by Paul Jenkins, from Jeffrey Martens' lab at the University of Michigan.

REFERENCES

1. Adio, S., et al., *Review: regulation mechanisms of Kinesin-1.* J Muscle Res Cell Motil, 2006. **27**(2): p. 153-60.
2. Cross, R. and J. Scholey, *Kinesin: the tail unfolds.* Nat Cell Biol, 1999. **1**(5): p. E119-21.
3. Aronov, S., et al., *Visualization of translated tau protein in the axons of neuronal P19 cells and characterization of tau RNP granules.* J Cell Sci, 2002. **115**(Pt 19): p. 3817-27.
4. Dietrich, K.A., et al., *The kinesin-1 motor protein is regulated by a direct interaction of its head and tail.* Proc Natl Acad Sci U S A, 2008. **105**(26): p. 8938-43.
5. Hackney, D.D. and M.F. Stock, *Kinesin Tail Domains and Mg(2+) Directly Inhibit Release of ADP from Head Domains in the Absence of Microtubules.* Biochemistry, 2008.
6. Cai, D., et al., *Kinesin-1 structural organization and conformational changes revealed by FRET stoichiometry in live cells.* J Cell Biol, 2007. **176**(1): p. 51-63.
7. Hackney, D.D. and M.F. Stock, *Kinesin's IAK tail domain inhibits initial microtubule-stimulated ADP release.* Nat Cell Biol, 2000. **2**(5): p. 257-60.
8. Al-Bassam, J., et al., *Distinct conformations of the kinesin Unc104 neck regulate a monomer to dimer motor transition.* J Cell Biol, 2003. **163**(4): p. 743-53.
9. Lee, J.R., et al., *An intramolecular interaction between the FHA domain and a coiled coil negatively regulates the kinesin motor KIF1A.* EMBO J, 2004. **23**(7): p. 1506-15.
10. Yamada, K.H., T. Hanada, and A.H. Chishti, *The effector domain of human Dlg tumor suppressor acts as a switch that relieves autoinhibition of kinesin-3 motor GAKIN/KIF13B.* Biochemistry, 2007. **46**(35): p. 10039-45.
11. Chu, P.J., J.F. Rivera, and D.B. Arnold, *A role for Kif17 in transport of Kv4.2.* J Biol Chem, 2006. **281**(1): p. 365-73.
12. Guillaud, L., M. Setou, and N. Hirokawa, *KIF17 dynamics and regulation of NR2B trafficking in hippocampal neurons.* J Neurosci, 2003. **23**(1): p. 131-40.
13. Setou, M., et al., *Kinesin superfamily motor protein KIF17 and mLin-10 in NMDA receptor-containing vesicle transport.* Science, 2000. **288**(5472): p. 1796-802.
14. Chennathukuzhi, V., et al., *The kinesin KIF17b and RNA-binding protein TB-RBP transport specific cAMP-responsive element modulator-regulated mRNAs in male germ cells.* Proc Natl Acad Sci U S A, 2003. **100**(26): p. 15566-71.
15. Takano, K., et al., *NXF2 is involved in cytoplasmic mRNA dynamics through interactions with motor proteins.* Nucleic Acids Res, 2007. **35**(8): p. 2513-21.

16. Evans, J.E., et al., *Functional modulation of IFT kinesins extends the sensory repertoire of ciliated neurons in Caenorhabditis elegans.* J Cell Biol, 2006. **172**(5): p. 663-9.

17. Illuchev, D., et al., *Relationships between blood oxygen parameters in patients with chronic obstructive lung disease.* Folia Med (Plovdiv), 1993. **35**(1-2): p. 5-21.

18. Pan, X., et al., *Mechanism of transport of IFT particles in C. elegans cilia by the concerted action of kinesin-II and OSM-3 motors.* J Cell Biol, 2006. **174**(7): p. 1035-45.

19. Scholey, J.M., et al., *Intraflagellar transport motors in Caenorhabditis elegans neurons.* Biochem Soc Trans, 2004. **32**(Pt 5): p. 682-4.

20. Snow, J.J., et al., *Two anterograde intraflagellar transport motors cooperate to build sensory cilia on C. elegans neurons.* Nat Cell Biol, 2004. **6**(11): p. 1109-13.

21. Insinna, C., et al., *The homodimeric kinesin, Kif17, is essential for vertebrate photoreceptor sensory outer segment development.* Dev Biol, 2008. **316**(1): p. 160-70.

22. Jenkins, P.M., et al., *Ciliary targeting of olfactory CNG channels requires the CNGB1b subunit and the kinesin-2 motor protein, KIF17.* Curr Biol, 2006. **16**(12): p. 1211-6.

23. Mukhopadhyay, S., et al., *Distinct IFT mechanisms contribute to the generation of ciliary structural diversity in C. elegans.* EMBO J, 2007. **26**(12): p. 2966-80.

24. Imanishi, M., et al., *Autoinhibition regulates the motility of the C. elegans intraflagellar transport motor OSM-3.* J Cell Biol, 2006. **174**(7): p. 931-7.

25. Guillaud, L., R. Wong, and N. Hirokawa, *Disruption of KIF17-Mint1 interaction by CaMKII-dependent phosphorylation: a molecular model of kinesin-cargo release.* Nat Cell Biol, 2008. **10**(1): p. 19-29.

26. Jacobson, C., B. Schnapp, and G.A. Banker, *A change in the selective translocation of the Kinesin-1 motor domain marks the initial specification of the axon.* Neuron, 2006. **49**(6): p. 797-804.

27. Nakata, T. and N. Hirokawa, *Microtubules provide directional cues for polarized axonal transport through interaction with kinesin motor head.* J Cell Biol, 2003. **162**(6): p. 1045-55.

28. Cai, D., K.J. Verhey, and E. Meyhofer, *Tracking single Kinesin molecules in the cytoplasm of mammalian cells.* Biophys J, 2007. **92**(12): p. 4137-44.

29. Yildiz, A. and P.R. Selvin, *Kinesin: walking, crawling or sliding along?* Trends Cell Biol, 2005. **15**(2): p. 112-20.

30. Verhey, K.J., et al., *Light chain-dependent regulation of Kinesin's interaction with microtubules.* J Cell Biol, 1998. **143**(4): p. 1053-66.

31. Kawaguchi, K. and S. Ishiwata, *Nucleotide-dependent single- to double-headed binding of kinesin.* Science, 2001. **291**(5504): p. 667-9.

32. Coy, D.L., et al., *Kinesin's tail domain is an inhibitory regulator of the motor domain.* Nat Cell Biol, 1999. **1**(5): p. 288-92.

33. Blasius, T.L., et al., *Two binding partners cooperate to activate the molecular motor Kinesin-1.* J Cell Biol, 2007. **176**(1): p. 11-7.

34. Murrell, J.R. and D.D. Hunter, *An olfactory sensory neuron line, odora, properly targets olfactory proteins and responds to odorants.* J Neurosci, 1999. **19**(19): p. 8260-70.

35. Vale, R.D., *The molecular motor toolbox for intracellular transport.* Cell, 2003. **112**(4): p. 467-80.

36. Kull, F.J. and S.A. Endow, *Kinesin: switch I & II and the motor mechanism.* J Cell Sci, 2002. **115**(Pt 1): p. 15-23.

37. Kimple, R.J., et al., *Structural determinants for GoLoco-induced inhibition of nucleotide release by Galpha subunits.* Nature, 2002. **416**(6883): p. 878-81.

38. Kull, F.J., R.D. Vale, and R.J. Fletterick, *The case for a common ancestor: kinesin and myosin motor proteins and G proteins.* J Muscle Res Cell Motil, 1998. **19**(8): p. 877-86.

39. Setou, M., et al., *Glutamate-receptor-interacting protein GRIP1 directly steers kinesin to dendrites.* Nature, 2002. **417**(6884): p. 83-7.

40. Lupas, A., M. Van Dyke, and J. Stock, *Predicting coiled coils from protein sequences.* Science, 1991. **252**(5009): p. 1162-1164.

Chapter 3:
Motile Properties of Dimeric KIF1A Motors Upon Release of Autoinhibition

Molecular motors of the kinesin superfamily use the energy of ATP to move along or modify the microtubule cytoskeleton. Kinesin-3 family members, mammalian KIF1A and C. *elegans* Unc104, specifically couple this ATP driven motility to transport many types of intracellular cargo including synaptic vesicle precursors [1-3]. Labeling KIF1A or Unc104 proteins with GFP has allowed motors clustered on vesicular membranes to be visualized and tracked. These motors move at 0.8-1.0 μm/second in an anterograde direction down axons of murine primary hippocampal neurons or in live worms [4-6].

To ensure that ATP is not wasted by kinesin motors uncoupled to cargo, kinesin motors must be tightly regulated. Indeed, many studies have shown that the first identified, and most well-characterized kinesin motor, Kinesin-1 (also known as conventional kinesin or KIF5), is autoinhibited in the absence of cargo ([7-9] and reviews [10, 11]. This work has led to the general hypothesis that all cargo transporting kinesins must have both active and inhibited states. Recently more examples of kinesin autoinhibition have come to light as the Kinesin-2 family member, Osm-3, and Kinesin-3 family members, Gakin/KIF13B, KIF1A, and Unc104 are also inhibited [12-17]. Autoinhibition of KIF1A/Unc104, is mediated by two different regions. First microtubule binding is inhibited by the forkhead-associated (FHA) domain and the C-terminally adjacent coiled-coil (CC2) [14, 15]. Second, the neck coil (NC) and first coiled-coil region (CC1) of Unc104 has been suggested to play a role in the transition from a monomeric state incapable of long-distance motility to an active dimeric state [14]. Whether this regulatory mechanism is also conserved in mammalian KIF1A has not yet been tested.

KIF1A/Unc104 motors have some of the fastest reported velocities and longest run lengths of the kinesin superfamily [2, 4-6, 18-20]. However, the most unique or controversial quality of KIF1A is that it has been proposed to act as a monomer [16, 21, 22]. Most cargo transporting kinesins are dimeric and are believed to coordinate their two motor heads in an alternating hand-over-hand fashion, moving in 8nm steps down the microtubule [23]. However, results from hydrodynamic analysis of recombinant and endogenous KIF1A/Unc104 motors suggest they are monomers [2, 17, 19, 24]. Thus, a novel motility mechanism was proposed to explain how KIF1A/Unc104's single motor domain could generate processive movement. In the model, KIF1A/Unc104 diffuses along the microtubule with ATP hydrolysis powering a slight rotation of the head that provides enough mechanical force to bias diffusion towards the plus-ends of microtubules. The processivity of KIF1A/Unc104 also depends heavily on a positively charged K-loop inserted near the motor domain's microtubule binding interface. Electrostatic interactions between this lysine rich region and the negatively charged C-terminal tails of tubulin help the single-headed motor stay attached in a weak binding state while diffusing [16, 21, 22, 25, 26].

The biased diffusion model has been controversial because *in vitro* experiments report that monomeric KIF1A motors move at very slow velocities (0.14μm/second) compared to the fast velocities reported for GFP-tagged KIF1A/Unc104 motors expressed *in vivo* [5, 6, 16, 20-23]. Monomeric KIF1A motors also stall under low load (0.15 pN), which is likely not sufficient to drive vesicle transport in a crowed cellular environment [21]. Finally, monomeric Unc104 constructs do not show the same biased diffusion movement as KIF1A [19, 20]. Thus, a second model for KIF1A/Unc104 motility was put forth, suggesting that *in vivo*, KIF1A/Unc104 dimerize on vesicular membranes in order to achieve processive transport of cargo. This model is supported by several lines of evidence. First, studies show that Unc104 constructs artificially dimerized by the addition of a leucine zipper or the coiled-coil stalk region of Kinesin-1, are highly processive. The forced-dimer Unc104 motors show motile properties similar to other dimeric kinesins and to the motility properties of GFP-tagged KIF1A/Unc104 motors expressed *in vivo* [20]. Second, Unc104 proteins can drive the processive transport of liposomes by binding phosphotidylinositol(4,5)bisphosphate ($PIP_{4,5}P_2$)

molecules. This processive transport is greatly enhanced by high concentrations of $PIP_{4,5}P_2$, or experimental conditions that locally concentrate $PIP_{4,5}P_2$ on the liposome membrane. This suggests locally concentrating the Unc104 motor on cargo vesicles facilitates its dimerization and consequently its ability to move processively [4, 27]. Third, recombinant KIF1A motors expressed in reticulocyte lysates can dimerize [17]. Finally, the fact that the closely related Kinesin-3 family members, *Dictyostelium* Unc104 (DdUnc104) and Kif1C exist in a dimeric state, also lends support to the KIF1A/Unc104 processive dimer model [28, 29]. Yet, a KIF1A motor that is dimerized via its own sequences and that moves processively has not yet been demonstrated.

What are the KIF1A/Unc104 regions that may facilitate dimerization? The short predicted coiled-coils are likely candidates, but as they are much shorter, and in some cases, significantly weaker than the extended coiled-coil segments present in other kinesin family members, they have largely been overlooked and understudied. However, the NC is likely to be important as mutations in this region, abolished the ability of Unc104 forced dimers to move processively, suggesting it must function in some way to coordinate the two motor domains of the forced dimer [20]. Additionally cryoelectron microscopy studies and studies on synthesized peptides equivalent to the NC of KIF1A or Unc104 also suggest this short coiled-coil is capable of dimerization [14, 17, 30]. None of the other predicted coiled-coil regions have been implicated in dimerization, but they also have not been studied.

We set out to examine the overall structure and regulatory regions of KIF1A motors and to correlate processive motor activity with dimeric state. We show that full-length KIF1A motors can dimerize, but these dimers are still in an autoinhibited state where they are prevented from binding microtubules and moving processively. Our data agree with previous studies that this autoinhibition is mediated by the CC2/FHA region and CC1. Dimerization requires the full NC, but likely other coiled-coils contribute. Finally, we support the model that KIF1A moves processively as a dimer. Although we observed monomeric motor constructs that moved for short time periods via one-dimensional diffusion, we show that processive movement for long time periods requires dimerization and likely a motility mechanism more reminiscent of kinesins that move hand-over-hand.

RESULTS

Full length KIF1A is inactive in mammalian cells

In order to investigate the regulatory mechanisms and monomeric/dimeric state of KIF1A, we tagged rat KIF1A with a fluorescent protein (FP) on the N- or C-terminus and expressed it in mammalian cells. Kinesin-1 motors have been successfully labeled and studied in their native cellular environment by this approach, thereby avoiding many of the pitfalls associated with purifying and labeling kinesin motors *in vitro* [7, 31]. As Unc104 proteins tagged with a FP on their C-terminus are able to rescue the paralyzing phenotypes caused by Unc104 mutations in C *elegans*, the FP tag appears to have no deleterious effects on the cargo binding, regulatory, or motility properties of the motor [6].

We first investigated whether full-length KIF1A was able to bind microtubules. KIF1A was tagged with a monomeric version of Citrine (mCit, a variant of YFP), and expressed in COS cells where it showed a diffuse, cytoplasmic localization (Figure 3.1 A). Previous studies on Kinesin-1 have shown that steady-state expression patterns often do not reveal whether the motor is actively binding and moving on microtubules. However, by exposing the motors to the non-hydrolysable ATP analog, AMPPNP, active motors can be trapped on the microtubule as they are unable to change from a strong microtubule bound conformation [7, 32]. Live COS cells were permeabilized with the bacterial toxin streptolysin O (SLO) then treated with AMPPNP. The cytosolic localization of mCit-KIF1A was not altered by AMPPNP (Figure 3.1 A and B), revealing that full-length KIF1A is inhibited from binding microtubules. This data agrees with previous reports suggesting KIF1A/Unc104 is an autoinhibited motor.

Full length KIF1A forms a compact dimeric protein in mammalian cells

As two regulatory mechanisms have been proposed to explain the KIF1A/Unc104 inhibited state, specifically the presence of inhibitory domains or a monomer-to-dimer transition, it is important to determine whether full-length KIF1A exists as a monomer or dimer. Three experimental approaches were taken to address this question, specifically, co-immunoprecipitation, chemical crosslinking, and fluorescence resonance energy transfer (FRET) stoichiometry. For co-immunoprecipitation experiments, mCit- and

Myc-tagged KIF1A proteins were co-expressed in COS cells. Cells were then lysed and immunoprecipitated with either control antibodies (IgG) or antibodies to the Myc tag. mCit-KIF1A co-precipitated with Myc-KIF1A in the presence of Myc antibodies but not control antibodies. Similar results were seen for KIF1A motors tagged with mCit on the N-terminus and monomeric cyan fluorescent protein (mCFP) on the C-terminus (mCit-KIF1A-mCFP, Figure 3.1C). These results support a dimeric, rather than monomeric, state for KIF1A when it is expressed in mammalian cells.

Chemical crosslinking, the second experimental approach used to test the monomeric or dimeric state of KIF1A, has been used previously to demonstrate that Kinesin-1 and some Kinesin-3 motors are dimers [20, 29]. Cell lysates from mCit-KIF1A expressing COS cells were treated with dimethylpimilimidate (DMP) then run on a SDS-PAGE gel and blotted for the mCit tag. The mCit-KIF1A protein ran at the expected molecular weight (~170 kD) in the absence of crosslinker, but showed reduced mobility in the gel when treated with DMP (Figure 3.1D, lanes 1,2). The KHC domain of Kinesin-1, which is a well proven dimer, also showed an up-shifted bands in the presence of DMP when similarly tagged with mCit (Figure 3.1D, lanes 3 and 4). Control experiments with lysates containing the mCit tag alone showed no up-shifted band of reduced mobility, proving that the decreased mobility seen for mCit-KIF1A and mCit-KHC was not due to the tag (Figure 3.1D, lanes 5 and 6). These results again suggest that KIF1A, like Kinesin-1, can exist as a dimer.

The final approached used to resolve the KIF1A monomer-dimer question, FRET stoichiometry, was chosen as it could also give information about the overall conformation of KIF1A. FRET stoichiometry was recently used to elucidate conformational changes that occur in Kinein-1 when it changes from an autoinhibited state to an active state [7]. FRET stoichiometry uses three fluorescence images to calculate an average FRET efficiency (E_{AVE}; for more details see materials and methods). E_{AVE} values vary between 0% (no FRET) for unlinked donor mCFP and acceptor mCit fluorophores, and 37% for mCFP and mCit linked by a 16 amino acid polypeptide chain [7, 33, 34].

To test the prediction that KIF1A is a dimer, mCFP-KIF1A and mCit-KIF1A were co-expressed in COS cells and an average FRET efficiency between the donor and

acceptor FPs was calculated. The motor-to-motor FRET of KIF1A was low, but measurable (E_{AVE} = 3.0%) and was very comparable to the motor-to-motor FRET of the Kinesin-1 holoenzyme that has its motor domains separated by KLC in its inactive state (E_{AVE} = 2.1%, Figure 3.1 E and F) [7] . As there was a detectable FRET signal for KIF1A, these results do not support a monomeric conformation, but rather support the idea that KIF1A is dimeric, but in the inactive molecule the motor domains do not reside side by side However, the possibility that KIF1A exists as a mixture of monomers and dimers *in vivo* cannot be excluded.

FRET stoichiometry was put to further use in order to test the model that KIF1A folds into a compact conformation. This model is based on previous studies using rotary shadowing of recombinant KIF1A [2]. The single motor construct, mCit-KIF1A-CFP, was generated in order to put donor and acceptor FPs on KIF1A's motor and tail domains. When expressed in COS cells with Myc-KIF1A, mCit-KIF1A-CFP resulted in an E_{AVE} that was again low, but detectable (E_{AVE} = 4.8%). This value was significantly different from the motor-to-tail FRET efficiency of the Kinesin-1 holoenzyme, whose motor and tail domains are in very close proximity in the folded, inactive state (E_{AVE} = 15.8%, Figure 3.1 G and H) [7]. These results support the conclusion that KIF1A, in native conditions, is not an extended molecule (where we would expect no FRET) nor does it have a conformation with the motor or tail domains as closely located as in the case of Kinesin-1 (expect high FRET). Nevertheless, KIF1A is likely folded in a compact conformation which places the N-terminal motor and C-terminal tail within at least ~8-10 nm of each other.

The combination of these results shows that KIF1A can form dimers *in vivo*, but is inhibited from binding microtubules. Thus, dimerization is not sufficient for motor activation and a mechanism other than a monomer-to-dimer transition must be used in order to shift KIF1A from and inactive to active state.

Separate mechanisms regulate microtubule binding and processive motility of KIF1A motors

Analysis of the domain structure of KIF1A/Unc104, shows the motor domain is followed by two very short coiled-coils (referred to as the neck coil, NC; and coiled-coil

1, CC1), a forkhead-associated (FHA) domain, two more short coil-coils (CC2 and 3), a large undefined region, and a C-terminal PH domain (Figure 3.2 A and B). Whether any or all of the short predicted coiled-coils are necessary or sufficient for dimerization is unknown. To identify the regions of KIF1A involved in autoinhibition and dimerization under native expression conditions, truncated versions if KIF1A were created (Figure 3.2 B) by placing a mCit tag after CC2, KIF1A(1-726), after CC1, KIF1A(1-491), or after the NC, KIF1A(1-393).

The SLO/AMPPNP assay described above was used first to investigate the microtubule binding ability of each truncation. Live cell imaging of COS cells expressing the mCit-tagged KIF1A truncations showed that after SLO and AMPPNP treatment, KIF1A(1-726)-mCit remained cytosolic (Figure 3.3 C,D,E), indicating that this construct, which has roughly half of the KIF1A residues missing (727-1696), still maintains the autoinhibited state of the full-length molecule. Further truncation of CC2 and the FHA domain caused KIF1A(1-491)-mCit to relocate from a diffuse cytosolic localization, to a microtubule-locked localization after treatment with AMPNP. Thus, the CC2 and FHA domains (residues 492-726) are responsible for keeping KIF1A inhibited and unable to interact with microtubules. These results are consistent with previous work on truncated KIF1A/Unc104 [14, 15] which also implicated the CC2/FHA region as important in maintaining KIF1A's autoinhibited state. Removal of the CC1 domain, yielded more interesting results, as KIF1A(1-393)-mCit localized to microtubules even in the absence of AMPPNP. In this case the motor was accumulated on microtubules in the periphery of the cell suggesting that it was constantly undergoing processive movement. Addition of AMPPNP did result in a shift in the remaining cytosolic KIF1A(1-393) to a microtubule bound state which was most apparent in the central regions of the cell. Therefore, although the CC2/FHA region prevents KIF1A from binding microtubules, the CC1 region may play an additional role in regulating KIF1A's motile properties.

To further test CC1's role in regulating processive motility, we tested all constructs in two processive motility assays. Since multiple studies have demonstrated that active kinesin motors often accumulate at the tips of cell processes [15, 35, 36], we first analyzed the processive motility of KIF1A in the neuronal-like cell line, CAD. Second, we tested processive motility *in vitro* using a single molecule motility assay. For

this assay, KIF1A constructs were tagged on their C-terminus with three tandem copies of mCit for improved signal-to-noise ratio and decreased photobleaching and photoblinking [31]. Cell lysates from COS cells expressing the 3xmCit-tagged KIF1A constructs were added to a flow chamber containing taxol-stabilized microtubules and assayed on a total internal reflection fluorescence (TIRF) microscope. By timelapse imaging at 100ms intervals, individual motors could be seen moving along microtubules. Only motility events that lasted at least 500ms were included in the analyzed data set to ensure that the same motor could be tracked through 5 timelapse images. In order to directly compare the number of motility events and the motile properties of velocity and track length for each KIF1A motor construct, the amount of expressed protein was normalized by western blot and each construct was analyzed for the same total amount of time.

As expected from the microtubule binding experimental results, full-length (FL) KIF1A and KIF1A(1-726) were inactive for processive movement as they did not accumulate at the tips of CAD cell neuronal processes but were instead diffusely localized primarily in the cell body (Figure 3.3 A). They additionally showed very few motility events *in vitro* (Figure 3.3 B-D). Interestingly, KIF1A(1-491) was also diffusely localized in CAD cells and moved only rarely *in vitro*. This reveals that while the CC2/FHA region of KIF1A regulates microtubule binding of the full-length motor, an additional region must control motility. KIF1A(1-393), on the other hand, showed dramatic accumulation to the tips of neuronal processes, with very little cell body localization and exhibited a large number of motility events *in vitro*. Thus, CC1, or amino acids 394-490, must play an inhibitory role in KIF1A, mediating to some degree the motility control mechanism.

KIF1A(1-393)'s average velocity of 1.36 ± 0.04 μm/sec and average track length of 1.24 ± 0.06 μm per event (Figure 3.3 D), are comparable to previous *in vivo* and *in vitro* measurements for KIF1A/Unc104 motors where velocities ranged from 0.8-1.7 μm/sec with track lengths up to several μm [2, 4-6, 14, 19]. The slight differences in velocity and run lengths observed for the FL, 1-726, and 1-491 motors as compared to 1-393 are likely not significant due to the very few events used to calculate them. These

few motility events are likely due to stochastic activation of the auto-inhibited motors by random conformational changes.

The CC1 domain prevents dimerization and processive motility of KIF1A(1-491)

What is the mechanism by which processive motility is inhibited in the KIF1A(1-491) motor? Results from Albassam et al [14] provide a likely explanation. Using cryoelectron microscopy they noted that CC1 could fold back on the NC forming a parallel intramolecular coiled-coil that limited the motor to a monomeric conformation. In a second conformation, they reported that the motor was likely dimerized with the NC and CC1 forming intermolecular coils with their respective counterparts on the adjacent dimer subunit[14]. Thus, the CC1 may inhibit the processive motility of dimeric KIF1A by uncoupling its two motor heads. This would be analogous to the situation in Kinesin-1 where the KLC subunits prevent processive motility in the inhibited state by unwinding the neck and pushing the motor domains apart [7]. In the case of the KIF1A truncation (1-491), the CC1 may prevent dimerization altogether.

To test this hypothesis and whether or not truncated forms of KIF1A are monomers or dimers, chemical crosslinking, co-immunoprecipitation and photobleaching experiments were done. In the absence of crosslinker, all truncations ran at sizes representing their approximate molecular weight. When treated with DMP, however, both the (1-726)-mCit and (1-393)-mCit proteins where present in up-shifted bands of restricted mobility (Figure 3.4 A), indicating they exist as dimers. (1-491)-mCit, on the other hand, showed only a small fraction of protein shifted to a higher molecular weight, with the remaining majority shifted downward to species of faster mobility. This suggests that (1-491) is primarily a monomer. The novel downshift further indicates that the monomer has a compact conformation that permits an intramolecular crosslink. This internal crosslink could be indicative of the parallel coiled-coil between the NC and CC1 seen by Albassam et al, but could also have occurred elsewhere such as in the motor domain. Co-immunoprecipitation experiments gave similar results with the exception of 1-491. Myc- and mCit-tagged versions of the KIF1A truncations were co-expressed in COS cells and immunoprecipitated with control antibodies (IgG) or antibodies to the Myc tag. A significant portion of mCit tagged truncations 1-726, 1-508 (a truncation very

similar to 1-491, that behaves identically to 1-491 in all assays), 1-491, and 1-393 were co-precipitated with Myc constructs of an equivalent length in the presence of Myc antibodies. Thus, 1-726 and 1-393 behave as dimers in both assays, but 1-491 showed varied results.

The final method used to test the dimeric state of KIF1A truncations involved tagging them with 3xmCit tags, then analyzing the fluorescence intensity values of individual motors over time as they photobleach. As each mCit molecule photobleaches, the total fluorescence intensity of the motor construct drops at rather consistent intervals. Thus, a dimeric 3xmCit-tagged motor would show up to six bleaching steps, whereas, a monomeric motor would only have up to three steps. Dimers and monomers are expected to have some variation in their number of bleaching steps as some mCit molecules will have the tendency to blink, bleach simultaneously, or bleach prior to analysis. As this assay tests dimerization at the single molecule level, it can potentially reveal more information about the pool of motors than the previous assays which treated all motors as a group.

Cell lysates from COS cells expressing 3xmCit-tagged versions of full-length or truncated KIF1A motors were added to flow chambers where the 3xmCit-tagged motors were adsorbed directly to the coverglass or locked on microtubules in the presence of AMPPNP. The bleaching behavior of single motors over time was recorded in the TIRF microscope and the number of bleaching steps for individual fluorescent motors was then plotted as a histogram (Figure 3.4 C; representative fluorescence intensity traces are shown in Figure 3.4 D). A truncated Kinesin-1 construct, KHC(1-891)-3xmCit, was used as a dimeric motor positive control. This motor showed a maximum of six bleaching steps with a large proportion of the individual motors bleaching with more than three steps proving they are dimers. The histograms for KIF1A full-length (FL), 1-726, and 1-393 look almost identical to that of KHC(1-891), consistent with the above results that they are dimeric. Although truncations 1-491 and 1-508, also had some motors bleach in six steps, most of the motors bleached in two or three steps, which is consistent with the conclusion that they are monomers.

Although KIF1A has long been referred to as a monomeric kinesin, the data from these three dimerization experiments, provide conclusive evidence that the KIF1A

truncations 1-726 and 1-393 (Figure 4) can dimerize similar to the FL protein (Figure 1). However, KIF1A constructs that are terminated after CC1, (1-491 and 1-508) are primarily monomeric. Formation of an intramolecular coil between the NC and CC1 would explain KIF1A(1-491)'s monomeric state, as it contains no other regions capable of mediating dimerization. Formation of a NC/CC1 intramolecular coil in 1-726 and FL would not necessarily preclude dimerization as CC2 and/or CC3 could compensate. The small portion of dimers detected for 1-491 are likely due to a intermolecular coiled-coil conformation of the NC and CC1. The discrepancy between the three assays for the 1-491 construct may be due to individual assay conditions that influence the amount of motors forming intra- or inter-molecular coils. In particular, the binding of bulky antibodies to the Myc tag may place strain on monomeric intramolecular coils and favor instead intermolecular coils and dimerization.

KIF(1-393) moves processively as a dimer

As two models for KIF1A's processive motility have been proposed, one involving the biased diffusion of monomers and the other involving the hand-over-hand stepping of dimers, we used two-color TIRF imaging to simultaneously track the motility of (1-393) motors labeled with two fluorescent proteins, mCit and mCherry in order to conclusively prove that our KIF1A (1-393) truncation moves in its dimeric state. (1-393)-3xmCit and (1-393)-3xmCherry motors were co-expressed in COS cells and lysates were added to flow chambers with polymerized microtubules. Although mCit labeled motors could homodimerize with other mCit motors and thus show motility events with only mCit fluorescence, similar to what one would expect if the motors were monomers, these homodimers would be brighter than mCit motors heterodimerized with mCherry motors, or mCit motors that were monomers. For 109, 3xmCit fluorescent spots tracked, 44 tracked with a corresponding mCherry fluorescent spot (a representative track is shown in Figure 3.4 E). As the mCit fluorescence of these two colored motility events was significantly less (356.8 +/- 51.4) than the fluorescence of mCit spots moving independently of mCherry spots (513.4 +/- 54.0), a majority if not all of the mCit-only spots must also be dimers. At least two factors may explain why the average mCit maximum fluorescence intensity measurements of the mCit/mCherry heterodimers (three

mCits and three mCherrys) are not half the fluorescence intensity of mCit homodimers (6 mCits). First, self-quenching of mCit fluorescent proteins is more likely to occur in homodimeric motors (six mCits) than heterodimeric motors (three mCits). Second, because homodimeric motors are brighter (with six mCits) they also have a wider range of fluorescence intensity levels that are detectible above the signal-to-noise threshold for analysis than the low levels of mCit fluorescence in the heterodimeric motors (with only three mCits). This is the most conclusive demonstration that KIF1A moves in a processive fashion as a dimeric motor. Previous studies have used Unc104 constructs that were forced dimers due to addition of leucine zippers or truncations that contained the CC2/FHA or CC1 inhibitory regions and thus had only rare motility events [4, 14, 18, 20].

Dimerization of KIF1A via the Neck Coil domain

Much of the data supporting or refuting the biased-diffusion model of motility have used very short KIF1A or Unc104 constructs that contained only the motor domain and limited amounts of the NC. In some cases the constructs tested were monomers, in other cases it was just assumed that they were monomeric (for more details see, Figure 3.5 A) [14, 16, 20-22]. As KIF1A(1-393) is a dimer, but only 12-24 residues longer than some reported monomeric constructs, we sought to determine the minimal amount of NC that is required for dimerization and processive motility. Truncations of KIF1A motors with varying amounts of the NC, specifically 1-381, 1-377, and 1-369, were constructed based on previously described motors (Figure 3.5A). These constructs were compared to 1-393 for their ability to dimerize in crosslinking and photobleaching assays. When lysates from cells expressing the mCit C-terminally tagged truncations were treated with the crosslinker DMP and run on a SDS-PAGE gel, only the KIF1A(1-393)-mCit protein showed an up-shifted band of reduce mobility as compared to untreated lysates. KIF1A(1-381)-mCit, KIF1A(1-377)-mCit, and KIF1A(1-369)-mCit showed no change in their electrophoretic behavior when treated with DMP (Figure 3.5 B). Analysis of 3xmCit tagged truncations in our photobleaching assay yielded complimentary results. 1-393 showed a maximum of six bleaching steps with a large proportion of the individual motors bleaching with more than 3 steps, whereas 1-381 and 1-369 showed primarily

only 2 or 3 bleaching steps (Figure 3.5 C and D). These results suggest that the presence of the entire NC, as well as sequences C-terminal to this region, is required for dimerization of mammalian KIF1A. Even small truncations of the NC region convert the motor to a monomeric state. This is consistent with studies on synthesized peptides where several residues beyond G387 were required to prevent dissociation of the coiled-coil [30].

Motile characteristics of monomeric and dimeric KIF1A motors

We next set out to compare the motile properties of monomeric and dimeric KIF1A motors. We first tested the ability of the NC constructs to bind to microtubules under native conditions using the SLO/AMPPNP assay. COS cells expressing (1-393)-mCit, (1-381)-mCit or (1-369)-mCit were permeabilized with SLO then treated with AMPPNP. Only 1-393 accumulated at the cell periphery in the absence of AMPPNP; however, all three constructs became locked on microtubules in the presence of AMPPNP (Figure 3.6, A and B). Expressing all constructs in CAD cells yielded similar results where only the dimeric motor, (1-393)-mCit, accumulated in neurite tips whereas the monomeric motors (1-381)-mCit and (1-369)-mCit showed a diffuse localization and were limited primarily to cell bodies (Figure 3.6 C). These results confirm that the full NC of KIF1A, which confers the ability to dimerize, is required for processive motility in mammalian cells, but not for the ability to bind microtubules.

To investigate the motile characteristics of monomeric and dimeric KIF1A constructs *in vitro* single molecule motility experiments were carried out. Lysates from COS cells expressing (1-393)-3xmCit, (1-381)-3xmCit or (1-369)-3xmCit were added to flow chambers containing polymerized microtubules and motility events were tracked by timelapse TIRF microscopy using 100ms intervals. Again, only motility events that lasted at least 500ms were included in the analyzed data set. As shown before, in Figure 3.3, dimeric (1-393)-3xmCit motors produce a large number of motility events with an average velocity of 1.36 μm/sec and an average run length of 1.24 μm/run (Figure 3.6 D-F). Because the monomeric truncations 1-381 and 1-369 did not show evidence of processive motility *in vivo* (Figure 3.6 C), we were surprised at the number of motility events we observed for these same motors *in vitro* (Figure 3.6 D-F). However, the

number of observed motility events for 1-381 and 1-369 (n=100 and 93 respectively) were significantly reduced as compared to 1-393 (n=376). The velocity and track lengths also differed between the dimeric 1-393 truncation and the monomeric 1-381 and 1-369 truncations. Both monomeric motors consistently moved over shorter distances than the dimeric 1-393, resulting in average track lengths of 0.42 μm for 1-381, and 1.02 μm for 1-369. The velocity profiles where a little more varied, as 1-381 moved at a reduced average speed (0.80 ± 0.04 μm/second), but 1-369 moved at an increased average speed (1.98 ± 0.17 μm/second, Figure 3.6 D-F). Analysis of the velocity histogram for 1-369 reveals a wide variation in measured velocities with no Gaussian distribution characteristic of other processive kinesin motors and the 1-393 velocity data (Figure 3.6 D). The track length histogram for 1-369 (Figure 3.6 E) also deviates from an exponential decay profile likely reflecting the huge variation in velocities.

The rather stringent requirement that motility events had to last at least 500 ms, did exclude a large proportion of motility events that were short in duration, particularly for the monomeric truncations 1-369 and 1-381. In order to better understand monomeric versus dimeric motility mechanisms, we reanalyzed a subset of our single molecule motility assays for the constructs KIF1A (1-369)-3xmCit and KIF1A (1-393)-3xmCit to include motility events lasting at least 300 msec. This analysis included more short motility events, but potentially more false positives as well. Inclusion of the short motility events, resulted in an expected decrease in the average track lengths for both 1-369 and 1-393 (0.65 ± 0.04 μm and 0.90 ± 0.05 μm, respectively; Figure 3.7 C). However, the increase in average velocity was rather surprising (2.19 ± 0.10 μm/second and 1.88 ± 0.07 μm/second, respectively, Figure 3.7 B). Kymographs showing representative motility events for both 1-369 and 1-393 motors are shown in Figure 3.7 A.

Plotting the single molecule velocity and track length data as a function of time spent in 1-directional motility reveals that the motile properties of monomeric KIF1A(1-369) and dimeric KIF1A(1-393) are truly different (Figure 3.7 D and E). Monomeric (1-369)-3xmCit motors spent short periods of time (< 1 sec) moving at a wide variety of speeds, over a broad range of distances (Figure 3.7 D and E, middle left panels, red circles). The fact that the measured velocities vary so widely and the track lengths are

not dependent on the length of time spent in motion suggests that these motors are moving by one-dimensional diffusion. The dimeric construct (1-393)-3xmCit exhibited this same diffusive type of motility for a portion of its motility events (Figure 3.7 D and E, top left panels, red circles), but added a second type of motility where motors spent longer periods of time (>1 sec) moving at a constant speed of ~1.2 μm/second for distances that reflected time spent in motility at this same constant speed (Figure 3.7 D and E, top left panels, blue circles). This second type of motion, moving at a constant speed for longer time periods, was the only type of motility seen for a truncated version of the Kinesin-1 heavy chain subunit, KHC(1-891)-3xmCit, which is known to be a dimeric motor that that utilizes a hand-over-hand motility mechanism to drive its processive motility (Figure 7D, E bottom left panel, blue circle). Taken together, these results indicate that KIF1A(1-393)-3xmCit motors display motile properties characteristic of both single-headed processivity (which is diffusive) and two-headed processivity (which is likely due to a hand-over-hand stepping mechanism).

Dimeric but not monomeric KIF1A motors display ATP-driven processive motility

A key aspect of single-headed processivity is one-dimensional diffusion that relies heavily on a weak binding state to microtubules [22]. This weak binding state occurs when the motor has ADP in its nucleotide pocket. Thus, to distinguish whether monomeric 1-369 and dimeric 1-393 KIF1A motors move by one-dimensional diffusion or another mechanism, we ran the *in vitro* single molecule motility assays in the presence of ADP rather than ATP. The motility profile of monomeric (1-369)-3xmCit motors was not changed in the presence of ADP (compare middle left and right panels of Figure 3.7 D and E); confirming that it moves processively by one-dimensional diffusion (but for relatively short time periods only). In contrast, the motile characteristics of dimeric motors were highly dependent on nucleotide. In the presence of ADP, dimeric KIF1A(1-393) motors continued to display short motility events of various velocities and run length (Figure 3.7 D and E, top right panel, red circles) similar to the monomeric, diffusive 1-369 motors. However, the switch to ADP eliminated the ability of dimeric motors, KIF1A(1-393)-3xmCit and KHC(1-891)-3xmCit, to move for longer periods of time, at a constant velocity and over distances that were dependent on the time spent in

motion (Figures 7 D and E, top and bottom panels, respectively, blue circles). Thus, although KIF1A(1-393) motors are dimers, they can move to some extent by one-dimensional diffusion for short periods of time. However for longer processive motility events, they require their two heads and ATP, reminiscent of other kinesins that use a hand-over hand stepping mechanism.

DISCUSSION

Dimerization of KIF1A

KIF1A/Unc104 motors have long been referred to as monomeric kinesins and indeed, truncated constructs containing only the motor domain do show diffusion mediated, processive motility [16, 21, 22]. The proposal that full-length KIF1A/Unc104 motors are monomeric comes from gel filtration and sucrose density gradient centrifugation experimental that show recombinant and endogenous KIF1A/Unc104 proteins have mobilities that reflect their inherent molecular weight, and not double it, as would be expected if they existed as dimers [2, 17, 19, 24, 37]. Here we have used four different assays that each demonstrates a dimeric state for full-length KIF1A expressed in mammalian cells (chemical crosslinking, co-immunoprecipitation, FRET, and photobleaching). Although these experiments were done with over-expressed proteins, it is unlikely that a monomer-to-dimer switch occurred due to high concentrations, as the crosslinking, co-immunoprecipitation, and photobleaching assays involved significant dilution. Similar methods have been applied to show that other closely related Kinesin-3 family members, specifically, KIF1C and *Dictyostelium* Unc104, are also dimers [17, 28, 29]. Our FRET analysis confirms the compact conformation seen for KIF1A/Unc104 in electron microscopy studies, which leaves open the possibility that this compact conformation impacted the mobility of KIF1A in previous hydrodynamic studies leading to the conclusion that KIF1A/Unc104 was monomeric rather than dimeric as we conclude.

We show that the short NC of KIF1A is sufficient for dimerization and processive motility. Importantly, the full NC and likely several residues C-terminal to the NC are required for this dimerization, as constructs containing only part of the NC were shown to be monomers in our analysis as well as in previous reports [14, 16, 17, 20-22, 30]. The

dimerization and processive motility characteristics of Kinesin-1 are also sufficiently mediated by its NC [38, 39], but its other coiled-coils in the stalk domain also function in dimerization and regulation [10]. Likewise, KIF1A's CC1 and CC2 regions have additional motor regulatory and dimerization functions. This is demonstrated in part by our results showing that truncation of KIF1A after CC1 (or residue 491), results in a primarily monomeric motor that can bind microtubules but cannot move processively. CC1 is thus inhibitory to the dimerization of this particular construct, and consequently, two-headed processive movement. Results from Al- Bassam et al give an explanation for the monomeric conformation of our KIF1A(1-491) as they show by cryo-EM , that a Unc104 construct of similar length formed a parallel intramolecular coil between CC1 and the NC, limiting it to a monomeric state. In a slightly different experimental condition, the CC1 and NC were able to form dimerizing intermolecular coils [40]. As full-length KIF1A and the longer truncation, KIF1A(1-726), were both shown to be dimeric in all of our assays, presence of CC1 must not impose a monomeric conformation on the full-length molecule.

In the full-length molecule, the CC2 domain could function in dimerization and compensate for the NC if it is trapped in an intramolecular coil with CC1 rather than a dimerizing intermolecular coil with its counterpart on a second molecule. The formation of the NC/CC1 intramolecular coil could be a critical autoinhibitory mechanism used to separate and uncoordinated the two motor domains of dimeric KIF1A. A similar case is true for Kinesin-1 where the TPR domains (or for fungal Kinesin-1, the globular tail) unwind the neck coil and physically separate the motor domains [7, 41]. Future work is required to determine if the NC/CC1 intramolecular coil exists in the inhibited, full-length KIF1A motor or whether it is just an artifact of truncation.

Autoinhibition of KIF1A

Autoinhibition is a common regulatory strategy used in diverse biological systems [42, 43]. Autoinhibition of kinesins ensures that in the absence of cargo, motors do not hydrolyze excessive ATP in useless motility. It also allows for temporal and spatial control of motor activity, ensuring kinesins are available and ready when needed for

cargo loading and transport [10, 11]. Auto-inhibition has now been shown to regulate members of the Kinesin-1, Kinesin-2, and Kinesin-3 families [10, 12, 13, 15].

Consistent with previous studies [2, 14-17, 19], we show that full-length KIF1A expressed in mammalian cells is autoinhibited, being incapable of microtubule binding *in vivo* as well as processive motility *in vivo* and *in vitro*. Our work provides the additional conclusion that dimerization is not sufficient for activation. Truncation of KIF1A reveals that two regions mediate this autoinhibited state. First the CC2+FHA region prevents microtubule binding. This is consistent with results from Lee et al, who further showed that neither the FHA domain nor CC2 is sufficient for inhibition. Rather, inhibition requires a direct binding interaction between the FHA domain and CC2. As no direct contact of this FHA/CC2 linkage with the motor was detected, it is unclear how microtubule binding is prevented [15]. Although their evidence is weak, the authors suggest the FHA/CC2 interaction limits dimerization and thus a monomer-to-dimer switch may be important for activating the full-length motor. Our results, however, show that full-length KIF1A, and the KIF1A(1-726) truncation which contains the FHA/CC2 region, are convincing dimers but still inhibited for microtubule binding. Thus dimerization is not sufficient for activation. More structural data is needed to show exactly how the CC2/FHA region prevents microtubule binding. Possibly, the compact conformation of inhibited, dimeric KIF1A, places the motor near these regions, allowing the CC2/FHA linkage to sterically block access to microtubules.

The second region of KIF1A that mediates its autoinhibited state is CC1. Removal of CC1 allows KIF1A(1-393) constructs to not only bind microtubules, but to also move processively along them. This finding is again consistent with the results by Lee et al [15]. We add however that this processive movement is due to a two-motor mechanism, as KIF1A(1-393) constructs labeled individually with mCit or mCherry tags move together in a two-color single molecule motility assay and that constructs truncated after CC1 are prevented from undergoing processive movement due to the fact that they are primarily monomeric. As mentioned above, CC1 probably functions to inhibit the full-length molecule, not by preventing dimerization, but by locally separating and uncoupling the two motor heads.

Mechanisms of KIF1A motility

Understanding the processive motility mechanism used by KIF1A/Unc104 has been complicated by the fact that KIF1A/Unc104's regulatory regions (CC1, FHA, and CC2) all lie very close to the motor domain in primary sequence. In contrast, Kinesin-1's motor domain is well separated from the two regions that mediate its autoinhibited state. One resides at the opposite end of the same subunit (IAK region of KHC tail), and the other is part of a completely separate subunit (TPR domains of KLC) [10]. Thus, processive motility of Kinesin-1 can be seen with very limited truncation of KHC. Indeed, truncating Kinesin-1 at various places along the stalk results in active, processive motors. In order to deal with KIF1A/Unc104's more complicated domain makeup, researchers studying KIF1A/Unc104 have opted to study the processive movement of constructs that contain only the motor domain (sometimes containing a partial NC) or longer constructs that contain either one or both of the CC1 and FHA/CC2 inhibitory regions. This has led to two models for KIF1A motility, first that KIF1A moves processively as a monomer via one-dimensional diffusion along the microtubule [16, 21, 22, 44]; and second, that KIF1A moves processively as a dimer, but requires high local concentrations in order to dimerize [4, 14, 15, 18, 20].

Monomeric Motility. Our data supports the conclusion that monomeric KIF1A constructs have the ability to move processively for short time periods via a one-dimensional diffusion mechanism. Specifically, we show that the motility of monomeric KIF1A(1-369) and (1-381) motors occurs for at a large range of speeds allowing the motor to travel various distances. Additionally, KIF1A monomers can diffuse along the microtubule surface in presence of both ATP and ADP, which is a defining characteristic of the one-dimensional diffusion model of processivity and consistent with previous work [21, 22]. In contrast to our results, previous studies have reported very slow average velocities (0.14μm/sec) and long microtubule dwell times for KIF1A monomeric motors [16, 21, 22]. This discrepancy is likely explained by the fact that our analysis 1) excluded motors that bound to microtubules but did not move and 2) terminated motility events if the motor stopped moving but remained attached to microtubules. Consequently our results reflect the fact that monomeric, diffusion-based motility never lasts more than a few hundred milliseconds. Because monomeric motors move for only

short time periods and as others have reported stall under low loads (0.12 pN) [21], it is unlikely to be sufficient to carry cargos long distances *in vivo*.

KIF1A is rather unique among the Kinesin superfamily because it shows this one-dimensional diffusion. The only other kinesin protein shown to exhibit diffusion along microtubules is Mitotic Centromere Associated Kinesin (MCAK), a member of the Kinesin-13 family [45]. It's reported one-dimensional diffusion is similar to KIF1A in that can be very fast, does not require ATP hydrolysis, and is due to electrostatic interactions between positively charged residues on the motor domains and negatively charged residues on the C-terminal tails of α/β-tubulin [16, 21, 22, 45]. Also like KIF1A, the one-dimensional diffusive motion of MCAK is not thought to contribute to the motor force that drives cellular function but may serve to position and/or tether the motors increasing the probability of a successful event. For KIF1A this tethering could possibly explain why KIF1A dimeric motors have some of the longest reported track lengths in single molecule motility assays, running up to 10 μm in a single motility event, and on average, about double the track length of Kinesin-1 (Figures 3.3 and 3.7 and [20]). Indeed a positive correlation between track length and strength of electrostatic interactions with tubulin was clearly demonstrated by Thorn et al who saw increased processive run lengths with Kinesin-1 after adding positively charged residues to the neck coiled-coil [46].

Dimeric Motility. Although we did see monomeric KIF1A constructs move, we conclude that KIF1A must dimerize for long distance, long lasting, processive motility to occur. KIF1A(1-393) constructs move as dimers, and in the presence of ATP they travel much farther distances at one constant speed (1.36 μm/second) with motility events lasting up to several seconds. This motion occurs with an average velocity and run lengths that are comparable to the motility reported for 1) full-length KIF1A/Unc104 motors in *in vitro* microtubule gliding assays (1.2 μm/sec [2]; 1.7 μm/sec [19], 1.7 μm/sec [20]) and 2) KIF1A/UNC104 driven vesicles *in vivo* (1.0 μm/sec [5, 6]). Thus, the physiological form that drives processive motion of cargoes in cells is likely to be the dimeric motor. We propose the mechanism driving this dimeric processive motility is the conventional hand-over-hand mechanism; yet, we acknowledge that more detailed studies are required to confirm this hypothesis.

Although similar dimeric processivity has been reported previously [20], this is the first time motile properties have been evaluated for a KIF1A/Unc104 construct that is dimerized via its own endogenous sequences without the inclusion of inhibitory domains. Previous studies that utilized constructs with inhibitory regions concluded that high motor concentrations were required to drive KIF1A/Unc104 into a dimeric, active state [18, 20]. It is possible, however, that by including inhibitory domains, high concentrations of motor were necessary to capture enough rare motility events for analysis. Indeed we saw limited motility events for the inhibited but dimeric full-length KIF1A, as well as, the KIF1A(1-726) motor construct which is truncated after CC2. This construct is similar in length to the Unc104(1-653) motor that was used to conclude the necessity for high motor concentrations [18, 20]. Although we cannot directly compare the protein concentrations used in the two cases, our KIF1A(1-393) motor that is dimeric and uninhibited has significantly more motility events when tested at similar expression levels to KIF1A(1-726), proving that motility events for KIF1A(1-726) were primarily limited by the FHA/CC2 region and not protein concentration. In the studies of Klopfenstein et al who used Unc104 motors truncated after CC1 (Unc104(1-446)), high local concentrations may have, indeed, been required to drive the truncated Unc104 motor into a dimeric, active state. By adding the PH domain back to the end of their truncated Unc104(1-446) motor, they could drive the processive motility of $PIP_{4,5}P_2$ containing liposomes. They found that by clustering $PIP_{4,5}P_2$ on membranes by the addition of cholesterol, they increased Unc104's ability to processively move the liposomes. As we and Al-Bassam et al show that the NC and CC1 form an intramolecular coil that limits constructs truncated after CC1 to be monomers, locally concentrating the Unc104(1-446:PH) motor could facilitate a monomer to dimer switch that would allow processive motility of liposomes to occur. As full-length KIF1A can exist as a dimer independent of cargo binding, this "high concentration" model of motor activation may be limited in application. Future studies looking at full-length KIF1A, with real cargo, will be necessary to determine whether or not local concentration of the motor has any role in regulating activity state or processivity.

MATERIALS AND METHODS

Plasmids and antibodies: Full-length or truncated KIF1A constructs tagged with mCit, 3xmCit, or Myc were generated using convenient restriction sites or by PCR amplification from a rat KIF1A cDNA vector (gift of Bruce Schnapp) and cloned into the mCit-N1 or C1 vectors (modified from Clontech's EYFP-N1/C1 vectors by replacing EYFP with sequence for monomeric Citrine) the 3xmCit-N1 vector previously described [31], or the pRK5-myc vector. Rat KIF1A(1-393)-mCit, however, was a gift from Gary Banker. All plasmids were sequence verified. KHC(1-891)-3xmCit has been described previously [31]. The following antibodies were used: Myc (Sigma and 9E10 hybridoma ascites), GFP (used to recognize mCit; Invitrogen), HA (12CA5 hybridoma ascites; used as control IgG) and FLAG (Sigma, used as control IgG).

Cells, transfection and immunoprecipitation: COS and CAD cells were cultured, transfected, and processed for immunofluorescence as previously described (COS, [31]; CAD, [47, 48]. For immunoprecipitation experiments, transfected COS cells were resuspended in lysis buffer (LB; 25 mM Hepes/KOH, 115mM potassium acetate, 5 mM sodium acetate, 5 mM $MgCl_2$, 0.5 mM, EGTA, 1% Triton X-100, and protease inhibitors; pH 7.4); and, after removing insoluble material by centrifugation at 20,000xg at 4°C for 10mins, extracts were incubated with the specified antibodies for 2.5-18 hr at 4°C. Protein A agarose beads were then added and mixture was incubated for and additional 30-60 minutes at 4°C. Beads were pelleted and washed two times with lysis buffer, resuspended in Laemmli sample buffer, and analyzed by SDS-PAGE and Western blot.

Crosslinking: For crosslinking experiments cells were lysed in a Borate buffer (50mM NaBorate, 100mM potassium acetate, 2 mM $MgCl_2$, 1mM EGTA, 1% Triton X-100, and protease inhibitors; pH 8.57). After removing insoluble material by centrifugation, lysates were incubated for 30 minutes with 20 mM dimethylpimilimidate (DMP, Sigma). Lysates were then quenched for 10 minutes with an equal volume of 50mM NH_4Cl_2 in PBS. After adding Laemmli sample buffer, crosslinked lysates were analyzed by SDS-PAGE and Western blot.

In vivo microtubule binding assay: COS cells were plated onto glass-bottomed dishes (MatTek) and transfected with plasmids encoding the proteins of interest.

Twenty-four hours later, cells were viewed on a Nikon TE2000 inverted microscope with a Plan-APO 60X/NA 1.4 objective and Photometrics CS ES2 camera. Cells were treated with 0.1 μg/ml Streptolysin O in permeabilization buffer 1 (25 mM Hepes/KOH, 115mM potassium acetate, 5 mM sodium acetate, 5 mM $MgCl_2$, 0.5 mM, EGTA, and 10mg/ml BSA; pH 7.4) for 1 min. After washing 3 times with Buffer 1, cells were incubated with Buffer 1 containing 2mM AMPPNP. Cells were monitored every minute for an additional 15 minutes.

The Relocation Index was calculated on a frame by frame basis using ImageJ as described [7]. Briefly two image masks were made from the last timelapse frame encompassing either the microtubule region (MT) or the rest of the cell, excluding the nucleus and regions of aggregated motor (Other). The total fluorescence pixel intensities—Sum_{MT} and Sum_{Other}—was determined and a ratio (R) of Sum_{MT} over Sum_{Other} was calculated for each frame. The Relocation index for each frame is defined as the percent change of R as compared with R before the addition of AMPPNP.

FRET stoichiometry: FP-tagged versions of KIF1A or RnKHC (RnKIF5C) were transfected into COS cells. 24 hours later, cells were viewed on wide-field microscope equipped for FRET stoichiometry. FRET stoichiometry uses three fluorescence images from a calibrated microscope to calculate three parameters that describe each pixel: (a) R_M, the mole ratio of acceptor- to donor-labeled proteins, (b) E_A, the apparent acceptor FRET efficiency (FRET efficiency x fraction of acceptor molecules in complex), and (c) E_D, the apparent donor FRET efficiency (FRET efficiency x fraction of donor molecules in complex). Because protein expression levels influence the fraction of donor or acceptor molecules in FRET complex for non-linked molecules, we analyzed cells with R_M close to 1.0 and we calculated an average FRET efficiency, E_{AVE} = (ED + EA)/2, which is less sensitive to expression ratio [33, 34].

In vitro single molecule motility assays and photobleaching analysis: Motility and photobleaching assays were performed in flow chambers created from a 25x25 #1.5 coverglass and microtubule slide assembled with double-sided tape (~30ul chamber volume). Cy5-labeled microtubules in BRB80 buffer (80mM Pipes/KOH, 1mM EGTA, and 2mM $MgCl_2$; pH 6.8) with 10μM taxol were flowed into the chamber, followed by addition of 40ul of 0.1mg/ml casein/BRB80 to coat the chamber surfaces. After 5-10 minutes, chambers were washed twice in P12 buffer (12 mM Pipes/KOH, 1 mM EGTA,

and 2 mM $MgCl_2$, pH 6.8) with 10 μM taxol. Motor proteins were prepared by lysing transfected COS cells in LB with 1mM ATP. Lysates were cleared by centrifugation at 20,000xg for 10mins and then flash-frozen by immersion in liquid nitrogen and stored at -80°C. 0.25-1μl cell lysate was added to flow-chambers with 50 μl of oxygen scavenger buffer (1 mM DTT, 1 mM $MgCl_2$, 2 mM ATP, 10 mM glucose, 0.1 mg/ml glucose oxidase, 0.08 mg/ml catalase, 10 mg/ml BSA, and 10 μM taxol in P12; however, in photobleaching experiments or motility experiments performed with ADP, the 2mM ATP was replaced by 2mM AMPPNP or 2mM ADP respectively). Then, the chamber was sealed with wax and assayed for motility or photobleaching using objective-type total internal reflection fluorescence microscopy (TIRFM) on a custom-modified microscope (Axiovert 135TV; Carl Zeiss MicroImaging, Inc.) equipped with an 1.45 NA α-plan Fluor objective, 2.5x optovar, 505DCXR dichroic and ET510LP emission filters, and a back-illuminated EMCCD camera (Cascade 512B; Roper Scientific). The 488-nm line of a tunable, single-mode, fiber-coupled argon ion laser (Melles Griot) was used for streaming images every 100ms for 30-35 second. For two-color TIRFM, a second 594 nm laser diode was coupled with the 488nm laser (535DCXR) for excitation. mCit and mCherry fluorescence emissions were first passed though a FT505/590 dual-band dichroic mirror and then projected separately onto each halves of the CCD camera by a Dualview beam-splitter (Optic Insights) equipped with a FT498 dichroic and HQ540/70M and HQ610LP emission filters (Filters are all from Chroma Technology Corp).

All of the fluorescence imaging analysis, including FRET, Relocation Index, single molecule tracking in one or two-colors, and single molecule photobleaching were analyzed using home made plug-ins written for ImageJ (NIH). Single molecule tracking measurements for each construct come from at least two independent protein preparations and include motile events lasting at least 0.5 or 0.3 seconds. For photobleaching, only stationary, diffraction-limited fluorescence spots that were well separated from neighboring spots were included in analysis. Fluorescence intensity (with background intensity subtracted) was measured as described previously [31] and plotted as a function of time. Bleaching steps were determined using these individual plots.

FIGURES

Figure 3.1: Full-length KIF1A exists as a dimeric motor that is inactive for microtubule binding *in vivo*. (A and B) Live cell microtubule binding assay. COS cells expressing full-length KIF1A tagged with mCit were imaged while permeabilized with SLO and treated with AMPPNP. (A) Still images from a movie, before and after AMPPNP treatment. (B) Quantification of the percentage of KIF1A fluorescence that changes from a cytoplasmic localization to a microtubule (MT)-associated localization (Relocation Index; see materials and methods for details) over time. N=16 cells. Error bars +/- SEM. (C) Co-immunoprecipitation. COS cells were co-transfected with plasmids encoding mCit-KIF1A and Myc-KIF1A, or mCit-KIF1A-CFP and myc-KIF1A. Lysates were immunoprecipitated with an anti-Myc antibody or control IgG antibody, separated by SDS-PAGE, and immunoblotted with anti-Myc and anti-mCit antibodies. (D) Crosslinking. Lysates from COS cells over-expressing mCit-KIF1A, mCit-KHC, or mCit were treated with or without DMP, then separated by SDS-PAGE, and immunoblotted with anti-mCit antibodies. (E) Motor to motor FRET in COS cells expressing mCit-KIF1A and CFP-KIF1A (top panels); or Kinesin-1 (mCit-KHC + CFP-KHC + HA-KLC). (G) Motor to tail FRET in live COS cells expressing mCit-KIF1A-CFP and myc-KIF1A (top panels); or Kinesin-1 (mCit-KHC-CFP + Myc-KHC + HA-KLC) (bottom panels). (F and H) Average FRET efficiency (Eave) is quantitated. Error bars +/- SEM. Acknowledgements: Lynne Blasius from the Verhey lab contributed the crosslinking data in (D). The FRET data (E-H) was contributed by Dawen Cai also from the Verhey lab.

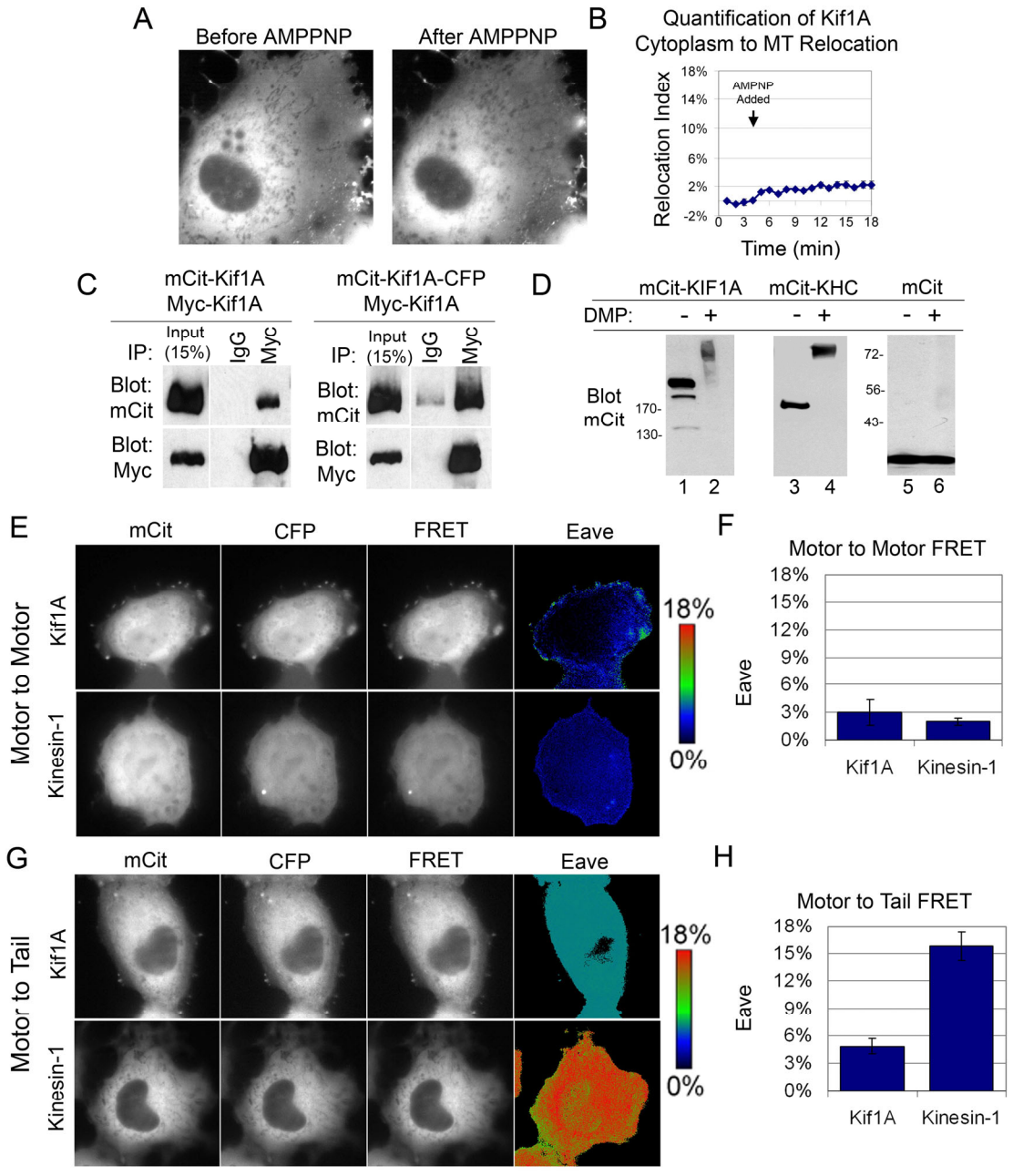
A
Before AMPPNP
After AMPPNP
B
Quantification of Kif1A
Cytoplasm to MT Relocation
Relocation Index
18%
14%
10%
6%
2%
-2%
AMPNP
Added
0 3 6 9 12 15 18
Time (min)
C
mCit-Kif1A
Myc-Kif1A
mCit-Kif1A-CFP
Myc-Kif1A
IP:
Input (15%)
IgG
Myc
Blot: mCit
Blot: Myc
D
mCit-KIF1A
mCit-KHC
mCit
DMP:
- +
- +
- +
Blot mCit
170-
130-
72-
56-
43-
1 2 3 4 5 6
E
mCit
CFP
FRET
Eave
Motor to Motor
Kif1A
Kinesin-1
18%
0%
F
Motor to Motor FRET
Eave
18%
15%
12%
9%
6%
3%
0%
Kif1A
Kinesin-1
G
mCit
CFP
FRET
Eave
Motor to Tail
Kif1A
Kinesin-1
18%
0%
H
Motor to Tail FRET
Eave
18%
15%
12%
9%
6%
3%
0%
Kif1A
Kinesin-1

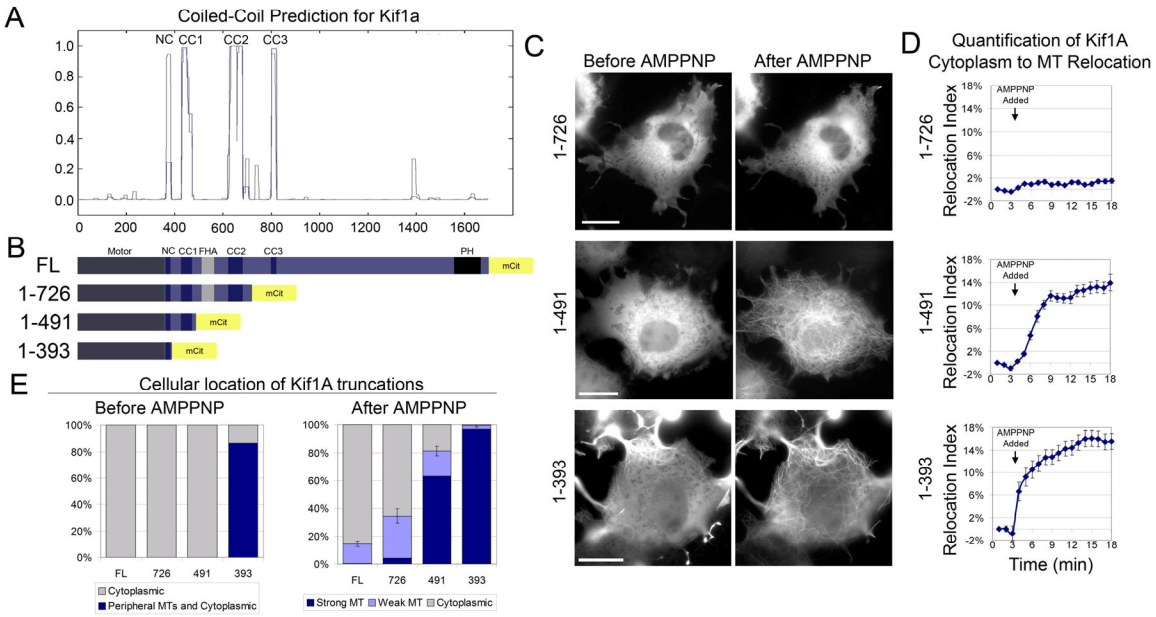

Figure 3.2: Truncated of KIF1A relieves autoinhibition of microtubule binding. (A) Coiled-coil prediction for KIF1A (NP_032466); Gray dotted line, prediction using a window of 14 amino acids; Blue line, prediction using a window of 21 amino acids (COILS, Lupas Method). NC, Neck coiled-coil; CC1-3, coiled-coil 1-3. (B) Schematic of mCit tagged full-length (FL) and truncated KIF1A constructs. (C-E) Live cell microtubule binding assay. COS cells expressing truncated KIF1A constructs were imaged while permeabilized with SLO and treated with AMPPNP. (C) Still images from movies taken before and after AMPPNP treatment. Scale 20µm. (D) Quantification of the average percentage of KIF1A fluorescence that changes from a cytoplasmic localization to a microtubule (MT) associated localization (Relocation Index) over time. Error bars +/- SEM. 1-726, N=17; 1-491, N=11; 1-393, N=12. (E) Percent of cells whose KIF1A truncations localize to the indicated cellular locations before and after AMPPNP treatment. Averages from 3-5 independent experiments; 50-100 cells each. Error bars +/- SEM. MT, microtubules.

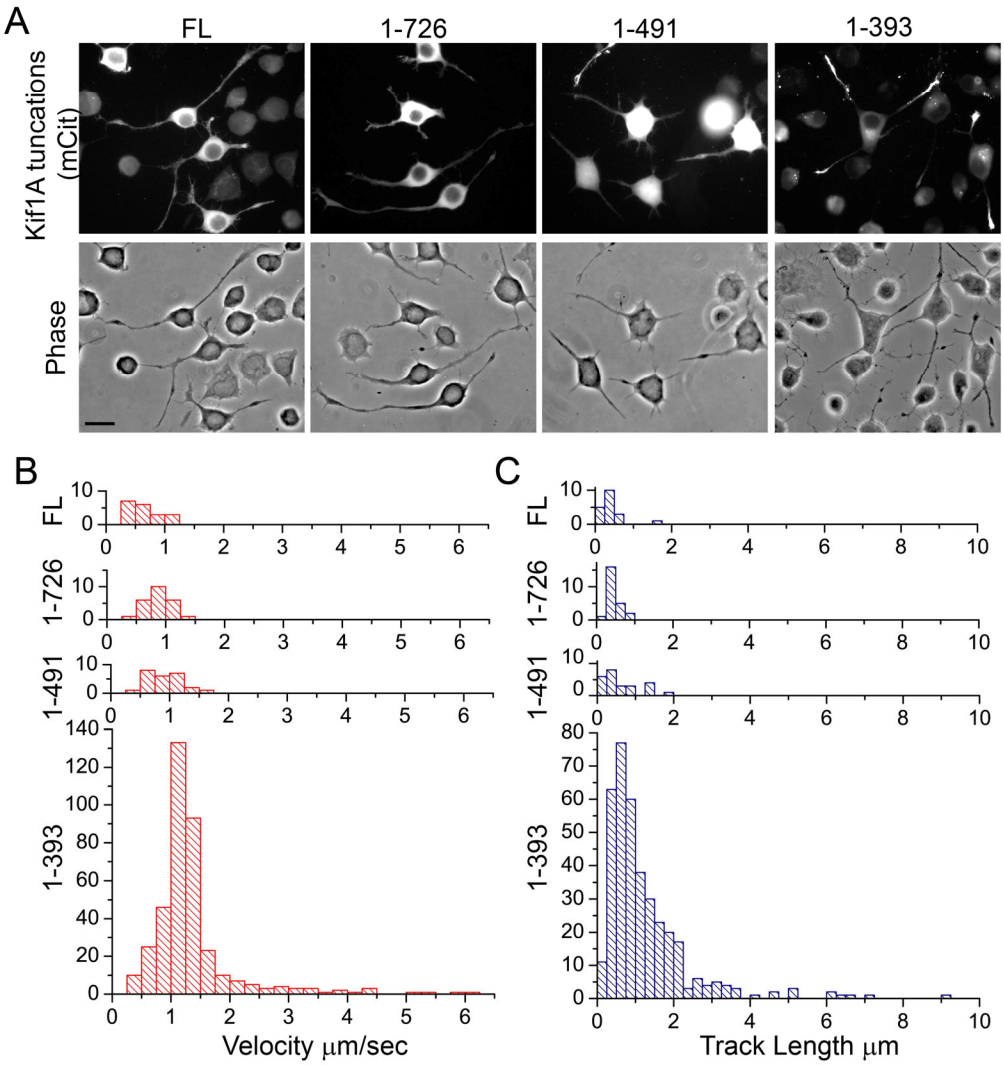

D

Kif1A Construct	Number of Tracks	Average Velocity μm/sec	Average Track Length μm	Neurite Accumulation
FL	19	0.65 +/- .06	0.44 +/- .08	No
1-726	24	0.85 +/- .04	0.43 +/- .03	No
1-491	25	0.89 +/- .06	0.65 +/- .09	No
1-393	376	1.36 +/- .04	1.24 +/- .06	Yes

Figure 3.3: Processive motility of truncated KIF1A constructs. (A) Processive motility *in vivo*. CAD cells were transfected with full-length (FL) or truncated KIF1A constructs and differentiated for 40-48 hrs. Representative images are shown. Scale 20μm. (B-D) Processive motility *in vitro*. COS cells were transfected with 3xmCit tagged FL or truncated KIF1A constructs. Motor proteins in cell lysates were incubated with Taxol-stabilized microtubules and single molecule assays were carried out using a TIRF microscope. (B) Velocity histograms. (C) Track length histograms. (D) Table of motile properties, Average +/- SEM.

Figure 3.4: KIF1A truncations dimerize and KIF1A(1-393) moves processively as a dimer. (A) Crosslinking. Western blot of lysates from COS cells expressing Myc-tagged KIF1A truncations 1-393, 1-491, and 1-726 treated with or without DMP. Arrows indicate bands of reduced mobility upon crosslinking, arrowheads and construct labels refer to band sizes in the absence of DMP. (B) Co-immunoprecipitation. COS cells were co-transfected with plasmids encoding Myc and mCit tagged KIF1A constructs of the same length. Lysates were analyzed by western blot either directly (input lysate) or after immunoprecipitation with anti-Myc or control IgG antibodies. (C and D) Photobleaching analysis of 3xmCit-labeled KIF1A motors. Lysates from COS cells expressing 3xmCit tagged FL or truncated constructs were either locked onto microtubules with AMPPNP or absorbed directly to the coverglass of the flow chamber then imaged with TIRF microscopy. (C) Distribution of the number of photobleaching steps for each KIF1A construct or a dimeric truncated Kinesin-1 construct, KHC(1-891). (D) Representative examples of the stepwise photobleaching occurring over time for 3xmCit-KIF1A or Kinesin-1 fluorescent spots located within the light-diffraction-limit. AU, arbitrary units. (E and F) Two-color single molecule motility assay. COS cells were co-transfected with 3xmCit- and 3xmCherry tagged KIF1A(1-393) plasmids. Lysates containing labeled motors were then subjected to a two-color *in vitro* single molecule motility assay. Kymograph of a representative dual-labeled/dimerized KIF1A(1-393) motor moving along a microtubule. (H) Table indicating the number and average spot intensities of dual-labeled (mCit and mCherry) or single-labeled (mCit only) motile tracks detected in two-color single molecule motility assays.
Acknowledgements: The crosslinking data in (A) was contributed by Lynne Blasius, Verhey Lab.

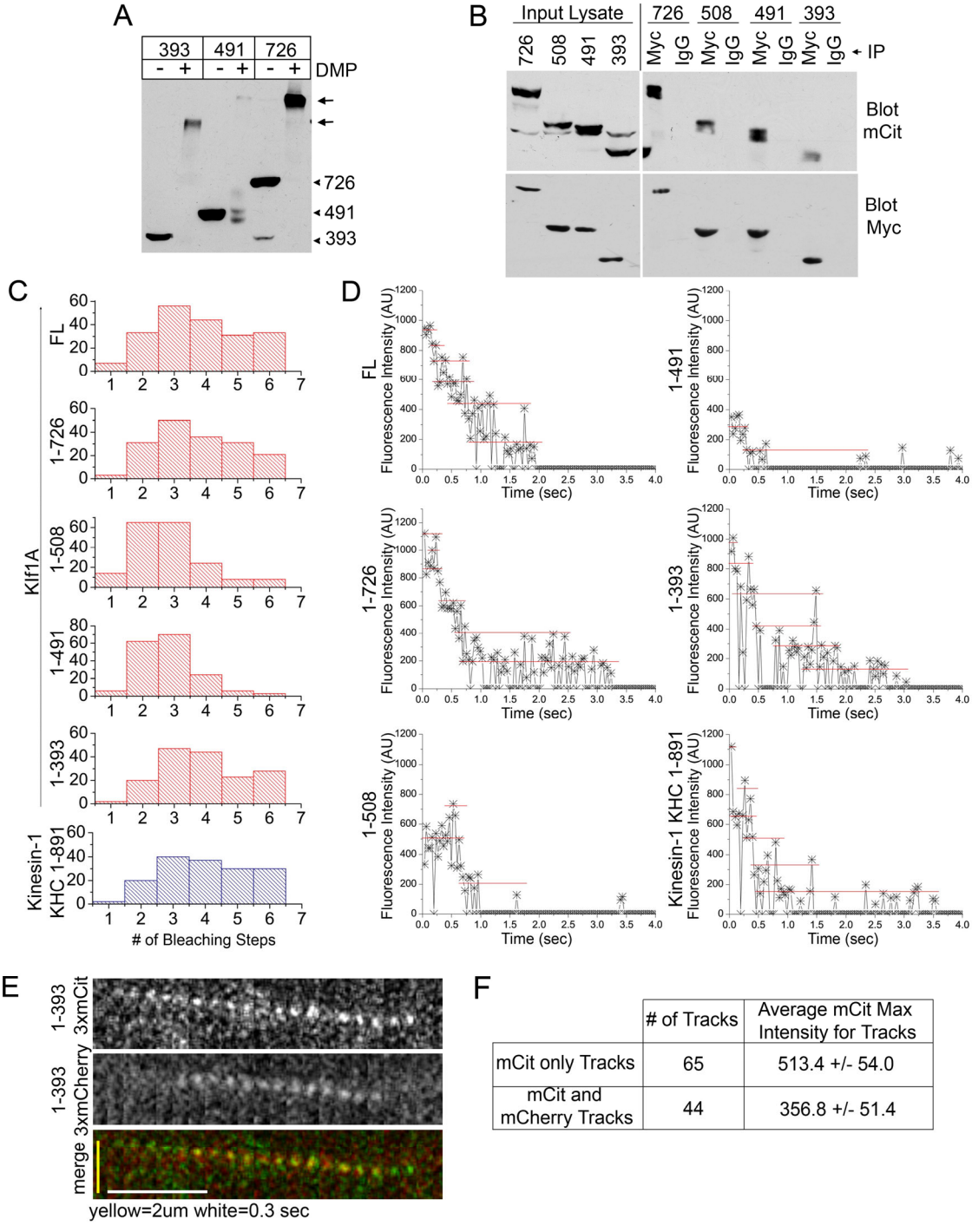

	# of Tracks	Average mCit Max Intensity for Tracks
mCit only Tracks	65	513.4 +/- 54.0
mCit and mCherry Tracks	44	356.8 +/- 51.4

Figure 3.5: The full neck coil (NC) and adjacent residues are required for dimerization of KIF1A. (A) Sequence comparisons of the region around the NC of the KIF1A/Unc104 family. Identical residues are in red; similar residues are in orange. Below the sequence comparison is a schematic of KIF1A constructs containing all or portions of the NC with reference to equivalent KIF1A or Unc104 constructs used in previous studies. (B) Crosslinking. Lysates from COS cells overexpressing Myc-tagged NC truncations were treated with or without DMP, separated by SDS-PAGE, and immunoblotted with anti-Myc antibodies. Arrow shows the dimer-sized band formed only by the longest construct 1-393. (C and D) Photobleaching analysis of 3xmCit-labeled NC constructs by TIRF microscopy. (C) Histogram of the number of photobleaching steps for each 3xmCit tagged NC construct. (D) Representative examples of the stepwise photobleaching occurring over time for 3xmCit-truncated KIF1A fluorescent spots located within the light-diffraction-limit. AU, arbitrary units. Acknowledgement: Kristen Verhey compiled the alignment and construct schematic in (A). Lynne Blasius of the Verhey lab contributed the crosslinking data in (B).

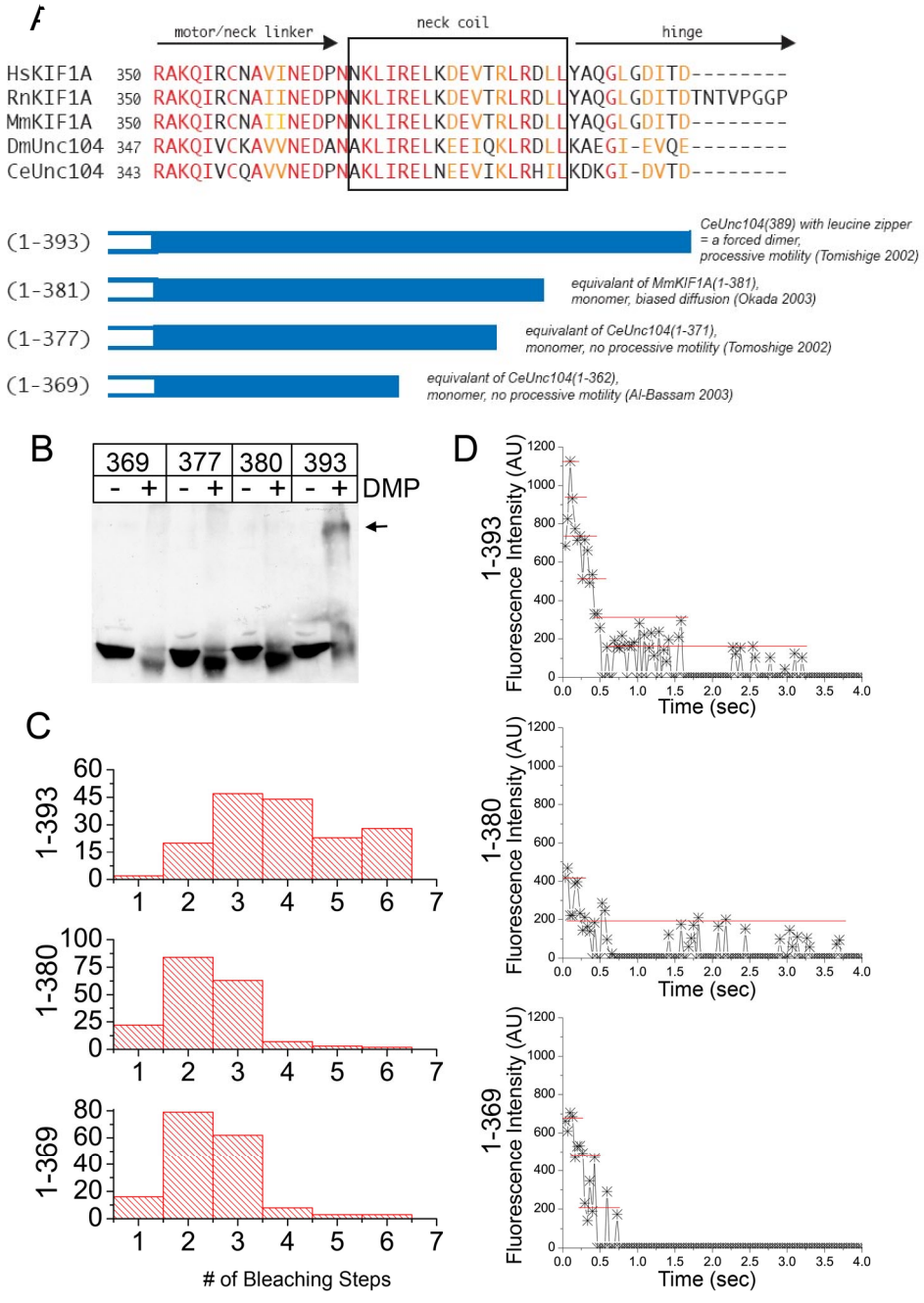
A
motor/neck linker
neck coil
hinge
HsKIF1A 350 RAKQIRCNAVINEDPNNKLIRELKDEVTRLRDLLYAQGLGDITD--------
RnKIF1A 350 RAKQIRCNAIINEDPNNKLIRELKDEVTRLRDLLYAQGLGDITDTNTVPGGP
MmKIF1A 350 RAKQIRCNAIINEDPNNKLIRELKDEVTRLRDLLYAQGLGDITD--------
DmUnc104 347 RAKQIVCKAVVNEDANAKLIRELKEEIQKLRDLLKAEGI-EVQE--------
CeUnc104 343 RAKQIVCQAVVNEDPNAKLIRELNEEVIKLRHILKDKGI-DVTD--------
(1-393)
CeUnc104(389) with leucine zipper = a forced dimer, processive motility (Tomishige 2002)
(1-381)
equivalant of MmKIF1A(1-381), monomer, biased diffusion (Okada 2003)
(1-377)
equivalant of CeUnc104(1-371), monomer, no processive motility (Tomoshige 2002)
(1-369)
equivalant of CeUnc104(1-362), monomer, no processive motility (Al-Bassam 2003)
B
369 377 380 393
- + - + - + - +
DMP
C
1-393
1-380
1-369
# of Bleaching Steps
D
1-393
1-380
1-369
Fluorescence Intensity (AU)
Time (sec)

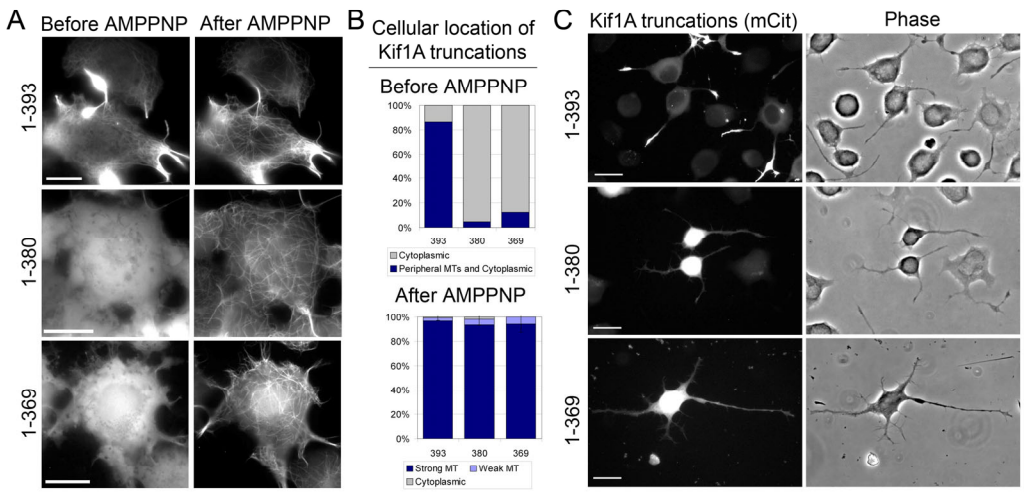

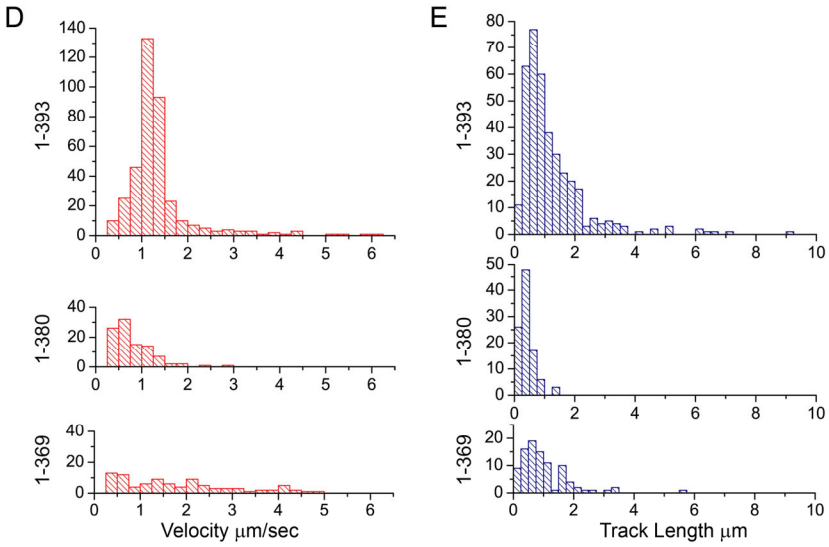

F

Kif1A Construct	Number of Tracks	Average Velocity μm/sec	Average Track Length μm	Neurite Accumulation
1-393	376	1.36 +/- 0.04	1.24 +/- 0.06	Yes
1-380	100	0.80 +/- 0.04	0.42 +/- 0.02	No
1-369	93	1.98 +/- 0.17	1.02 +/- 0.09	No

Figure 3.6: Long-distance processive motility, but not microtubule binding, requires KIF1A dimerization. (A-B) Live cell microtubule binding assay. COS cells expressing truncated KIF1A constructs were imaged during SLO permeabilization and AMPPNP treatment. (A) Representative before and after AMPPNP treatment images shown. Scale 20μm. (B) Percent of cells whose NC constructs localize to the indicated cellular locations before and after AMPPNP treatment. Averages from 2-3 independent experiments; ~50 cells each. Error bars +/- SEM. MT, microtubules. (C) *In vivo* processive motility assay. CAD cells were transfected with truncated KIF1A constructs and differentiated for 40-48 hrs. Scale 20μm. (D-F) *In vitro* single molecule motility assay. COS cells were transfected with 3xmCit tagged truncated NC constructs. Motor proteins in cell lysates were incubated with Taxol-stabilized microtubules in a flow chamber and assayed with TIRF microscopy for motility. Images were taken every 100ms and measurements include motile events lasting at least 0.5 seconds. (D) Distribution of velocities. (E) Track length distribution. (F) Table of motile properties, mean+/-SEM.

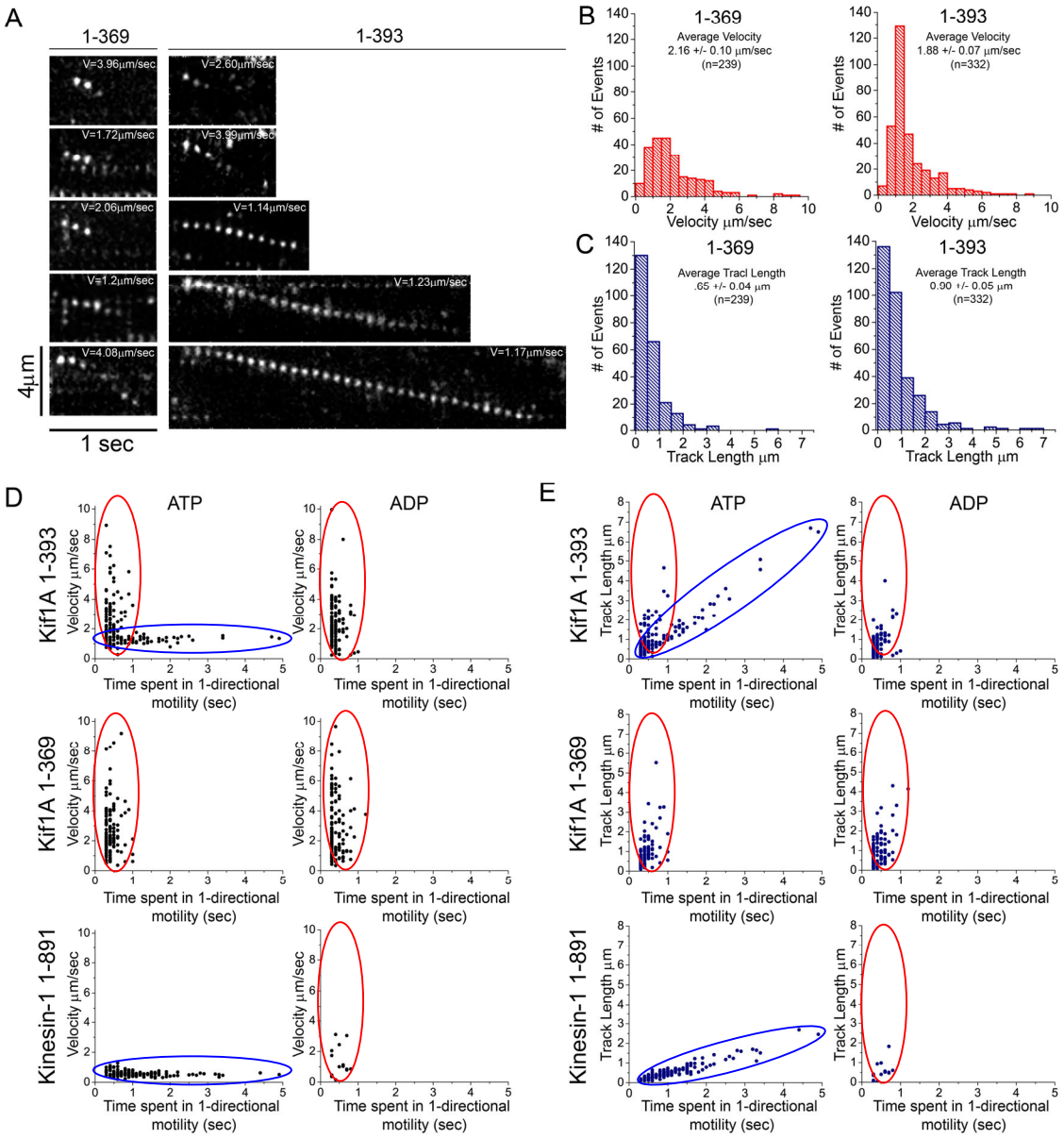

Figure 3.7: ATP-dependent processive motility is a property of dimeric but not monomeric KIF1A motors. (A-E) *In vitro* single molecule motility assay. COS cells were transfected with dimeric (1-393)-3xmCit or monomeric (1-369)-3xmCit KIF1A constructs. Motor proteins in cell lysates along with 1mM ATP were incubated with Taxol-stabilized microtubules in a flow chamber and assayed with TIRF microscopy for motility. Images were taken every 0.1 seconds and measurements include motile events lasting at least 0.3 seconds. (A) Representative kymographs. (B) Velocity histograms. (C) Track Length histograms. (D and E) Comparison of monomeric and dimeric motile properties in the presence of ATP or ADP. Distribution of velocities (D) or Track Lengths (E) for KIF1A(1-393), (1-369), or Kinesin-1, KHC(1-891) in the presence of ATP or ADP as a function of time spent in 1-directional motility.

REFERENCES

1. Hall, D.H. and E.M. Hedgecock, *Kinesin-related gene unc-104 is required for axonal transport of synaptic vesicles in C. elegans.* Cell, 1991. **65**(5): p. 837-47.
2. Okada, Y., et al., *The neuron-specific kinesin superfamily protein KIF1A is a unique monomeric motor for anterograde axonal transport of synaptic vesicle precursors.* Cell, 1995. **81**(5): p. 769-80.
3. Yonekawa, Y., et al., *Defect in synaptic vesicle precursor transport and neuronal cell death in KIF1A motor protein-deficient mice.* J Cell Biol, 1998. **141**(2): p. 431-41.
4. Klopfenstein, D.R. and R.D. Vale, *The lipid binding pleckstrin homology domain in UNC-104 kinesin is necessary for synaptic vesicle transport in Caenorhabditis elegans.* Mol Biol Cell, 2004. **15**(8): p. 3729-39.
5. Lee, J.R., et al., *Characterization of the movement of the kinesin motor KIF1A in living cultured neurons.* J Biol Chem, 2003. **278**(4): p. 2624-9.
6. Zhou, H.M., I. Brust-Mascher, and J.M. Scholey, *Direct visualization of the movement of the monomeric axonal transport motor UNC-104 along neuronal processes in living Caenorhabditis elegans.* J Neurosci, 2001. **21**(11): p. 3749-55.
7. Cai, D., et al., *Kinesin-1 structural organization and conformational changes revealed by FRET stoichiometry in live cells.* J Cell Biol, 2007. **176**(1): p. 51-63.
8. Dietrich, K.A., et al., *The kinesin-1 motor protein is regulated by a direct interaction of its head and tail.* Proc Natl Acad Sci U S A, 2008. **105**(26): p. 8938-43.
9. Hackney, D.D. and M.F. Stock, *Kinesin Tail Domains and Mg(2+) Directly Inhibit Release of ADP from Head Domains in the Absence of Microtubules.* Biochemistry, 2008.
10. Adio, S., et al., *Review: regulation mechanisms of Kinesin-1.* J Muscle Res Cell Motil, 2006. **27**(2): p. 153-60.
11. Cross, R. and J. Scholey, *Kinesin: the tail unfolds.* Nat Cell Biol, 1999. **1**(5): p. E119-21.
12. Imanishi, M., et al., *Autoinhibition regulates the motility of the C. elegans intraflagellar transport motor OSM-3.* J Cell Biol, 2006. **174**(7): p. 931-7.
13. Yamada, K.H., T. Hanada, and A.H. Chishti, *The effector domain of human Dlg tumor suppressor acts as a switch that relieves autoinhibition of kinesin-3 motor GAKIN/KIF13B.* Biochemistry, 2007. **46**(35): p. 10039-45.
14. Al-Bassam, J., et al., *Distinct conformations of the kinesin Unc104 neck regulate a monomer to dimer motor transition.* J Cell Biol, 2003. **163**(4): p. 743-53.
15. Lee, J.R., et al., *An intramolecular interaction between the FHA domain and a coiled coil negatively regulates the kinesin motor KIF1A.* EMBO J, 2004. **23**(7): p. 1506-15.

16. Okada, Y. and N. Hirokawa, *A processive single-headed motor: kinesin superfamily protein KIF1A.* Science, 1999. **283**(5405): p. 1152-7.

17. Rashid, D.J., et al., *Monomeric and dimeric states exhibited by the kinesin-related motor protein KIF1A.* J Pept Res, 2005. **65**(6): p. 538-49.

18. Klopfenstein, D.R., et al., *Role of phosphatidylinositol(4,5)bisphosphate organization in membrane transport by the Unc104 kinesin motor.* Cell, 2002. **109**(3): p. 347-58.

19. Pierce, D.W., et al., *Single-molecule behavior of monomeric and heteromeric kinesins.* Biochemistry, 1999. **38**(17): p. 5412-21.

20. Tomishige, M., D.R. Klopfenstein, and R.D. Vale, *Conversion of Unc104/KIF1A kinesin into a processive motor after dimerization.* Science, 2002. **297**(5590): p. 2263-7.

21. Okada, Y., H. Higuchi, and N. Hirokawa, *Processivity of the single-headed kinesin KIF1A through biased binding to tubulin.* Nature, 2003. **424**(6948): p. 574-7.

22. Okada, Y. and N. Hirokawa, *Mechanism of the single-headed processivity: diffusional anchoring between the K-loop of kinesin and the C terminus of tubulin.* Proc Natl Acad Sci U S A, 2000. **97**(2): p. 640-5.

23. Yildiz, A. and P.R. Selvin, *Kinesin: walking, crawling or sliding along?* Trends Cell Biol, 2005. **15**(2): p. 112-20.

24. Otsuka, A.J., et al., *The C. elegans unc-104 gene encodes a putative kinesin heavy chain-like protein.* Neuron, 1991. **6**(1): p. 113-22.

25. Kikkawa, M., Y. Okada, and N. Hirokawa, *15 A resolution model of the monomeric kinesin motor, KIF1A.* Cell, 2000. **100**(2): p. 241-52.

26. Kikkawa, M., et al., *Switch-based mechanism of kinesin motors.* Nature, 2001. **411**(6836): p. 439-45.

27. Klopfenstein, D.R., E.A. Holleran, and R.D. Vale, *Kinesin motors and microtubule-based organelle transport in Dictyostelium discoideum.* J Muscle Res Cell Motil, 2002. **23**(7-8): p. 631-8.

28. Pollock, N., et al., *Reconstitution of membrane transport powered by a novel dimeric kinesin motor of the Unc104/KIF1A family purified from Dictyostelium.* J Cell Biol, 1999. **147**(3): p. 493-506.

29. Dorner, C., et al., *The kinesin-like motor protein KIF1C occurs in intact cells as a dimer and associates with proteins of the 14-3-3 family.* J Biol Chem, 1999. **274**(47): p. 33654-60.

30. Shimizu, Y., et al., *Stalk region of kinesin-related protein Unc104 has moderate ability to form coiled-coil dimer.* Biochem Biophys Res Commun, 2005. **337**(3): p. 868-74.

31. Cai, D., K.J. Verhey, and E. Meyhofer, *Tracking single Kinesin molecules in the cytoplasm of mammalian cells.* Biophys J, 2007. **92**(12): p. 4137-44.

32. Kawaguchi, K. and S. Ishiwata, *Nucleotide-dependent single- to double-headed binding of kinesin.* Science, 2001. **291**(5504): p. 667-9.

33. Beemiller, P., A.D. Hoppe, and J.A. Swanson, *A phosphatidylinositol-3-kinase-dependent signal transition regulates ARF1 and ARF6 during Fcgamma receptor-mediated phagocytosis.* PLoS Biol, 2006. **4**(6): p. e162.

34. Hoppe, A., K. Christensen, and J.A. Swanson, *Fluorescence resonance energy transfer-based stoichiometry in living cells.* Biophys J, 2002. **83**(6): p. 3652-64.

35. Jacobson, C., B. Schnapp, and G.A. Banker, *A change in the selective translocation of the Kinesin-1 motor domain marks the initial specification of the axon.* Neuron, 2006. **49**(6): p. 797-804.

36. Nakata, T. and N. Hirokawa, *Microtubules provide directional cues for polarized axonal transport through interaction with kinesin motor head.* J Cell Biol, 2003. **162**(6): p. 1045-55.

37. Nangaku, M., et al., *KIF1B, a novel microtubule plus end-directed monomeric motor protein for transport of mitochondria.* Cell, 1994. **79**(7): p. 1209-20.

38. Morii, H., et al., *Identification of kinesin neck region as a stable alpha-helical coiled coil and its thermodynamic characterization.* Biochemistry, 1997. **36**(7): p. 1933-42.

39. Tripet, B., R.D. Vale, and R.S. Hodges, *Demonstration of coiled-coil interactions within the kinesin neck region using synthetic peptides. Implications for motor activity.* J Biol Chem, 1997. **272**(14): p. 8946-56.

40. Al-Bassam, J., et al., *Analysis of the weak interactions of ADP-Unc104 and ADP-kinesin with microtubules and their inhibition by MAP2c.* Cell Motil Cytoskeleton, 2007. **64**(5): p. 377-89.

41. Bathe, F., et al., *The complex interplay between the neck and hinge domains in kinesin-1 dimerization and motor activity.* Mol Biol Cell, 2005. **16**(8): p. 3529-37.

42. Pufall, M.A. and B.J. Graves, *Autoinhibitory domains: modular effectors of cellular regulation.* Annu Rev Cell Dev Biol, 2002. **18**: p. 421-62.

43. Schlessinger, J., *Signal transduction. Autoinhibition control.* Science, 2003. **300**(5620): p. 750-2.

44. Nitta, R., et al., *KIF1A alternately uses two loops to bind microtubules.* Science, 2004. **305**(5684): p. 678-83.

45. Helenius, J., et al., *The depolymerizing kinesin MCAK uses lattice diffusion to rapidly target microtubule ends.* Nature, 2006. **441**(7089): p. 115-9.

46. Thorn, K.S., J.A. Ubersax, and R.D. Vale, *Engineering the processive run length of the kinesin motor.* J Cell Biol, 2000. **151**(5): p. 1093-100.

47. Blasius, T.L., et al., *Two binding partners cooperate to activate the molecular motor Kinesin-1.* J Cell Biol, 2007. **176**(1): p. 11-7.

48. Verhey, K.J., et al., *Cargo of kinesin identified as JIP scaffolding proteins and associated signaling molecules.* J Cell Biol, 2001. **152**(5): p. 959-70.

Chapter 4:
Cooperative Versus Independent Transport of Different Cargoes by Kinesin-1

Motor proteins of the kinesin, myosin, and dynein families utilize the energy of ATP hydrolysis to transport organelles, membrane vesicles, and protein complexes along the cytoskeleton in order to organize cellular components for proper cell morphology and function [1, 2]. Critical to understanding the cellular roles of motor proteins is deciphering how motors attach to specific cargoes. Recent work has identified multiple binding partners for individual motor proteins. In some cases, these binding partners are soluble adaptor proteins that mediate the attachment of motor proteins to membrane-bound cargoes [2, 3]. How motor proteins distinguish cargo partners and bind to specific cargoes at specific times and cellular locations is unknown.

The founding member of the kinesin superfamily, Kinesin-1 (formerly conventional kinesin or Kif5), is a heterotetramer composed of two kinesin heavy chain (KHC) and two kinesin light chain (KLC) subunits. Both KHC and KLC have been implicated in cargo binding [4, 5]. For KLC, most cargoes bind to the TPR bundle, although a role for the alternatively spliced C-terminal sequences has also been demonstrated [6, 7]. TPR bundles are protein-protein interaction domains comprised of tandem TPR motifs. Each TPR motif contains a degenerate 34-amino acid repeat arranged in two antiparallel α-helices linked by a tight turn. Adjacent TPR motifs then pack against each other to form a half-cylindrical bundle [8, 9]. Structural and biochemical analyses of the protein-protein interactions mediated by TPR domains have described two distinct mechanisms for partner protein binding. In several cases, the extreme C-terminal residues of the binding partner have been shown to bind in an extended conformation to the concave face (groove) of the TPR domain [10-12]. Alternatively, internal sequences of the partner protein can bind to the loop regions that connect helices on the edge of the TPR bundle [13]. Thus, target recognition by TPR domains is likely to be versatile and may enable the assembly of multi-protein

complexes. Such an assembly function has been proposed for structurally similar helical repeat domains such as armadillo repeats, ankyrin repeats and 14-3-3 proteins [14-17].

The first cargo proteins identified to bind Kinesin-1 via the TPR bundle were the c-Jun NH_2-terminal kinase (JNK)-interacting protein (JIP) group of scaffold proteins [18-20]. Based on their sequence similarities, JIP's can be divided into two classes [21]. JIP1 (also called islet brain 1) and JIP2 share a similar domain structure consisting of an N-terminal JNK-binding domain and C-terminal SH3 and PTB domains. JIP3 (also known as JSAP1) and JIP4 (also known as JLP) contain a JNK-binding domain and several coiled-coil domains. Despite this disparity in domain structure, the JIP proteins function as scaffolding proteins to coordinate the cellular localization and activity of JNK signaling complexes [21]. Interestingly, the extreme C-terminal sequences of JIP1 and JIP2 are required for binding to the TPR bundle of KLC whereas internal segments of JIP3 and JIP4 are required for KLC binding [18, 20, 22, 23], suggesting that JIP1 binds in the TPR groove whereas JIP3 binds outside of the TPR groove. Through their interactions with Kinesin-1, the JIP proteins likely also play a critical role in membrane trafficking as loss-of-function alleles of JIP homologs in *C. elegans* and *Drosophila* cause defects in axonal transport with phenotypes similar to KHC loss-of-function alleles [18, 24, 25].

In recent years, other cargoes that bind to Kinesin-1 via the TPR bundle have been identified, including Kidins220/ARMS, Calsyntenin/Alcadein, Collapsin Response Mediator Protein-2, Huntington Associated Protein-1, Alzheimer Precursor Protein (APP), torsinA, 14-3-3 and Vaccinia virus's A36R protein [26-34]. The identification of multiple cargoes for Kinesin-1 raises the question of how one motor coordinates the transport of its many potential cargoes. One possibility is that binding sites for different cargoes may not be accessible at the same time such that cargoes compete with each other for binding and transport (competitive transport model). A second possibility is that different cargoes may undergo cooperative transport whereby one cargo facilitates the binding and transport of another cargo (cooperative transport model). A third possibility is that different cargoes neither compete nor cooperate for transport but rather are transported independent of each other (independent transport model). We set out to test whether the transport of different cargoes by Kinesin-1 is competitive, cooperative or

independent of each other. Our results suggest that transport of most Kinesin-1 cargoes that bind via the TPR bundle of KLC is not competitive but rather independent of each other. However, transport of JIP1 and JIP3 is cooperative due to interactions of JIP1 and JIP3 with KLC as well as with each other.

RESULTS

Independent transport of the JIP proteins and other Kinesin-1 cargoes

Since many different cargoes have been identified for Kinesin-1 [4, 5], we focused on known binding partners of Kinesin-1 rather than organelles that can employ multiple motors via unknown linkage mechanisms. In addition, since both the KHC and KLC subunits have been implicated in Kinesin-1 cargo binding, we focused on cargo proteins that bind via the KLC subunit, specifically JIP1, JIP3, Kidins220/ARMS, and PAT1. Kidins220/ARMS is a transmembrane protein whose cytoplasmic tail binds to KLC [27]. Kinesin-1 activity is required for the transport of JIP1, JIP3 and Kidins220/ARMS to neurite tips in neuronal cells [19, 20, 27]. PAT1 was identified as a binding partner of KLC in a yeast two-hybrid screen using the TPR motifs of KLC as the bait, and the interaction between KLC and PAT1 has been confirmed by Dichtenberg et al [35] as well as by co-immunoprecipitation of GST-tagged PAT1 and HA-tagged KLC expressed in COS cells (Figure Supp 4.1).

To test whether distinct cargoes are transported together or independent of each other, we first used live cell imaging of fluorescent protein (FP)-tagged cargoes. Unfortunately, we were unable to visualize JIP proteins undergoing transport in live cells, presumably due to the low number of molecules on a transport cargo [36]. In addition, such studies cannot distinguish independent versus competitive transport. Thus, to test whether distinct Kinesin-1 cargo proteins are transported competitively, cooperatively or independently of each other, we used competition experiments in neuronal cells. We hypothesized that over-expression of one cargo should result in reduced transport and mislocalization of other cargoes if the two proteins compete for Kinesin-1-mediated transport, enhanced transport if the two proteins are transported cooperatively, and no effect on transport if the two proteins are transported independently.

We first explored the effect of over-expression of a cargo protein on the localization of its endogenous protein. Such experiments were feasible for JIP3 and Kidins220/ARMs using antibodies that recognize the endogenous proteins but not truncated KLC-binding constructs. Differentiated CAD cells (a neuronal-like cell line) were transfected with plasmids encoding the KLC-binding regions of JIP3 [Myc-JIP3(138-621), Figure 5 D] or Kidins220/ARMS [cyan fluorescent protein (CFP)-Kidins220/ARMS(1129-1426), [27] and Figure Supp 4.1]. Over-expression of Myc-JIP3(138-621) resulted in mislocalization of the endogenous JIP3 protein (Figure 4.1 A,B) and over-expression of CFP-Kidins220/ARMS (1129-1426) interfered with transport of the endogenous Kidins220/ARMS protein (Figure 4.1 C,D). These results indicate that competition for Kinesin-1 transport exists between transfected and endogenous cargo proteins. Thus, transport of individual Kinesin-1 cargoes is saturable.

We then tested the effect of over-expression of a cargo protein on the localization of other cargo proteins. Differentiated CAD cells were transfected with plasmids encoding GFP-tagged Kidins220/ARMS and the localization of endogenous JIP1 and JIP3 proteins was analyzed in transfected and untransfected cells. Over-expression of GFP-Kidins220/ARMS had no effect on the localization of JIP1 (Figure 4.2 A,D) or JIP3 (Figure 4.2 A,E) to neurite tips. Since Kidins220/ARMS is a transmembrane protein and accumulates in the endoplasmic reticulum when over-expressed (Figure 4.1 A), we also tested whether over-expression of the KLC-binding region of Kidins220/ARMS as a soluble fragment could compete with JIP1 or JIP3 for Kinesin-1 transport. As with the full length Kidins200/ARMS protein, over-expression of CFP-Kidins220/ARMS (1129-1426) had no effect on JIP1 (Figure 4.2 A,D) or JIP3 (Figure 4.2 A,E) localization. In the converse experiments, over-expression of Myc-JIP1 or Flag-JIP3 in differentiated CAD cells had no effect on the localization of endogenous Kidins220/ARMS protein to neurite tips (Figure 4.2 B,F). These results indicate that Kidins220/ARMS and the JIP proteins do not compete for Kinesin-1 transport. Moreover, immunoprecipitation experiments indicate that there is no competition between Kidins220/ARMS and JIP1 or JIP3 for Kinesin-1 binding (Figure Supp 4.2). Thus, the transport of distinct Kinesin-1 cargoes is saturable but not competitive with other cargoes.

Similar experiments were carried out to assess whether PAT1 and the JIP proteins could compete with each other for Kinesin-1 transport to neurite tips. Differentiated CAD cells were transfected with plasmids encoding Flag-tagged PAT1 and the localization of endogenous JIP1 and JIP3 proteins was analyzed in transfected and untransfected cells. In cells overexpressing Flag-PAT1, the localization of endogenous JIP1 (Figure 4.2 C,D) and JIP3 (Figure 4.2 C,E) proteins was similar to that of untransfected cells, suggesting that there is no competition between PAT1 and the JIP proteins for Kinesin-1-mediated transport. Similar experiments to investigate the effect of JIP1 or JIP3 over-expression on PAT1 localization could not be performed due to a lack of suitable antibodies.

We further analyzed the ability of Kinesin-1 cargoes to be transported cooperatively, independently or competitively by analyzing whether cargoes that bind via the KHC subunit could compete with JIP1 or JIP3 for Kinesin-1 mediated transport in neuronal cells. Over-expression of p120catenin constructs that bind to KHC (full length or an N-terminal truncation ΔN [37]) had no effect on the localization of JIP1 or JIP3 (Figure Supp. 4.3). These results indicate there is no competition or cooperation for Kinesin-1-mediated transport, but rather that transport of different Kinesin-1 cargoes is independent of each other.

JIP1 facilitates JIP3 transport by Kinesin-1 and vice versa

We next set out to determine whether different JIP proteins, namely JIP1 and JIP3, are transported by Kinesin-1 in a competitive, cooperative, or independent manner. Differentiated CAD cells were transfected with plasmids encoding Myc-tagged full length JIP1. In cells expressing high levels of Myc-JIP1, the amount of endogenous JIP3 localized at neurite tips was similar to that in untransfected cells (Figure 4.3 A,C), suggesting that there is no competition between JIP1 and JIP3 for Kinesin-1-mediated transport. Surprisingly, in differentiated CAD cells expressing Myc-JIP1 at levels similar to the endogenous JIP1 protein (based on localization of the myc-tagged protein to the neurite tip), there is a 2 fold increase in the amount of JIP3 at the tips of neurites (Figure 4.3 B,C). Similar results were obtained (Figure 4.3 C) upon expression of a truncated version of JIP1 that binds both JIP3 and KLC but not JNK [Myc-JIP1(307-711), Figure

4.6]. In contrast, low level expression of Myc-JIP1 had no effect on the localization of endogenous Kidins220/ARMS and vice versa (Figure 4.2 D,F). These results suggest that JIP1 facilitates transport of JIP3.

Similar experiments were carried out to test whether JIP3 could affect the transport of JIP1 by Kinesin-1. In differentiated CAD cells expressing high levels of full-length Flag-JIP3 or a truncated version that binds both JIP1 and KLC [JIP3(138-621), Figure 4.6], there was no change in the amount of endogenous JIP1 at neurite tips (Figure 4.3 D,F). But in cells expressing low levels of Flag-JIP3 or JIP3(138-621), there was an approximately 2-2.5 fold increase in the amount of JIP1 at neurite tips (Figure 4.3 E,F). Low level expression of Flag-JIP3 had no effect on the localization of endogenous Kidins220/ARMS and vice versa (Figure 4.2 E,F). Thus, JIP3 facilitates transport of JIP1 by Kinesin-1.

JIP1 and JIP3 bind to different sites on the KLC TPR bundle

To undergo cooperative transport by Kinesin-1, JIP1 and JIP3 may cooperate for binding to the KLC subunit. To test this, Myc-JIP1, Flag-JIP3, and HA-KLC proteins were expressed separately in COS cells. Equal amounts of cell lysates were mixed together in various combinations prior to immunoprecipitating KLC with an anti-HA antibody. More Myc-JIP1 and Flag-JIP3 were coprecipitated with HA-KLC when all three proteins were present in the mixture than when the JIP proteins were present individually (Figure 4.4 A,B). These results suggest that JIP1 and JIP3 cooperate for binding to the KLC TPR bundle and transport to neurite tips.

Previous studies on TPR-containing proteins identified two mechanisms of partner protein binding that may explain, at least in part, how JIP1 and JIP3 can cooperate for binding to the KLC TPR bundle. To identify sites in the KLC TPR bundle responsible for the interactions with JIP1 and JIP3, we undertook two approaches. In our first approach, we targeted specific residues for site-directed mutation based on a structural model of the KLC TPR repeats (Figure 4.4 C). The sequences of TPRs 2-5 of rat KLC1-C (residues 247 - 411) were overlaid onto known crystal structures of other TPR bundles (Figure Supp 4.4). Residues in the groove and along the edges of the KLC TPR bundle that are likely to be involved in partner protein binding (Figure 4 C) were

altered to Alanine in the two-hybrid bait vector pGBD [20]. In the BLUE mutant, charged residues in the loops that link successive TPR repeats were altered, whereas in the ORANGE mutant, charged and/or bulky residues in the tight turns within a TPR repeat were altered (Figure 4.4 C). The YELLOW and GREEN mutations targeted residues that (a) are conserved across many TPR bundles and (b) whose side chains have been shown to project into the groove of other TPR bundles. Specifically, the YELLOW mutant targeted conserved Asparagine residues which form a continuous ladder through the superhelix and play a critical role in binding the C-terminal peptide backbone of target proteins [10-12, 38]. The GREEN mutant targeted conserved hydrophobic residues in the TPR groove (Figure 4 C). The ability of the mutant KLC TPR bundles to bind JIP1 and JIP3 was then tested in a directed two-hybrid assay. As shown in Figure 4 D, mutations along the top of the TPR bundle (BLUE) abolished binding to both JIP1 and JIP3. Interestingly, mutations inside the TPR groove (YELLOW and GREEN) or along the bottom of the TRP bundle (ORANGE) abolished JIP1 binding but not JIP3 binding, suggesting that the C-terminal residues of JIP1 do indeed bind within the KLC TPR groove whereas JIP3 binds via a different site.

In a second approach to identify residues in the KLC TPR bundle required for binding to JIP1 and JIP3, random mutagenesis of the KLC TPR bundle (amino acids 199-488) was carried out using error-prone PCR (EP-PCR). Most clones retained the ability to interact with both JIP1 and JIP3 in the directed two-hybrid assay. Sequencing revealed either wildtype sequences (e.g. 14A, Figure 4.4 D), single mutations (e.g. 27A, Figure 4.4 D) or multiple mutations spread across the TPR bundle (e.g. 47A and 63A, Figure 4.4 D). We identified several EP-PCR mutants that lost the ability to interact with JIP1 but retained an interaction with JIP3 (22A, 28A, 33A, 64A, Figure 4.4 D). Sequencing of these clones showed that a variety of residues are involved in contacting the JIP1 C-terminal tail. Surprisingly, only one clone was identified that lost the ability to interact with JIP3 but retained an interaction with JIP1 (48A, Figure 4.4 D). Consistent with previous results [23], two pieces of data suggest that the N-terminal half of the KLC TPR domain is critical for the KLC-JIP3 interaction. First, mutations that abolish JIP3 binding (clone 48A) are all clustered in the first three TPR motifs and second, a truncated TPR domain (clone 28A) that contains only the first 3.5 TPR motifs retains an interaction with

JIP3. The fact that we have identified mutations that selectively abolish JIP1 or JIP3 binding suggests that the two scaffolding proteins bind to distinct sites and via distinct mechanisms to the TPR bundle. Specifically, these results support the hypothesis that the JIP1 C-terminal tail binds in the groove of the TPR bundle whereas internal sequences in JIP3 bind outside the groove. This is the first demonstration that a single TPR domain can use distinct surfaces for binding different partner proteins.

To confirm the binding specificity of these site-directed or EP-PCR mutants for JIP1 and JIP3 in mammalian cells, coimmunoprecipitation experiments were performed in COS cells as they contain minimal levels of endogenous Kinesin-1 and JIP proteins [39, 40]. For these experiments, truncated versions of the mutant KLC proteins were created due to ease of cloning, since truncated (amino acids 1-488) and full-length (amino acids 1-560) versions of KLC display identical interactions with JIP1 and JIP3 [20]. HA-tagged wild-type and mutant KLC proteins were coexpressed with either Myc-JIP1 or Flag-JIP3. Lysates were precipitated with antibodies to the Myc or Flag tags. Similar to the results of the directed two-hybrid assay, the YELLOW, GREEN and 33A mutants showed reduced binding to JIP1 (Figure 4.4 E, lanes 7-9, Figure 4.4 G) but not to JIP3 (Figure 4.4 F, lanes 7-9, and Figure 4.4 H), whereas the 48A mutant showed reduced binding to JIP3 but not JIP1 (Figure 4.4 E,F, lane 10, and Figure 4.4 G,H). These results confirm that distinct residues in the KLC TPR bundle are responsible for the interactions with JIP1 and JIP3.

The two JIP binding sites on the KLC TPR bundle facilitate transport of the JIP proteins

To test whether both binding sites on the KLC TPR bundle contribute to the transport of JIP1 and JIP3, we expressed wildtype and mutant KLC TPR bundles in differentiated CAD cells. Over-expression of the wild-type KLC TPR bundle resulted in a loss of JIP1 and JIP3 tip localization by trapping cargo away from Kinesin-1 in a non-motile complex (Figure 4.5 and [20, 41]). We hypothesized that over-expression of a mutant KLC TPR bundle that retains an interaction with JIP3 but lost the interaction with JIP1 (e.g. GREEN; Figure 4.4) will have a dominant negative effect on both JIP1 and JIP3 transport, and thus neurite tip localization, in the cooperative model, but will

selectively abolish only JIP3 transport if the JIP proteins can bind independently to KLC (independent model). As shown in Figure 4.5, over-expression of the GREEN mutant in differentiated CAD cells caused a significant decrease in both JIP1 (Figure 4.5 A,C) and JIP3 (Figure 5 B,D) tip localization. Similarly, over-expression of the 48A mutant that lost the interaction with JIP3 but retains an interaction with JIP1 (Figure 4.4) caused a significant decrease in both JIP1 (Figure 4.5 A,C) and JIP3 (Figure 4.5 B,D) tip localization. In control experiments, over-expression of the BLUE mutant, which lost the interaction with both JIP1 and JIP3 (Figure 4.4), had no effect on transport of either JIP protein (Figure 4.5). These results indicate that both JIP1 and JIP3 binding sites of the KLC TPR bundle contribute to JIP transport and support the conclusion that JIP1 and JIP3 are transported in a cooperative manner by Kinesin-1.

Oligomerization of JIP1 and JIP3

Binding of JIP1 and JIP3 to distinct sites on the KLC TPR bundle likely contributes to their cooperative transport. Yet the possibility remained that JIP1 and JIP3 could interact with each other independent of their interaction with KLC. Binding as a JIP1/JIP3 oligomer could allow a stronger interaction with the two binding sites on KLC. Previous studies have shown that JIP1, JIP2, and JIP3 homo-oligomerize and that JIP2 can hetero-oligomerize with JIP1 and JIP3 [40, 42, 43]. To test whether JIP1 can interact with JIP3, we performed coimmunoprecipitation experiments in transfected COS cells. When lysates expressing Myc-JIP1 and Flag-JIP3 were immunoprecipitated with an antibody to the Myc tag, both JIP1 and JIP3 were precipitated (Figure 4.6 B, lane 9). Furthermore, the endogenous JIP1 and JIP3 proteins in differentiated CAD cells hetero-oligomerize as shown by coimmunopreciptation of JIP3 with an antibody to JIP1 (Figure 4.6 F). Taken together, these results indicate that JIP1 and JIP3 can form an oligomeric complex. Thus, distinct binding sites on KLC for JIP1 and JIP3 and an interaction between JIP1 and JIP3 contribute to cooperative transport.

To define the regions of JIP1 responsible for the interactions with JIP3 and KLC, a series of Myc-tagged truncated and mutant versions of JIP1 were generated (Figure 4.6 A). Full length and truncated/mutant JIP1 proteins were coexpressed in COS cells with Flag-JIP3 (Figure 4.6 B) or HA-KLC (Figure 4.6 C) and immunoprecipitated with an

antibody to the Myc tag. JIP3 was coimmunoprecipitated with all of the truncated and mutated JIP1 proteins that contain an intact PTB domain (Figure 4.6 B, lanes 9-13), but not with a construct containing just the SH3 domain of JIP1 (Figure 6 B, lane 14). These results indicate that JIP3 interacts specifically with the PTB domain of JIP1. This binding region is distinct from the JIP1 sequences required for interaction with KLC as the coprecipitation of HA-KLC was lost upon mutation (Y709A, Figure 4.6 C, lane 11) or truncation (307-701, Figure 4.6 C, lane 12) of the C-terminal residues of JIP1, in agreement with previous results [20]. Although the extreme C-terminal residues of JIP1 are necessary for the interaction with KLC, they are not sufficient, as a construct containing only the PTB and C-terminal residues of JIP1 failed to coprecipitate KLC (Figure 4.6 C, lane 13). These data indicate that JIP1 can form distinct interactions with JIP3 and KLC.

To define the regions of JIP3 required for the interactions with JIP1 and KLC, Myc-tagged truncated versions of JIP3 were created [(138-621) and (138-433), Figure 4.6 A]. The truncated JIP3 proteins were coexpressed in COS cells with Flag-JIP1 (Figure 4.6 D) or HA-KLC (Figure 4.6 E) and immunoprecipitated with an antibody to the Myc tag. While the longer construct, JIP3(138-621) coprecipitated both JIP1 (Figure 4.6 D, lane 5) and KLC (Figure 4.6 E, lane 5), the shorter fragment of JIP3 containing residues 138-433 interacted only weakly with JIP1 (Figure 4.6 D, lane 6) and not at all with KLC (Figure 4.6 E, lane 6). These results suggest that residues 138-433 of JIP3 are partly sufficient for the interaction with JIP1; however, residues 433-621 are required for complete JIP1 and KLC binding.

A JIP1/JIP3/KLC complex is necessary for efficient JIP1 or JIP3 binding and transport

Previously we showed that KLC's binding sites for both JIP1 and JIP3 contribute to efficient transport of JIPs in neuronal cells (Figure 4.5). Having defined the regions of JIP1 and JIP3 required for binding KLC (Figure 4.6), we next tested whether JIP1 and JIP3 binding of the KLC TPR bundle is required for efficient transport of both JIP proteins. In control experiments, high level expression of JIP1 constructs that bind both JIP3 and KLC [JIP1(307-711), Figure 4.6] or that bind to neither JIP3 nor KLC

[JIP1(307-565), Figure 4.6] had no effect on localization of JIP3 to neurite tips (Figure 4.7 A,B). Similar control experiments showed that high level expression of JIP3 constructs that bind to both JIP1 and KLC [JIP3 full length and JIP3(138-621), Figure 4.6] did not disrupt JIP1 transport (Figure 4.7 C,D). In contrast, high expression of JIP1 proteins that bind JIP3 but not KLC [(307-701), Y709A, and PTB, Figure 4.6], resulted in a significant decrease in the amount of JIP3 protein localized at neurite tips (Figure 4.7 A,B). In addition, high expression of a JIP3 construct that binds weakly to JIP1 but not at all to KLC [JIP3(138-433), Figure 4.6] resulted in a significant decrease in JIP1 levels at neurite tips (Figure 4.7 C,D). These results suggest that although JIP1 and JIP3 can bind independently to the KLC TPR bundle, binding of both proteins to Kinesin-1 is required for efficient transport of the JIP proteins.

High expression of Myc-JIP1(307-701) may act to disrupt JIP3 localization by preventing an efficient interaction of JIP3 with Kinesin-1. Upon over-expression of Myc-JIP1(307-701) in differentiated CAD cells, less endogenous JIP3 protein was coimmunoprecipitated with Kinesin-1 (Figure 4.7 E) as compared to the vector control or expression of a JIP1 construct (307-711) that binds to both JIP3 and KLC (Figure 4.7 E). These results suggest that high expression of Myc-JIP1(307-701) results in a decreased interaction between endogenous JIP3 and Kinesin-1 proteins.

JIP1 is required for JIP3 transport and vice versa

To further explore the cooperative transport of JIP1 and JIP3 by Kinesin-1, we tested whether JIP1 is required for transport of JIP3 and vice versa using RNAi to knock down expression of JIP1 or JIP3 in differentiated CAD cells. To establish the knockdown efficiency and specificity of our shRNA plasmids, COS cells were cotransfected with mouse Flag-JIP1 or Flag-JIP3 and shRNA plasmids directed against JIP1 or JIP3. An empty shRNA vector was used as a control. Expression of the JIP1 shRNA plasmid resulted in decreased Flag-JIP1 expression (Figure 4.8 A, lane 2) whereas Flag-JIP3 expression was unaffected (Figure 4.8 B, lane 2). Expression of the JIP3 shRNA plasmid resulted in decreased JIP3 expression (Figure 4.8 B, lane 3) whereas JIP1 expression was unaffected (Figure 4.8 A, lane 3). Immunoblotting the same lysates for β-tubulin shows that equal protein levels were loaded.

The JIP1 or JIP3 shRNA plasmids were then transfected into differentiated CAD cells using a CFP plasmid as a marker for transfected cells. After 48 hrs, cells were fixed and immunostained for endogenous JIP1 or JIP3 proteins. Transfection of the shRNA plasmid against JIP1 resulted in loss of staining for endogenous JIP1 protein (Figure 4.8 C,E), verifying the efficacy and specificity of the JIP1 shRNA construct, as well as a significant decrease in JIP3 localization at neurite tips (Figure 4.8 D,F). Similarly, shRNA-mediated knockdown of JIP3 resulted in a loss of JIP3 staining (Figure 4.8 D,F) as well as a significant decrease in JIP1 localization at neurite tips (Figure 4.8 C,E). In the case of JIP3 knockdown, only cells that retained normal neurite morphology were selected for quantification since, in some cells, knockdown of JIP3 resulted in a complete loss of neurites or the formation of short, thin, and highly branched neurites as previously observed [44, 45]. Taken together, the RNAi, dominant negative and coimmunoprecipitation experiments support the conclusion that transport of JIP1 and JIP3 to neurite tips is dependent on the formation of a JIP1/JIP3/KLC complex.

DISCUSSION

Cooperative versus Independent transport of Kinesin-1 Cargoes

To understand how motor proteins function in vesicle transport, it is important to determine how motors link to their cargoes and how transport is regulated. In the case of Kinesin-1, recent work has identified many proteins that bind to the KHC and KLC subunits [4, 5]. This raises several models for how transport of disparate cargoes by one motor might be coordinated. One possibility is that binding sites for different cargoes may not be accessible at the same time, such that cargoes compete with each other for transport. Our results suggest this model is insufficient to describe cargo transport by Kinesin-1 as over-expression of cargoes that bind via KLC (Kidins220/ARMS, JIP1/JIP3 and PAT1) did not compete with other cargoes for transport. In addition, no competition was detected between cargoes that bind via KHC and those that bind via KLC (p120catenin and JIP1/JIP3, respectively). Overall, our results support a second model for coordination of multiple cargoes - that transport of disparate cargoes is saturable yet independent of each other. The third model, cooperative transport, is viable in the case of

Kinesin-1 mediated transport of JIP1 and JIP3, as these proteins bind to separate sites on the KLC TPR bundle yet facilitate each other's binding and transport.

These results are compatible with those of Bracale et al who showed that over-expression of the KLC-binding region of Kidins220/ARMS does not impair Kinesin-1 driven transport of vaccinia virus to the plasma membrane [27]. However, Araki et al have shown that over-expression of JIP1 caused a reduction in anterograde velocity of GFP-Alcadein vesicles and reduced binding of Alcadein to KLC [26]. Likewise, over-expression of Alcadein caused a reduction in anterograde velocity of APP-GFP vesicles [26]. In addition, Horiuchi et al have shown that over-expression of APLIP1, a JIP1 ortholog, in *Drosophila* causes defects in axonal transport [24]. Further investigation, from the structural to the cellular level, is clearly required to understand how the transport of disparate cargoes is coordinated.

That transport of an individual cargo can be saturated yet not compete with other cargoes suggests that the Kinesin-1 motor is not rate-limiting for transport. It has been suggested that the majority of Kinesin-1 protein, particularly in neuronal cells, is not participating in microtubule-based transport but rather is in a folded inactive state [4, 39]. This seemingly excess of Kinesin-1 protein may function to ensure an ample supply of motors that can be activated on demand. A similar mechanism may function in myosin-driven transport as mammalian Myosin V is also regulated by autoinhibition [46, 47].

The rate-limiting factor for Kinesin-1 transport may be unidentified accessory proteins required for selective cargo loading. In the case of JIPs, the formation of a JIP1/JIP3 oligomer may be rate limiting for Kinesin-1-mediated transport as low level expression of either JIP1 or JIP3 enhanced transport of the other JIP protein. Yet the fact that high level expression of either JIP1 or JIP3 did not enhance transport suggests that unidentified accessory factors may be diluted out by the over-expressed protein.

Our results are applicable to other cellular processes in which a diverse set of proteins depends on a common component for trafficking within the cell. Particularly relevant are studies showing that the clathrin-mediated endocytosis of disparate receptors and their ligands is saturable but not competitive [48]. Recent work has shown that the rate-limiting factor is not the common clathrin core components, but rather sorting connectors or adaptors that regulate the selective trafficking of specific cargoes [49].

Whether kinesin-cargo interactions are regulated by similar mechanisms is unknown. In the case of cytoplasmic dynein, transport of a wide variety of cargoes is thought to derive from a diverse set of cargo-binding accessory polypeptides that bind to dynein heavy chain [50]. These accessory polypeptides may bind in a mutually exclusive fashion to assemble distinct dynein-cargo combinations [51, 52] or may bind simultaneously to assemble multi-cargo complexes [53]. While over-expression of the light chain rp3 displaces the Tctex-1 light chain from dynein and blocks the apical delivery of rhodopsin [52], the differential tissue distribution of these light chains suggests that such competition may not exist *in vivo* [54].

Cooperative transport of JIP1 and JIP3 via a JIP1/JIP3/KLC complex

Our results show that although JIP1 and JIP3 can interact independently with KLC in yeast-two-hybrid and coimmunoprecipitation experiments, they bind with higher affinity when part of a complex (JIP1/JIP3/KLC). This complex is necessary for efficient JIP1 and JIP3 transport as evidenced by both RNAi knockdown and dominant negative expression experiments. Our demonstration of an interaction between JIP1 and JIP3 is in contrast to a previous report that JIP3 binds to the C-terminal PTB domain of JIP2 but not JIP1 [40]. This discrepancy is most likely explained by the fact that the JIP1b splice variant (711 amino acids) used in this study contains a complete PTB domain whereas the previous study likely used a shorter JIP1a splice variant (660 amino acids) containing only a partial PTB domain [43]. Thus, a complete JIP1 PTB domain is required for the interaction of JIP1 with JIP3.

The biological significance of cooperative transport of JIP1 and JIP3 is not clear. Some reports have indicated that JIP1 and JIP3 play distinct roles in cellular processes such as stress signaling and apoptosis, cell migration, and neuronal development [21, 55]. In our studies, we noticed that knockdown of JIP1 protein by RNAi resulted in increased neurite outgrowth, whereas loss of JIP3 protein resulted in decreased neurite outgrowth, similar to a previous report [45, 56]. However, recent reports have suggested that JIP1 and JIP3 can cooperate to control cellular events such as phosphorylation and accumulation of APP at neurite tips [45, 56], axon guidance [57], and JNK activation following glucose deprivation [58]. In this respect, cooperative transport of JIP1 and

JIP3 by Kinesin-1 could facilitate the inclusion of many proteins into the transport complex and crosstalk between unique subsets of JNK regulators and substrates [21, 42, 59]. Indeed, the macromolecular complex transported by Kinesin-1 via JIP1 and JIP3 most likely includes multiple other proteins such as members of the JNK cascade and transmembrane receptor proteins [21, 60].

Multiple mechanisms for partner protein binding by the KLC TPR domain

Our experiments indicate that the TPR bundle of KLC uses at least two independent regions for partner protein binding. First, the inside surface of the TPR groove binds to the extreme C-terminal residues of JIP1, similar to the binding of other TPR repeat-containing proteins such as Hop, PP5, and Pex5 and their interacting partners [10-12]. Second, the outer convex surface of the TPR bundle binds to internal residues in JIP3, analogous to the binding interface of the TPR-containing protein $p67^{phox}$ and its partner Rac [13]. Thus, although previous studies have demonstrated that both the groove and outer surfaces of TPR bundles can bind to partner proteins, KLC is the first TPR-containing protein known to utilize both mechanisms. In addition, in the case of KLC, these multiple interaction surfaces enable the cooperative assembly of a JIP1/JIP3/KLC complex.

Several features noted in other TPR bundles are important for JIP binding to KLC. First, substrate recognition and engagement by TPR bundles involves a variety of residues spread across a large surface area in the groove or along the outside of the TPR domain [8]. Consistent with this, single mutations in the KLC TPR domain were not sufficient to abolish the interaction with JIP1 or JIP3. Second, an Asparagine array lines the concave face of the bundle and likely contributes to peptide orientation in the groove [10-12, 38]. In the case of KLC, mutation of the Asparagine array abolished the interaction with JIP1 but not JIP3, supporting the conclusion that the C-terminal peptide of JIP1 sits in the KLC TPR groove.

KLC's TPR domain is known to mediate binding of Kinesin-1 to other proteins including Kidins220/ARMS, Pat1, Calsyntenin/Alcadein, Collapsin Response Mediator Protein-2, Huntington Associated Protein-1, APP, torsinA, 14-3-3 and Vaccinia virus's A36R protein [26-34]. In most of these cases, the mechanism of interaction is unknown,

as the residues required for binding have not been identified. In a recent study, quadruple mutations at positions L280, L287, A294, and L301 in KLC abolished the interaction with JLP, a JIP4 splice variant [23]. Our structural model predicts that these residues contribute to helical packing between the second and third TPR motifs. This is consistent with the structural function of residues in similar positions of the Leu7 subclass of TPR-containing proteins [61]. Thus, it seems likely that the loss of JLP binding was due to alterations in overall TPR domain structure rather than a novel leucine zipper interaction between KLC and JLP, as was proposed. Another recent study showed that two conserved WDDS motifs in the cytoplasmic C-terminal tail of Calsyntenin/Alcadein are required for efficient binding to KLC1 [26, 33]. As one WDDS is internal and the other within the last 10 amino acids, Calsyntenin/Alcadein may bind to KLC using either or both of the binding mechanisms identified in this study. Thus, it will be interesting to learn whether this diverse group of proteins binds to one of our two identified sites in KLC's TPR domain or whether the TPR bundle contains additional cargo binding interfaces.

MATERIALS AND METHODS

Plasmids: Plasmids encoding HA (hemagglutinin)-tagged rat KLC1 and the six TPR motifs (amino acids 199-488) have been previously described [20, 62]. For co-immunoprecipitation with JIP1 and JIP3, mutant TPR domains from pGBD-KLC TPR were subcloned into pCDNA3-HA-KLC to create truncated mutant KLC proteins (amino acids 1-488) using convenient restrictions sites. For expression of wild-type and mutant KLC TPR domains as dominant negative proteins, mutant TPR domains were subcloned from pGBD-KLC TPR into pCDNA3-HA-KLC TPR (amino acids 199-488).

Flag-tagged mouse JIP1, JIP2, and JIP3 [40, 43, 63] were a kind gift of R. Davis (University of Massachusetts Medical School). The splicing variant of JIP1 used in this study is JIP1b, also known as islet brain 1(IB1), which contains the full PTB domain that the JIP1a variant lacks [43]. Myc-tagged human full length JIP1, as well as the truncations or mutants 307–711, Y709A, 307-701, and PTB (554-711) have been described previously [20, 64]. Myc-JIP1(307-565) was generated by PCR amplification using primers with convenient restrictions sites for cloning into the pRK5-Myc vector.

Truncated JIP3 constructs [JIP3(138-433) and (138-621)] were obtained from clones identified in a yeast two-hybrid screen [20] and transferred from the two-hybrid prey vector pACT2 into the pCDNA3-myc vector. Flag-PAT1, GST-PAT1(1-351), and GST-PAT1(352-585) were a gift of J. Dictenberg and G. Bassell (Albert Einstein College of Medicine, Bronx, NY). GFP-Kidins220/ARMS [27] was a gift from G. Schiavo (Cancer Research UK). CFP-Kidins220/ARMS (1129-1426) was subcloned from the full length construct using convenient restriction sites. ECFP-p120catenin and ECFP-p120cateninΔN2 (deletion of amino acids 28-233) [37] were a gift from K.J. Green (Northwestern University, Chicago, IL).

Antibodies: The following antibodies were used: polyclonal and monoclonal antibodies to the Myc tag (Sigma C3956, Millipore 06-549, and 9E10 hybridoma ascites), HA tag (Sigma H6908, Upstate 07-221, and 12CA5 hybridoma ascites), and Flag tag (Sigma F7425 and Sigma F3165); polyclonal JIP1 (#152, [20]); polyclonal JIP3 (against *Drosophila* JIP3 (Syd2) N-terminal residues 1–772, or C-terminal residues 1066-1328 [65], gifts from L.S.B. Goldstein, University of California, San Diego); Monoclonal and polyclonal Kidins220/ARMS ([27], gifts from G. Schiavo, Cancer Research UK); monoclonal KHC (H2, Covance); and β-tubulin (E7, Developmental Studies Hybridoma Bank, Univ. Iowa). Polyclonal anti-KHC antibodies (B1-1) were generated against the KHC motor domain peptide CDKNRVPYVKGCTER (rat Kif5c amino acids 159-172). Secondary antibodies for immunofluorescence microscopy, Fluorescein and Rhodamine Red-X, were purchased from Jackson ImmunoResearch.

Structural Model of KLC TPR motifs 1-5. The sequences of TPRs 2-5 of rat KLC1-C (residues 247-411) were overlaid onto crystal structures of other TPR bundles (Figure Supp 4), specifically the TPR region of human Pex5 (PDB code 1FCH; residues A451-A552) and the TPR region of $p67^{phox}$ (PDB code 1E96; residues B120-B151) using the graphics program O [66]. The first TPR of KLC (residues 210-246) was then modeled by spatial alignment with the helical regions of Pex5 (1FCH, residues A383-A445). The sixth TPR repeat of KLC could not be accurately represented in the model through sequence or structural alignments to other TPR regions due to a long insertion between the fifth and sixth TPR motifs that is unique to KLC.

Directed yeast two-hybrid assay: A construct containing the six TPR motifs (amino acids 199-488) of rat KLC1 in the two-hybrid bait vector pGBD has been described [20]. Two-hybrid prey plasmids containing fragments of JIP1 and JIP3 in plasmid pACT2 were obtained in a two-hybrid screen [20]. Directed mutation of specific residues in amino acids 199-370 of the KLC TPR domain was carried out by Gene Synthesis [67]. EP-PCR to generate random mutations in KLC TPR motifs (amino acids 199-488) was carried out as described [68, 69]. Briefly, the region was amplified by PCR reactions in which $MnCl_2$ was substituted for $MgCl_2$. Amplified products were subcloned back into the pGBD-KLC TPR plasmid using convenient restriction sites. Mutant clones were picked randomly and mini-prep DNA was transformed into the yeast strain AH109 (Clontech).

Screening of the mutant TPR's ability to bind to JIP1 and JIP3 was carried out by yeast mating. Yeast strain AH109 expressing wild-type or mutant pGBD-KLC TPR clones was mated to yeast strain Y189 expressing pACT2-JIP1(478-711) or pACT2-JIP3(138-680) in 96 well plates. Diploid yeast were sequentially plated on double (-leu,-trp) and triple (-leu,-trp,-his + 3-aminotriazole and -leu,-trp,-ade) drop-out plates. Successful mating was evidenced by growth on double drop-out (-leu,-trp) plates. A positive interaction between the KLC TPR domain and JIP1 or JIP3 was evidenced by growth on -leu,-trp,-his and on -leu,-trp,-ade drop-out plates.

Clones that lost the ability to interact with either JIP1 or JIP3 were selected for further analysis. Yeast plasmids were transformed back into *E.coli* for DNA sequencing. A few clones that retained interactions with both JIP1 and JIP3 were also selected for DNA sequencing. In most cases, no mutations were found, however, in some cases single or double mutations were found. Clones that lost the ability to interact with both JIP1 and JIP3 were not selected since these could include truncated KLC TPR domains as well as misfolded proteins.

Cell culture and Fluorescence Microscopy: COS and CAD cells were cultured as described [20] and transfected with *Trans*IT-LT1 (Mirus). Cells were processed for immunofluoresence as in [20] and mounted in 50% glycerol, 0.5% n-propyl gallete in PBS or using Prolong Gold (Invitrogen). Images were collected with either an Olympus BX51 microscope with UplanFl 60X/NA 1.25 objective and Olympus DP70 CCD

camera, or a Nikon TE2000 microscope Plan-Fl 40X/NA 0.75 or a Plan-APO 60X/NA 1.4 objective and Photometrics CS ES2 camera. Quantification of neurite tip immunofluorescence intensity was done using Image J (NIH). Neurite tips were hand-selected with an elliptical selection tool and the average pixel fluorescence intensity was measured. In order to pool values from two or three independent experiments for statistical analysis (student's t-test), measurements within each sample were normalized by first subtracting cell background fluorescence (determined from measurements within neurite shafts), then dividing each transfected or non-transfected tip measurement by the average intensity of all non-transfected neurite tips within the same experimental sample.

Immunoprecipitation: COS or CAD cells were resuspended in lysis buffer (40mM Hepes pH 7.5, 120 mM NaCl, 1 mM EDTA, 10mM sodium pyrophosphate, 10mM ß-glycerophosphate, 50 mM NaF, 0.5% NP40, 0.1% Brij-35, and protease inhibitors). Extracts were incubated with the specified antibodies for 2.5-18 hr at 4°C then incubated with protein A agarose beads for 20 min at 4°C. Beads were washed two times with lysis buffer, resuspended in Laemmli sample buffer, and analyzed by SDS-PAGE and Western blot.

RNAi: A shRNA (short hairpin RNA) plasmid targeting mouse JIP1 was made using DNA oligos designed with a 19mer sense sequence (selected using Dharmacon's website), 9 nucleotide loop, 19mer antisense sequence, and 6T pol III stop sequence (sense: 5'-tttGGCTCACCGTGCACTTTAAttcaagagaTTAAAGTGCACGGTGAGC Cttttt-3' and antisense: 5'-tagaaaaaaGACCGTGTGTCTCGATCATtctcttgaaATGATCG AGACACACGGT-3'). Annealed oligos were cloned into the Bbs1 and Xba1 sites of the pU6-puro vector (modified from pU6pro [70] by addition of a puromycin resistence gene into the PvuII site). The shRNA plasmid targeting mouse JIP3 was made the same way using a previously verified JIP3 shRNA sequence [71] (sense: 5'-tttGCAGGCCGAG GAGAAATTCAttcaagagaTGAATTTCTCCTCGGCCTGtttttt-3' and antisense: 5'-ctagaaaaaaCAGGCCGAGGAGAAATTCAtctcttgaaTGAATTTCTCCTCGGCCTG-3'). All plasmids were verified by DNA sequencing. Knockdown efficiency was verified by co-transfecting the shRNA or control plasmids into COS cells with Flag-tagged mouse JIP1 or JIP3 plasmids. Protein expression of Flag-JIP1 or JIP3 in control and knockdown cells was analyzed by Western blot and immunofluorescence.

FIGURES

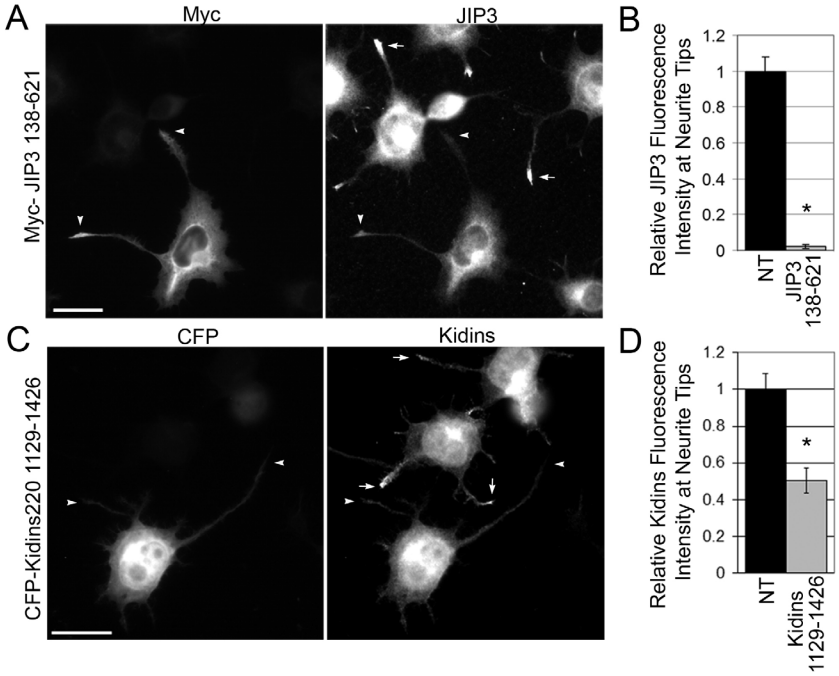

Figure 4.1: Transport of specific cargo proteins by Kinesin-1 is saturable. (A,C) Differentiated CAD cells overexpressing the KLC-binding region of (A) JIP3 [Myc-JIP3(138-621)] or (C) Kidins220/ARMS [CFP-Kidins220/ARMS(1129-1426)] were fixed and stained for (A) the Myc tag and the endogenous JIP3 protein or (C) the Kidins220/ARMS protein. Arrowheads, neurite tips of transfected cells; arrows, neurite tips of non-transfected cells. Scale bar = 20 μm. (B and D) Quantification of endogenous (B) JIP3 or (D) Kidins220/ARMS fluorescence intensity at neurite tips of non-transfected cells (NT) or cells overexpressing the indicated proteins. * $p<0.01$. Error bars = +/- SEM. N>100 neurites for each construct.

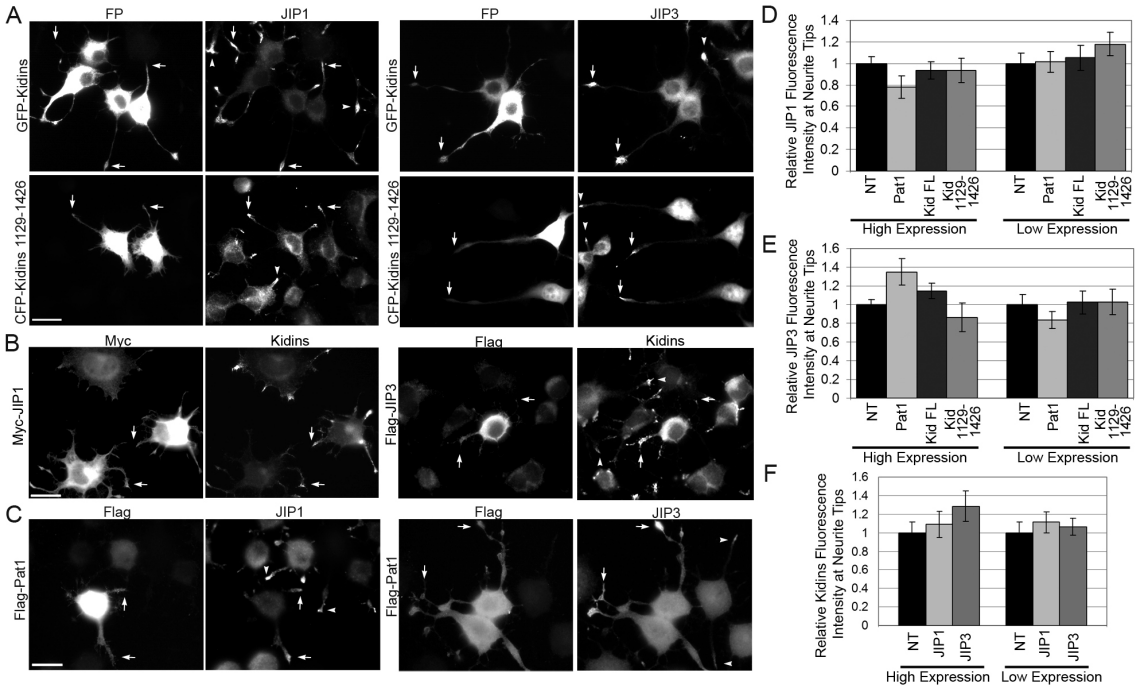

Figure 4.2: Kinesin-1 cargoes that bind via KLC do not compete with each other for transport. (A) Differentiated CAD cells expressing GFP-Kidins220/ARMS or CFP-Kidins220/ARMS(1129-1426) were stained for the endogenous JIP1 (left set of panels) or JIP3 (right set of panels) proteins. FP, fluorescent protein. (B) Differentiated CAD cells expressing Myc-JIP1 (left panels) or Flag-JIP3 (right panels) were double labeled for the expressed proteins (Myc or Flag tags) and for the endogenous Kidins220/ARMS protein. (C) Differentiated CAD cells expressing Flag-PAT1 were double labeled for the Flag tag and the endogenous JIP1 (left panels) or JIP3 (right panels). Arrows, neurite tips of transfected cells; arrowheads, neurite tips of non-transfected cells. Scale bar = 20 μm. (D-F) Quantification of (D) JIP1, (E) JIP3, (F) or Kidins220/ARMS fluorescence intensity at neurite tips of non-transfected cells (NT) or cells overexpressing the indicated proteins. N>100 neurites for each construct. Error bars = +/- SEM. ($p>0.01$ for all transfected constructs). Acknowledgements: Some data collection for this figure was done by Gloria T. Jih, Verhey lab.

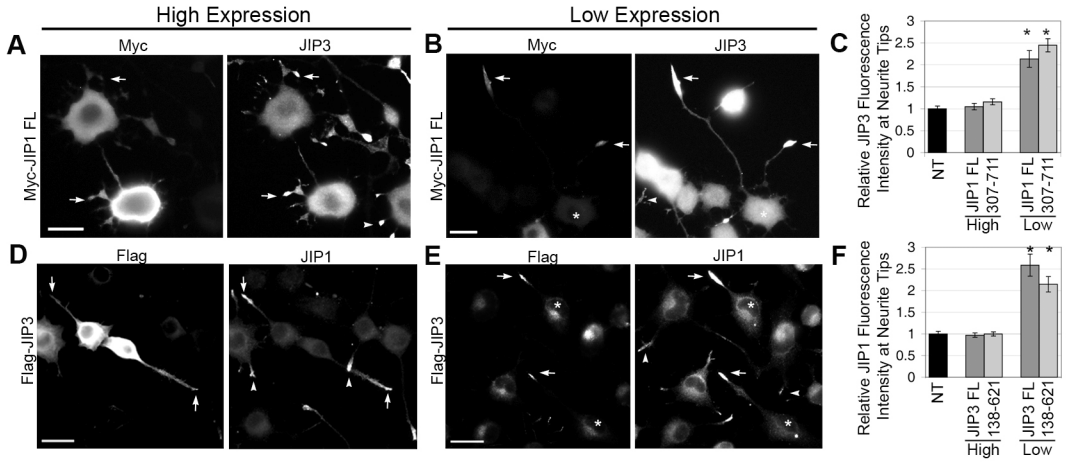

Figure 4.3: JIP1 facilitates JIP3's transport to neurite tips and JIP3 facilitates JIP1's transport. (A and B) Differentiated CAD cells expressing (A) high levels or (B) low levels of Myc-tagged JIP1 were fixed and stained with antibodies to the Myc tag and endogenous JIP3. Asterisk, cell body of transfected cell. Arrows, neurite tips of transfected cells. Arrowheads, neurite tips of non-transfected cells. Scale bar = 20 μm. (C) Quantification of JIP3 fluorescence intensity at neurite tips of non-transfected cells (NT) or cells expressing high or low levels of full-length (JIP1 FL) or N-terminally truncated JIP1 (307-711). N>75 neurites for each construct and expression level. Error bars = +/- SEM. * $p<0.01$. (D and E) Differentiated CAD cells expressing (D) high levels or (E) low levels of Flag-tagged JIP3 were fixed and stained with antibodies to the Flag tag and endogenous JIP1 protein. (F) Quantification of JIP1 fluorescence intensity at neurite tips of non-transfected cells (NT) or cells expressing high or low levels of full-length (JIP3 FL) or truncated JIP3 (138-621). N>150 neurites for each construct and expression level. Error bars = +/- SEM. * $p<0.01$.

Figure 4.4: The KLC TPR domain contains distinct binding sites for JIP1 and JIP3 which facilitate cooperative binding. (A and B) Cooperative binding of JIP1 and JIP3 to KLC. Lysates of COS cells expressing Flag-JIP3, Myc-JIP1, or HA-KLC were combined and analyzed by western blot either directly (total lysate) or after immunoprecipitation with an anti-HA antibody. (B) Quantification from six independent experiments of the fold increase in JIP1 (J1) or JIP3 (J3) pull-down in the absence and presence of the other JIP protein. * $p<0.01$; Error bars = +/- SEM. (C) Structural model of KLC's TPR motifs 1-5. The TPRs are depicted as a grey ribbon diagram. Residues targeted for mutation are depicted as ball-and-stick. The conserved Asparagines across the concave face are indicated in YELLOW whereas a series of hydrophobic residues that follow a similar line are shown in GREEN. The conserved K(Y/F)K residues within each TPR motif are shown in ORANGE whereas the conserved basic residues in the loops that link successive TPR motifs are shown in BLUE. (D) Results of directed yeast-two-hybrid assay. Yeast expressing wildtype or the indicated mutant versions of the KLC TPR domain as bait were mated to yeast expressing JIP1 or JIP3 as prey. The residues targeted for mutation are indicated (BLUE, YELLOW, GREEN, and ORANGE). For random mutation by EP-PCR, the mutated residues were determined after sequencing of the indicated clones. (E-H) Coimmunoprecipitation assay. COS cells were transiently transfected with plasmids encoding (E) Myc-JIP1 or (F) Flag-JIP3 along with wildtype (WT) or indicated mutant (mut) KLC TPR proteins. Lysates were immunoprecipitated with (E) anti-Myc or (F) anti-Flag antibodies, separated by SDS-PAGE, and immunoblotted with antibodies to the HA, Flag, or Myc tags as indicated. (G and H) Western Blot band intensities from three independent experiments were quantified using Image J. Shown is the percentage of total KLC (WT or Mut.) that was Co-IPed with (E) JIP1 or (F) JIP3 normalized to WT. # $p<0.05$; Error bars = +/- SEM. Acknowledgements: The structural model of KLC's TPR bundle (C) was contributed by Jeanne Stuckey from the University of Michigan. The yeast-two-hybrid experiment in (D) was contributed by Kelly Griffin, Verhey lab.

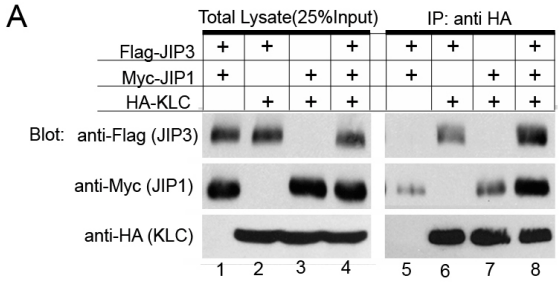

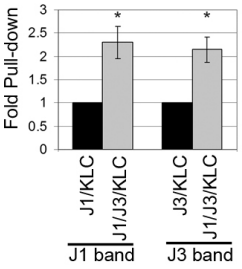

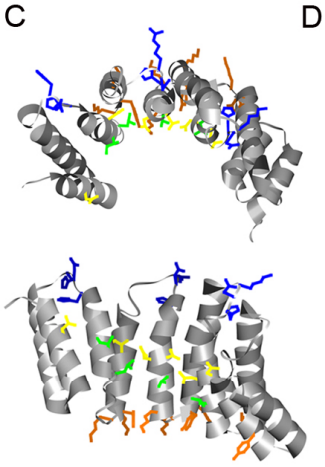

D

Yeast-two Hybrid			
KLC TPR mutant	**Binds to JIP1?**	**Binds to JIP3?**	**Mutations**
WT	yes	yes	
BLUE	no	no	H249A, D250A, H251A, R291A, D292A, H293A, K333A, D334A, H335A
YELLOW	no	yes	N218A, N259A, N301A, N302A, N343A, N344A
GREEN	no	yes	I260A, L263A, V305A, L347A
ORANGE	no	yes	K270A, Y271A, K272A, K309A, K312A, Y313A, K314A, K354A, Y355A
EP-PCR #14A	yes	yes	Wild-type
EP-PCR #22A	no	yes	L300P, I326N
EP-PCR #27A	yes	yes	A202S
EP-PCR #28A	no	yes	R214C, L347stop
EP-PCR #33A	no	yes	N279A, C320Y, R327G, L347W, K382R, Y404F
EP-PCR #47A	yes	yes	A202V, G206S, A224V, R310C, V380M
EP-PCR #48A	yes	no	R214H, G227W, A232T, R310H, L319M, D334N
EP-PCR #63A	yes	yes	G205C, K312M, E435G, D459G
EP-PCR #64A	no	yes	E196G, A199T, N259S, L345Q, Q370P, Y391F, R433G
EP-PCR #66A	yes	yes	K270E, K354M

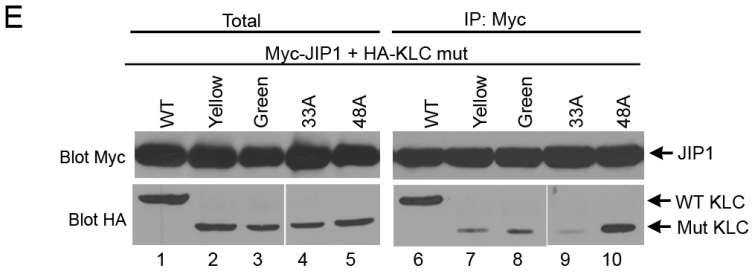

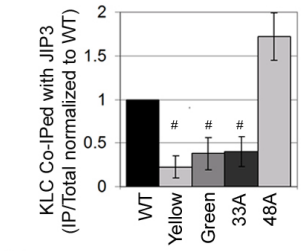

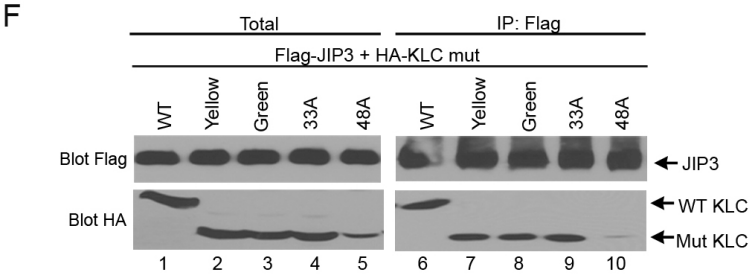

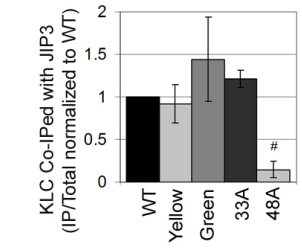

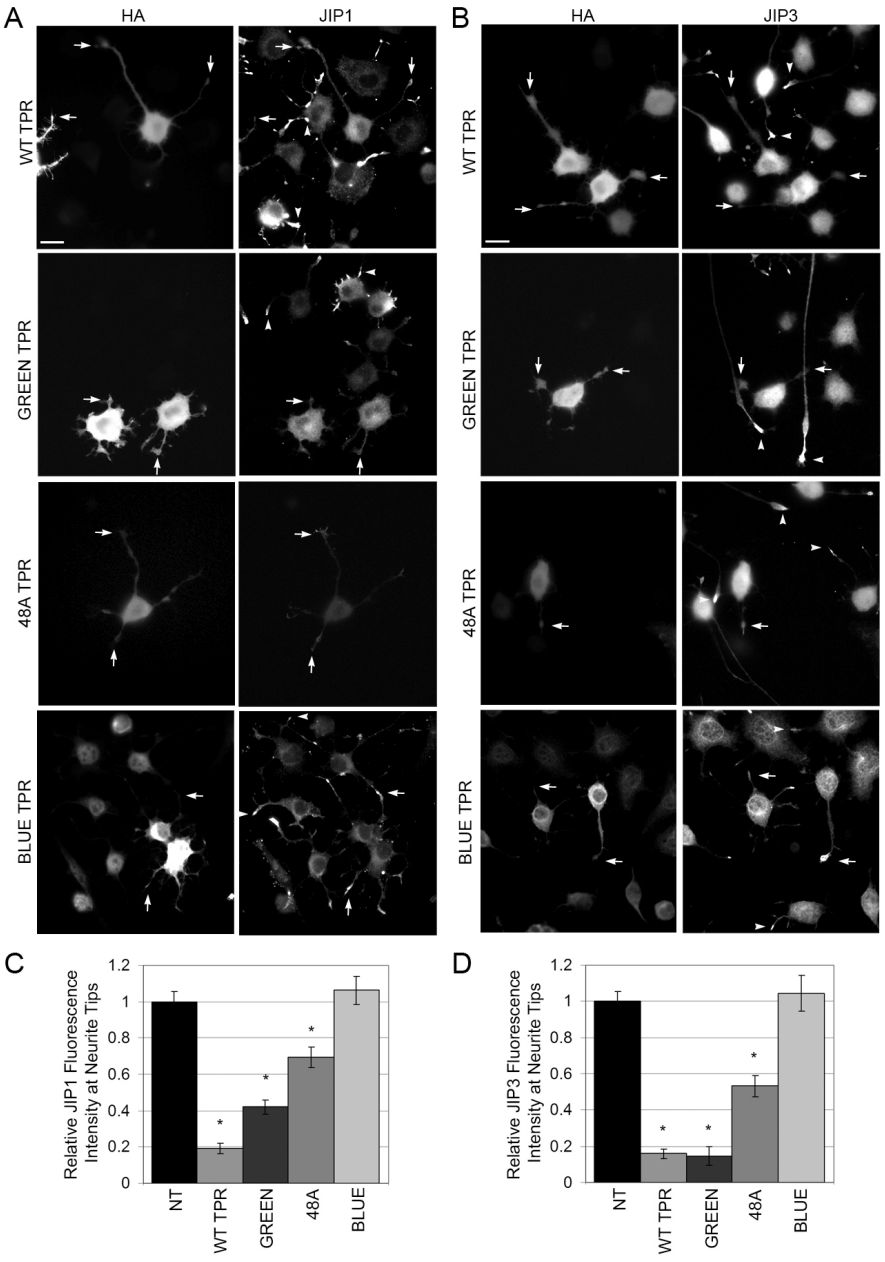

Figure 4.5: KLC TPR mutants functionally block both JIP1 and JIP3 transport to neurite tips. **(**A and B) Differentiated CAD cells expressing HA-tagged wildtype (WT) or mutant KLC-TPR bundles (GREEN, 48A, BLUE) were double labeled for the HA tag and for endogenous (A) JIP1 or (B) JIP3 proteins. Arrows, neurite tips of transfected cells; Arrowheads, neurite tips of non-transfected cells. Scale bar = 20 μm. (C and D) Quantification of (C) JIP1 or (D) JIP3 fluorescence intensity at neurite tips of non-transfected cells (NT) or cells expressing the indicated WT or mutant TPR bundles. Compared to control non-transfected cells, a significant (* $p<0.01$) decrease in JIP1 or JIP3 staining intensity is seen in cells transfected with the WT, GREEN, and 48A TPR bundles, but not the BLUE TPR bundle. N>200 neurites for each construct. Error bars = +/- SEM.

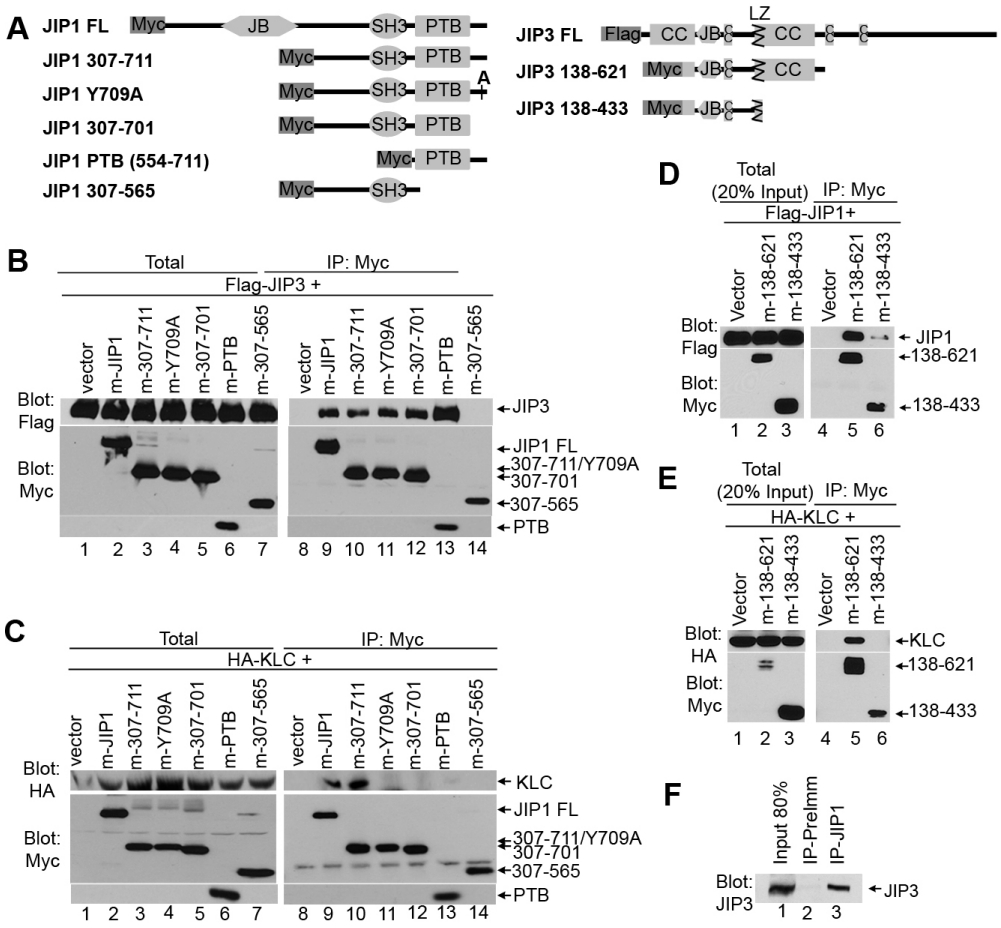

Figure 4.6: Oligomerization of JIP1 and JIP3. **(**A) Schematic illustration of full length or truncated JIP1 and JIP3 constructs. JB, JNK binding domain; PTB, phosphotyrosine binding domain; CC, coiled coil; LZ, leucine zipper. (B and C) Mapping of JIP1 domains. COS cells were cotransfected with the indicated Myc-JIP1 (m-JIP1) constructs and either (B) Flag-JIP3 or (C) HA-KLC. Cells were lysed and protein levels were analyzed by western blot directly (total) or after immunoprecipitation (IP) with anti-Myc antibodies. (D and E) Mapping of JIP3 domains. COS cells were co-transfected with a control vector or the indicated Myc-JIP3 (m-JIP3) constructs and either (D) Flag-JIP1 or (E) HA-KLC. Cells were lysed and protein levels were analyzed by western blot directly (total) or after immunoprecipitation (IP) with anti-Myc antibodies. (F) Interaction between endogenous JIP1 and JIP3 proteins. Lysates of differentiated CAD cells were immunoprecipitated with an anti-JIP1 antibody (IP-JIP1) or with the control pre-immune serum (IP-PreImm). The presence JIP3 in the immunoprecipitate was determined by immunoblotting with an antibody to JIP3.

Figure 4.7: Interaction of JIP1 with KLC is required for JIP3 transport and vice versa. (A and B) Over-expression of JIP1 constructs. Differentiated CAD cells expressing the indicated truncated versions of Myc-JIP1 were immunostained with antibodies to the Myc tag and the endogenous JIP3 protein. Arrows, neurite tips of transfected cells. Arrowheads, neurite tips of non-transfected cells. Scale bar = 20 μm. JIP3 fluorescence intensity at neurite tips was quantified (B) for non-transfected cells (NT) or cells expressing the indicated JIP1 constructs. N>170 neurites for each construct. Error bars = +/- SEM. * $p<0.01$. (C and D) Over-expression of JIP3 constructs. Differentiated CAD cells expressing full length (FL) Flag-JIP3 or the indicated truncated versions of Myc-JIP3 were immunostained with antibodies to the Flag or Myc tags and the endogenous JIP1 protein. JIP1 fluorescence intensity at neurite tips was quantified (D) for non-transfected cells (NT) or cells expressing the indicated JIP3 constructs. N>200 neurites for each construct. Error bars = +/- SEM. * $p<0.01$. (E) Effect of JIP1 dominant negative constructs on JIP3 binding to KLC. Lysates of differentiated CAD cells expressing full length or the indicated constructs of Myc-JIP1 were immunopreprecipitated (IP) with antibodies to the endogenous KHC protein. Precipitates were analyzed by western blot for the presence of the endogenous KHC and JIP3 proteins.

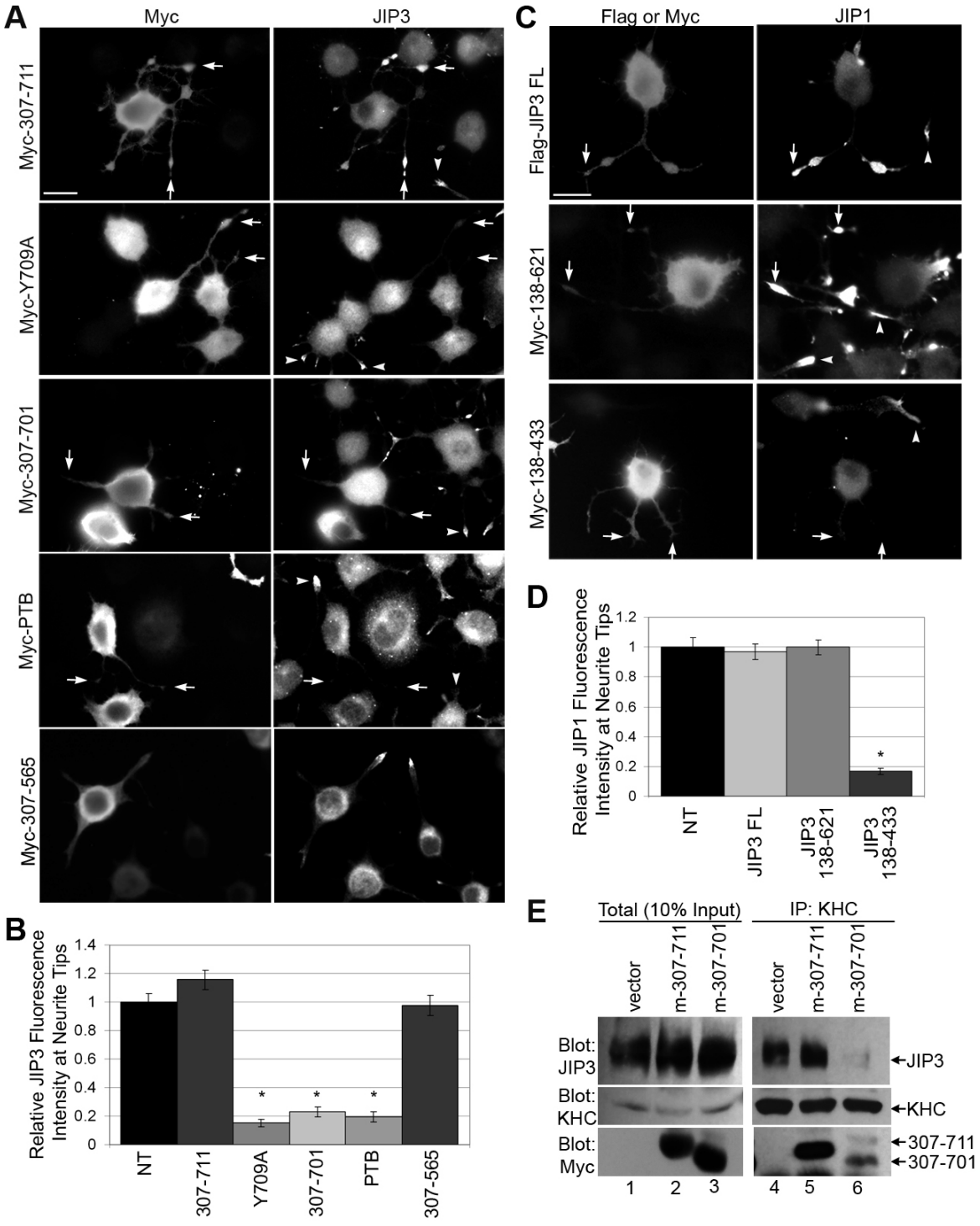
A
Myc
JIP3
Myc-307-711
Myc-Y709A
Myc-307-701
Myc-PTB
Myc-307-565
B
Relative JIP3 Fluorescence Intensity at Neurite Tips
1.4
1.2
1
0.8
0.6
0.4
0.2
0
NT
307-711
Y709A
307-701
PTB
307-565
C
Flag or Myc
JIP1
Flag-JIP3 FL
Myc-138-621
Myc-138-433
D
Relative JIP1 Fluorescence Intensity at Neurite Tips
1.2
1
0.8
0.6
0.4
0.2
0
NT
JIP3 FL
JIP3 138-621
JIP3 138-433
E
Total (10% Input)
IP: KHC
vector
m-307-711
m-307-701
Blot: JIP3
Blot: KHC
Blot: Myc
JIP3
KHC
307-711
307-701
1
2
3
4
5
6

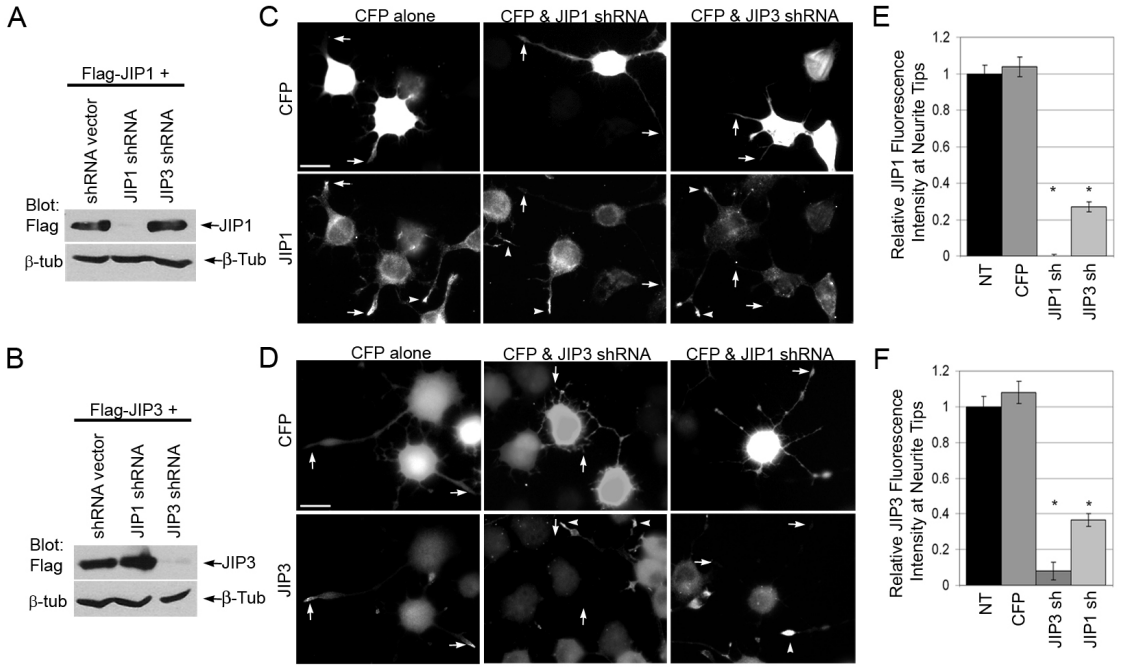

Figure 4.8: Knockdown of JIP1 abrogates JIP3 transport and vice versa. (A and B) Specificity of RNAi knockdown. COS cells were co-transfected with Flag-JIP1 (A) or Flag-JIP3 (B) and either an empty shRNA vector or shRNA plasmids targeting JIP1 or JIP3. The levels of remaining JIP1 and JIP3 proteins were determined by immunoblotting total cell lysates with an anti-Flag antibody. Equal loading of total protein is indicated by blotting with an anti-β-tubulin antibody. (C and D) Differentiated CAD cells were transfected with a plasmid encoding CFP alone or together with JIP1 shRNA or JIP3 shRNA plasmids. Cells were fixed and immunostained with antibodies to the endogenous (C) JIP1 or (D) JIP3 proteins. Left panels: transfection with CFP has no effect on (C) JIP1 or (D) JIP3 tip localization or protein level. Middle panels: JIP1 and JIP3 shRNA transfected cells show efficient knockdown of endogenous JIP1 or JIP3 respectively. Right panels: JIP3 shRNA-transfected cells show a defect in JIP1 tip localization (C) and JIP1 shRNA-transfected cells have a defect in JIP3 tip localization (D). Arrows, neurite tips of transfected cells; arrowheads, neurite tips of non-transfected cells. Scale bar = 20 μm. (E and F) Quantification of the relative JIP1 (E) or JIP3 (F) fluorescence intensity at neurite tips in transfected cells as compared to non-transfected (NT) cells. N>160 neurites for each construct. Error bars = +/- SEM. * $p<0.01$.

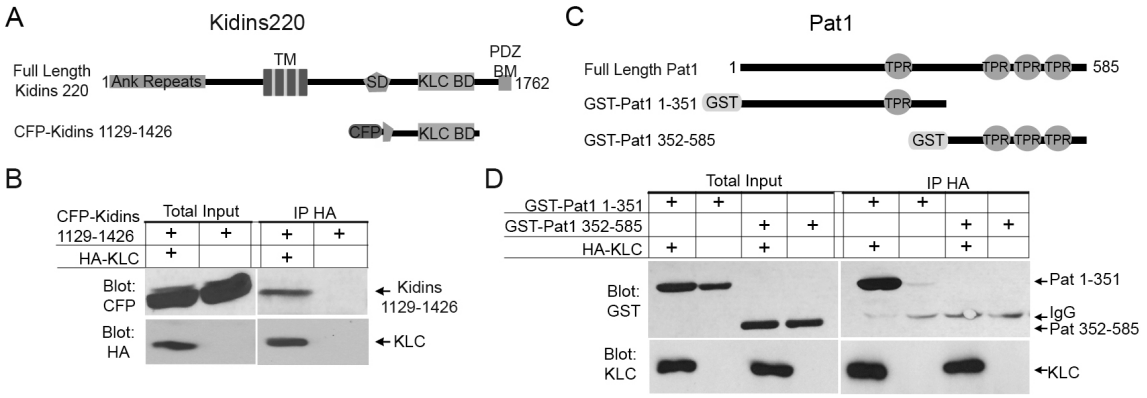

Figure Supplemental 4.1: Binding of Kidins220/ARMS and PAT1 to KLC. (A) Schematic illustration of full length Kidins220/ARMS and the truncated, cytoplasmic construct CFP-Kidins220/ARMS(1129-1426). Ank, ankyrin repeats; TM, transmembrane domains; SD, SAM domain; KLC BD, KLC binding domain as determined by Bracale *et al,* 2007; PDZ BM, PDZ binding motif. (B) Coimmunoprecipitation of Kidins220/ARMS with KLC. Lysate from COS cells transfected with CFP-Kidins220/ARMS(1129-1426) was mixed with lysate from untransfected cells or cells transfected with HA-KLC . Mixed lysates were then immunoprecipitated with anti-HA antibodies and analyzed by western blot. (C) Schematic illustration of PAT1 and truncated GST-PAT1 constructs. (D) GST-PAT1(1-351) or GST-PAT1(352-585) recombinant proteins were mixed with lysates from COS cells that had been transfected with HA-KLC or left untransfected. Mixtures were immunoprecipitated with anti-HA antibodies and analyzed by western blot. KLC binds within amino acids 1-351 of PAT1.

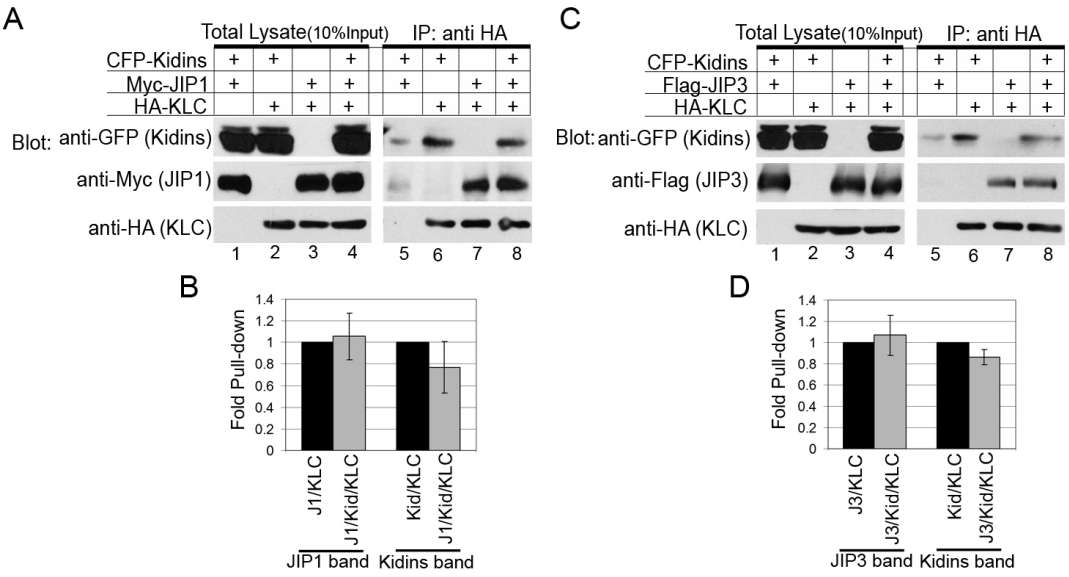

Figure Supplemental 4.2: Kidins220/ARMS does not compete with JIP1 or JIP3 for binding to KLC. Lysates of COS cells expressing Myc-JIP1, Flag-JIP3, CFP-Kidins220/ARMS(1129-1426), and HA-KLC were combined and analyzed by western blot either directly (total lysate) or after immunoprecipitation with an anti-HA antibody. (A and B) Kidins220/ARMS and JIP1 do not compete for binding to KLC. (A) Representative western blot of co-immunoprecipitation of JIP1 and Kidins220/ARMS with KLC. Co-precipitation of Kidins220/ARMS with KLC (lane 6) or of JIP1 with KLC (lane 7) is not altered by the presence of the other cargo protein (lane 8). (B) Quantification of five independent experiments. Error bars = +/- SEM. $p>0.05$ for all combinations. (C and D) Kidins220/ARMS and JIP3 do not compete for binding to KLC. (C) Representative western blot of coimmunoprecipitation of JIP3 and Kidins220/ARMS with KLC. Coprecipitation of Kidins220/ARMS with KLC (lane 6) or of JIP3 with KLC (lane 7) is not altered by the presence of the other cargo protein (lane 8). (D) Quantification of six independent experiments. Error bars = +/- SEM. $p>0.05$ for all combinations.

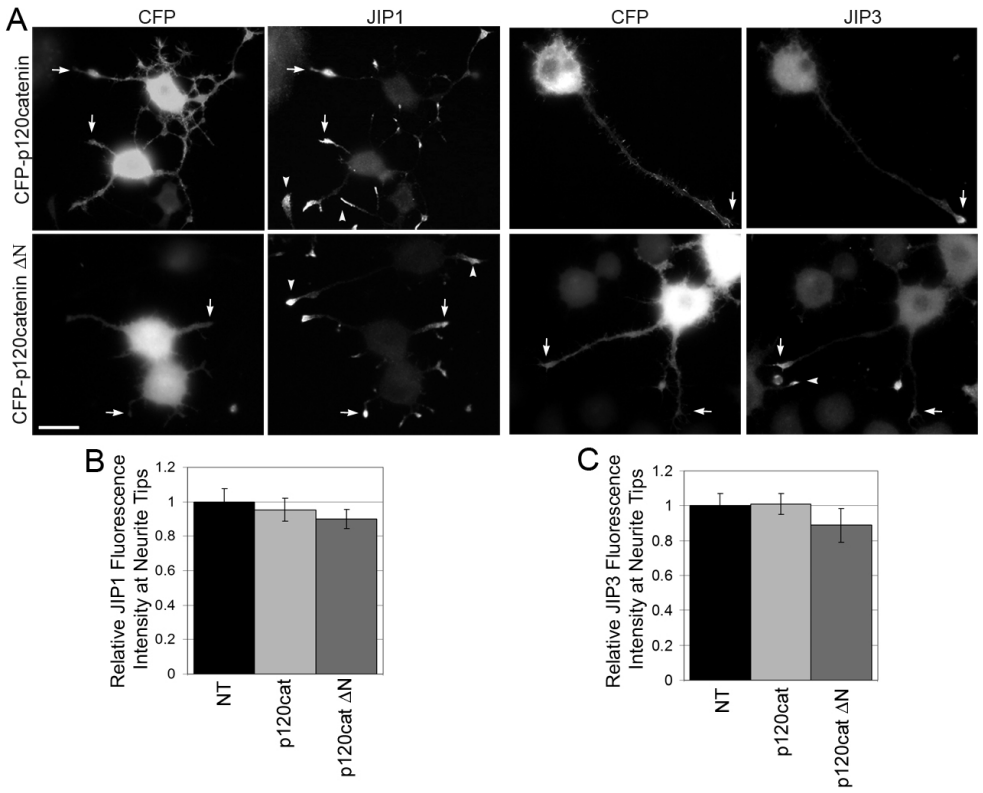

Figure Supplemental 4.3: p120catenin, a KHC-binding Kinesin-1 cargo, does not compete with JIP1 or JIP3 for transport. (A) Differentiated CAD cells expressing CFP-p120catenin or an N-terminally truncated version of p120-catenin, ΔN, were stained for endogenous JIP1 (left panels) or JIP3 (right panels). Arrows, neurite tips of transfected cells; arrowheads, neurite tips of non-transfected cells. Scale bar = 20 μm. (B and C) Quantification of JIP1 (B) or JIP3 (C) fluorescence intensity at neurite tips of non-transfected cells (NT) or cells transfected with the indicated p120catenin construct. N>100 neurites for each construct. Error bars = +/- SEM. ($p>0.01$ for all transfected constructs).

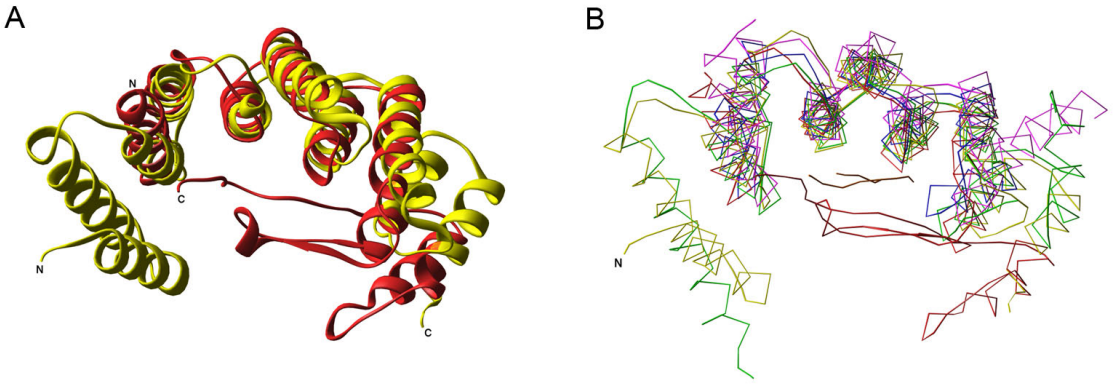

Figure Supplemental 4.4: Alignment of the structural model of KLC TPR repeats 1-5 with known TPR domain structures. The sequences of TPRs 2-5 of rat KLC1-C were overlaid onto the known crystal structures of human Pex5 and $p67^{phox}$. The first TPR of KLC (residues 210 –246) was then modeled by spatial alignment with the helical regions of Pex5. The sixth TPR repeat of KLC could not accurately be represented in the model through sequence or structural alignments to other TPR regions due to a long insertion between the fifth and sixth TPR motifs that is unique to KLC. (A) Ribbon diagrams depicting the structural alignment of the TPR domains of $p67^{phox}$ residues B2 – B186 (red, PDB code 1E96) aligned with the model of KLC1, residues 210 – 411, shown in yellow. (B) Manual alignment of the Cα atoms of the TPR region of the KLC1 structural model with four known TPR crystal structures. Yellow, KLC1 residues 210 – 411. Magenta, PP5 residues 19 – 170 (PDB code: 1A17). Blue, Hop residues A2 – A118 (PDB code 1ELW). Red, $p67^{phox}$ residues B2 –B186 (PDB code 1E96). Green, Pex5 residues A420 – A602 (PDB code 1FCH). Depicted in brown are the co-crystallized binding partners of Hop (Hsp70 C-terminal peptide (C5 – C12), PDB code 1ELW) and $p67^{phox}$ (peroxisomal targeting peptide (C1 – C5), PDB code 1E96). Acknowledgement: This figure was generously provided by Jeanne Stuckey, University of Michigan.

REFERENCES

1. Caviston, J.P. and E.L. Holzbaur, *Microtubule motors at the intersection of trafficking and transport.* Trends Cell Biol, 2006. **16**(10): p. 530-7.
2. Hirokawa, N. and R. Takemura, *Molecular motors and mechanisms of directional transport in neurons.* Nat Rev Neurosci, 2005. **6**(3): p. 201-14.
3. Gunawardena, S. and L.S. Goldstein, *Cargo-carrying motor vehicles on the neuronal highway: transport pathways and neurodegenerative disease.* J Neurobiol, 2004. **58**(2): p. 258-71.
4. Adio, S., et al., *Review: regulation mechanisms of Kinesin-1.* J Muscle Res Cell Motil, 2006: p. 1-8.
5. Gindhart, J.G., *Towards an understanding of kinesin-1 dependent transport pathways through the study of protein-protein interactions.* Brief Funct Genomic Proteomic, 2006. **5**(1): p. 74-86.
6. Gyoeva, F.K., E.M. Bybikova, and A.A. Minin, *An isoform of kinesin light chain specific for the Golgi complex.* J Cell Sci, 2000. **113**(Pt 11): p. 2047-54.
7. Wozniak, M.J. and V.J. Allan, *Cargo selection by specific kinesin light chain 1 isoforms.* Embo J, 2006. **25**(23): p. 5457-5468.
8. D'Andrea, L.D. and L. Regan, *TPR proteins: the versatile helix.* Trends Biochem Sci, 2003. **28**(12): p. 655-62.
9. Main, E.R., et al., *Design of stable alpha-helical arrays from an idealized TPR motif.* Structure (Camb), 2003. **11**(5): p. 497-508.
10. Cliff, M.J., et al., *Conformational diversity in the TPR domain-mediated interaction of protein phosphatase 5 with Hsp90.* Structure, 2006. **14**(3): p. 415-26.
11. Gatto, G.J., Jr., et al., *Peroxisomal targeting signal-1 recognition by the TPR domains of human PEX5.* Nat Struct Biol, 2000. **7**(12): p. 1091-5.
12. Scheufler, C., et al., *Structure of TPR domain-peptide complexes: critical elements in the assembly of the Hsp70-Hsp90 multichaperone machine.* Cell, 2000. **101**(2): p. 199-210.
13. Lapouge, K., et al., *Structure of the TPR domain of p67phox in complex with Rac.GTP.* Mol Cell, 2000. **6**(4): p. 899-907.
14. Coates, J.C., *Armadillo repeat proteins: beyond the animal kingdom.* Trends Cell Biol, 2003. **13**(9): p. 463-71.
15. Kobe, B. and A.V. Kajava, *The leucine-rich repeat as a protein recognition motif.* Curr Opin Struct Biol, 2001. **11**(6): p. 725-32.
16. Li, J., A. Mahajan, and M.D. Tsai, *Ankyrin repeat: a unique motif mediating protein-protein interactions.* Biochemistry, 2006. **45**(51): p. 15168-78.
17. Yaffe, M.B., *How do 14-3-3 proteins work?-- Gatekeeper phosphorylation and the molecular anvil hypothesis.* FEBS Lett, 2002. **513**(1): p. 53-7.

18. Bowman, A.B., et al., *Kinesin-dependent axonal transport is mediated by the sunday driver (SYD) protein.* Cell, 2000. **103**(4): p. 583-94.

19. Byrd, D.T., et al., *UNC-16, a JNK-signaling scaffold protein, regulates vesicle transport in C. elegans.* Neuron, 2001. **32**(5): p. 787-800.

20. Verhey, K.J., et al., *Cargo of kinesin identified as JIP scaffolding proteins and associated signaling molecules.* J Cell Biol, 2001. **152**(5): p. 959-70.

21. Whitmarsh, A.J., *The JIP family of MAPK scaffold proteins.* Biochem Soc Trans, 2006. **34**(Pt 5): p. 828-32.

22. Kelkar, N., C.L. Standen, and R.J. Davis, *Role of the JIP4 scaffold protein in the regulation of mitogen-activated protein kinase signaling pathways.* Mol Cell Biol, 2005. **25**(7): p. 2733-43.

23. Nguyen, Q., et al., *JLP associates with kinesin light chain 1 through a novel leucine zipper-like domain.* J Biol Chem, 2005. **280**(34): p. 30185-91.

24. Horiuchi, D., et al., *APLIP1, a kinesin binding JIP-1/JNK scaffold protein, influences the axonal transport of both vesicles and mitochondria in Drosophila.* Curr Biol, 2005. **15**(23): p. 2137-41.

25. Hurd, D.D. and W.M. Saxton, *Kinesin mutations cause motor neuron disease phenotypes by disrupting fast axonal transport in Drosophila.* Genetics, 1996. **144**(3): p. 1075-85.

26. Araki, Y., et al., *The novel cargo Alcadein induces vesicle association of kinesin-1 motor components and activates axonal transport.* Embo J, 2007. **26**(6): p. 1475-1486.

27. Bracale, A., et al., *Kidins220/ARMS is transported by a kinesin-1-based mechanism likely to be involved in neuronal differentiation.* Mol Biol Cell, 2007. **18**(1): p. 142-152.

28. McGuire, J.R., et al., *Interaction of Huntingtin-associated protein-1 with kinesin light chain: implications in intracellular trafficking in neurons.* J Biol Chem, 2006. **281**(6): p. 3552-3559.

29. Ichimura, T., et al., *Phosphorylation-dependent interaction of kinesin light chain 2 and the 14-3-3 protein.* Biochemistry, 2002. **41**(17): p. 5566-72.

30. Kamal, A., et al., *Axonal transport of amyloid precursor protein is mediated by direct binding to the kinesin light chain subunit of kinesin-I.* Neuron, 2000. **28**(2): p. 449-59.

31. Kamm, C., et al., *The early onset dystonia protein torsinA interacts with kinesin light chain 1.* J Biol Chem, 2004.

32. Kimura, T., et al., *Tubulin and CRMP-2 complex is transported via Kinesin-1.* J Neurochem, 2005. **93**(6): p. 1371-82.

33. Konecna, A., et al., *Calsyntenin-1 docks vesicular cargo to kinesin-1.* Mol Biol Cell, 2006. **17**(8): p. 3651-63.

34. Ward, B.M. and B. Moss, *Vaccinia virus A36R membrane protein provides a direct link between intracellular enveloped virions and the microtubule motor kinesin.* J Virol, 2004. **78**(5): p. 2486-93.

35. Dictenberg, J.B., et al., *ZBP1 mediates dendritic mRNA granule localization through a direct interaction with a novel Kinesin Light Chain (KLC)-like Protein in Neurons.* Mol Biol Cell, 2006. **17 (Supp)**: p. 1162.

36. Reed, N.A., et al., *Microtubule acetylation promotes kinesin-1 binding and transport.* Curr Biol, 2006. **16**(21): p. 2166-72.

37. Chen, X., et al., *p120 catenin associates with kinesin and facilitates the transport of cadherin-catenin complexes to intercellular junctions.* J Cell Biol, 2003. **163**(3): p. 547-57.

38. Jinek, M., et al., *The superhelical TPR-repeat domain of O-linked GlcNAc transferase exhibits structural similarities to importin alpha.* Nat Struct Mol Biol, 2004. **11**(10): p. 1001-7.

39. Cai, D., et al., *Kinesin-1 structural organization and conformational changes revealed by FRET stoichiometry in live cells.* J Cell Biol, 2007. **176**(1): p. 51-63.

40. Kelkar, N., et al., *Interaction of a mitogen-activated protein kinase signaling module with the neuronal protein JIP3.* Mol Cell Biol, 2000. **20**(3): p. 1030-43.

41. Sato, S., et al., *Scaffold protein JSAP1 is transported to growth cones of neurites independent of JNK signaling pathways in PC12h cells.* Gene, 2004. **329**: p. 51-60.

42. Kristensen, O., et al., *A unique set of SH3-SH3 interactions controls IB1 homodimerization.* Embo J, 2006. **25**(4): p. 785-97.

43. Yasuda, J., et al., *The JIP group of mitogen-activated protein kinase scaffold proteins.* Mol Cell Biol, 1999. **19**(10): p. 7245-54.

44. Bayarsaikhan, M., et al., *Regulation of N-cadherin-based cell-cell interaction by JSAP1 scaffold in PC12h cells.* Biochem Biophys Res Commun, 2007. **353**(2): p. 357-62.

45. Muresan, Z. and V. Muresan, *c-Jun NH2-terminal kinase-interacting protein-3 facilitates phosphorylation and controls localization of amyloid-beta precursor protein.* J Neurosci, 2005. **25**(15): p. 3741-51.

46. Liu, J., et al., *Three-dimensional structure of the myosin V inhibited state by cryoelectron tomography.* Nature, 2006. **442**(7099): p. 208-11.

47. Thirumurugan, K., et al., *The cargo-binding domain regulates structure and activity of myosin 5.* Nature, 2006. **442**(7099): p. 212-5.

48. Warren, R.A., et al., *Distinct saturable pathways for the endocytosis of different tyrosine motifs.* J Biol Chem, 1998. **273**(27): p. 17056-17063.

49. Haucke, V., *Cargo Takes Control of Endocytosis.* Cell, 2006. **127**: p. 35-37.

50. King, S.J., et al., *Subunit organization in cytoplasmic dynein subcomplexes.* Protein Sci, 2002. **11**(5): p. 1239-50.

51. Tynan, S.H., et al., *Light Intermediate Chain 1 Defines a Functional Subfraction of Cytoplasmic Dynein Which Binds to Pericentrin.* J Biol Chem, 2000. **275**(42): p. 32763-32768.

52. Tai, A.W., J.Z. Chuang, and C.H. Sung, *Cytoplasmic dynein regulation by subunit heterogeneity and its role in apical transport.* J Cell Biol, 2001. **153**(7): p. 1499-509.

53. Mok, Y.-K., K.W.-H. Lo, and M. Zhang, *Structure of Tctex-1 and Its Interaction with Cytoplasmic Dynein Intermediate Chain** J Biol Chem, 2001. **276**(17): p. 14067-14074.

54. King, S.M., et al., *Cytoplasmic dynein contains a family of differentially expressed light chains.* Biochemistry, 1998. **37**(43): p. 15033-15041.

55. Waetzig, V., Y. Zhao, and T. Herdegen, *The bright side of JNKs-Multitalented mediators in neuronal sprouting, brain development and nerve fiber regeneration.* Prog Neurobiol, 2006. **80**(2): p. 84-97.

56. Muresan, Z. and V. Muresan, *Coordinated transport of phosphorylated amyloid-beta precursor protein and c-Jun NH2-terminal kinase-interacting protein-1.* J Cell Biol, 2005. **171**(4): p. 615-25.

57. Ha, H.Y., et al., *The axon guidance defect of the telencephalic commissures of the JSAP1-deficient brain was partially rescued by the transgenic expression of JIP1.* Dev Biol, 2005. **277**(1): p. 184-99.

58. Song, J.J. and Y.J. Lee, *Cross-talk between JIP3 and JIP1 during glucose deprivation: SEK1-JNK2 and Akt1 act as mediators.* J Biol Chem, 2005. **280**(29): p. 26845-55.

59. Kukekov, N.V., Z. Xu, and L.A. Greene, *Direct interaction of the molecular scaffolds POSH and JIP is required for apoptotic activation of JNKs.* J Biol Chem, 2006. **281**(22): p. 15517-24.

60. Verhey, K.J. and T.A. Rapoport, *Kinesin carries the signal.* Trends Biochem Sci, 2001. **26**(9): p. 545-50.

61. Magliery, T.J. and L. Regan, *Beyond consensus: statistical free energies reveal hidden interactions in the design of a TPR motif.* J Mol Biol, 2004. **343**(3): p. 731-45.

62. Verhey, K.J., et al., *Light chain-dependent regulation of Kinesin's interaction with microtubules.* J Cell Biol, 1998. **143**(4): p. 1053-66.

63. Whitmarsh, A.J. and R.J. Davis, *Structural organization of MAP-kinase signaling modules by scaffold proteins in yeast and mammals.* Trends Biochem Sci, 1998. **23**(12): p. 481-5.

64. Meyer, D., A. Liu, and B. Margolis, *Interaction of c-Jun amino-terminal kinase interacting protein-1 with p190 rhoGEF and its localization in differentiated neurons.* J Biol Chem, 1999. **274**(49): p. 35113-8.

65. Cavalli, V., et al., *Sunday Driver links axonal transport to damage signaling.* J Cell Biol, 2005. **168**(5): p. 775-87.

66. Jones, T.A., et al., *Improved methods for building protein models in electron density maps and the location of errors in these models.* Acta Crystallogr A, 1991. **47 (Pt 2)**: p. 110-9.

67. Moore, D.D., *Gene Synthesis*, in *Current Protocols in Molecular Biology*, F.M. Ausubel, et al., Editors. 2002, J. Wiley and Sons. p. 8.2.8-8.2.13.

68. Fromant, M., S. Blanquet, and P. Plateau, *Direct random mutagenesis of gene-sized DNA fragments using polymerase chain reaction.* Anal Biochem, 1995. **224**(1): p. 347-53.

69. Wilson, D.S. and A.D. Keefe, *Random Mutagenesis by PCR*, in *Current Protocols in Molecular Biology*, F.M. Ausubel, et al., Editors. 2002, J. Wiley and Sons. p. 8.3.1-8.3.4.

70. Yu, J.Y., S.L. DeRuiter, and D.L. Turner, *RNA interference by expression of short-interfering RNAs and hairpin RNAs in mammalian cells.* Proc Natl Acad Sci U S A, 2002. **99**(9): p. 6047-52.

71. Matsuguchi, T., et al., *JNK-interacting protein 3 associates with Toll-like receptor 4 and is involved in LPS-mediated JNK activation.* Embo J, 2003. **22**(17): p. 4455-64.

Chapter 5:
Microtubule Post-Translational Modifications Direct Kinesin-1 into Axons

Unidirectional signal transduction by neuronal cells is intimately linked to their highly polarized morphology. The biogenesis and maintenance of distinct axon/dendrite compartments depends on transport of specific vesicles and proteins along microtubules to their proper cellular locations. Despite much effort, it is still unclear how polarity is established. Several signaling pathways and proteins have been identified that control neurite outgrowth and/or axon specification including: the PI3K/Akt/GSK3β pathway; the Par3/Par6/aPKC complex; SAD kinases; Ras, Rac, Cdc42, and Rap1b small GTPases; APC, and CRMP-2 [1, 2]. Many of these signaling pathways regulate components of the actin cytoskeleton to facilitate growth cone motility, as well as components of microtubule-based transport systems for targeted delivery of vesicles and protein complexes [1, 2]. As specification and maintenance of neuronal polarity rely on microtubule-based transport, understanding the molecular mechanisms responsible for the polarized transport of kinesin motors to axons and/or dendrites is critical to understanding neuronal organization and polarity.

The process of cellular polarization has been studied in cell culture, typically with primary hippocampal neurons [3]. Unpolarized (stage 1) cells start their differentiation process by extending multiple apparently identical neurites (stage 2). Polarity is established a short time later when one neurite undergoes a period of rapid extension and becomes the axon (stage 3). The remaining neurites will then become dendrites (stages 4 and 5).

Upon polarization (stage 3), several signaling components become localized to the growth cone of the developing axon (Par3/Par6/aPKC complex, APC, PIP_3, JIP1, as well as members of the Rho family GTPases: Rac, Cdc42, and Rap1b and some of their activating GEFs) [4-15]. Several mechanisms have been proposed to account for this

polarized localization including 1) selective transport down the axon by kinesin motors, 2) selective degradation by the ubiquitin/proteasome system in minor neurites, or 3) localized activation or production of signaling components in the developing axon [1, 2, 16-21]. In the case of selective microtubule transport, the Kinesin-1 motor and its cargo protein JNK-interacting protein (JIP)-1 accumulate preferentially in the developing axon [11, 16, 17]. Kinesin-1 also transports CRMP2, a protein essential for axon specification [22]. The Kinesin-3 family member, Gakin, delivers PIP_3-containing vesicles via its interaction with the PIP_3-interacting protein, PIP_3BP, thus contributing to the PIP_3 accumulation that initiates signaling cascades important for axon specification [13, 15, 23]. Finally the Kinesin-2 family member, KIF3, has been implicated in transporting proteins essential for axon elongation and specification (APC and the Par3 complex), but whether this involves selective transport to the developing axon, or general transport to all neurites is still unclear [4, 14].

How the developing axon in stage 3 is chosen from apparently equivalent neurites in stage 2 is still unclear. Recent work has shown that kinesin motors can distinguish between apparently equivalent neurites in stage 2, even before morphological differentiation has taken place. Using live cell imaging of fluorescently-tagged, constitutively active versions of the Kinesin-1 motor KIF5C, Jacobson et al showed that Kinesin-1 accumulates in a subset of neurites in a very dynamic fashion [16]. The Kinesin-1 cargo JIP1 also localizes to a subset of neurites in nonpolarized cells and may play a role in axonal specification and growth [11, 24]. Thus, the selectivity of endogenous and over-expressed Kinesin-1 motors for specific neurites is one of the earliest known molecular differences between seemingly equivalent neurites in stage 2 cells.

What are the molecular signals that drive the selective transport of Kinesin-1 motors in neurites of unpolarized stage 2 neurons and axons of polarized stage 3 neurons? Recent work has raised the possibility that Kinesin-1 “reads” biochemical cues that specify a qualitatively and/or functionally distinct set of microtubule tracks in selected neurites and axons. Previous work has shown that stage 3 axons are enriched in stable microtubules as compared to minor neurites [25, 26]. Stable microtubules comprise a subset of the total microtubules in cells whose low turnover enables a long half-life (t ½ =

hours) as compared to dynamic microtubules (t ½ = minutes). Stable microtubules are resistant to depolymerization by microtubule-destabilizing drugs such as nocodazole and become marked by a variety of post-translational modifications (PTMs) in an age-dependent manner. Thus, stable microtubules may serve as an axonal signal for Kinesin-1. In support of this possibility, in vitro assays have shown that Kinesin-1 has a binding preference for microtubules containing the PTMs of acetylation, detyrosination, and polyglutamylation [24, 26-30]. In addition, hyperacetylation of microtubules can misdirect Kinesin-1 transport of JIP1 in stage 2 primary hippocampal neurons [24].

Whether one particular microtubule PTM or a combination of PTMs provides a biochemical cue that directs Kinesin-1 to the developing axon in stage 3 cells is unknown. Here we test the possibility that microtubule acetylation directs Kinesin-1 axonal sorting by analyzing the transport of expressed constitutively active Kinesin-1 motors and endogenous Kinesin-1 cargoes in primary hippocampal neurons. We show that Kinesin-1 can be influenced by microtubule acetylation in stage 2 neurons but not in stage 3 neurons. Rather, in stage 3 neurons, Kinesin-1 "reads" axonal cues that can override the acetylation input. This axonal cue can be incorporated into dendrites by low concentration taxol treatment or inhibition of GSK3β. Both treatments correlate with an increase in multiple microtubule PTMs. These results suggest that multiple microtubule biochemical inputs may create a "code" that directs kinesin motors to specific subcellular destinations.

RESULTS

Kinesin-1 prefers neurites and axons with higher levels of modified microtubules

Kinesin-1 has been shown to preferentially transport down axons in stage 3 and later primary hippocampal neurons [16, 17]. However, the molecular mechanism for this axonal sorting is unknown. It is possible that the mechanism is related to a specific property of the microtubule population in axons. Previous work has shown that axons contain a higher percentage of stable microtubules than dendrites [25, 26]. Thus, we asked whether the microtubule PTMs often associated with stable microtubules are enriched in axons. To do this, we stained stage 3 primary hippocampal neurons with antibodies that recognize the known microtubule PTMs of α-tubulin acetylation, α-

tubulin detyrosination, and polyglutamylation of both α- and β-tubulin. The ratio of modified tubulin to total tubulin in the axon was compared to minor neurites. The levels of acetylated α-tubulin and polyglutamylated α-tubulin were significantly higher in the developing axon than in the minor neurites (Figure 5.1 A and B). Other labs have also demonstrated accumulation of detyrosinated microtubules in axons (Gary Banker, personal communication). We conclude that microtubule PTMs are enriched in axons and therefore may provide a biochemical cue for Kinesin-1 that drives polarized transport.

We then tested whether the microtubule PTMs are also enriched in minor neurites chosen by Kinesin-1 in unpolarized stage 2 primary hippocampal neurons. Recent work has shown that one neurite in stage 2 neurons is often enriched in stable microtubules [25]. Yet it is unknown whether the presence of stable microtubules and/or the PTMs that mark this subpopulation correlate with the presence of proteins known to accumulate in one neurite of stage 2 neurons. As Kinesin-1 is one of the earliest known markers of the newly specified axon and often localizes to one or a few stage 2 neurites, we tested whether the preferential trafficking of Kinesin-1 motors also correlates with increased levels of microtubule PTMs. We used constitutively active versions of Kinesin-1 (CA-Kinesin-1) that contain a dimeric motor domain required for microtubule-based motility but lack the C-terminal tail domains required for autoinhibition and cargo-binding [Kif5c(1-560) or Kif5c(1-509)]. When tagged with fluorescent proteins and expressed in neuronal cells, such truncated motors provide a direct readout of Kinesin-1 activity regulated primarily by the microtubule/motor interface [16, 17, 31]. Stage 2 hippocampal neurons expressing CA-Kinesin-1 were fixed and stained for total α-tubulin and the various PTMs. The ratio of modified tubulin to total tubulin was then compared between neurites with or without significant CA-Kinesin-1 accumulation. For the acetylation and polyglutamylation modifications, the level of modified tubulin was higher in neurites with CA-Kinesin-1 accumulation than in neurites that lack CA-Kinesin-1 (Figure 5.1 C-E). These results suggest that the preferential accumulation of microtubule PTMs in one neurite of stage 2 neurons may serve to direct Kinesin-1 trafficking into that neurite, thus promoting axon growth and specification.

Microtubule acetylation influences the localization of the Kinesin-1 cargo JIP1 in unpolarized (stage 2) but not polarized (stage 3) neurons

That microtubule PTMs regulate Kinesin-1 transport is supported by recent data showing that hyperacetylation of microtubules in stage 2 primary hippocampal neurons results in a misdirection of Kinesin-1 transport [24]. In this study, the localization of the Kinesin-1 cargo JIP1 in fixed cells was used as a read-out of the activity of the endogenous Kinesin-1 motor. In primary neurons, the localization of JIP1 to a subset of neurites in stage 2 cells, and to the developing axon in stage 3 cells, is dependent on Kinesin-1 activity [11, 24, 32]. Stage 2 primary hippocampal neurons were treated with 125nM trichostatin A (TSA), a general deacetylase inhibitor, or with 5-10μM tubacin, a specific inhibitor of the tubulin deacetylase HDAC6, for 3 hours to hyperacetylate microtubules (Figure 5.2 C, F). Cells were then fixed and stained for acetylated tubulin and the endogenous JIP1 protein. In control cells, JIP1 was localized to a subset of neurites whereas hyperacetylation resulted in a redirection of JIP1 to a greater percentage of neurites (Figure 5.2 A and B, [24]). Thus, preferential transport of JIP1 to a subset of neurites by the endogenous Kinesin-1 motor can be influenced specifically by the acetylation PTM present on microtubules.

We thus tested whether microtubule acetylation can influence Kinesin-1 transport of JIP1 to axons in stage 3 neurons. Stage 3 primary hippocampal neurons were treated with TSA or tubacin and then fixed and stained for the endogenous JIP1 protein. Surprisingly, in polarized stage 3 neurons, increased acetylation (Figure 5.2 D and E) had no effect on JIP1 transport. In both control and treated cells, JIP1 accumulated exclusively in the developing axon and not minor neurites (Figure 5.2 D and E). These results suggest that the PTM of α-tubulin acetylation is not sufficient to provide the biochemical cue that drives axonal transport of Kinesin-1.

Microtubule acetylation does not influence the motility of CA-Kinesin-1 motors in polarized (stage 3) neurons

That alterations in microtubule acetylation influence JIP1 localization in stage 2 cells but not in stage 3 cells could be explained by differences in the cellular environment (e.g. axonal retention of JIP1) other than Kinesin-1 transport. Thus, to test directly

whether acetylation influences Kinesin-1 motors in stage 3 neurons, we analyzed the effects of increased acetylation on CA-Kinesin-1 motors. Primary hippocampal neurons were electroporated with CA-Kinesin-1-EGFP at the time of plating. Upon reaching stage 3, the cells were treated with DMSO control, 2μM tubacin, or 100nM TSA and then observed using time-lapse live-cell imaging. Before treatment, CA-Kinesin-1 accumulated specifically in the developing axon. After treatment with TSA or tubacin for 1 to 2 hours, no movement of CA-Kinesin-1 motors to minor neurites was observed (Figure 5.3 A and B) despite significant increases in the levels of acetylated tubulin within the same time period (Figure 5.3 C).

An alteration of CA-Kinesin-1 localization in this experiment would require that CA-Kinesin-1 motors localized at the tip of the developing axon return to the cell body before choosing minor neurites. Thus, we performed a second set of experiments designed to allow newly-made CA-Kinesin-1 motors equal opportunity to choose hyperacetylated axons or minor neurites without the need to first diffuse out of the axon. Stage 3 or stage 5 mouse hippocampal neurons were treated for 3-4 hours with DMSO, 125nM TSA, or 10μM tubacin. The cells were then transfected with CA-Kinesin-1-mCherry together with YFP to illuminate the entire cell, and allowed to express the exogenous proteins under additional treatment for 4-5 hours. CA-Kinesin-1 motors accumulated preferentially in the developing axon and not in minor neurites in both control and treated stage 3 cells (Figure 5.3, D and E). Similarly, CA-Kinesin-1 motors accumulated in axons rather than dendrites in stage 5 cells (Figure 5.3 E).

Thus, although increased microtubule acetylation can influence Kinesin-1 transport in stage 2 cells (Figure 5.2), it did not alter the preferential localization of the Kinesin-1 cargo JIP1 or the preferentially transport of CA-Kinesin-1 motors to axons in polarized cells (Figures 5.2 and 5.3). Hyperacetylation caused by deacetylase inhibitors also did not cause multiple axons. Treating cells with 5μM tubacin from 3hrs after plating until 6 days *in vitro* does not increase the percentage of cells with multiple axons (Figure 5.3 F and [25]). We conclude that acetylation is not the primary signal that drives axonal trafficking of Kinesin-1. Rather, Kinesin-1 apparently recognizes some other biochemical property of microtubules present in axons that is absent or decreased in other processes (minor neurites or dendrites).

Taxol treatment alters microtubule modifications and selective Kinesin-1 transport in both stage 2 and stage 3 primary hippocampal neurons

Although changes in microtubule acetylation are not sufficient to alter the preferential transport of Kinesin-1 to axons in polarized cells, treatment of differentiated neurons (stage 5) with low doses of the microtubule-stabilizing drug, taxol, has been shown to redirect CA-Kinesin-1 motors to dendrites [17]. In our hands, treatment of stage 5 primary hippocampal neurons did indeed result in the accumulation of CA-Kinesin-1 motors in both dendritic and axonal growth cones (Figure 5.4 A and C). This effect was also seen earlier in differentiation, as treatment of stage 3 neurons with low levels of taxol also resulted in accumulation of CA-Kinesin-1 motors in minor neurites (Figure 5.4 B and C). These results suggest that promoting microtubule stabilization in non-axonal processes is sufficient to override the axonal signal used by Kinesin-1.

We next explored the dynamics of taxol-induced changes in microtubule PTMs and Kinesin-1 transport. Primary hippocampal neurons that had been electroporated with CA-Kinesin-1-mCit at the time of plating, were treated with DMSO control or with 10nM or 100nM Taxol and observed using time-lapse live cell imaging. In unpolarized stage 2 cells where Kinesin-1 was initially evenly distributed throughout the cell, the motor accumulated in all neurite tips within 10-20 minutes after taxol treatment (Figure 5.5 A, B, and D), but not after DMSO treatment (data not shown, Figure 5.2 A and B). In treated cells, CA-Kinesin-1 fluorescence stayed relatively constant in all neurite tips for the duration of the recording (Figure 5.5 A and B) ; whereas, some untreated cells showed transient activity of CA-Kinesin-1 towards one or a few neurites over time as previously reported [16] . It is interesting that in these stage 2 cells, although there are plenty of microtubule tracks for constitutively active Kinesin-1 to take to the ends of neurites, Kinesin-1's processivity is still limited. Upon taxol treatment the biochemical properties of the microtubules must be altered such that Kinesin-1 finds the tracks more suitable and quickly responds by accumulating at neurite tips.

In polarized stage 3 cells, CA-Kinesin-1-mCit showed a similar change in trafficking upon taxol treatment. Prior to treatment, most CA-Kinesin-1 was accumulated in the axon with only a minor portion present in the cell body. Within 10-20 mins of taxol treatment, the minor neurites showed a significant accumulation of CA-

Kinesin-1 (Figure 5.5 C and D). The CA-Kinesin-1 fluorescence in minor neurites continued to increase at a gradual rate over the 4 hour period imaged. At the end of the imaging period, CA-Kinesin-1 was accumulated at the tips of 95% of axons and 66% of minor neurites. However cells treated with DMSO had CA-Kinesin-1 in axons only (98% of axons, 3% of dendrites) (Figure 5.5 E and F).

To determine the changes in microtubule PTMs occurring over this time course of taxol treatment, a mix of stage 2/stage 3 primary hippocampal neurons were treated for 0-60 minutes with 100nM Taxol. Cells were collected, lysed, run on SDS-PAGE gel, and then immunoblotted for total β-tubulin and for specific tubulin modifications (acetylated α-tubulin, detyrosinated α-tubulin, or polyglutamylated tubulin). Like TSA or tubacin treatment, taxol treatment caused a rapid (within 7.5 min) increase in the level of α-tubulin acetylation (Figure 5.5 G). Importantly, taxol treatment also caused a rapid (within 7.5 min) increase in the other known microtubule PTMs, detyrosination of α-tubulin and polyglutamylation of α- and β-tubulin (Figure 5.5 G). Importantly, this is the same time scale of taxol treatment that results in alterations in CA-Kinesin-1 trafficking in unpolarized stage 2 neurites and polarized stage 3 minor neurites. These results demonstrate that alterations in microtubule stability and/or PTMs regulate the selective transport of Kinesin-1 in both unpolarized and polarized neurons.

We thus asked what effects taxol treatment has on the transport of endogenous Kinesin-1 motors and on neuronal polarity. Stage 2 and Stage 3 primary hippocampal neurons were treated with DMSO control or with 10nM or 100nM taxol for 3 hours. The cells were then fixed and stained with antibodies to the Kinesin-1 cargo, JIP1, and acetylated α-tubulin. In stage 2 cells, taxol treatment resulted in redistribution of JIP1 from a subset of neurites to the majority of neurite tips (Figure 5.6 A and B). In stage 3 cells, taxol treatment caused JIP1 to accumulate in both future dendrites and axons, rather than just specifically in axons, as seen in control cells (Figure 5.6 C and D). To determine the PTM changes associated with this treatment, a mixture of stage 2 and 3 cortical cells were treated with 10 or 100nM taxol for 3 hours. Cells were then collected, lysed, and analyzed by western blot. Taxol treatment resulted in a significant increase in the amount of tubulin acetylation, detyrosination, and polyglutamylation (Figure 5.6 E; increased acetylation levels also visible by immunofluorescence Figure 5.6 A and C).

Microtubule stabilization induced by long-term taxol treatment is also sufficient to induce multiple axons in differentiated neurons. Staining of cells with antibodies to the axonal marker Tau-1 and the dendritic marker MAP2 demonstrates that untreated cells have a single Tau-1-positive axon leaving the cell body whereas taxol-treated cells have multiple Tau-1-positive axons that protrude from the cell body (Figure 5.6 F and G; [25]). Thus, taxol treatment results in changes within the microtubule cytoskeleton that dictate an axonal-like morphology and assemblage of proteins.

Inhibition of GSK3β signaling abolishes selective Kinesin-1 transport in stage 3 primary hippocampal neurons

Alterations in axon/dendrite identity can also be induced by pharmacological inhibition of the protein kinase GSK3β. In hippocampal cells, inhibition of GSK3β specifically toward primed substrates like APC and CRMP-2 can induce the formation of multiple axons or alternatively axons with increased branching [33-35]. The ability to form multiple axons suggests the possibility that events downstream of GSK3β activity limit the occurrence of microtubule based "axonal" signals. We first tested whether CA-Kinesin-1 motors could recognize and follow the cues provided by the multiple axons generated upon GSK3β inhibition. Cells that were nucleofected with CA-Kinesin-1-mCit at the time of plating were cultured in 5μM of the GSK3β inhibitor SB216763 for 6 days. Staining cells with antibodies to the axonal marker Tau-1 and the dendritic marker MAP2 demonstrates that pharmacological inhibition of GSK3β resulted in a significant increase in the number of cells with multiple axons (Figure 5.7 A), consistent with previous reports [33, 35]. When the treated cells were stained with an antibody to GFP to enhance the mCit signal on CA-Kinesin-1-mCit, the active Kinesin-1 motors accumulated in all axonal tips (Figure 5.7 B), suggesting GSK3β inhibition generated genuine axons containing the microtubule based axonal cue recognized by Kinesin-1.

We next asked whether Kinesin-1 could be redirected into the minor neurites of early polarizing neurons (stage 3) or the dendrites of fully differentiated (stage 5) neurons using shorter time periods of GSK3β inhibition. Stage 3 or 5 neurons were treated for 2-4 hours with DMSO control or with 5-10μM SB216763. Cells were then lipofectamine transfected with CA-Kinesin-1-mCherry together with YFP as a whole cell marker. After

additional treatment and expression time of 4-6 hours, cells were fixed and imaged. Inhibition of GSK3β for a total of ~ 8 hours resulted in significant CA-Kinesin-1-mCherry accumulation in minor neurites (stage 3) or dendrites (stage 5) in addition to the axon (Figure 5.7 D-F). Finally, we tested whether GSK3β inhibition could influence Kinesin-1 transport in unpolarized stage 2 cells. Treating stage 2 cells with 10μM SB216763 increased the percentage of neurites with JIP1 accumulation (Figure 5.7 G and H).

As inhibition of GSK3β resulted in an increase in "axonal signal" recognized by Kinesin-1, we tested how microtubule PTMs were altered with GSK3β inhibition. Cells were treated with 5-10μM SB216763, lysed, run on SDS-PAGE gels, and then immunoblotted for total α-tubulin and for the known tubulin PTMs (acetylated α-tubulin, detyrosinated α-tubulin, and polyglutamylated tubulin.) Similar to taxol treatment, inhibition of GSK3β with 5-10 μM SB216763 resulted in an increase in all microtubule PTMs (Figure 5.7 I and J). We conclude that increased microtubule modifications upon inhibition of GSK3β could serve as a signal to influence Kinesin-1 transport in polarized primary hippocampal neurons.

DISCUSSION

Role of microtubule PTMs in regulating Kinesin-1 transport

Kinesin-1 has been shown to have increased binding to and motility on acetylated microtubules over non-acetylated microtubules [24]. Hyperacetylation of microtubules (due to inhibition of the tubulin deacetylase HDAC6) can influence kinesin transport in unpolarized cells, promoting transport of the Kinesin-1 cargo, JIP1, to a greater percentage of neurites (Figure 2, [24]). These results indicate that acetylated microtubules do play a positive role in regulating the kinesin-1/microtubule interaction. However, our results show that hyperacetylation has no effect on kinesin-1 transport in polarized cells, as assayed by both the localization of JIP1 and over-expressed CA-Kinesin-1 motors. Additionally hyperacetylation does not alter polarity in neuronal cultures as one would expect if acetylation provided the key "axonal" signal to microtubule motors (this study and [25]).

In polarized cells, it seems the microtubules have additional biochemical signals that direct Kinesin-1 transport even in the presence of high levels of microtubule acetylation. Our data shows that the selective transport of Kinesin-1 in polarized neurons correlates with increased levels of multiple microtubule PTMs in the axon compared to minor neurites. Thus, another microtubule biochemical modification (i.e. detyrosination, polyglutamylation, or other PTMs or microtubule properties not directly tested) or a combination of these modifications could provide the "axonal" signal to Kinesin-1. Detyrosination, polyglutamylation, and presence of MAPs each have suggested regulatory roles in the kinesin-1/microtubule interaction [24, 26-30, 36, 37]. Additionally, low concentration taxol treatment and GSK3β inhibition (both treatments which can transform dendrites into axons) result in increased levels of all PTMs tested. In the case of HDAC6 inhibition, where only the level of acetylation is increased, the additional biochemical changes occurring on the microtubules of the developing axon, must override the hyperacetylation of minor neurites or dendrites allowing Kinesin-1 to correctly transport only to the axon.

Previous work has shown that Kinesin-1 reacts to the presence of microtubule post-translation modifications other than acetylation. Kinesin-1 shows preferential binding to detyrosinated microtubules over tyrosinated microtubules [24], and is more likely to transport along detyrosinated tracks than the total number of microtubule tracks in a fibroblast cells [29]. Detyrosination microtubules also have been implicated as playing an essential role in the cellular localization of recycling endosome compartments and the kinesin mediated trafficking of TfR vesicles from these endosomal compartments to the plasma membrane [38]. The carboxypeptidase that removes the c-terminal tyrosine of α-tubulin has yet to be identified; but tubulin tyrosine ligase (TTL) replaces it, resulting a continuous detyrosination/tyrosination cycle [39-41]. In TTL knockout mice, the level of detyrosinated tubulin is artificially high, and results in perinatal death due to disorganized neuronal networks. In culture, cortical or hippocampal neurons from these mice polarize at a faster rate than wildtype cells and have a small but significant increase in the number of cells with multiple axons. Additionally growth rates of axons and minor neurites were increased, but also more erratic [42]. These results suggest that microtubule detyrosination may be important for normal polarization and neurite growth.

However, because the effect on individual cells is small other microtubule properties may also contribute to or dominate the axonal signal. Future experiments are required to test whether detyrosination plays a specific role in directing Kinesin-1 to axons.

Polyglutamylation is another tubulin modification that could influence Kinesin-1 trafficking. Polyglutamylation of α-tubulin influences transport of synaptic vesicles by the kinesin family member KIF1A [27]. Kinesin-1 has been shown to have a binding preference for microtubules that can be glutamylated [24, 30]. In polarized epithelial cells, polyglutamylated microtubules provide preferred tracks for Golgi-to-plasma membrane vesicle transport. The presence of these polyglutamylated tracks require septin2 fibers [43], which have been shown in yeast to coordinate polarized membrane growth [44, 45]. It is important to note that polyglutamylation has much more variety than other post-translational modifications. Glutamylation occurs on both α- and β-tubulin and involves the addition of one to six glutamates [40, 41, 46]. Early work has suggested that Kinesin-1 and other MAPs may have preference for certain glutamate chain lengths [30, 47]. Although recently the family of proteins involved in polyglutamylation of both α- and β-tubulin has been identified [48], the enzymes that function specifically in developing neurons has not been fully elucidated. Thus, alterations of the levels of polyglutamylation in neuronal cells will have to wait until the enzymes are more fully characterized.

Since one can only study tubulin post-translational modifications in fixed cells, it is still unclear whether the dynamic changes in kinesin-1 motility seen in stage 2 cells, where the motor switches rapidly between apparently identical neurites, are related to changes in microtubule stability and/or tubulin post-translational modifications. Yet, we were able to show that the relative levels of acetylated and polyglutamylated tubulin is higher in neurites that accumulate kinesin than in the other neurites.

Also unclear are the signaling cascades that promote PTMs on select microtubules or neurites. Our data suggests that the signaling pathways leading to GSK3β inhibition in the axon, which have already been shown to play a role in axon specification and maintenance [1, 33], may be sufficient to increase the levels of tubulin post-translational modifications in one neurite. This stabilization of microtubules and increase in PTMs is likely due to multiple downstream targets of GSK3β. APC and CRMP2 bind, stabilized,

and/or promote growth of microtubules—activities that are inhibited by GSK3β phosphorylation and are required for axon specification and growth [1, 14, 34, 35, 49]. Additional targets of GSK3β are Tau, MAP1b, MAP2, and neurofilaments [1]. Rac activity is also essential for axon specification and growth and may be tied to GSK3β activity through positive feedback loops [1, 7, 50]. Rac has been shown to promote microtubule growth and stabilization in the axon by locally inhibiting the microtubule severing/destabilizing protein stathmin/Op18 [6].

Other regulators of selective Kinesin-1 transport

Although there is evidence Kinesin-1 is directly influenced by microtubule PTMs, we cannot rule out the possibility that the axonal signal may consist to some extent on properties secondary to changes in microtubule structure such as the presence or absence of MAPs. Previous studies have well established that axonal versus dendritic microtubules have differences in the localization patterns and phosphorylation states of various MAPs. Recent work using single molecule in vitro assays has shown that tau provides road blocks for Kinesin-1, leading to kinesin dissociation from microtubules or reduced attachment rates [36, 37]. In neurons, with over-expressed MAPs, cargo transport of all types is significantly reduced, but can be rescued by dissociation of MAPs from microtubules by phosphorylation [51]. In fibroblasts, MAP4 plays an inhibitory role in vesicle trafficking that is independent of its role in microtubule stability [52]. Interestingly, microtubule PTMs and MAPs may functionally antagonize each other so that PTMs promote and direct kinesin-based transport whereas MAPs inhibit the same transport events. The association of certain MAPs with microtubules has been shown, but not always consistently, to be altered upon taxol treatment or GSK3β inhibition. Treating cells that are overexpressing tau with taxol (1μM) causes tau to rapidly dissociate from microtubules [53]. Another study showed treating neurons with 10μM taxol interferes with the binding of some but not all endogenous MAPs (increase binding of endogenous tau, but less binding of Map2 and charin MAPs) [54]. Additionally GSK3β activity is known to regulate the binding of multiple MAPs such as MAP1b, Tau, APC, and CRMP-2 [1, 34, 35, 49, 55].

MATERIALS AND METHODS

Plasmids and Antibodies: CA-Kinesin plasmids, KHC 1-509 mCit and KHC 1-560 mCit, mCherry, or YFP, were generated from rat Kif5c using PCR or convenient restriction sites and subcloned into the β-actin expression vector (S. Impey; [16]). All constructs were sequence verified. For western blots and immunofluorescence the following antibodies were used: β-tubulin E7 (Developmental Studies Hybridoma Bank), α-tubulin DM1α (Sigma) or ab18251 (Abcam); acetylated α-tubulin 6-11B-1 (Sigma T6793), or a rabbit polyclonal antibody we generated against a α-tubulin peptide; detyrosinated α-tubulin ab24622 (Abcam) or a rabbit polyclonal antibody we generated against a α-tubulin c-terminal peptide; polyglutamylated tubulin, GT335 (recognizes mono- and poly-glutamylated α- and β-tubulin; Gift of Carsten Janke). Polyclonal anti-GFP (Invitrogen) was used in some immunofluorescence experiments to enhance the GFP signal of transfected CA-Kinesin. Antibodies to neuronal polarity markers Tau-1 (Milipore MAB375) and MAP2 (Milipore AB5622) as well as JIP1 152 [56] were also used for immunofluorescence.

Cell Culture: Primary hippocampal cultures were prepared from either E16 CD1 embryonic mice or E18 embryonic rats as described in [57]. Neurons from mice were cultured in Neuralbasal media with B27 supplement and neurons from rats were cultured in DMEM with N2 supplement. Identical experiments performed in both mouse or rat neurons gave the same results. Transfection of DNA plasmids was done either at time of plating via electroporation using the Amaxa Nucleofector 1, or 1-5 days after plating using lipofectamine2000. Cells were treated for the indicated times and concentrations with Taxol (Sigma); the tubulin deacetylase inhibitors trichostatin A (TSA; Sigma), or a close structural analog of tubacin, MAZ1370, that is more potent in cell-based assays and referred to in the text as tubacin for simplicity (R. Maxitschek, personal communication); or the GSK3β inhibitor SB216763 (Sigma).

Microscopy and Image Processing: *Live cell imaging*. Cells were plated on glass-bottom dishes (MatTek) coated with poly-D-lysine and cultured in glial conditioned media. Cells were maintained at 32-34 degrees C for the duration of recording using an objective warmer and a Nikon TE2000 microscope with a Plan-APO 60X/NA 1.4 objective and Photometrics CS ES2 camera. *Fixed cells.* Cells were processed for

immunofluorescence as described [32]. Images were taken on Nikon TE2000 microscope with Photometrics CS ES2 camera or an Olympus BX51 microscope with an Olympus DP70 CCD camera. Images were processed with NIH Image J software, Metamorph, or Photoshop. Neurites were counted positive for JIP1 or CA-Kinesin-1 accumulation if the fluorescence intensity (due to immunostaining or fluorescent protein tags) in the growth cone was three-folds higher than the fluorescence intensity of the neurite shaft.

FIGURES

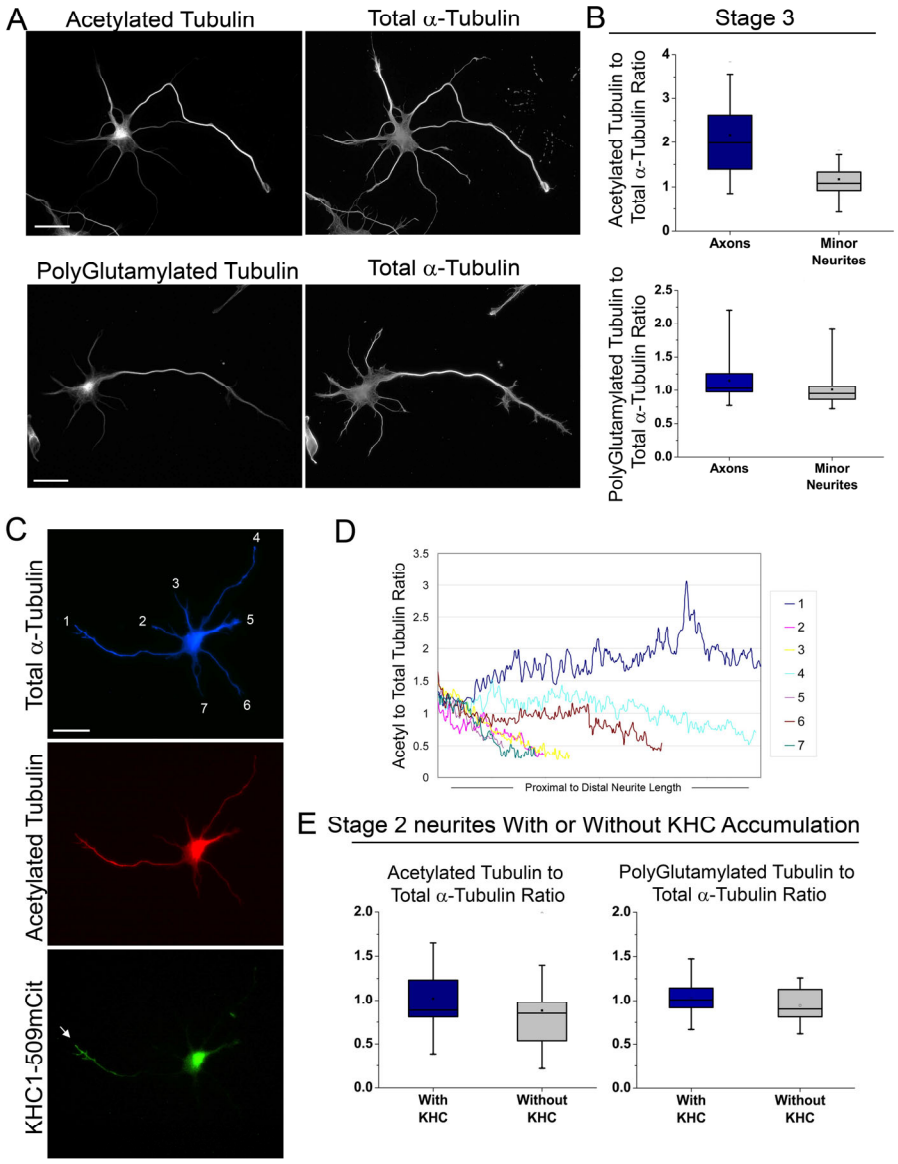

Figure 5.1: Axons and Stage 2 neurites preferred by Kinesin-1 have higher levels of modified microtubules. (A) Immunofluorescence of Stage 3 hippocampal neurons probed with antibodies to α-tubulin and either acetylated, or polyglutamylated tubulin. (B) Quantification of the ratio of PTMs to total tubulin in axons or minor neurites. (Student's T-test: Acetylation p=0.00001; Polyglutamylation p=0.0005). (C) Immunofluorescence of Stage 2 hippocampal neurons expressing CA-Kinesin-1-mCit stained with antibodies to α-tubulin (top) and acetylated α-tubulin (middle). CA-Kinesin-1 accumulates only in a subset of stage 2 neurites (bottom). (D) Quantification of the acetylated α-tubulin to total α-tubulin ratio along the proximal to distal length of each stage 2 neurite shown in C. CA-Kinesin-1 accumulated in neurite 1, which has the highest relative level of acetylated tubulin. (E) Quantification of the ratio of PTMs to total tubulin in stage 2 neurites with or without CA-Kinesin-1 accumulation. (Student's T-test: Acetylation p=0.02; Polyglutamylation p=0.003). Scale for all images=20μM

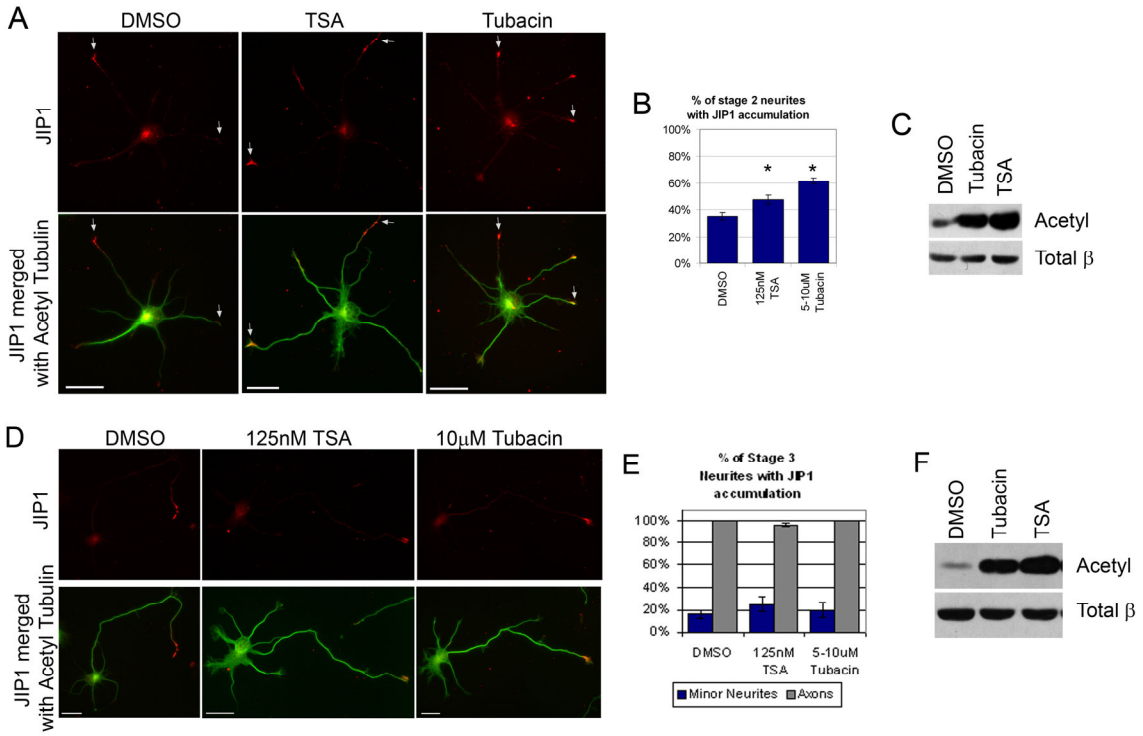

Figure 5.2: Microtubule acetylation influences JIP1 localization in unpolarized stage 2 hippocampal neurons but not in polarized stage 3 neurons. (A and B) Stage 2 hippocampal neurons were treated for 3 hours with DMSO, 125nM TSA, or 5-10μM tubacin. (A) Cells were fixed and stained for antibodies to endogenous JIP1 and acetylated α-tubulin. Scale=20μM. (B) Quantification of the percent of stage 2 neurites with JIP1 tip accumulation. Error bars= SEM. Student's T-test: **$p<0.05$ *$p<0.01$. (C) Stage 2 cortical cells were treated 3 hours with DMSO, 125nM TSA, or 10μM tubacin. Cells were then collected, lysed, and analyzed by western blot using antibodies to acetylated α-tubulin or total α-tubulin. (D and E) Stage 3 hippocampal neurons were treated for 3 hours with DMSO, 125nM TSA, or 10μM tubacin. (D) Cells were fixed and stained for antibodies to endogenous JIP1 and acetylated α-tubulin. Arrows, growth cones of minor neurites. Arrowheads, axonal growth cones. Scale=20μM. (E) Quantification of the percent of stage 3 minor neurites and axons with JIP1 tip accumulation. Error bars= SEM. Student's T-test: $p>0.05$ for all conditions. (F) Stage 3 cortical cells were treated 3 hours with DMSO, 125nM TSA, or 10μM tubacin. Cells were then collected, lysed, and analyzed by western blot using antibodies to acetylated α-tubulin or total α-tubulin.

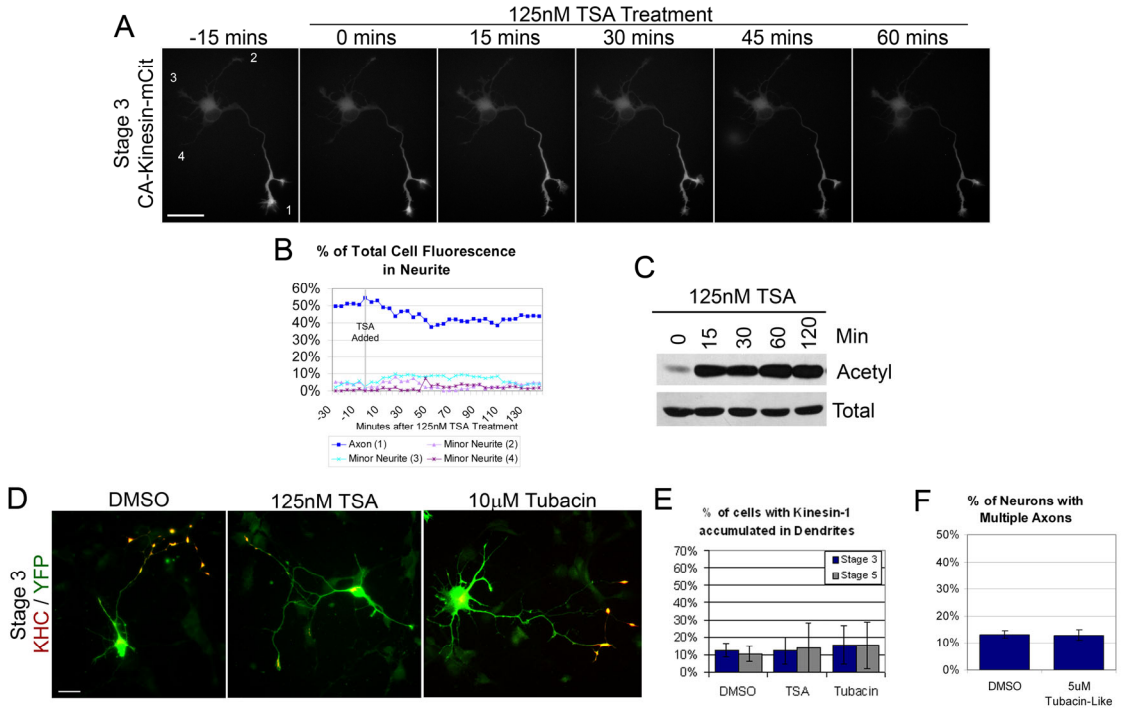

Figure 5.3: Microtubule acetylation does not influence CA-Kinesin-1 motors in polarized stage 3 primary hippocampal neurons. (A) Stage 3 hippocampal neuron expressing CA-Kinesin-1 shown at the indicated times before (-15 min) and after (15, 30, 45 and 60 mins) treatment with 250nM TSA. CA-Kinesin-1 does not accumulate in minor neurites upon TSA treatment. (B) Quantification of the experiment in A. (C) Stage 3 hippocampal cells were treated from 0-2 hours with 125nM TSA. Western blots of cell lysates were probed with anti-acetylated α-tubulin or total α-tubulin antibodies. (D) Stage 3 hippocampal cells were treated for 2-4 hours with DMSO, 125nM TSA, or 10μM tubacin. Cells were then lipofectamine transfected with CA-Kinesin-1-mCherry and YFP. Cells were allowed to express the truncated kinesin under additional treatment for 4-5 hours then fixed and imaged. Scale=20μM. (E) Quantification of the percentage of stage 3 minor neurites or stage 5 dendrites that have accumulation of CA-Kinesin-1-mCherry in growth cones after treatment described in D. Error bars=SEM. Students T-test: $p>0.05$ for all conditions. (F) Quantification of the percentage of hippocampal neurons at 6DIV with >1 axon after being cultured in 5μM tubacin from time of plating.

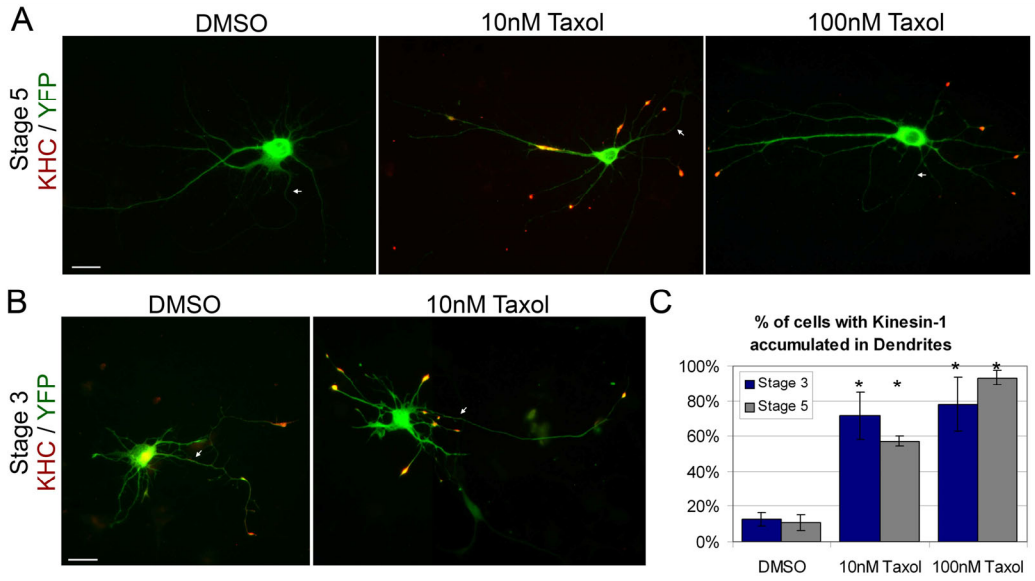

Figure 5.4: Taxol treatment redirects CA-Kinesin-1 motors to dendrites in polarized cells. (A-C) Stage 5 (A) or Stage 3 (B) hippocampal cells were treated for 2-4 hours with DMSO, 10nM or 100nM taxol. Cells were then lipofectamine transfected with CA-Kinesin-1-mCherry and YFP. Cells were allowed to express the truncated kinesin under additional treatment for 4-5 hours then fixed and imaged. Arrows indict axonal processes leaving the cell body. (C) Quantification of the percentage of stage 3 minor neurites or stage 5 dendrites that have accumulation of CA-Kinesin-1 mCherry in growth cones. Error bars=SEM. Students T-test: *$p<0.01$.

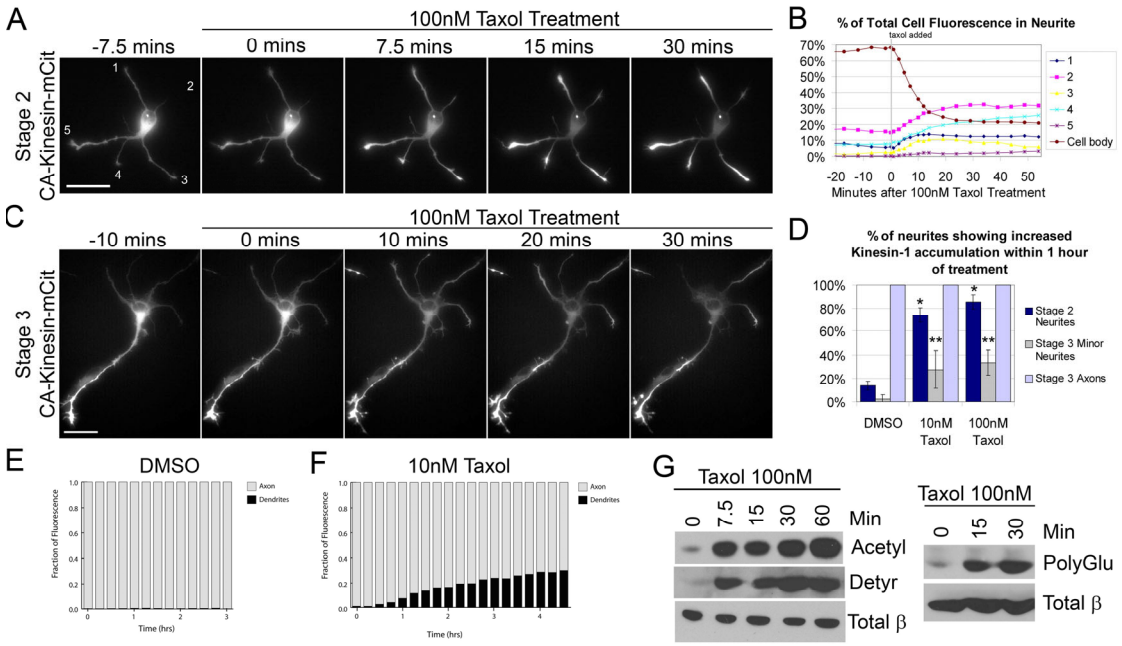

Figure 5.5: Within minutes, taxol treatment redirects Kinesin-1 to minor neurites and increases the levels of modified microtubules. (A and C) Stage 2 (A) or Stage 3 (C) hippocampal neuron expressing CA-Kinesin-mCit. Time lapse before and after 0-30 minutes of treatment with 100nM taxol. CA-Kinesin redistributes to all Stage 2 neurite tips and some Stage3 minor neurites upon taxol treatment. (B) Quantification of the percent of total fluorescence in each stage 2 neurite from the cell in A. (D) Quantification of the percentage of stage 2 neurites or Stage 3 minor neurites and axons that have increased CA-Kinesin-mCit accumulation after 1 hour taxol treatment. Error bars=SEM. Student's T-test *$p<0.01$ **$p<0.05$ (E and F) Time course quantification of DMSO (E) or 10nM taxol (F) treatment-induced dendritic accumulation of CA-Kinesin over a 4 hour treatment period. (G) A mix of Stage 2/Stage 3 hippocampal neurons were treated for 0-1 hr with 100nM taxol. Cell were collected and cell lysates were analyzed by western blot with antibodies to acetylated α-tubulin, detyrosinated α-tubulin, polyglutamylated tubulin, or total β-tubulin. Scale bars=20μM . Acknowledgements: (E) and (F) were contributed by Catherine Jacobson from Gary Banker's lab at Oregon Health and Science University.

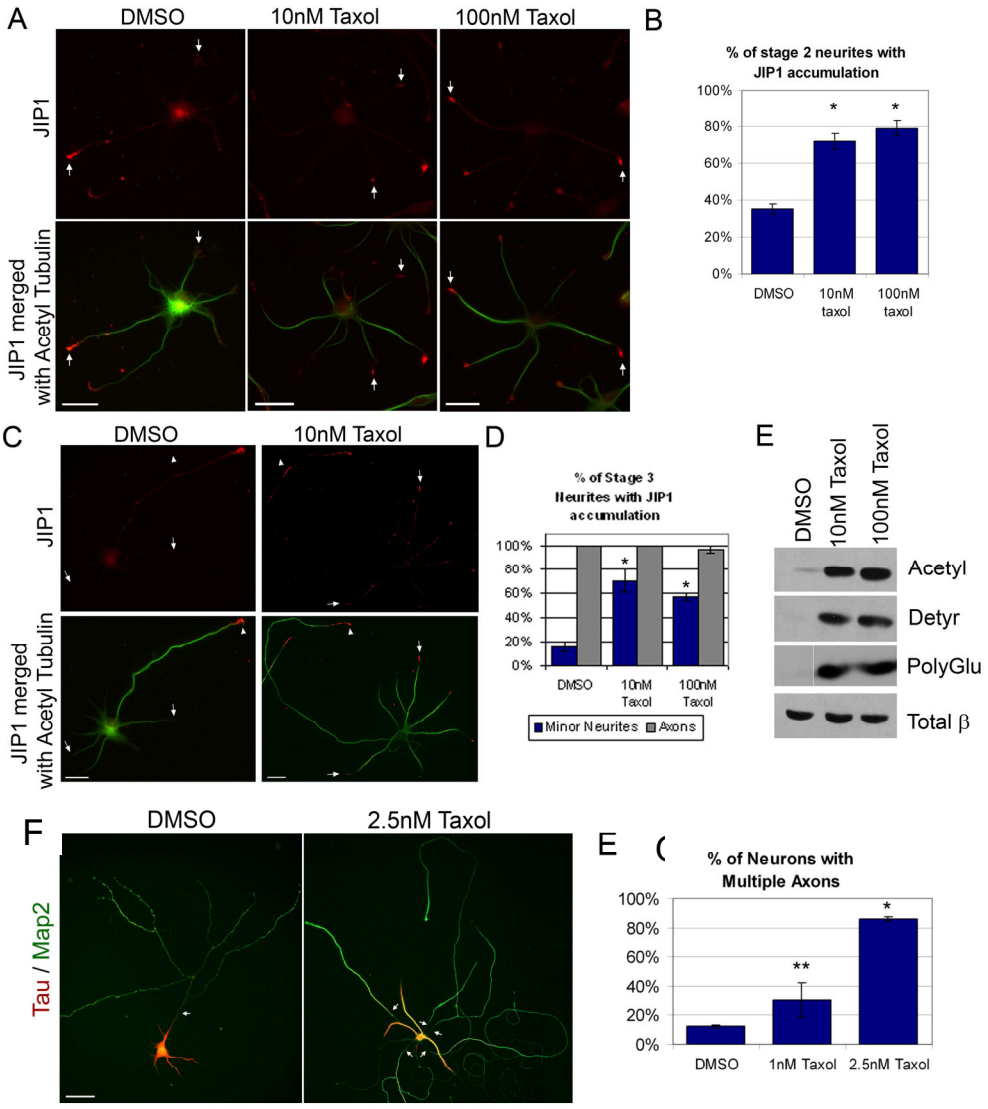

Figure 5.6: Taxol treatment causes a redistribution in the localization of JIP1 and the formation of multiple axons. A and C) Stage 2 (A) or Stage 3 (C) hippocampal neurons were treated for 3 hours with DMSO, 10nM, or 100 nM taxol then fixed and stained with antibodies to JIP1 and acetylated α-tubulin. Arrows=growth cones of stage 2 neurites or stage 3 minor neurites. Arrowheads= axonal growth cones. Scale=20μM. B and D) Quantification of the percentage of stage 2 neurites (B) or percentage of stage 3 minor neurites or axons (D) with JIP1 accumulation after DMSO or taxol treatment. Error bars=SEM. Student's T-test *p<0.01. E) A mix of Stage 2/Stage 3 cortical neurons were treated for 3hrs with DMSO, 10nM Taxol, or 100nM Taxol. Cell were collected and cell lysates were analyzed by western blot with antibodies to acetylated α-tubulin, detyrosinated α-tubulin, polyglutamylated tubulin, or total β-tubulin. Polyglutamylated lanes are from the same blot. F and G) Culturing cells in taxol results in the formation of multiple axons. Hippocampal neurons were cultured in DMSO, 1nM taxol, or 2.5nM taxol from time of plating until 6DIV. F) Cells were fixed and probed with antibodies to Tau or Map2. Arrows indict axonal processes leaving the cell body. G) Quantification of the percentage of neurons with >1 axon. Error bars=SEM. Students T-test: **p<0.05, *p<0.01. Scale=20μM for all images.

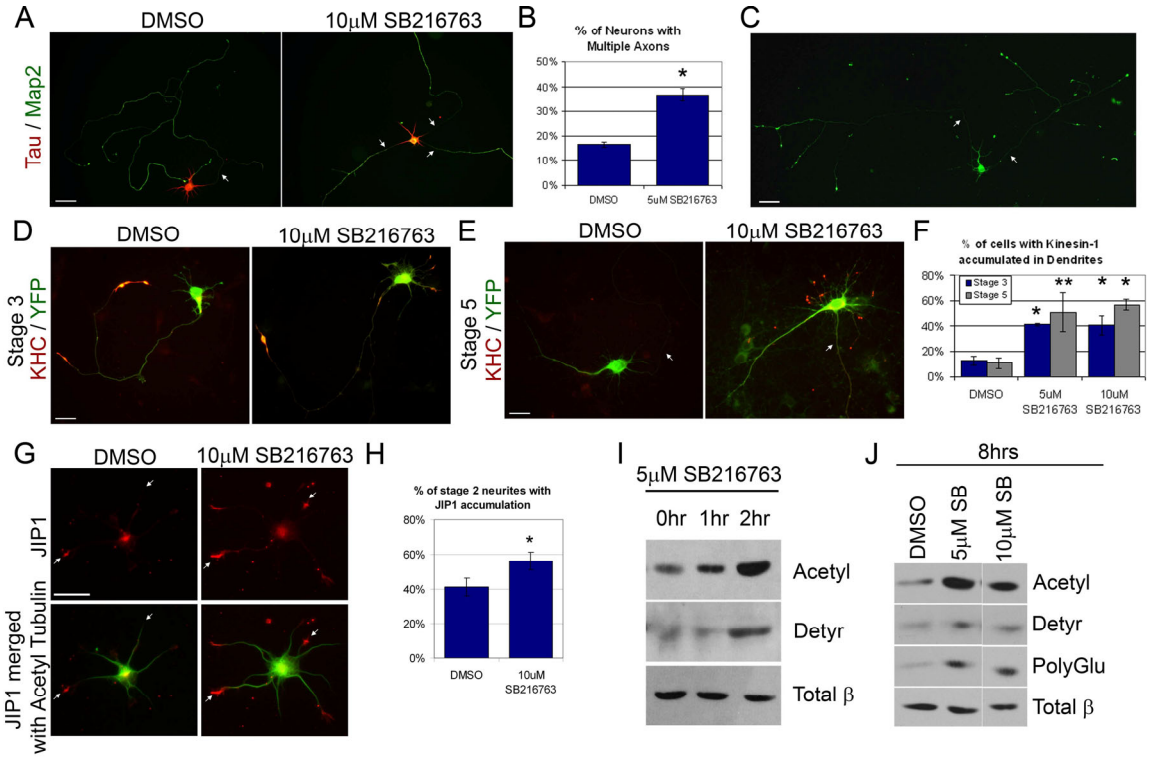

Figure 5.7: GSK3β inhibition influences Kinesin-1 transport in polarized cells and results in increased levels of modified microtubules. (A and B) Long-term GSK3β inhibition results in multiple axons in many cells. Hippocampal neurons were cultured in DMSO or 10μM SB216763 from time of plating until 6DIV. (A) Cells were fixed and probed with antibodies to Tau or Map2. Arrows indict axonal processes leaving the cell body. (B) Quantification of the percentage of neurons with >1 axon. Error bars=SEM. Students T-test: *p<0.01. (C) Kinesin-1 accumulates in the growth cones of all the axonal processes made by long-term GSK3β inhibition. Hippocampal cells were electroporated with CA-Kinesin-mCit at time of plating and cultured in 5μM SB216763 for 6 days. Cells were then fixed and probed with antibodies to mCit. Arrows indict axonal processes leaving the cell body. (D-E) Stage 3 hippocampal cells were treated for 2-4 hours with DMSO, 5μM or 10μM SB216763. Cells were then lipofectamine transfected with CA-Kinesin-mcherry and YFP. Cells were allowed to express the truncated kinesin under additional treatment for 4-5 hours then fixed and imaged. (F) Quantification of the percentage of stage 3 minor neurites or stage 5 dendrites that have accumulation of CA-Kinesin-mCherry in growth cones. Error bars=SEM. Students T-test: **p<0.05, *p<0.01. (G and H) Stage 2 hippocampal cells were treated for 8 hours with DMSO or 10μM SB216763. (G) Cells were fixed and stained for antibodies to endogenous JIP1 and acetylated α-tubulin. Scale=20μM. (H) Quantification of the percent of stage 2 neurites with JIP1 tip accumulation. Error bars= SEM. Student's T-test: *p<0.01. (I) Stage 3 hippocampal neurons were treated for 0-2 hrs with 5μM SB216763. Cells were then collected, lysed, and analyzed by western blot with antibodies to acetylated α-tubulin, detyrosinated α-tubulin, or total β-tubulin. (J) Stage 3 cortical neurons were treated for 8 hrs with 5μM or 10μM SB216763. Cell lysates were then analyzed by western blot with antibodies to acetylated α-tubulin, detyrosinated α-tubulin, polyglutamylated tubulin, or total β-tubulin. All bands probed with similar antibody came from the same gel. Scale=20μM for all figure images.

REFERENCES

1. Arimura, N. and K. Kaibuchi, *Neuronal polarity: from extracellular signals to intracellular mechanisms.* Nat Rev Neurosci, 2007. **8**(3): p. 194-205.
2. Wiggin, G.R., J.P. Fawcett, and T. Pawson, *Polarity proteins in axon specification and synaptogenesis.* Dev Cell, 2005. **8**(6): p. 803-16.
3. Dotti, C.G., C.A. Sullivan, and G.A. Banker, *The establishment of polarity by hippocampal neurons in culture.* J Neurosci, 1988. **8**(4): p. 1454-68.
4. Schwamborn, J.C., M.R. Khazaei, and A.W. Puschel, *The interaction of mPar3 with the ubiquitin ligase Smurf2 is required for the establishment of neuronal polarity.* J Biol Chem, 2007. **282**(48): p. 35259-68.
5. Schwamborn, J.C. and A.W. Puschel, *The sequential activity of the GTPases Rap1B and Cdc42 determines neuronal polarity.* Nat Neurosci, 2004. **7**(9): p. 923-9.
6. Watabe-Uchida, M., et al., *The Rac activator DOCK7 regulates neuronal polarity through local phosphorylation of stathmin/Op18.* Neuron, 2006. **51**(6): p. 727-39.
7. Govek, E.E., S.E. Newey, and L. Van Aelst, *The role of the Rho GTPases in neuronal development.* Genes Dev, 2005. **19**(1): p. 1-49.
8. Nishimura, T., et al., *Role of the PAR-3-KIF3 complex in the establishment of neuronal polarity.* Nat Cell Biol, 2004. **6**(4): p. 328-34.
9. Matsuo, N., et al., *Roles of STEF/Tiam1, guanine nucleotide exchange factors for Rac1, in regulation of growth cone morphology.* Mol Cell Neurosci, 2003. **24**(1): p. 69-81.
10. Santos Da Silva, J., V. Schubert, and C.G. Dotti, *RhoA, Rac1, and cdc42 intracellular distribution shift during hippocampal neuron development.* Mol Cell Neurosci, 2004. **27**(1): p. 1-7.
11. Dajas-Bailador, F., E.V. Jones, and A.J. Whitmarsh, *The JIP1 scaffold protein regulates axonal development in cortical neurons.* Curr Biol, 2008. **18**(3): p. 221-6.
12. Toriyama, M., et al., *Shootin1: A protein involved in the organization of an asymmetric signal for neuronal polarization.* J Cell Biol, 2006. **175**(1): p. 147-57.
13. Shi, S.H., L.Y. Jan, and Y.N. Jan, *Hippocampal neuronal polarity specified by spatially localized mPar3/mPar6 and PI 3-kinase activity.* Cell, 2003. **112**(1): p. 63-75.
14. Shi, S.H., et al., *APC and GSK-3beta are involved in mPar3 targeting to the nascent axon and establishment of neuronal polarity.* Curr Biol, 2004. **14**(22): p. 2025-32.
15. Menager, C., et al., *PIP3 is involved in neuronal polarization and axon formation.* J Neurochem, 2004. **89**(1): p. 109-18.

16. Jacobson, C., B. Schnapp, and G.A. Banker, *A change in the selective translocation of the Kinesin-1 motor domain marks the initial specification of the axon.* Neuron, 2006. **49**(6): p. 797-804.

17. Nakata, T. and N. Hirokawa, *Microtubules provide directional cues for polarized axonal transport through interaction with kinesin motor head.* J Cell Biol, 2003. **162**(6): p. 1045-55.

18. Schwamborn, J.C., et al., *Ubiquitination of the GTPase Rap1B by the ubiquitin ligase Smurf2 is required for the establishment of neuronal polarity.* EMBO J, 2007. **26**(5): p. 1410-22.

19. Bryan, B., et al., *Ubiquitination of RhoA by Smurf1 promotes neurite outgrowth.* FEBS Lett, 2005. **579**(5): p. 1015-9.

20. Zhang, Y., H.R. Wang, and J.L. Wrana, *Smurf1: a link between cell polarity and ubiquitination.* Cell Cycle, 2004. **3**(4): p. 391-2.

21. Yan, D., L. Guo, and Y. Wang, *Requirement of dendritic Akt degradation by the ubiquitin-proteasome system for neuronal polarity.* J Cell Biol, 2006. **174**(3): p. 415-24.

22. Kimura, T., et al., *Tubulin and CRMP-2 complex is transported via Kinesin-1.* J Neurochem, 2005. **93**(6): p. 1371-82.

23. Horiguchi, K., et al., *Transport of PIP3 by GAKIN, a kinesin-3 family protein, regulates neuronal cell polarity.* J Cell Biol, 2006. **174**(3): p. 425-36.

24. Reed, N.A., et al., *Microtubule acetylation promotes kinesin-1 binding and transport.* Curr Biol, 2006. **16**(21): p. 2166-72.

25. Witte, H., D. Neukirchen, and F. Bradke, *Microtubule stabilization specifies initial neuronal polarization.* J Cell Biol, 2008. **180**(3): p. 619-32.

26. Baas, P.W., et al., *Microtubule dynamics in axons and dendrites.* J Neurosci Res, 1991. **30**(1): p. 134-53.

27. Ikegami, K., et al., *Loss of alpha-tubulin polyglutamylation in ROSA22 mice is associated with abnormal targeting of KIF1A and modulated synaptic function.* Proc Natl Acad Sci U S A, 2007. **104**(9): p. 3213-8.

28. Liao, G. and G.G. Gundersen, *Kinesin is a candidate for cross-bridging microtubules and intermediate filaments. Selective binding of kinesin to detyrosinated tubulin and vimentin.* J Biol Chem, 1998. **273**(16): p. 9797-803.

29. Dunn, S., et al., *Differential trafficking of Kif5c on tyrosinated and detyrosinated microtubules in live cells.* J Cell Sci, 2008. **121**(Pt 7): p. 1085-95.

30. Larcher, J.C., et al., *Interaction of kinesin motor domains with alpha- and beta-tubulin subunits at a tau-independent binding site. Regulation by polyglutamylation.* J Biol Chem, 1996. **271**(36): p. 22117-24.

31. Lee, J.R., et al., *An intramolecular interaction between the FHA domain and a coiled coil negatively regulates the kinesin motor KIF1A.* EMBO J, 2004. **23**(7): p. 1506-15.

32. Verhey, K.J., et al., *Cargo of kinesin identified as JIP scaffolding proteins and associated signaling molecules.* J Cell Biol, 2001. **152**(5): p. 959-70.

33. Jiang, H., et al., *Both the establishment and the maintenance of neuronal polarity require active mechanisms: critical roles of GSK-3beta and its upstream regulators.* Cell, 2005. **120**(1): p. 123-35.

34. Kim, W.Y., et al., *Essential roles for GSK-3s and GSK-3-primed substrates in neurotrophin-induced and hippocampal axon growth.* Neuron, 2006. **52**(6): p. 981-96.

35. Yoshimura, T., et al., *GSK-3beta regulates phosphorylation of CRMP-2 and neuronal polarity.* Cell, 2005. **120**(1): p. 137-49.

36. Dixit, R., et al., *Differential regulation of dynein and kinesin motor proteins by tau.* Science, 2008. **319**(5866): p. 1086-9.

37. Seitz, A., et al., *Single-molecule investigation of the interference between kinesin, tau and MAP2c.* EMBO J, 2002. **21**(18): p. 4896-905.

38. Lin, S.X., G.G. Gundersen, and F.R. Maxfield, *Export from pericentriolar endocytic recycling compartment to cell surface depends on stable, detyrosinated (glu) microtubules and kinesin.* Mol Biol Cell, 2002. **13**(1): p. 96-109.

39. Erck, C., R. Frank, and J. Wehland, *Tubulin-tyrosine ligase, a long-lasting enigma.* Neurochem Res, 2000. **25**(1): p. 5-10.

40. Hammond, J.W., D. Cai, and K.J. Verhey, *Tubulin modifications and their cellular functions.* Curr Opin Cell Biol, 2008. **20**(1): p. 71-6.

41. Verhey, K.J. and J. Gaertig, *The tubulin code.* Cell Cycle, 2007. **6**(17): p. 2152-60.

42. Erck, C., et al., *A vital role of tubulin-tyrosine-ligase for neuronal organization.* Proc Natl Acad Sci U S A, 2005. **102**(22): p. 7853-8.

43. Spiliotis, E.T., et al., *Epithelial polarity requires septin coupling of vesicle transport to polyglutamylated microtubules.* J Cell Biol, 2008. **180**(2): p. 295-303.

44. Barral, Y., et al., *Compartmentalization of the cell cortex by septins is required for maintenance of cell polarity in yeast.* Mol Cell, 2000. **5**(5): p. 841-51.

45. Gladfelter, A.S., J.R. Pringle, and D.J. Lew, *The septin cortex at the yeast mother-bud neck.* Curr Opin Microbiol, 2001. **4**(6): p. 681-9.

46. van Dijk, J., et al., *Polyglutamylation is a post-translational modification with a broad range of substrates.* J Biol Chem, 2008. **283**(7): p. 3915-22.

47. Bonnet, C., et al., *Differential binding regulation of microtubule-associated proteins MAP1A, MAP1B, and MAP2 by tubulin polyglutamylation.* J Biol Chem, 2001. **276**(16): p. 12839-48.

48. Janke, C., et al., *Tubulin polyglutamylase enzymes are members of the TTL domain protein family.* Science, 2005. **308**(5729): p. 1758-62.

49. Zhou, F.Q., et al., *NGF-induced axon growth is mediated by localized inactivation of GSK-3beta and functions of the microtubule plus end binding protein APC.* Neuron, 2004. **42**(6): p. 897-912.

50. Nishimura, T., et al., *PAR-6-PAR-3 mediates Cdc42-induced Rac activation through the Rac GEFs STEF/Tiam1.* Nat Cell Biol, 2005. **7**(3): p. 270-7.

51. Mandelkow, E.M., et al., *MARK/PAR1 kinase is a regulator of microtubule-dependent transport in axons.* J Cell Biol, 2004. **167**(1): p. 99-110.

52. Bulinski, J.C., et al., *Overexpression of MAP4 inhibits organelle motility and trafficking in vivo.* J Cell Sci, 1997. **110 (Pt 24)**: p. 3055-64.

53. Samsonov, A., et al., *Tau interaction with microtubules in vivo.* J Cell Sci, 2004. **117**(Pt 25): p. 6129-41.

54. Black, M.M., *Taxol interferes with the interaction of microtubule-associated proteins with microtubules in cultured neurons.* J Neurosci, 1987. **7**(11): p. 3695-702.

55. Goold, R.G. and P.R. Gordon-Weeks, *Glycogen synthase kinase 3beta and the regulation of axon growth.* Biochem Soc Trans, 2004. **32**(Pt 5): p. 809-11.

56. Meyer, D., A. Liu, and B. Margolis, *Interaction of c-Jun amino-terminal kinase interacting protein-1 with p190 rhoGEF and its localization in differentiated neurons.* J Biol Chem, 1999. **274**(49): p. 35113-8.

57. Kaech, S. and G. Banker, *Culturing hippocampal neurons.* Nat Protoc, 2006. **1**(5): p. 2406-15.

Chapter 6:
Conclusion

The first kinesin motor was identified in squid axons about 20 years ago [1]. Since then, much work has been done to elucidate the chemo-mechanical properties and identity of kinesin superfamily members [2-4]. However many details are still unclear regarding the general and specific mechanisms used by individual members of the kinesin superfamily for motor regulation; cargo recognition, loading, and unloading; polarized sorting; microtubule track selection; and coordination of multiple motors. The work that has been described in Chapters 2-5 of this dissertation, addresses some of the remaining questions regarding KIF1A and KIF17 autoinhibition and motility, coordination and make-up of Kinein-1/cargo complexes, and Kinesin-1's polarized sorting in neurons. This work has shed light on both general mechanisms conserved among the kinesin superfamily, as well as, more specific mechanisms that regulate only individual family members.

AUTOINHIBITION

Autoinhibition of kinesins ensures that in the absence of cargo, motors do not hydrolyze excessive ATP in useless motility. It also allows for temporal and spatial control of motor activity ensuring that kinesins are available and ready when needed for cargo loading and transport. As the motor domain is the only region conserved among the kinesin superfamily, new regulatory regions and mechanisms must have evolved as novel cargo binding and structural domains were added to the basic motor core. By comparing the results from my KIF1A and KIF17 autoinhibition studies with those done previously on KIF1A, Osm-3, Kinesin-1, and Gakin/KIF13b, some general mechanisms of autoinhibition stand out as being conserved among all or a subset of these studied kinesins.

1) Separate mechanisms mediate inhibition of microtubule binding and processive motility.

Studies using deleted or mutated versions of Kinesin-1 or KIF1A suggest that autoinhibition is mediated by two independent mechanisms. The first mechanism prevents the motor from binding microtubules. In Kinesin-1 this is mediated by the KHC tail, but reinforced by the KLC domains [5-8]. In KIF1A it is mediated by the FHA domain and CC2 (Chapter 3 and [9, 10]). The second mechanism prevents the coordinated stepping of the two heads in cases where the motor does bypass the first inhibitory mechanism. The proposed model for this motor uncoupling involves an unwinding of the neck coiled-coil, allowing for a physical separation of the motor domains. KIF1A prevents processive motility or motor coordination through the formation of an intramolecular coiled-coiled between the NC and CC1 of the adjacent stalk (Chapter 3 and [9]). Evidence for this intramolecular coiled-coil has only been seen thus far in truncated proteins, so its presence and role in the motor regulation of full-length KIF1A requires further verification. In Kinesin-1, the KLC TPR domains push the motor domains apart, unwinding the neck in the process [5]. Yet, in the case of fungal Kinesin-1 that does not have KLC subunits, the KHC tail has also been suggested to play this inhibitory role by binding to a non coiled-coil conformation of the neck [11]. Although Kinesin-1 and KIF1A utilize both inhibitory schemes in a similar way, it is possible other kinesins use only one mechanism, or that the same type of motor activity (i.e. microtubule binding or processivity) is inhibited in a slightly different way.

2) Motor function is inhibited via direct contact of the motor or neck domains with C-terminal tail or stalk regions

Evidence from Kinesin-1, KIF17, KIF1A, and Gakin show that the inhibition mechanisms outline above are often mediated by direct intramolecular contacts involving a small region of the tail or stalk and either the motor or neck domains. In the case of Kinesin-1, a positively charged coiled-coil region of the KHC tail contacts a highly negative patch in the neck. This facilitates a second contact of the IAK tail residues with the switch I helix of the motor domain [6, 11-13]. KIF17 also likely employs an electrostatic interaction mechanism, as the very positively charged CC2 directly interacts

with the motor domain (Chapter 2). Finally the MBS region of Gakin's stalk has been shown to contact the motor domain inhibiting the microtubule stimulated ATPase activity [14]. KIF1A's intramolecular coiled-coil is the most unique, but once again represents a case where the neck is bound by a C-terminal stalk region [9].

An autoinhibition mechanism mediated by direct contact requires that the motor protein has some degree of structural flexibility in order to allow the protein to fold back on itself. Kinesin-1 employs hinges, with glycine and proline residues, in order to break up its extended coiled-coil regions permitting the protein to fold lengthwise head to tail [12]. Osm-3 (the C. *elegans* homologue of KIF17) appears to have a similar mechanism, as the presence of a 15-20 residue hinge between coiled-coil 1 and 2 is required for folding it into a more compact inhibited conformation [15]. Comparison of Osm-3 and KIF17 structures and regulatory mechanisms bring some ambiguity to this model of Osm-3 inhibition, however, as the hinge region of Osm-3 is right next to and somewhat analogous to the CC2 in KIF17 that, in chapter 2, was shown to interact directly with the motor domain. Whether this region in Osm-3 truly acts as a structural hinge or as a direct motor regulatory region requires further study. Electron microscopy studies on recombinant KIF1A suggest that rather than folding lengthwise head to tail, KIF1A alternatively forms a very compact, more globular structure [16, 17]. As no direct contact has been found between the motor domain and the FHA domain, which has been shown to inhibit microtubule binding [10], we can only guess at the regulatory mechanism. However, one possibility is that the compact conformation of KIF1A places the FHA domain near the motor allowing it to block access of the motor to microtubules via steric hindrance.

Unanswered Questions. Although for each motor analyzed thus far, direct contact of an inhibitory domain with either the motor or neck domains has been discovered, more detailed studies are required to learn the exact contact sites as well as the particulars of how these interactions result in inhibited motor functions. Does binding of the stalk/tail region to the motor or neck 1) prevent access of one or both motor domains to microtubules 2) prevent the exchange of ADP for ATP from the nucleotide binding pocket thus locking the motor in a weak microtubule bound state or 3) inhibit ATP hydrolysis. Additionally do these events occur by directly blocking access to

the motor's active sites or through more indirect mechanisms, such as allosteric conformational changes? More structural knowledge of individual stalk/tail regions as well as full-length molecules would be helpful to gain understanding of how the motor folds on itself and inhibits the motor.

3) Cargo binding relieves autoinhibition.

Gakin provides the simplest example thus far where binding of cargo relieves motor inhibition. Binding of a single cargo, Dlg, to the MBP region of Gakin which directly interacts with the motor domain, allows the motor to move along microtubules and hydrolyze ATP [14]. The FHA domain of Gakin was also identified as a cargo binding site for phosphotidylinositol(3,4,5)trisphosphate binding protein (PIP_3BP) [18], but whether binding to this site also relieves Gakin's autoinhibitory mechanism remains to be seen. The case of Kinesin-1 reveals some of the complexities of motor/cargo complexes as binding of two proteins is necessary to relieve autoinhibition. FEZ binds to KHC's tail IAK region and JIP1 binds the TPR domains of KLC [19]. Whether other cargo proteins can replace the role of FEZ or JIP1 in motor activation requires further study.

Kinesin-1 and Gakin show that inhibitory regions are equivalent to cargo binding regions. How this model will change when considering all cargos and potential binding sites remains to be seen. In the case of KIF17 and KIF1A the potential correlation between inhibitory regions and cargo binding domains is lacking primarily due to the lack of evidence as to cargo identity and the locations of cargo binding domains.

Unanswered Questions. As implied in this discussion, there are still many open questions in regards to this cargo mediated activation model. The biggest hole resides in the identity of specific cargos for each motor. Beyond that, additional questions remain such as: How many separate binding cargos are needed to achieve full activation for each motor? Where on the motor do they bind? If they don't bind directly to inhibitory regions, how is motor conformation altered in order to achieve activation? Are there proteins that serve solely as motor regulatory proteins rather than cargo that have other functions at the transport destination?

KIF1A motility: Long distance, processive movement requires two heads.

Although KIF1A has motile properties as a monomer, where it can take advantage of electrostatic interactions between the positively charged K-loop in its motor domain and the negatively charged tubulin tails of the microtubule lattice in order to glide along microtubules without the need of ATP [20-22], my results show KIF1A only moves efficiently over long-distances as a dimer (Chapter 3 and [23]). The kinesin motor MCAK has also been shown to move in a "biased-diffusion" manner [24]. In both cases, the diffusional motion does not require energy, has velocities ranging from very fast to very slow, is due to electrostatic interactions, and does not contribute to the force driven cellular function of the motor. Thus for any long range movement, using a hand-over-hand stepping mechanism, where at least one head is always strongly attached to the microtubule ensures that the motor does not dissociate prematurely.

What then is the role for the added diffusion ability? The electrostatic interaction that permits diffusion likely functions as a tether to accelerate rebinding of the unbound, actively stepping motor domain, thus, reducing the chance of complete detachment. This tethering would in general increase the processivity or distance traveled by the motor and possibly explain why KIF1A has some of the longest run lengths in single molecule motility assays, running up to 10μm in a single run, and on average about double the run length of Kinesin-1 (Chapter 3 and [23]). Indeed a positive correlation between run length and strength of electrostatic interactions was clearly demonstrated by Thorn et al who saw increased processive run lengths with Kinesin-1 after adding positively charged residues to the neck coiled-coil [25].

Microtubule-based diffusion or tethering may have additional *in vivo* roles beyond increasing processivity. Vesicles in a cell often undergo "salutatory" motion where they have periods of rapid movement followed by pauses where little displacement occurs [26]. Pausing is likely a result of motors encountering barriers, or road blocks, in their path. If the motor diffuses along the microtubule in various directions, it may find a way to negotiate around the barrier without completely dissociating from the microtubule.

Specific future directions for KIF17

My studies on KIF17 show that the coiled-coil 2 region (CC2) inhibits the processive motility of KIF17 by directly binding to the motor domain. To gain a better understanding of how the CC2 region of KIF17 inhibits motor activity, it would be useful to narrow down the specific residues in CC2, as well as in the motor domain that mediate this interaction. I identified the region between 738 and 795 as containing the inhibitory and motor binding region. It is unlikely that this entire 57 residue CC2 region is essential for motor binding and/or inhibition. In support of this hypothesis, mutating CC2 reside G754 to glutamate or residues 764-772 to alanine was sufficient to relieve motor inhibition. These mutations could have relieved autoinhibition by removing essential amino acids necessary for the motor domain/CC2 binding interface or for structural conformations necessary to bring essential CC2 region residues into contact with the motor domain. To distinguish these two possibilities it would be necessary to test whether a CC2 construct with these mutations is still able to interact with the motor.

In order to find the minimal region of CC2 that is important for motor domain binding and/or autoinhibition a few approaches could be undertaken. 1) Making more mutations within CC2 (such as by spacing alanine mutations in 5 or 10 amino acid stretches throughout CC2). 2) Making truncations that end within the CC2 region (such as 1-785 and 1-775). 3) Making KIF17 constructs with small internal deletions within CC2. Or 4) testing short peptides spanning part of the CC2 region for their ability to bind the motor domain or inhibit the processive motility of active KIF17 constructs in *trans*. Each of these approaches could point out important and non-essential residues for autoinhibition and motor binding. Once a smaller region of CC2 has been identified, crosslinking CC2 peptides to the KIF17 motor domain followed by mass-spectrometry and/or cryo-EM could be used similar to the recent study on Kinesin-1 [13] to determine where exactly on the motor domain the CC2 region binds. If it is analogous to Kinesin-1 [13], the motor's switch-I region is a likely CC2 binding interface, but other motor regions are also possible.

Another major future question regarding KIF17 autoinhibition is how the motor is activated and specifically whether cargo binding is sufficient for this activation. KIF17's cargo proteins, Mint1 and NXF-2, bind the C-terminal tail [27, 28] that in our studies

showed little sign of motor inhibition and certainly no direct motor domain contact. It is possible however, that binding of cargo to this tail region sterically blocks the ability of CC2 to contact the motor. However my studies also suggest that binding of Mint1 alone to KIF17 is not sufficient to activate the motor. Yet, it is possible that other proteins that bind Mint1 play a role in KIF17 activation, or alter the conformation of Mint1, such that when it is in a multi-protein complex, it is sufficient to activate KIF17. Thus testing whether co-expression of KIF17 with Mint1, mLin2, and mLin7, or alternatively, truncated forms of Mint1 are sufficient to activate the motor would be required before a role for Mint1 in KIF17 activation could be ruled out.

Alternatively Mint1 may need other cargo proteins to independently bind KIF17 for activation. Indeed Kinesin-1 requires that two cargo proteins bind in order to release it from autoinhibition. It is possible that CC2 itself serves as a cargo binding region. As more direct binding partners and cargo binding sites are identified for KIF17 it will become clearer whether the CC2 regulatory region is itself a cargo binding domain and the mechanisms by which KIF17 inhibition is released. Yeast-two hybrid assays have proven very useful in identifying kinesin cargos and thus this experimental method should be applied to KIF17's CC2 region or other domains in order to find novel binding partners that can be studied for their role in activating KIF17 for microtubule binding and/or motility.

KIF17's cargo binding tail (847-1028), although likely not a major player in motor autoinhibition, was shown to be necessary for KIF17's localization to the peripheral tips of cilia. Presumably this cilia accumulation is due to the loading of KIF17 into cilia by IFT cargo or IFT machinery that regulates cilia access. As KIF17 accumulated at the peripheral tips of cilia, rather than throughout cilia, this interaction with IFT cargo/machinery likely also activated KIF17 motor activity. However, it has not yet been tested whether the motor activity of KIF17 is necessary for this accumulation or whether KIF17 is able to hijack a ride on IFT cargo driven by other motors. Thus testing a motor dead KIF17 construct in the cilia localization assay would be helpful. If a motor dead KIF17 is unable to accumulate in cilia, then one could conclude that the IFT machinery activates KIF17 to move itself into cilia. Using the tail of KIF17 as bait in a yeast-two-hybrid assay using a prey cDNA library from olfactory cells or other cilia containing cells

could serve to identify the IFT cargo that KIF17 binds directly to in order to get into cilia and/or connect to IFT complexes so it can transport them.

Specific future directions for KIF1A

My work on KIF1A shows that it is an autoinhibited motor that moves processively as a dimer rather than a monomer. One limitation to my studies (and indeed all previous studies) is that full-length KIF1A is inactive and thus KIF1A's motile properties cannot be studied without making large truncations to remove autoinhibitory domains. My processive KIF1A construct (1-393) includes only about 1/4 of KIF1A's total protein residues. In order to confirm that full-length KIF1A also moves processively as a dimer (and not as a monomer using one-dimensional diffusion), it would be helpful to evaluate a full-length KIF1A construct that is relieved of autoinhibition. KIF1A constructs with single point mutations in either the FHA or coiled-coil 2 (CC2) domains have been shown to accumulate at neurite tips, suggesting that they are processive motors [10]. By testing these full-length, but uninhibited constructs in dimerization and one- or two-color single molecule motility assays, I would expect the motile properties of full-length KIF1A to look similar to dimeric KIF1A(1-393) rather than monomeric KIF1A(1-369). This additional data would more conclusively confirm that KIF1A moves processively over long distances as a dimeric motor and although it may have some ability to move via one-dimensional diffusion, this type of movement is erratic and short in duration and not likely to be the mechanism that allows for vesicular transport.

My work further shows that KIF1A autoinhibition is mediated by the CC2/FHA region that prevents microtubule binding, as well as by the CC1 region which inhibits processive motility. It is likely that CC1 inhibits processive motility by forming an intramolecular coiled-coil with the neck coil (NC). This intramolecular coiled-coil conformation rather than an intermolecular coiled-coil conformation would be sufficient to separate and uncoordinated the motors domains such that two-headed processive motility would be impossible. Evidence for both intermolecular and intramolecular conformations has been seen by cryo-EM, yet only with truncated proteins [9]. Thus it remains to be seen whether full-length KIF1A also utilizes the intramolecular NC/CC1

conformation to limit processive motility. The FRET stoichiometry studies shown in Chapter 3 do lend support to the hypothesis that the motor domains are separated in the full-length dimeric KIF1A molecule; however, more solid proof of the intramolecular coil is still necessary.

Kinesin-1 also has separated motor domains in its autoinhibited conformation. This conformation has been validated by a combination of crosslinking studies and FRET stoichiometry [5]. A similar type of crosslinking experiment could be applied to KIF1A. For Kinesin-1 a cysteine residue was added to the NC such that when two KHC peptides dimerized via coiled-coil formation a chemical crosslinker locked the closely located, novel cysteines together. If KIF1A with a cysteine residue added to the NC region crosslinked in dimeric form with disulfide linking chemical crosslinkers, an intermolecular NC/CC1 conformation would be confirmed. If no crosslinked product was found, an intramolecular NC/CC1 conformation would be plausible. Utilizing a full-length, but uninhibited, KIF1A construct (such as a FHA or CC2 mutation) as a positive control for the intermolecular conformation would lead to greater proof that a negative result in this assay was indicative of an intramolecular NC/CC1 conformation, especially if motor-to-motor FRET stoichiometry also revealed a higher FRET value for a mutant, uninhibited KIF1A construct compared to the wild-type, autoinhibited KIF1A.

The most open questions for KIF1A autoinhibition, like that of KIF17 autoinhibition, is the mechanism by which inhibition is relieved and specifically whether cargo binding serves as the switch. KIF1A has two regions known at this point in time to function in cargo binding. The PH domain and liprin-α binding region. The C-terminal PH domain connects KIF1A to vesicles by binding to phosphotidylinositol (4,5) bisphosphate ($PtdIns_{(4,5)}P_2$) lipids [29, 30]. As there does appear to be some specificity in the type of vesicles KIF1A carries, additional regulatory partners must exist to limit promiscuous binding. Indeed protease studies have revealed that protein components play a role in KIF1A vesicle binding [29, 30]. Where these essential protein components bind is less clear except that the cargo protein, liprin-α, binds to a part of CC2 but requires additional C-terminal residues [31].

The PH domain and indeed the entire second half of KIF1A has no observable motor regulatory role (Chapter 3 and [10]), implying that the model that all cargo binding

domains equal inhibitory domains is incorrect. However, clustering of $PtdIns_{(4,5)}P_2$ molecules on vesicular membranes does enhance the motile properties of KIF1A, suggesting that whatever conformational changes are promoted upon two PH domains interacting with lipids in close proximity, help to activate the motor [29].

As the liprin-α binding domain overlaps with CC2, binding of liprin-α to CC2 may be sufficient to relieve KIF1A autoinhibition. This hypothesis could be easily tested by co-expressing liprin-α with full-length KIF1A in COS and/or CAD cells then testing whether KIF1A is active for microtubule binding with the SLO/AMPPNP assay or whether it can move processively into neurite tips. If liprin-α is not sufficient to activate KIF1A, it may still play a role in motor activation with the help of other cargo binding proteins. As FHA domains are also protein-protein interaction domains, the FHA domain of KIF1A is another potential cargo binding region. It may be very informative to use the FHA domain (with or without the CC2 region) as bait in yeast-2 hybrid or GST-pull down experiments to search for novel KIF1A cargos and/or regulatory partners.

Important contributions to the field of kinesin regulation

By providing two more examples of kinesin motors that are regulated by autoinhibition, as well as elucidating some of mechanistic details by which this negative regulation occurs, my work on KIF17 and KIF1A helps the kinesin field better understand how the basic, conserved motor domain of kinesin proteins can be inhibited by so many unique stalk/tail regions. My work on KIF17 shows that processive motility is inhibited by the CC2 region directly interacting with the motor. As the cargo binding tail is essential to sorting KIF17 into subcellular compartments such as cilia, KIF17 has a level of regulation in addition to autoinhibition that is important for cargo transport. My work on KIF1A shows that this motor is an inhibited dimer, not a monomer as has long been proposed and points to the limitations of studying the motile properties of motor constructs that are too short or contain inhibitory regions. Dimerization is necessary for long-distance motility, but is not likely a step involved in KIF1A motor activation, with the exception that separated motor domains need to be coupled and coordinated before productive transport can occur. The strength of my studies resides in the fact that I used both *in vivo* and *in vitro* techniques to assay motor inhibition mechanisms. Thus the

conclusions benefit from the fact that proteins were studied in a native environment free from many of the troubles of protein purification but also at the single molecule level where the properties of individual motors could be analyzed rather than simply looking at groups of motors at a steady-state level.

CARGO COMPLEXES

Kinesin cargos take various forms ranging in size from large organelles, to small protein complexes. For the first 10-15 years after the discovery of kinesin motors, attempts to identify direct binding cargos were rather fruitless. Recently however, there has been an explosion in the number of identified direct or indirect binding partners for specific kinesins and some of the exact binding mechanisms have been elucidated. As there are at least 13 Kinesin-1 cargo proteins currently known to bind specifically to the TPR domains of KLC, not to mention the handful of others that bind KHC's tail [19, 32-44], an obvious question arises of how one motor can coordinate and carry out the transport of its many different cargoes. Results described in Chapter 4 and other studies suggest that cases of cooperative transport and competition exist.

In a cooperative transport model, the motor could combine independently binding cargo proteins into one multi-protein complex. This assembly function could bring together only specific subgroups of cargo, or allow for endless cargo combinations. The first scenario appears to function in the case of Kinesin-1 cargos JIP1 and JIP3. Both cargo proteins bind to KLC's TPR domains at independent sites, yet, because they also interact with each other they require co-transport within the same complex (Chapter 4, [45]). As JIP1 and JIP3 also function as scaffolding proteins for the kinases and substrates of the JNK signaling pathway [46], this same JIP1/JIP3/Kinesin-1 transport complex potentially contains may additional proteins, both soluble and transmembrane, that may have additional roles in cargo complex formation and/or release [40, 47].

In a competitive transport model, cargos binding to the same kinesin binding site, or to mutually exclusive binding sites may result in cargo competition. This scenario has been shown for the two Kinesin-1 cargos, Alcadein and a JIP1/APP complex [33]. On the other hand, my results shown in Chapter 4, as well as data from other research groups, show that while over-expression of a single Kinesin-1 binding cargo can saturate

and inhibit the transport of its own endogenous counterpart, it does not necessarily saturate all other cargos [35, 45]. Thus, competition between cargos is likely limited to certain cargo subsets and may often be a negligible factor due to the existence of a large pool of inactive kinesins seen in cellular fractionation and autoinhibition studies [1, 12, 48]. A case where the kinesin pool may be limiting for certain cargos resides in the hypothesis that different Kinesin-1 splice variants contain unique cargo binding sites. There are two gene isoforms of KLC, KLC1 and 2, and both of these are known to have multiple splice variations in the C-terminal cargo binding region [49-51]. Thus cargo that bind a specific splice variant may show competition with cargo binding that same splice variant but not cargos using other splice variants. This hypothesis remains to be tested, however, due to the lack of evidence for specific cargo that bind specific splice variants. Other factors that may be limiting to transport of a specific cargo, or subgroups of cargo, would be cooperative binding partners or other accessory proteins used to facilitate binding and/or transport.

Specific future directions for Kinesin-1 cargo complexes.

My work on JIP1/JIP3/Kinesin-1 complexes showed that JIP1 and JIP3 bind KLC's TPR bundle using unique binding sites. JIP1 binds inside the TPR groove and JIP3 binds outside the TPR groove. As the binding sites of other KLC TPR binding proteins have not been mapped in more detail than to the TPR domain in general, it is unknown whether other Kinesin-1 cargoes use one of the two TPR binding sites identified for JIP1 or JIP3 or whether there are other cargo binding interfaces on the TPR bundle. It would be simple to test other known KLC binding cargos with the KLC mutants described in chapter 4 using yeast-two-hybrid or co-immunoprecipitation assays in order to further map their binding interfaces. Additionally, as the error-prone PCR mutants generated for binding experiments with JIP1 and JIP3 had multiple point mutations, interesting constructs such as 48A should be further investigated and broken down into individual point mutations in order to determine which residues make up the binding interface and which residues are inconsequential.

My work additionally shows that JIP1 requires the presence of JIP3 in its Kinesin-1 transport complex (Chapter 4 and [45]). Previous studies have additionally shown that

it takes at least two proteins, FEZ and JIP1, in order to relieve the autoinhibition state of Kinesin-1 [19]. Together these studies exemplify some of the complexities of Kinesin-1/cargo transport, as at least three Kinesin-1 binding partners likely play a role in activating Kinesin-1 for long-distance motility. Although these three binding partners have been shown to be essential in separate studies, it has yet to be shown whether they are indeed in the same complex. Co-immunoprecipitation experiments could be helpful in validating the presence of all three Kinesin-1 binding cargos in the same complex. If precipitation of endogenous JIP1 or JIP3 pulled down FEZ or precipitation of endogenous FEZ pulled down JIP1 and JIP3 it could be concluded that indeed they are all part of the same complex. Additionally, it has been shown that JIP1 and FEZ can activate Kinesin-1 in a single molecule motility assay resulting in more motility events than when only Kinesin-1 is added. As JIP3 is also likely a part of this same complex and is necessary for JIP1 transport by Kinesin-1, one would expect that addition of JIP3 to the JIP1/FEZ/Kinesin-1 mix in a single molecule motility assay may result in even more motility events.

Finally, it is unclear what combinations of other Kinesin-1 cargo may be capable of activating Kinesin-1 for microtubule binding or long distance transport. Can KHC tail binding cargos such as FEZ and p120catenin be mixed and matched with KLC binding cargos such as JIP1/JIP3 or Kidins220 in order to activate Kinesin-1 or do only certain combinations constitute a Kinesin-1 activating cargo complex? Different Kinesin-1 cargo combinations could be tested by expressing them together in COS cells and testing microtubule binding using an SLO/AMPPNP assay, or alternatively, *in vitro* microtubule binding assays or single molecule motility assays could be done with mixtures of Kinesin-1 with different Kinesin-1 cargo combinations.

Important contributions to the field of cargo complexes and general future directions

Most cargo/Kinesin studies up to this point have focused on the identification of cargo and mapping of binding sites. My work, detailed in Chapter 4, is one of the first to investigate the relationships that exists between different cargo proteins that share the same motor. This work showed that JIP1 and JIP3 bind to separate sites on the KLC TPR

bundle, yet facilitate each other's binding and transport. As JIP1, JIP3, and FEZ are necessary to activate Kinesin-1 for long range transport, it is possible that a single Kinesin-1 interacting protein, may not be able to act as a full kinesin "cargo", that is a cargo capable of fully activating the motor. Although more research is still needed to identify Kinesin-1 cargo and their indirect or direct binding mechanisms, future research in the area of motor/cargo complexes will need to address how multiple interactions within a cargo complex, either between cargo and motors, or cargo and cargo, function to assemble a *complete* cargo complex that has the capacity to activate motors for efficient, long range transport.

MICROTUBULE PREFERENCE

Once kinesins are loaded with cargo, they must transport that cargo to its proper cellular destination. Although there are multiple mechanisms that mediate polarized membrane sorting, one involves the use of "smart" motors, or motors that have the intrinsic ability to move towards one particular cellular destination. Although all kinesin motors have a basic method of directionality dictating whether they move towards the plus-end or minus-end of microtubules, some motors appear to have the additional ability to move towards particular cellular locations or alternatively to reside in limited cellular compartments. The most evidence for this is in neuronal cells, which have two types of processes each requiring very different protein subsets to carry out their particular functions, specifically axons and dendrites. Kinesin-1 has been shown to move preferentially into and down the axon process, generally avoiding the more abundant dendrites (Chapter 5, [52, 53]). KIF1A on the other hand, transports down all processes showing no apparent partiality [52]. MKLP, KIF21b, and KIF17 have all been shown to be enriched in dendrites over axons, and at least in the case of MKLP and KIF21b this dendritic localization appears to be due to active motors preferentially moving into the dendritic compartments ([27, 53-56], Gary Banker personal communication, and Verhey lab unpublished data). As evidence in support of the "smart" motor model comes primarily from studies using constitutively active, truncated kinesin constructs, the mechanism mediating preferential sorting to axonal or dendritic compartments is thought to reside within the motor/microtubule binding interface [53].

For Kinesin-1 there is a growing body of evidence showing it has the intrinsic ability to pick up small variations that appear on only a subset of all possible microtubule tracks. *In vitro*, Kinesin-1 has been shown to have improved binding and in some reports better motility on microtubules post-translationally modified by acetylation, detyrosination, or polyglutamylation [57-61] . In fibroblasts, the subset of microtubules used by kinesin-1 is the same subset that is marked by the post-translational modifications (PTMs) of acetylation and detyrosination ([60] and Verhey lab unpublished data).

Important Contributions and Future Directions on Kinesin-1 and microtubule PTMs.

My results in Chapter 5, show that Kinesin-1's preference for axonal microtubule tracks in polarized neurons, and those of one or a small subset of neurites in unpolarized neurons also correlates with higher levels of modified microtubules. As altering only one modification, acetylation, could influence Kinesin-1 transport in unpolarized cells but not polarized cells, it is likely that Kinesin-1's axonal preference resides in the additive or synergistic combination of multiple modifications that each slightly enhance Kinesin-1's binding or motile properties on microtubules. Indeed the drug treatments of taxol, a microtubule stabilizing compound, or SB216763, a GSK3β inhibitor, both increased the levels of multiple microtubule PTMs throughout axons and dendrites leading to a loss of Kinesin-1's axonal preference. As GSK3β inhibition is necessary for axon specification and maintenance [62], these results further suggest that increased levels of microtubule PTMs may be a key factor to axon identity. Although there is evidence Kinesin-1 is directly influenced by microtubule PTMs, we cannot rule out the possibility that the axonal signal may consist to some extent on properties secondary to changes in microtubule structure such as the presence or absence of MAPs. However, MAPs have also been shown to have a preference for certain microtubule modifications, so their polarized compartmentalization may also depend on biochemical cues inherent to the microtubules they bind [63, 64].

It is thus proposed that microtubule modifications make up a tubulin code, similar to the modifications on histones [65, 66]. This code would mediate microtubule

functions specific to certain subsets of microtubules, such as in directing Kinesin-1 to axons. It is likely that various kinesin superfamily members will react to this tubulin PTM code in different ways. For example, as some smart motors move preferentially towards the axon, others move preferentially toward dendrites. Thus these two sets of motors may have opposite binding preferences for modified or unmodified microtubules or alternatively no preference at all. Indeed, in fibroblast cells, KIF1A and KIF17 appear to walk on all microtubules regardless of the presence or absence of modifications or even whether or not the microtubules are still growing (Verhey lab unpublished data). Additionally, in neurons with reduced amounts of α-tubulin polyglutamylation, the binding affinity to microtubules was differentially altered for a subset of kinesins and MAPs [59].

Obviously we are only at the very beginning of validating this tubulin code hypothesis and its role in directing kinesin polarized transport in neurons and other cell types. As Kinesin-1 is one of the lone kinesins tested for binding or varied ability to move along microtubules with different types of tubulin modifications, other kinesins with different sorting patterns need to be investigated in both *in vitro* biochemical assays and *in vivo* correlative assays. Indeed, even the sorting preferences of different kinesins need further validation.

Studying the cellular function of microtubule modifications in the past has largely been limited by the fact that most of the enzymes that modify tubulin where unknown. In the past few years, the tubulin deacetylase (HDAC6) and the polyglutamylating and polyglycylating enzymes (TTLLs) have been discovered. Thus, the role of polyglutamylation on Kinesin-1 transport in neurons can now be tested by over-expressing or knocking down different combinations of polyglutamylating enzymes and determining whether Kinesin-1's axonal sorting is modified. Likewise, the role of detyrosination in Kinesin-1 polarized axonal transport can be similarly investigated by over-expressing TTL, (tubulin tyrosine ligase) the enzyme that replaces the tyrosine residue onto the C-terminus of α-tubulin, or by using primary neurons from TTL knockout mice. Experiments such as these will provide much information in the future as to the specific roles played by individual tubulin modifications.

REFERENCES

1. Vale, R.D., T.S. Reese, and M.P. Sheetz, *Identification of a novel force-generating protein, kinesin, involved in microtubule-based motility.* Cell, 1985. **42**(1): p. 39-50.
2. Vale, R.D., *The molecular motor toolbox for intracellular transport.* Cell, 2003. **112**(4): p. 467-80.
3. Miki, H., Y. Okada, and N. Hirokawa, *Analysis of the kinesin superfamily: insights into structure and function.* Trends Cell Biol, 2005. **15**(9): p. 467-76.
4. Block, S.M., *Kinesin motor mechanics: binding, stepping, tracking, gating, and limping.* Biophys J, 2007. **92**(9): p. 2986-95.
5. Cai, D., et al., *Kinesin-1 structural organization and conformational changes revealed by FRET stoichiometry in live cells.* J Cell Biol, 2007. **176**(1): p. 51-63.
6. Hackney, D.D. and M.F. Stock, *Kinesin's IAK tail domain inhibits initial microtubule-stimulated ADP release.* Nat Cell Biol, 2000. **2**(5): p. 257-60.
7. Hackney, D.D. and M.F. Stock, *Kinesin Tail Domains and Mg(2+) Directly Inhibit Release of ADP from Head Domains in the Absence of Microtubules.* Biochemistry, 2008.
8. Verhey, K.J., et al., *Light chain-dependent regulation of Kinesin's interaction with microtubules.* J Cell Biol, 1998. **143**(4): p. 1053-66.
9. Al-Bassam, J., et al., *Distinct conformations of the kinesin Unc104 neck regulate a monomer to dimer motor transition.* J Cell Biol, 2003. **163**(4): p. 743-53.
10. Lee, J.R., et al., *An intramolecular interaction between the FHA domain and a coiled coil negatively regulates the kinesin motor KIF1A.* EMBO J, 2004. **23**(7): p. 1506-15.
11. Bathe, F., et al., *The complex interplay between the neck and hinge domains in kinesin-1 dimerization and motor activity.* Mol Biol Cell, 2005. **16**(8): p. 3529-37.
12. Cross, R. and J. Scholey, *Kinesin: the tail unfolds.* Nat Cell Biol, 1999. **1**(5): p. E119-21.
13. Dietrich, K.A., et al., *The kinesin-1 motor protein is regulated by a direct interaction of its head and tail.* Proc Natl Acad Sci U S A, 2008. **105**(26): p. 8938-43.
14. Yamada, K.H., T. Hanada, and A.H. Chishti, *The effector domain of human Dlg tumor suppressor acts as a switch that relieves autoinhibition of kinesin-3 motor GAKIN/KIF13B.* Biochemistry, 2007. **46**(35): p. 10039-45.
15. Imanishi, M., et al., *Autoinhibition regulates the motility of the C. elegans intraflagellar transport motor OSM-3.* J Cell Biol, 2006. **174**(7): p. 931-7.

16. Okada, Y., et al., *The neuron-specific kinesin superfamily protein KIF1A is a unique monomeric motor for anterograde axonal transport of synaptic vesicle precursors.* Cell, 1995. **81**(5): p. 769-80.

17. Hirokawa, N., *Kinesin and dynein superfamily proteins and the mechanism of organelle transport.* Science, 1998. **279**(5350): p. 519-26.

18. Horiguchi, K., et al., *Transport of PIP3 by GAKIN, a kinesin-3 family protein, regulates neuronal cell polarity.* J Cell Biol, 2006. **174**(3): p. 425-36.

19. Blasius, T.L., et al., *Two binding partners cooperate to activate the molecular motor Kinesin-1.* J Cell Biol, 2007. **176**(1): p. 11-7.

20. Okada, Y., H. Higuchi, and N. Hirokawa, *Processivity of the single-headed kinesin KIF1A through biased binding to tubulin.* Nature, 2003. **424**(6948): p. 574-7.

21. Okada, Y. and N. Hirokawa, *A processive single-headed motor: kinesin superfamily protein KIF1A.* Science, 1999. **283**(5405): p. 1152-7.

22. Okada, Y. and N. Hirokawa, *Mechanism of the single-headed processivity: diffusional anchoring between the K-loop of kinesin and the C terminus of tubulin.* Proc Natl Acad Sci U S A, 2000. **97**(2): p. 640-5.

23. Tomishige, M., D.R. Klopfenstein, and R.D. Vale, *Conversion of Unc104/KIF1A kinesin into a processive motor after dimerization.* Science, 2002. **297**(5590): p. 2263-7.

24. Helenius, J., et al., *The depolymerizing kinesin MCAK uses lattice diffusion to rapidly target microtubule ends.* Nature, 2006. **441**(7089): p. 115-9.

25. Thorn, K.S., J.A. Ubersax, and R.D. Vale, *Engineering the processive run length of the kinesin motor.* J Cell Biol, 2000. **151**(5): p. 1093-100.

26. Sheetz, M.P., *Motor and cargo interactions.* Eur J Biochem, 1999. **262**(1): p. 19-25.

27. Setou, M., et al., *Kinesin superfamily motor protein KIF17 and mLin-10 in NMDA receptor-containing vesicle transport.* Science, 2000. **288**(5472): p. 1796-802.

28. Takano, K., et al., *NXF2 is involved in cytoplasmic mRNA dynamics through interactions with motor proteins.* Nucleic Acids Res, 2007. **35**(8): p. 2513-21.

29. Klopfenstein, D.R., et al., *Role of phosphatidylinositol(4,5)bisphosphate organization in membrane transport by the Unc104 kinesin motor.* Cell, 2002. **109**(3): p. 347-58.

30. Klopfenstein, D.R. and R.D. Vale, *The lipid binding pleckstrin homology domain in UNC-104 kinesin is necessary for synaptic vesicle transport in Caenorhabditis elegans.* Mol Biol Cell, 2004. **15**(8): p. 3729-39.

31. Shin, H., et al., *Association of the kinesin motor KIF1A with the multimodular protein liprin-alpha.* J Biol Chem, 2003. **278**(13): p. 11393-401.

32. Schnapp, B.J., *Trafficking of signaling modules by kinesin motors.* J Cell Sci, 2003. **116**(Pt 11): p. 2125-35.

33. Araki, Y., et al., *The novel cargo Alcadein induces vesicle association of kinesin-1 motor components and activates axonal transport.* EMBO J, 2007. **26**(6): p. 1475-86.

34. Bowman, A.B., et al., *Kinesin-dependent axonal transport is mediated by the sunday driver (SYD) protein.* Cell, 2000. **103**(4): p. 583-94.

35. Bracale, A., et al., *Kidins220/ARMS is transported by a kinesin-1-based mechanism likely to be involved in neuronal differentiation.* Mol Biol Cell, 2007. **18**(1): p. 142-52.

36. Byrd, D.T., et al., *UNC-16, a JNK-signaling scaffold protein, regulates vesicle transport in C. elegans.* Neuron, 2001. **32**(5): p. 787-800.

37. Kamm, C., et al., *The early onset dystonia protein torsinA interacts with kinesin light chain 1.* J Biol Chem, 2004. **279**(19): p. 19882-92.

38. Konecna, A., et al., *Calsyntenin-1 docks vesicular cargo to kinesin-1.* Mol Biol Cell, 2006. **17**(8): p. 3651-63.

39. Taya, S., et al., *DISC1 regulates the transport of the NUDEL/LIS1/14-3-3epsilon complex through kinesin-1.* J Neurosci, 2007. **27**(1): p. 15-26.

40. Verhey, K.J., et al., *Cargo of kinesin identified as JIP scaffolding proteins and associated signaling molecules.* J Cell Biol, 2001. **152**(5): p. 959-70.

41. Yang, H.Y., P.E. Mains, and F.J. McNally, *Kinesin-1 mediates translocation of the meiotic spindle to the oocyte cortex through KCA-1, a novel cargo adapter.* J Cell Biol, 2005. **169**(3): p. 447-57.

42. Yang, J. and T. Li, *The ciliary rootlet interacts with kinesin light chains and may provide a scaffold for kinesin-1 vesicular cargos.* Exp Cell Res, 2005. **309**(2): p. 379-89.

43. Setou, M., et al., *Glutamate-receptor-interacting protein GRIP1 directly steers kinesin to dendrites.* Nature, 2002. **417**(6884): p. 83-7.

44. Kimura, T., et al., *Tubulin and CRMP-2 complex is transported via Kinesin-1.* J Neurochem, 2005. **93**(6): p. 1371-82.

45. Hammond, J.W., et al., *Co-operative versus independent transport of different cargoes by Kinesin-1.* Traffic, 2008. **9**(5): p. 725-41.

46. Whitmarsh, A.J., *The JIP family of MAPK scaffold proteins.* Biochem Soc Trans, 2006. **34**(Pt 5): p. 828-32.

47. Stagi, M., et al., *Unloading kinesin transported cargoes from the tubulin track via the inflammatory c-Jun N-terminal kinase pathway.* FASEB J, 2006. **20**(14): p. 2573-5.

48. Hollenbeck, P.J., *The distribution, abundance and subcellular localization of kinesin.* J Cell Biol, 1989. **108**(6): p. 2335-42.

49. Wozniak, M.J. and V.J. Allan, *Cargo selection by specific kinesin light chain 1 isoforms.* EMBO J, 2006. **25**(23): p. 5457-68.

50. DeBoer, S.R., et al., *Conventional kinesin holoenzymes are composed of heavy and light chain homodimers.* Biochemistry, 2008. **47**(15): p. 4535-43.

51. Cyr, J.L., et al., *Molecular genetics of kinesin light chains: generation of isoforms by alternative splicing.* Proc Natl Acad Sci U S A, 1991. **88**(22): p. 10114-8.

52. Jacobson, C., B. Schnapp, and G.A. Banker, *A change in the selective translocation of the Kinesin-1 motor domain marks the initial specification of the axon.* Neuron, 2006. **49**(6): p. 797-804.

53. Nakata, T. and N. Hirokawa, *Microtubules provide directional cues for polarized axonal transport through interaction with kinesin motor head.* J Cell Biol, 2003. **162**(6): p. 1045-55.

54. Xu, X., et al., *MKLP1 requires specific domains for its dendritic targeting.* J Cell Sci, 2006. **119**(Pt 3): p. 452-8.

55. Sharp, D.J., et al., *Identification of a microtubule-associated motor protein essential for dendritic differentiation.* J Cell Biol, 1997. **138**(4): p. 833-43.

56. Marszalek, J.R., et al., *Novel dendritic kinesin sorting identified by different process targeting of two related kinesins: KIF21A and KIF21B.* J Cell Biol, 1999. **145**(3): p. 469-79.

57. Reed, N.A., et al., *Microtubule acetylation promotes kinesin-1 binding and transport.* Curr Biol, 2006. **16**(21): p. 2166-72.

58. Liao, G. and G.G. Gundersen, *Kinesin is a candidate for cross-bridging microtubules and intermediate filaments. Selective binding of kinesin to detyrosinated tubulin and vimentin.* J Biol Chem, 1998. **273**(16): p. 9797-803.

59. Ikegami, K., et al., *Loss of alpha-tubulin polyglutamylation in ROSA22 mice is associated with abnormal targeting of KIF1A and modulated synaptic function.* Proc Natl Acad Sci U S A, 2007. **104**(9): p. 3213-8.

60. Dunn, S., et al., *Differential trafficking of Kif5c on tyrosinated and detyrosinated microtubules in live cells.* J Cell Sci, 2008. **121**(Pt 7): p. 1085-95.

61. Larcher, J.C., et al., *Interaction of kinesin motor domains with alpha- and beta-tubulin subunits at a tau-independent binding site. Regulation by polyglutamylation.* J Biol Chem, 1996. **271**(36): p. 22117-24.

62. Jiang, H., et al., *Both the establishment and the maintenance of neuronal polarity require active mechanisms: critical roles of GSK-3beta and its upstream regulators.* Cell, 2005. **120**(1): p. 123-35.

63. Bonnet, C., et al., *Differential binding regulation of microtubule-associated proteins MAP1A, MAP1B, and MAP2 by tubulin polyglutamylation.* J Biol Chem, 2001. **276**(16): p. 12839-48.

64. Boucher, D., et al., *Polyglutamylation of tubulin as a progressive regulator of in vitro interactions between the microtubule-associated protein Tau and tubulin.* Biochemistry, 1994. **33**(41): p. 12471-7.

65. Hammond, J.W., D. Cai, and K.J. Verhey, *Tubulin modifications and their cellular functions.* Curr Opin Cell Biol, 2008. **20**(1): p. 71-6.

66. Verhey, K.J. and J. Gaertig, *The tubulin code.* Cell Cycle, 2007. **6**(17): p. 2152-60.